Computational Fluid Dynamics Investigation into High Mast Illumination Poles: Influence of Light Fixture Type

By

Briceson August Junge

Submitted to the graduate degree program in Civil, Environmental, and Architectural Engineering and the Graduate Faculty of the University of Kansas in partial fulfillment of the requirements for the degree of Master of Science.

_____

Co-Chairperson William Collins

_____

Co-Chairperson Caroline Bennett

_____

Jian Li

_____

Mark Ewing

September 26th, 2022

LAWRENCE, KANSAS

Keywords: Fatigue, vortex shedding, high mast illumination poles, high mast light towers, computational fluid dynamics

The thesis committee for Briceson August Junge certifies that this is the approved version of the following thesis:

Computational Fluid Dynamics Investigation into High Mast Illumination Poles: Influence of Light Fixture Type

_____

Co-Chairperson William Collins

_____

Co-Chairperson Caroline Bennett

_____

Jian Li

_____

Mark Ewing

Approved Date: November 30, 2022

ABSTRACT

High mast illumination poles (HMIPs) are commonly used throughout the United States to illuminate large areas such as highways and rest stops. HMIPs have proven to be susceptible to fatigue under wind loading, yet interactions between the structure and wind remain poorly understood. Aeroelastic phenomenon, such as vortex shedding, have been shown to induce larger than normal deformations and stresses that can lead to premature fatigue in structural details near the base of the pole. The geometry of the structure is a contributor to how it will respond to wind loading. While HMIP geometry remains relatively the same, the type and number of luminaires installed at the top of the pole can differ greatly. This study aims to analyze how differences in luminaire installations can affect flow around the lighting assembly at the top of the pole. Flow past two types of luminaires commonly used in Kansas, LED and incandescent, was analyzed using 2D computational fluid dynamics (CFD) modeling. In addition to luminaire type, angle of attack of the wind, number of luminaires, and wind speed were varied. Lift and drag force time-histories were extracted from the CFD simulations, and the power spectral density (PSD) of the data was found. Using +/-10 percent bounds, the natural frequencies of the HMIP were compared to the peaks in the PSD curves to formulate conclusions regarding the susceptibility of poles to lock-in vortex shedding. The results of the study showed: 1) both luminaire types were susceptible to inducing vibrations that could lead to lock-in behavior across the first three natural frequencies of the poles, 2) the number of peaks in the PSD curves developed from each simulation that fell within a natural frequency range increased as the wind speed increased, 3) more peaks fell within the mode 1 range for the incandescent luminaires than for the LED luminaires, and 4) there was no clear indication that LED luminaires might incite a greater response than incandescent luminaires in the first mode.

TABLE OF CONTENTS

TABLE OF FIGURES

ACKNOWLEDGEMENTS

First and foremost, thank you to Dr. Caroline Bennett, Dr. William Collins, and Dr. Jian Li for giving me the opportunity to work with the fatigue and fracture research group while pursuing my Master's degree. You all provided excellent guidance and encouragement as well as showed patience with me, and for that, I am thankful. All the experience I gained working in the research group will serve me well in my career. I would also like to acknowledge the Kansas Department of Transportation for sponsoring my research.

I would like to thank Dr. Mark Ewing, Dr. Z. J. Wang, and Salman Rahmani of the Aerospace Department for their priceless insight and advice into computational fluid dynamics modeling and structural dynamics. They helped me and our group further our understanding of the subject and helped better the results of the project.

Thank you to the friends I made during my time in graduate school. To Mary Juno, Tristan Yount, Ryan Rulon, Grant Martin, Alireza Bahadori, and many others: Although our time in person may have been cut short, I thoroughly enjoyed it all.

To my family, you all were always there for me to fall back on. Finally, I want to thank my partner, Julia, for being by my side the whole way and always trying to push me to be better.

EXECUTIVE SUMMARY

High Mast Illumination Poles (HMIPs) are lighting towers that are greater than 55 ft (16.8 m) tall and are typically located along highways and rest stops. In March 2019, a wind event, referred to as the "bomb cyclone," caused several HMIPs in Kansas to excite and experience large-amplitude deflections on the order of several feet called "lock-in" behavior. Lock-in behavior is when the frequency of vibration matches a natural frequency of the structure and excess deformations will be observed. Vibrations is the poles are due to aeroelastic phenomenon like vortex shedding. Following this event, the poles were inspected and cracks were identified around the handhole openings in several of the structures. These poles were taken out of service having only been in place for approximately one year. Their premature failure caused significant concern. New, LED luminaires had been implemented with the construction of these poles. The Kansas Department of Transportation (KDOT) sought to learn if these had any influence on the behavior observed during this event over the older incandescent luminaires.

The goal of this thesis was to examine and compare the behavior of wind flow past LED and incandescent luminaires used in Kansas using computational fluid dynamics (CFD) modeling. 2-dimensional models were developed in Abaqus/CFD 2016 representing a projection of the full lighting assembly at the top of an HMIP. Simulations were created for each luminaire type on assemblies including 3 and 4 fixtures. The rotation and wind speed were varied throughout the simulations. 3-fixture simulations used rotations of 0, 30, and 60 degrees and 4-fixture simulations used rotations of 0, 22.5, and 45 degrees. All assemblies and rotations were simulated at wind speeds of 15 (6.7), 25 (11.2), 30 (13.4), 35 (15.6), and 45 (20.1) mph. A time-history of the force on the lighting assemblies in the along-wind and cross-wind directions was extracted from the models. Power spectral density (PSD) curves were developed, identifying the dominant

frequencies in the time-history data. The peaks in the curve were picked out and compared with the first 3 natural frequencies of the 4 representative HMIP types used in the state. The natural frequencies were determined using structural model of the poles using Abaqus/CAE 2017. +/-10 percent bounds around each natural frequency were used when comparing the peaks in the PSD data. When a peak fell within these bounds, it was constituted as a "hit" for that natural frequency mode. The hit counts were used to evaluate the behaviors observed and compare the behaviors of each fixture type, angle, and wind speed.

The results of the simulations showed the following: 1) both luminaire types were susceptible to inducing vibrations that could lead to lock-in behavior across the first three natural frequencies of the poles, 2) the number of peaks in the PSD curves developed from each simulation that fell within a natural frequency range increased as the wind speed increased, 3) more peaks fell within the mode 1 range for the incandescent luminaires than for the LED luminaires, and 4) there was no clear indication that LED luminaires might incite a greater response than incandescent luminaires in the first mode. Recommendations for future work include a continuation of this work for a broader spectrum of wind speeds, development of 3-dimensional models to capture the influence of changes in geometry along the depth of the luminaire on the flow behavior, and instrumentation of existing HMIP structures with different luminaire types to determine real responses and compare with the numerical predictions presented in this document.

INTRODUCTION AND BACKGROUND

High mast illumination poles (HMIPs) are light towers taller than 55 ft (16.8 m). They are ubiquitous throughout Kansas and other states and are typically located along freeways, at interchanges, and rest stops. The poles typically consist of tapered, long hollow steel sections with a lighting assembly attached to the top, as shown in Figure 1. Wind loading is the primary loading considered in the design and analysis of lighting and sign structures. Despite their widespread use, the industry's understanding of wind loading and the susceptibility of HMIPs to wind-induced aeroelastic phenomena, like vortex shedding and buffeting, remains significantly underdeveloped.

There have been numerous documented failures of HMIP structures throughout the United States. In February 2003, a winter storm led to the collapse of approximately 140 tapered aluminum light poles in western Illinois thought to be due to wind-induced vibrations (Caracoglia, 2007). The Wisconsin Department of Transportation reported cracking and failures of high-mast luminaire support structures and other support structures across the state (Foley, 2004). On November 12, 2003, a high-mast light pole fell along I-29, near Sioux City, Iowa (Dexter, 2004). On April 11, 2004, two high-mast lighting structures failed near Denver International Airport during a wind event (Goode & van de Lindt, 2007).

In March 2019, a wind event, referred to as the "bomb cyclone," caused several HMIPs in Kansas to excite and experience large-amplitude deflections on the order of several feet. Following this event, the poles were inspected and cracks were identified around the handhole openings in several of the structures, as shown in Figure 2. These poles were taken out of service. The poles taken out of service had only been in place for approximately one year, therefore, their premature failure caused significant concern. The University of Kansas was retained to conduct a forensics

investigation on the failed poles, and in parallel, engaged in an effort described in this paper to develop an improved understanding of the response of HMIPs to wind loading.

Figure 1: High Mast Illumination Pole Lighting Assembly with LED Luminaires (KDOT, 2019)

Figure 2: Cracking observed at the hand hole weld (KDOT, 2019)

Previous research into the interaction between wind and HMIP response has typically focused on instrumentation of existing poles and theoretical analysis of flow past the pole body, neglecting the lighting assembly. Ahearn and Puckett (2010) instrumented in-service HMIPs with

anemometers and accelerometers to analyze how the poles responded to wind loading. Data were also gathered for poles retrofitted with helical strakes and perforated shrouds to characterize effectiveness of retrofits at reducing dynamic responses. It was found that poles experienced lock-in behavior, mainly in the 3rd natural frequency mode (Ahearn & Puckett, 2010). Giosan (2005) used an analytical approach to incrementally calculate the susceptibility to vortex shedding near a natural frequency along the height of an HMIP. For the pole considered, it was found that shedding near the first four natural frequency modes at some points along the pole was possible within a practical wind speed range (Giosan, 2005). Peavy (2018) performed instrumentation of existing poles, computational fluid dynamics (CFD) modeling, and fluid-structure interaction (FSI) modeling of HMIPs. The 3D FSI model included the lighting assembly modeled as a thin projection of the shape attached to the top of the pole. Force and deflection data along the height of the pole were studied. Slower wind speeds around 5 mph (2.2 m/sec) were explored in the FSI model resulting in low deflections. The results proved it was difficult to predict the conditions at which excess vibrations will occur (Peavy, 2018).

1.1 Wind-Induced Vibrations

1.1.1 Vortex Shedding

Vortex shedding is an aeroelastic phenomenon that occurs when vortices form in the wake of a body and begin to interact and oscillate. This interaction results in forces on the body perpendicular to the direction of flow. A diagram of the phenomenon is shown in Figure 3. A "lock-in" phenomenon can occur when the vortex shedding frequency nears the natural frequency of the structure; under lock-in, the structure begins to excite and can experience excess deformations and stresses. Vortex shedding typically develops at sustained wind speeds between 10 mph (4.47 m/s) and 45 mph (20.1 m/s) and produces structural vibrations in the direction

perpendicular to the flow. Turbulence tends to be too high at wind speeds greater than 45 mph (20.1 m/s) for the phenomenon to occur. Wind speeds below 10 mph (4.47 m/s) are considered not significant enough to produce vortex shedding (AASHTO, 2001).

The Reynolds Number is defined as the ratio of inertia forces to viscous forces for fluid flow around an object or surface (NASA, 2009). Vortices begin to develop when the Reynolds number is between 5 and 40. Vortex shedding develops and is laminar when the Reynolds Number is above 40, then becomes turbulent between 300 to 300,000 Above this range, turbulence breaks up vortex formation (Lienhard, 1966). Currently, American Association of State Highway and Transportation Officials (AASHTO) specifications include design for wind loading on all components. Provisions are made conservative enough to aim to prevent possible damages due to fatigue from vortex shedding induced loading (AASHTO, 2013).

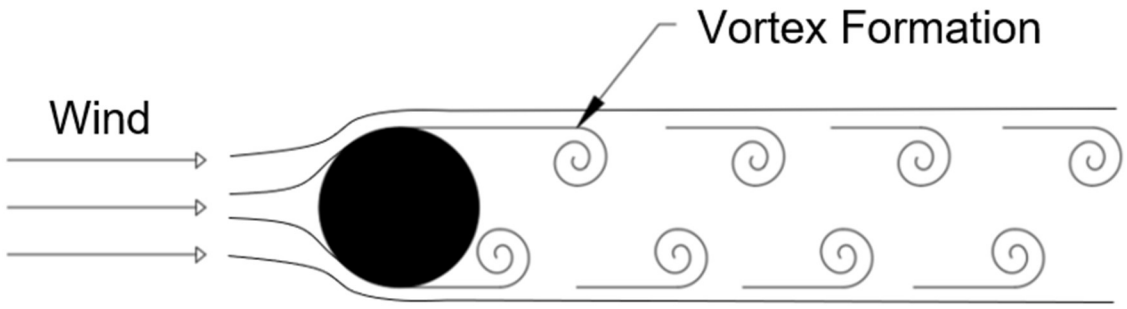

Figure 3: Formation of Vortex on Leeward Side of Body Causing Force Perpendicular to Flow Direction

1.1.2 Buffeting

Buffeting is an irregular motion of a structure or parts of a structure in a flow, excited by turbulence in the flow. This turbulence can be caused by increased flow velocity or separation of flow around a body upstream. The result of buffeting can be damaging to the structure (Fung, 1955). Vortex shedding and buffeting can be captured through a CFD model by analyzing a time-history of the pressure at a point on the leeward side of the object.

OBJECTIVE AND SCOPE

The objective of this study was to determine the influence of luminaire type on the susceptibility of HMIPs to vortex shedding using a computational fluid dynamics (CFD) modeling approach. Two types of luminaires were considered: LED and incandescent fixtures. The number of light fixtures was varied in the study, along with orientation of the fixtures with respect to wind flow and wind velocity. Time-histories of wind force on the lighting assembly projection were used to determine dominant frequencies produced by the wind flow and were compared with the first three natural frequency modes of poles commonly used in Kansas. This approach is able to provide insights for wind behavior as it flows across the assemblies, and which, if any, structural modes it may excite. This approach isolates the lighting assembly; therefore, it does not provide insight as to how the lighting assembly and pole respond together.

METHODOLOGY/MODELING APPROACH

The modeling approach adopted in this research was focused on capturing the global interaction of wind flow past the lighting assembly, specifically comparing different light fixture types, number of fixtures, orientations with respect to the wind, and wind speed. A two-dimensional CFD modelling approach for the lighting assemblies was selected, allowing global behavior to be captured while reducing computation demands in comparison with what is necessary in a three-dimensional analysis. Therefore, this approach considers a geometrically-projected section through the luminaires that neglects small geometric details.

Pressure data was extracted from the models at points on or near the surface on the leeward side of the body in the CFD model. Similarly, the total force components on the surface of the body could be extracted and yield similar results. A time-history of these force components were extracted and used for analysis. This shows how interactions in the wind with the body creates forces on the body. This data can be analyzed for the frequency of oscillation of these forces.

The data can be analyzed through inspection for things like the magnitude of force or pressure as well as through power spectral density (PSD) analysis. PSD curves will show the dominant frequencies that the time-history of pressure or force exhibits. The frequencies identified in each dataset can be compared to the natural frequencies of a given HMIP to judge its likelihood of inducing vortex induced vibrations (VIV).

3.1 Pole and Luminaire Geometry

The Kansas Department of Transportation (KDOT) provided drawings for HMIPs that are commonly installed throughout Kansas. KDOT HMIPs consist of a tapered, round pole constructed in either two or three sections. The bottom pole section is welded to a baseplate which

is bolted into the foundation. The two-section pole considered in this study is 30.5 m (100 ft) tall while the three-section poles considered have heights of 30.5 m, 33.5 m, and 36.6 m (100, 110, and 120 ft). The three-section pole is a newer design and provides an extra section of greater thickness at the base. The sections are connected with slip joint splices. An access hole (handhole) is located near the base of the pole to allow for lifting and lowering of the lighting fixture.

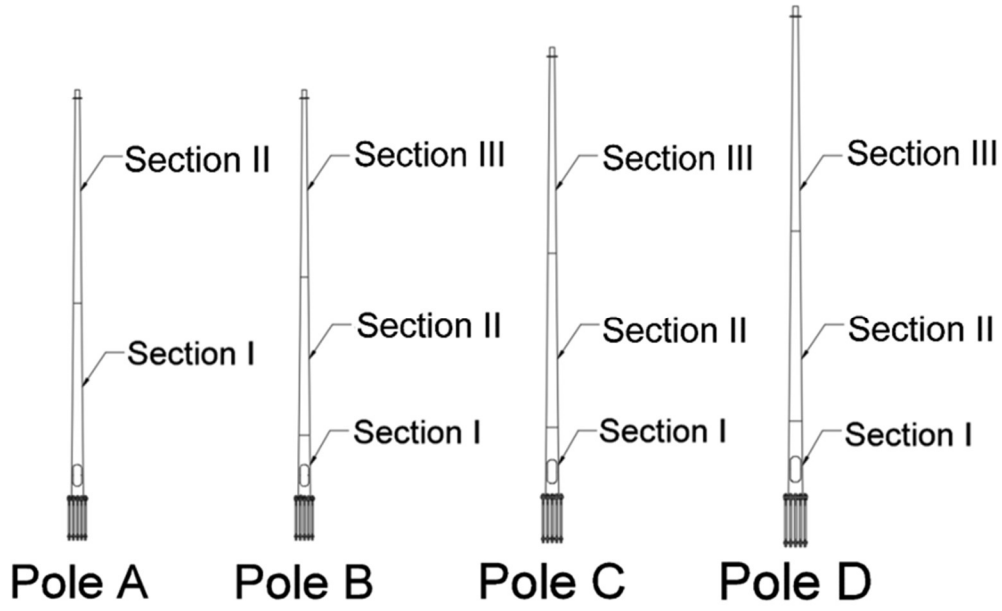

Figure 4: High Mast Illumination Pole Geometry

The lighting assembly located at the top of the pole includes luminaires attached to a lowering ring assembly. Movement of the lowering device is accomplished using an internal cable and pulley system. The number of luminaires attached to the lowering device depends on the amount of light required at that pole, with three to four luminaires commonly used for a single pole.

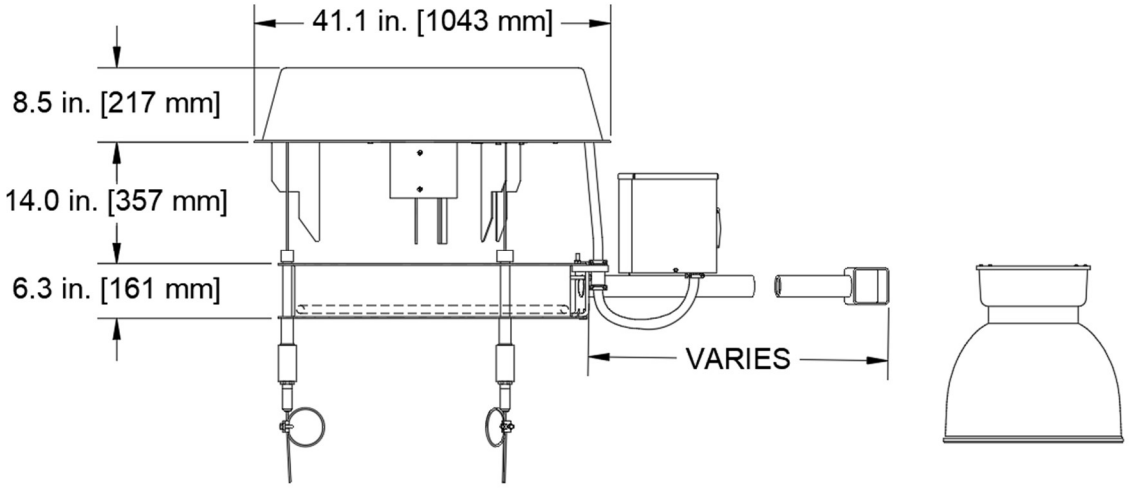

Figure 5: Lowering Ring Assembly

Two different types of luminaires were considered in this study: incandescent and LED. Until recently, KDOT used incandescent luminaires in all HMIP structures; however, newer structures utilize Holophane HMLED3 LED luminaires, which have a significantly slimmer profile and are brighter and more efficient than incandescent options. The LED luminaire is shown in Figure 6a. The most common incandescent luminaire used in the Kansas DOT lighting inventory is the Holophane HMSC High Mast Cutoff Series Luminaire, shown in Figure 6b.

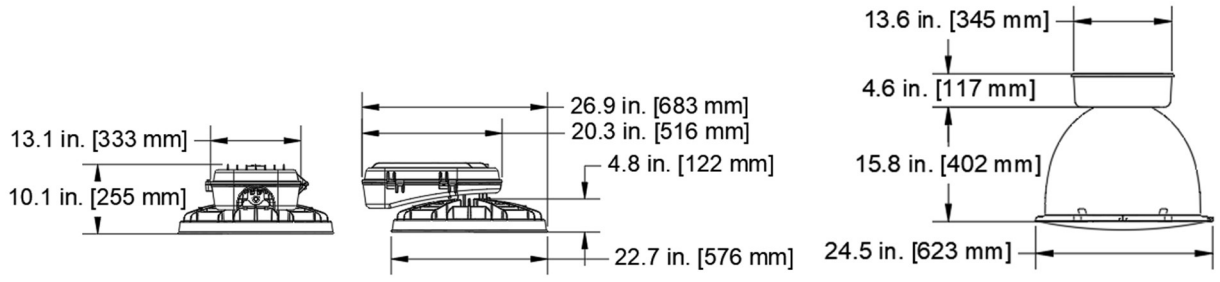

Figure 6: Luminaire Geometry (a) LED Luminaire (b) Incandescent Luminaire

3.2 Natural frequency analysis

The commercially available finite element analysis (FEA) software Abaqus/CAE (2017) was used to calculate the first three modes of natural vibration of the HMIP. A three-dimensional

structural model of the pole was developed based on the provided drawings. The lighting assembly was modeled as a lump mass at the top of the pole for simplicity in the natural frequency analysis.

Natural frequencies were determined for four different poles, as presented in Figure 5: a 100 ft (30.5 m) pole comprised of two tapered sections (Pole A), and 100 ft, 110 ft, and 120 ft (30.5 m, 33.5 m, and 36.6 m) poles comprised of three tapered sections (Poles B, C, and D, respectively). Pole geometries are presented in Table 1, with slip distance defined as the overlap between a pole section and the section below it. Pole specifications and drawings are provided in the Appendix. The poles are made of Gr. A572 steel, galvanized in the fabricated condition; material properties adopted in the models are listed in Table 2.

A linear perturbation frequency analysis step was created in Abaqus to compute the natural frequencies of the structure using Equations 1 and 2. The default settings for the step were used, and the first three dominant mode shapes were extracted. Torsional modes were disregarded in this analysis.

$$M^{NM}\ddot{u}^{M} + F^{N}(u^{M}) = 0 \qquad (1)$$

$$(-\omega^{2}M^{MN} + K^{MN})\varphi^{N} = 0 \qquad (2)$$

Where M^{MN} is the mass matrix, K^{MN} is the stiffness matrix, and φ^{N} is the eigenvectors or modes.

Table 1: High Mast Illumination Pole Tapered Section Measurements

Pole Label	Total Height, ft (m)	Section	Base Diameter, in. (mm)	Top Diameter, in. (mm)	Length ft (m)	Thickness, in. (mm)	Slip Distance, ft (m)
A	30.48 (100)	I	25.50 (647.7)	18.39 (467.1)	50.80 (15.48)	0.2500 (6.350)	N/A
		II	19.25 (491.6)	11.87 (301.5)	52.68 (5.867)	0.1880 (4.775)	28.31 (8.629)
B	30.48 (100)	I	26.00 (660.4)	23.42 (594.9)	18.40 (5.608)	0.5000 (12.70)	N/A
		II	24.50 (622.3)	18.63 (473.2)	41.90 (12.77)	0.2500 (6.350)	36.00 (10.97)
		III	19.50 (495.3)	12.88 (327.2)	47.32 (14.42)	0.1875 (4.763)	28.69 (8.745)
C	33.53 (110)	I	26.00 (660.4)	22.93 (582.4)	21.91 (6.678)	0.5000 (12.70)	N/A
		II	24.00 (609.6)	17.16 (435.9)	48.85 (14.89)	0.2500 (6.350)	35.25 (10.74)
		III	18.00 (457.2)	11.47 (291.3)	46.61 (14.21)	0.1875 (4.763)	26.44 (8.059)
D	36.58 (120)	I	26.00 (660.4)	21.95 (557.5)	28.93 (8.818)	0.5000 (12.70)	N/A
		II	23.00 (584.2)	16.18 (411.0)	48.73 (14.85)	0.2500 (6.350)	33.75 (10.29)
		III	17.00 (431.8)	10.08 (256.0)	49.46 (15.08)	0.1875 (4.763)	24.94 (7.602)

Table 2: Material Properties for A572 Steel

Material	Density (ρ)	Modulus of Elasticity (E)	Poisson's Ratio (ν)
	lb/ft^3 (kg/m^3)	**ksi (GPa)**	**-**
A572 Steel	490 (7849)	29,000 (200)	0.30

3.3 CFD Modeling

Commercially available finite element modeling (FEM) software programs, Abaqus/CFD 2016 (DSS, 2016), were used to create computational fluid dynamics models of air flowing around the different lighting assemblies; different wind velocities and angles of attack were included in the modeling effort. The models were used to analyze the behavior of the wind force parallel and perpendicular to the flow direction, to characterize the influence of specific luminaire details

(incandescent vs LED, and number of light fixtures) on aerodynamic response. To model flow, the lighting assembly geometry was “cut out” of a large, rectangular fluid domain.

The air domain and lighting assembly were modeled in two dimensions rather than three to simplify model construction and improve computational efficiency. It should be noted that this approach sacrifices the inclusion of small details on the luminaires and lowering ring, and neglects changes in luminaire shape through depth. However, the 2D approach has been successfully applied in numerous aerodynamic studies and is expected to represent global aerodynamic behavior for the lighting assemblies with reasonable accuracy, enabling comparison between incandescent and LED luminaires.

The modeled geometries are projections of the luminaire shapes and lowering ring in the lighting assembly configurations, as shown in Figure 7. The luminaires are spaced from the housing based on an 18-inch arm stretching from the lowering ring to the attachment point on the luminaire. Both fixtures attach to the arms on the back of their respective housings. Due to the placement of the LED fixture housings on the lowering ring, LED assemblies produce a larger projected total diameter than the equivalent incandescent assemblies. For both fixture types, the arms were omitted from the simulation geometry.

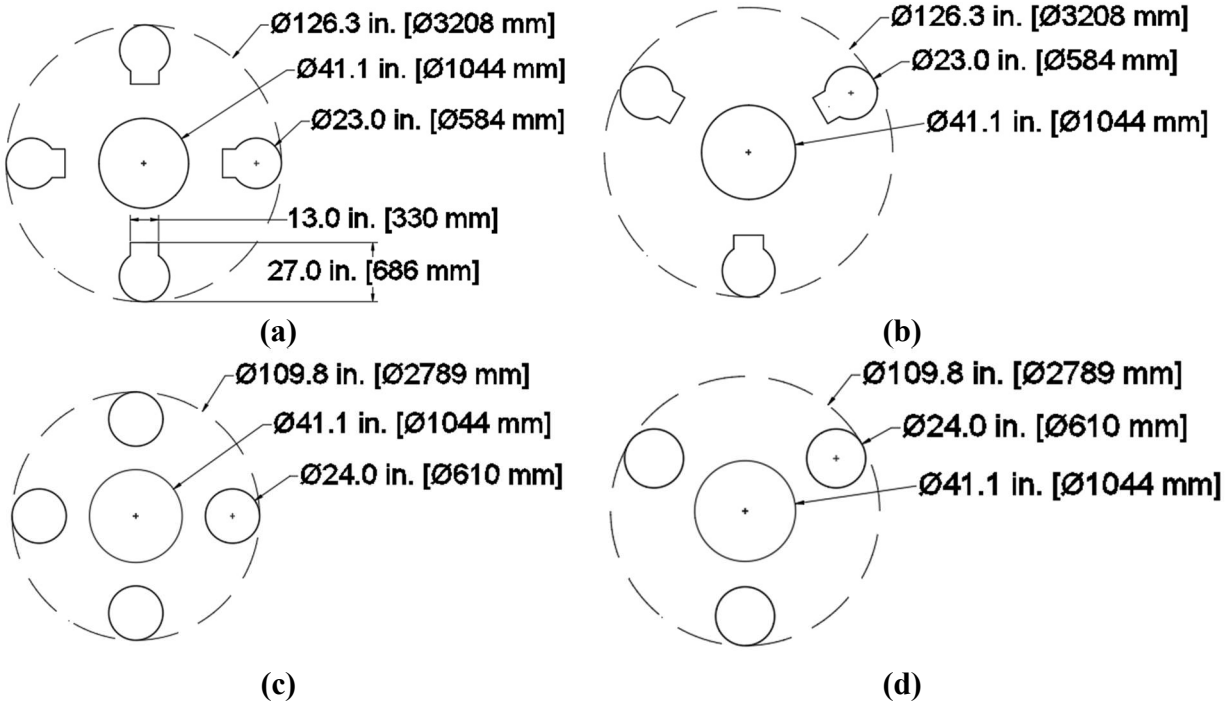

Figure 7: CFD Lighting Assembly 2D Geometry for (a) 4 LED Luminaires, (b) 3 LED Luminaires, (c) 4 Incandescent Luminaires, and (d) 3 Incandescent Luminaires

3.3.1 Abaqus/CFD Modeling

Abaqus/CFD 2016 was chosen to perform CFD simulations for this study. Abaqus is a three-dimensional modeling software; therefore, a pseudo two-dimensional modeling approach that used a fluid domain with a one-element thickness was adopted. This approach precludes any changes in velocity or pressure over the depth normal to the plane, thus modeling two-dimensional behavior. The lighting assembly was modeled as a void in the fluid domain. The fluid domain is shown in Figure 8.The fluid inlet was modeled as a velocity inlet, positioned five diameters from the nearest point of the center circle representing the housing of the lighting assembly. A diameter was defined as the diameter of the center circle of the geometry equal to 41 inches. The pressure outlet was positioned 15 diameters to the edge of the center circle. The initial pressure at the outlet was set at 0 psi. Far field boundaries (walls) were modeled as velocity inlets with velocity equal

in magnitude and direction to the front inlet. These were also positioned five diameters to the edge of the center circle. The lighting assembly geometry was defined to have no-slip boundaries where velocity is zero.

The fluid domain was carefully partitioned as shown in Figure 8 to allow for structured refinement of the mesh around the luminaire geometry. Partitions were offset 3 in. from each lighting assembly component. A seeding bias was placed normal to the boundaries to create inflation layers with a first element height of 0.01 in. (0.254 mm) which increased to 0.50 in. (12.7 mm). The mesh is unstructured within the box partition surrounding the full assembly to allow the mesh to conform around the geometry as different assemblies and rotations were modeled. The outsides of this box were seeded at 2 in. (50.8 mm), and the mesh increased to a 5 in. (127 mm) seed dimension in the region outside the interior box partition.

A dense mesh is necessitated near the wall boundaries to properly develop the boundary layer. The Spalart-Allmaras turbulence model works best with a y-plus value of approximately 1.0, where y-plus is a relative measurement of the first mesh element size against a boundary in a CFD model. Inflation layers in the mesh were created around the geometry where the first cell height was 0.01 in. (0.254 mm) and increased at a growth rate of 10 percent of the previous layer height. The first layer height of 0.01 in. (0.254 mm) corresponded to a y-plus value greater than 1, but this was the smallest mesh size that Abaqus allowed for.

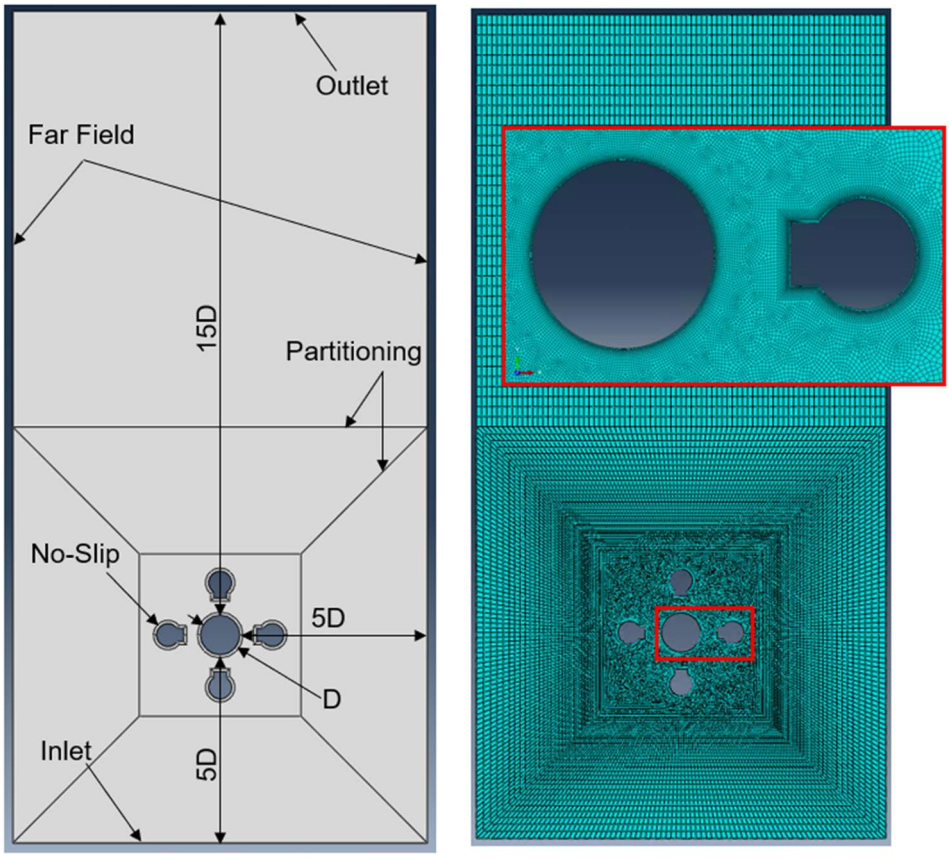

(a) (b)

Figure 8: Abaqus/CFD Fluid Domain

Fluid properties were defined as having the density and viscosity of standard air, as presented in Table 3. These properties correlate to air at sea level, at a temperature of 59 degrees Fahrenheit (15 degrees Celsius).

Table 3: Fluid Properties for Air

Material	ρ lb/ft^3 (kg/m^3)	μ lbf·s/ft^2 (Pa·s)
Air	2.37×10^{-3} (1.225)	3.740×10^{-7} (1.789×10^{-5})

The Reynolds Number can be calculated using Equation (3). The main factor influencing the Reynolds Number is air velocity, but air properties also have an effect as well. Notably, air properties change based on elevation and temperature. Density and pressure decrease as elevation

above sea level increases, corresponding with decreases in Reynolds Number. The density of air also decreases as temperature increases. Due to these factors, air properties can vary significantly based on location and weather. Over a temperature range of 0 to 100 degrees Fahrenheit (-17.8 to 37.8 Celsius), the Reynolds Number will differ by approximately 30 percent. Increasing altitude from sea level to 5,000 ft (1524 m) corresponds with a decrease in the Reynolds Number of approximately 9 percent.

$$Re = \frac{\rho V L}{\mu} \tag{3}$$

The Spalart-Allmaras turbulence solver was utilized in all CFD models created and executed using Abaqus (2016) CFD software (DSS 2016). The Spalart-Allmaras solver is a one-equation Reynolds-averaged Navier-Stokes (RANS) turbulence model approach. Default constants for the equation are listed in Table 4. In the solver controls, kinematic eddy viscosity was set to 0.01 in.^{2} /s (6.45×10-6 m^2 /s) in all areas.

Table 4: Spalart-Allmaras Turbulence Modeling Constants (DSS, 2016)

Constant	Value
C_{b1}	0.1355
C_{b2}	0.622
C_{v1}	7.1
C_{v2}	5
C_{w1}	3.2391
C_{w2}	0.3
C_{w3}	2
σ	0.6667
K	0.41

Simulations were executed for 12 seconds of flow time with a fixed step size of 0.01 seconds, allowing for enough data points for post processing of the data. Solver limitation settings chosen are listed in Table 5.

Table 5: Abaqus CFD Solver Settings

Solver	Momentum Equation	Pressure Equation	Transport Equation
Iteration Limit	600	1200	600
Convergence Checking Frequency	1	10	1
Linear Convergence Limit	1×10^{-12}	1×10^{-14}	1×10^{-12}

The Strouhal Number is a useful dimensionless quantity for describing vortex shedding frequency. The relationship between the Strouhal Number and the Reynolds Number is shown in Figure 9. A range of Strouhal Numbers is shown because different conditions can yield slightly different results at the same Reynolds Number, such as the shape of the body the fluid is moving across or the roughness of the surface. The relationship is defined by an equation from Re = 250 to Re =200,000. The Strouhal Number remains around 0.20 over this range. Above this value, the relationship is vague due to turbulent instabilities. This region is denoted with dashed lines. The Strouhal Number can be approximated while in the non-turbulent realm using the following equation:

$$S = 0.198(1 - \frac{19.7}{Re}) \quad (4)$$

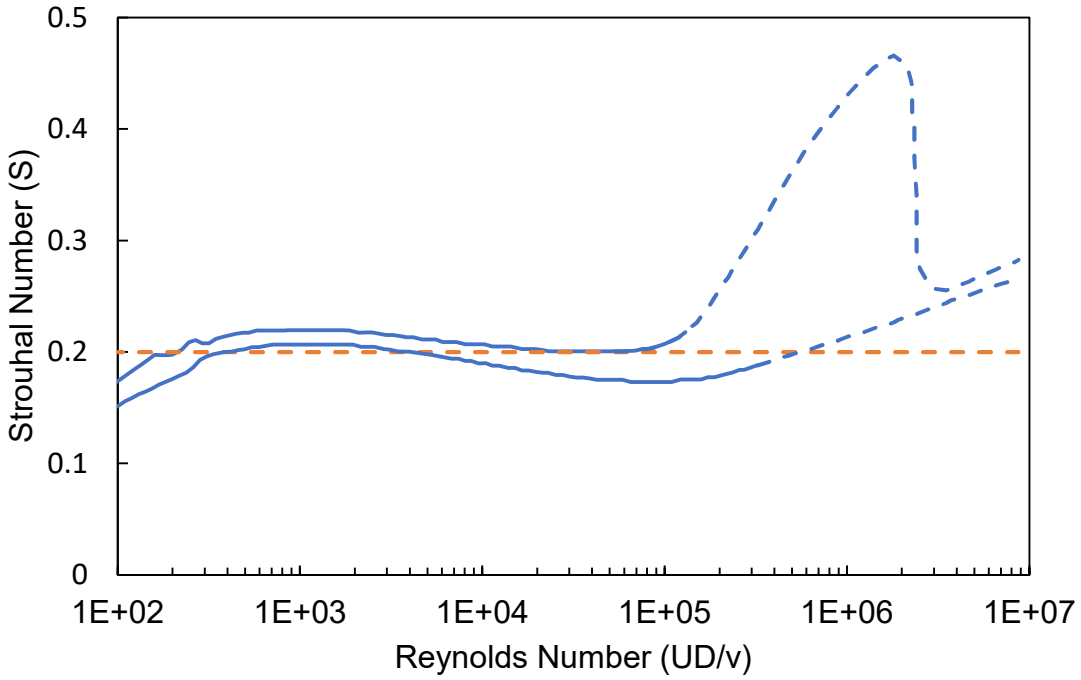

Figure 9: Relationship between Reynolds Number and Strouhal Number *(Blevins, 1990)*

The Strouhal Number can be calculated from experimental data using Equation (5), where f is the shedding frequency, D is the object diameter, and U is the free stream velocity.

$$S = \frac{fD}{U} \tag{5}$$

3.4 Model Matrix

Table 6 shows the modeling matrix. This was developed to capture common configurations with the luminaires in consideration. It was determined that three and four luminaire assemblies were the most common used in Kansas. The orientation of each luminaire assembly is defined with respect to the inlet. Orientations for each model begin at 0 degrees with one of the luminaires pointing towards the inlet, and models are rotated to capture the effects of orientation to fluid flow direction. The listed rotation is then applied from this position. Figure 10 shows the rotations considered. Four fixture assemblies were explored at 0, 22.5, and 45 degrees. Three fixture

assemblies at 0, 30, and 60 degrees. Velocity was initially based on velocity observed during the weather event causing the vibrations seen in the field. The wind speed measured at the nearest weather station was 35 mph (15.6 m/s) with gusts at 40 to 61 mph (17.9 to 27.3 m/s).

The data gathered from the CFD models includes the time history of the lift and drag coefficients and forces on the lighting assemblies. Lift is defined as the direction perpendicular flow and drag is parallel to flow. The lift and drag coefficients were calculated based on a reference length defined as the width of the geometry perpendicular to the flow direction.

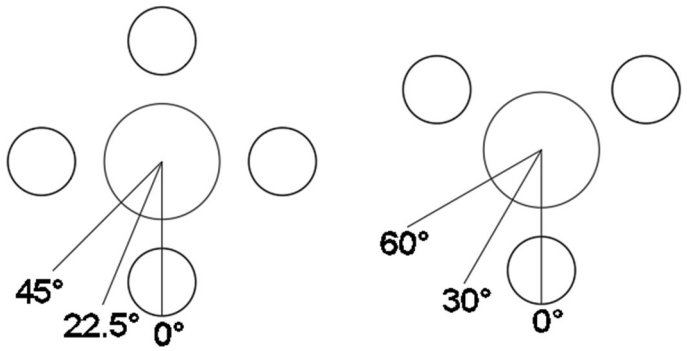

Figure 10: Lighting Assembly Model Rotations

Table 6: CFD Model Matrix

Luminaire Type	Number of Fixtures	Rotation (degrees)
Incandescent	3	0
		30
		60
	4	0
		22.5
		45
LED	3	0
		30
		60
	4	0
		22.5
		45

3.5 Power spectral density

After obtaining the results from the CFD simulation, MATLAB was utilized to determine the power spectral density of the time-history data. Power spectral density (PSD) is a representation of the signal power over frequencies (Stoica & Moses, 2005). The resulting curve shows the dominant frequencies present in the force data obtained in the CFD analysis. Figure 11 shows a PSD curve. Before finding the PSD, the average value of the data was subtracted out of each point to remove any static component. Also, a short portion at the beginning of the simulation was disregarded. This was to neglect the portion where the flow is starting up and the geometry is not experiencing a full response. Due to varying amplitudes and for clarity, the curves were each normalized respective to their own maximum values. The first three natural frequency modes of a given HMIP geometry are superimposed over the PSD curves. A frequency range is created for each mode by adding 10 percent above and below the value. The dominant frequencies present in the PSD curves can then be compared to the natural frequency ranges of a given pole.

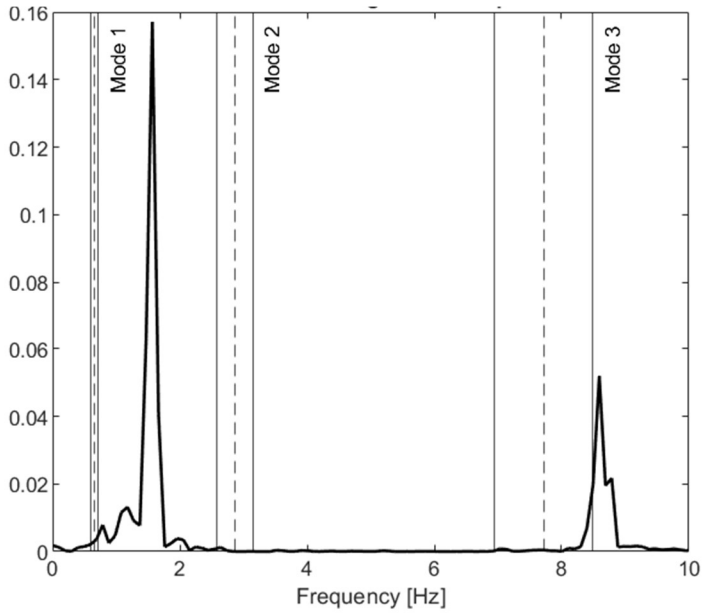

Figure 11: Power Spectral Density with Overlaid Natural Frequency Modes

RESULTS AND DISCUSSION

4.1 Natural Frequency Analysis Results

The resulting natural frequencies for the first three modes for each pole type considered are shown in Table 7. Frequencies were computed for the four lighting assembly configurations and four different pole geometries. Natural frequency varied slightly with changes in mass between the different lighting assembly configurations; however, they differed noticeably between pole geometries. The range of natural frequencies for the four pole geometries and various light fixture arrangements included in the study varied from 0.53-0.77 Hz for Mode 1, 2.13-3.33 Hz for Mode 2, and 5.35-8.62 Hz for Mode 3. Additionally, Table 11 through Table 14 shows frequency bands 10 percent above and below each natural frequency. These ranges were plotted with the power spectral density results of their respective configuration.

Table 7: HMIP Natural Frequencies with 3 Incandescent Fixtures

	Natural Frequency (Hz)			
Incandescent 3 Fixtures				
Mode	**Pole 1**	**Pole 2**	**Pole 3**	**Pole 4**
1	0.65	0.76	0.64	0.55
2	2.85	3.31	2.65	2.16
3	7.72	8.62	6.81	5.39

Table 8: HMIP Natural Frequencies with 4 Incandescent Fixtures

	Natural Frequency (Hz)			
Incandescent 4 Fixtures				
Mode	**Pole 1**	**Pole 2**	**Pole 3**	**Pole 4**
1	0.63	0.74	0.62	0.53
2	2.82	3.27	2.61	2.13
3	7.66	7.19	6.76	5.35

Table 9: HMIP Natural Frequencies with 3 LED Fixtures

	Natural Frequency (Hz)			
LED 3 Fixtures				
Mode	**Pole 1**	**Pole 2**	**Pole 3**	**Pole 4**
1	0.66	0.77	0.64	0.55
2	2.87	3.33	2.66	2.18
3	7.75	7.78	6.83	5.40

Table 10: HMIP Natural Frequencies with 4 LED Fixtures

	Natural Frequency (Hz)			
LED 4 Fixtures	**Mode**	**Pole 1**	**Pole 2**	**Pole 3**	**Pole 4**
	1	0.64	0.75	0.63	0.54
	2	2.84	3.29	2.63	2.15
	3	7.72	8.59	6.79	5.37

Table 11: HMIP Natural Frequency Ranges with 3 Incandescent Fixtures

		Pole 1		Pole 2		Pole 3		Pole 4	
Incandescent 3 Fixtures	**Mode**	**-10%**	**+10%**	**-10%**	**+10%**	**-10%**	**+10%**	**-10%**	**+10%**
	1	0.59	0.72	0.69	0.84	0.57	0.70	0.49	0.60
	2	2.57	3.14	2.98	3.64	2.38	2.91	1.95	2.38
	3	6.94	8.49	7.76	9.48	6.13	7.49	4.85	5.93

Table 12: HMIP Natural Frequency Ranges with 4 Incandescent Fixtures

		Pole 1		Pole 2		Pole 3		Pole 4	
Incandescent 4 Fixtures	**Mode**	**-10%**	**+10%**	**-10%**	**+10%**	**-10%**	**+10%**	**-10%**	**+10%**
	1	0.57	0.70	0.67	0.82	0.56	0.68	0.48	0.59
	2	2.54	3.10	2.94	3.60	2.35	2.88	1.92	2.35
	3	6.90	8.43	6.47	7.91	6.09	7.44	4.82	5.89

Table 13: HMIP Natural Frequency Ranges with 3 LED Fixtures

		Pole 1		Pole 2		Pole 3		Pole 4	
LED 3 Fixtures	**Mode**	**-10%**	**+10%**	**-10%**	**+10%**	**-10%**	**+10%**	**-10%**	**+10%**
	1	0.59	0.72	0.70	0.85	0.58	0.71	0.50	0.61
	2	2.58	3.16	3.00	3.66	2.40	2.93	1.96	2.39
	3	6.97	8.52	7.00	8.56	6.14	7.51	4.86	5.94

Table 14: HMIP Natural Frequency Ranges with 4 LED Fixtures

		Pole 1		Pole 2		Pole 3		Pole 4	
LED 4 Fixtures	**Mode**	**-10%**	**+10%**	**-10%**	**+10%**	**-10%**	**+10%**	**-10%**	**+10%**
	1	0.58	0.71	0.68	0.83	0.56	0.69	0.49	0.59
	2	2.55	3.12	2.96	3.62	2.37	2.90	1.93	2.36
	3	6.95	8.50	7.74	9.45	6.11	7.46	4.83	5.91

4.2 CFD Simulation Results

4.2.1 Abaqus/CFD Results

As previously described, time-histories of lift and drag forces acting on the light fixtures were extracted from the simulations. It was observed that the variation and amplitude of the lift

force tended to far exceed that of the drag force, as illustrated in Figure 12. For this reason, responses in the lift, or crosswind, direction were focused on. Time-history plots for all simulations are provided in Appendix A1. Generally, force tended to ramp up at the beginning of the simulations while the response was developing. This ramp portion of the data was disregarded in post-processing. The lift force typically oscillated around 0 force, while drag force tended to oscillate around a positive value. This value is the constant force component on the geometry. Before developing the PSD curves, the average force value was subtracted out of the data to remove this constant force component.

Figure 13 shows the power spectral density curves for an LED configuration with 3 fixtures oriented at a 0-degree rotation relative to the wind direction, subjected to wind velocity of 30 mph (13.4 m/s). PSD curves for all simulations are presented in Appendix A2. The spikes in the PSD represent dominant frequencies present in the time-history data. Four separate plots were created to overlay the natural frequency ranges for each pole type. Each plot uses the same PSD curve. The natural frequency ranges for the respective pole presented in Table 7 through Table 10 were overlaid on the plots, allowing consideration of the dominant frequencies from the time history responses in the context of the natural frequencies of the different pole geometries considered. For the cases presented in Figure 13, the response was greatest for frequencies less than 5 Hz, with the largest response at 1.17 Hz and next largest at 1.86 Hz. These two spikes did not occur within any of the natural frequency ranges, implying that resonance should not occur. However, smaller peaks were present that intersected mode 1 and mode 2 natural frequencies for all pole types, implying that resonance could still be possible at lower amplitude responses.

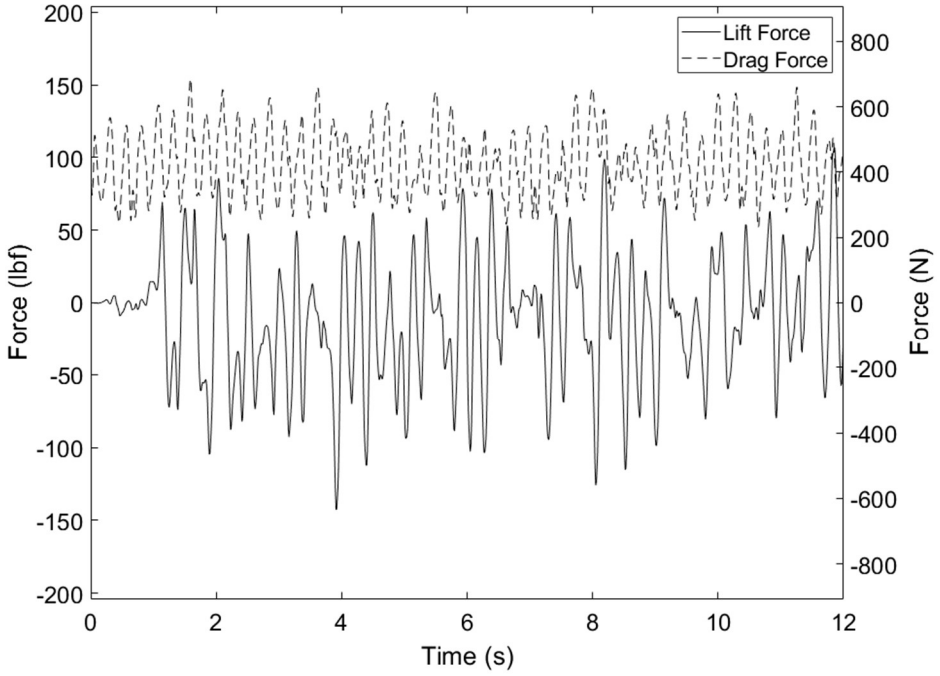

Figure 12: Time-history of lift and drag force for the 3 LED light fixture configuration with 0-degree rotation at 30 mph (13.4 m/s)

When considering the PSD data, a *peak* was defined as occurring when a local maximum existed that was greater than 5 percent of the maximum peak prominence of a given PSD curve. *Prominence* is the height of a local maximum measured from the valley in the curve separating it from the next highest peak. Because the PSD curves were normalized, the maximum possible prominence was 1.0. Adding a prominence requirement allowed for numerous small local maxima that were effectively noise in the data to be filtered out, and not be counted as a peak.

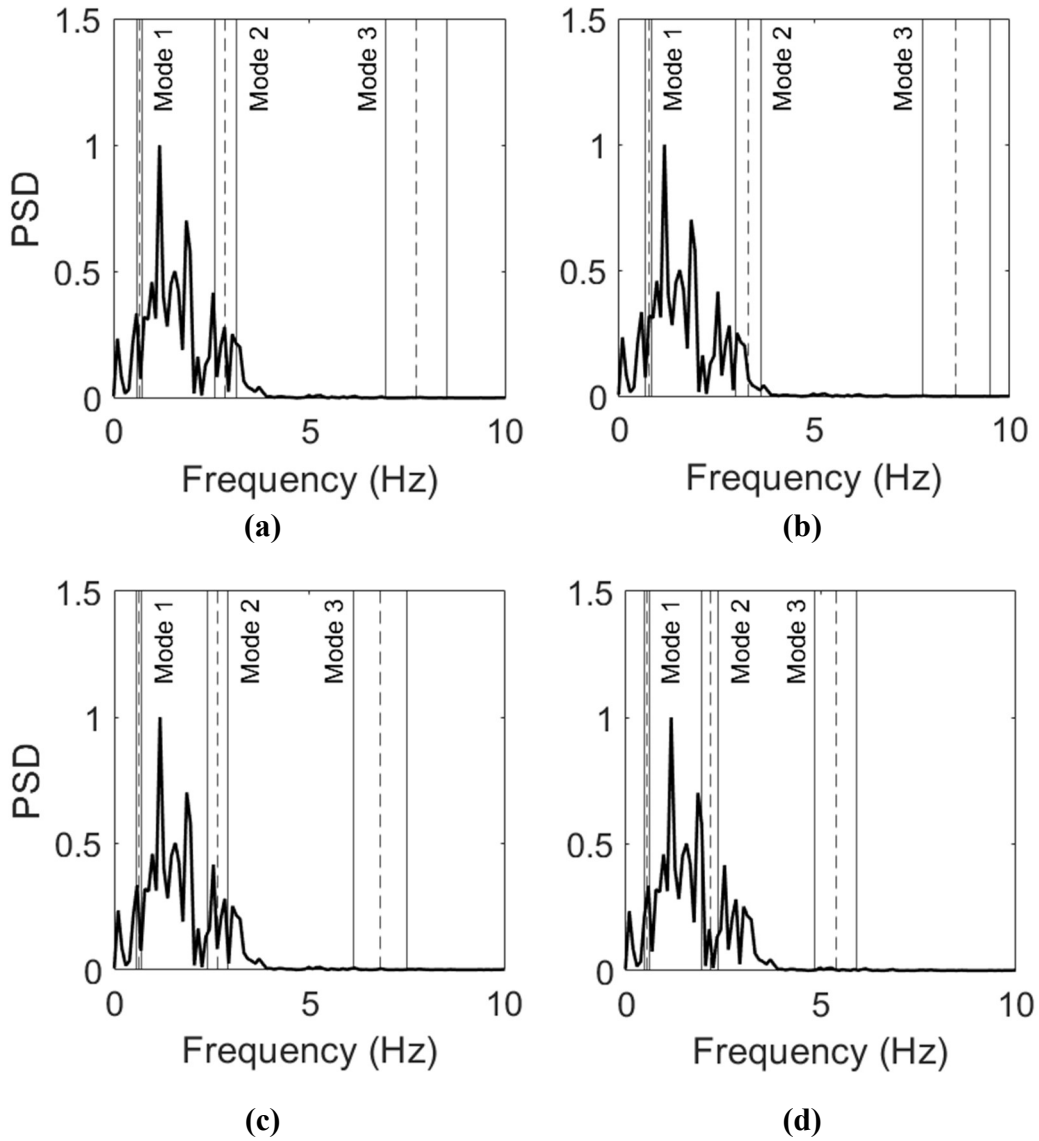

Figure 13: Power Spectral Density Curve of the Time-History of Crosswind Force on the Lighting Assembly for the 3 LED Configuration at a 0 Degree Rotation at 15 mph: (a) Pole A; (b) Pole B; (c) Pole C; (d) Pole D

Additional methods for defining peaks were explored. These alternative methods included considering minimum spacing between peaks and a minimum peak height, rather than minimum prominence. The requirement of a minimum spacing between peaks would come into effect when two peaks occur within a specified tolerance. The peak with higher prominence would be counted and the other would be neglected. This approach was found to not sufficiently filter the data and neglected important peaks. A minimum height requirement would specify a minimum value a local

maximum must exceed to be counted. On the normalized scale, this value was set to 0.10-0.30. The advantage to this approach is that peaks would not be omitted if they were characterized by high values but relatively low prominences. This approach was not selected because small peaks creating noise in the curve would not be filtered out when they were above the threshold value, resulting in a large number of peaks in some instances.

Peaks are determined relative to the data of a single simulation. This is flawed because a peak in a data set at a higher wind speed could be excluded when it has a higher amplitude than one that is not excluded at a lower wind speed when compared. To further identify the peaks in the data and compare them to peaks in other simulations, a series of color band comparison charts were created.

Figure 14 shows a color-band comparison chart for the 3 LED light fixture configuration oriented at a 0-degree position relative to the wind direction, with data represented for all wind speeds considered. The color bands represent amplitude of the PSD curves. These data were not normalized as was done in the PSD plots, so that changes in amplitude between variables could be considered. Translating the PSD curves to color bands allows for multiple curves to be placed adjacent to one another for comparison. Peaks in the data are identified with an 'X'. Like the individual PSD curves, a chart was created for each HMIP type and its respective natural frequency ranges were overlaid on the chart across all the bands. These ranges were not labeled for clarity. The mode 1 range is the lowest range with modes 2 and 3 ordered above it on the plots.

These plots were used to compare the light assembly configurations over the various wind speed and rotation ranges considered. For the configuration presented in Figure 14 (3 LEDs), peaks in the response data tended to shift to higher frequencies with increasing wind speed. The

amplitude of the data also increased with wind speed. Color band charts for all simulations are presented in Appendix A3.

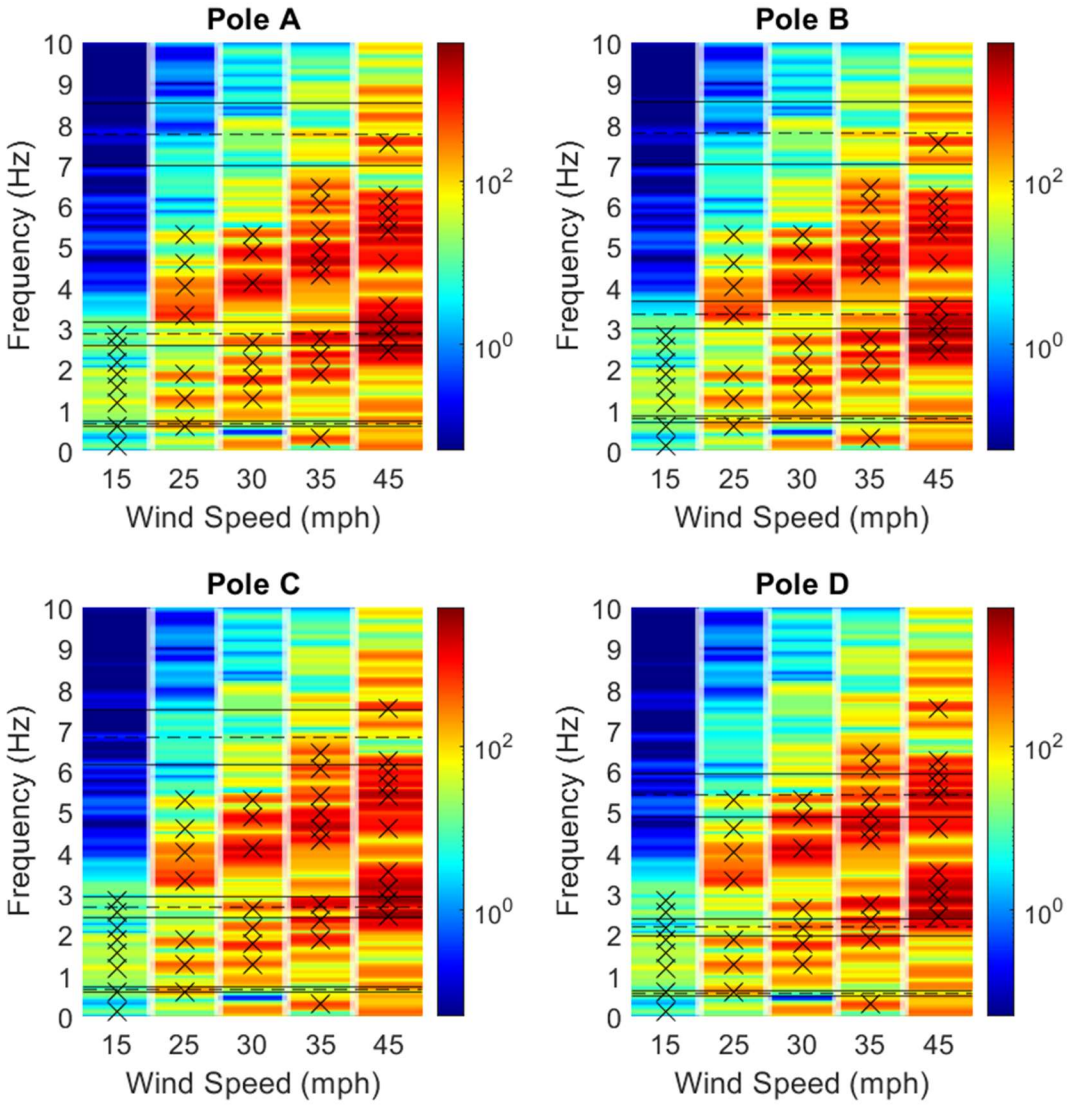

Figure 14: Color Band Comparison Chart of PSD Curves for 3 LED Fixture Configuration at 0-degree Rotation

To analyze broad patterns in the overall dataset, a series of bubble plots were created, indicating the number of times a dominant frequency in the PSD data fell within a natural frequency band for a given pole (Figure 15). The size of each bubble denotes the number of 'hits' occurred for a given assembly rotation and wind speed. Each hit count is denoted with numbers

overlaid on the bubbles. The mode 1 hits are indicated on the upper half of the bubbles with the number of hits proceeded by "M1". Modes 2 and 3 are labeled in similar fashion with mode 2 hits located in the center, and mode 3 on the lower half of the bubbles. Frequency bands were taken as 10 percent above and below the natural frequency for a given mode for each HMIP type (Table 11 through Table 14).

Hits were counted when a peak fell within the frequency range of a given mode. The ranges were applied two ways: 10 percent above and below the frequency of a given mode and 10 percent of a single mode applied across all three modes. When a 10 percent boundary was applied to each mode respectively, the result was ranges that increased in size as the mode increased. Figure 16 shows bubble plots developed with 10 percent bounds on each respective natural frequency. Applying 10 percent bounds of one of the modes across all of them resulted in a fixed size for all modes. This was done to try to address any bias in the data based on the size of a given range. The mode 1 range will naturally result in fewer hits than modes 2 and 3 due to the tighter range and vice versa. Figure 17 shows three bubble plots for the 4 incandescent fixture configuration where the range of one mode is applied to all modes. Figure 17a is the bubble plot where hits for each mode were counted with a range 10 percent above and below the first mode.

Generally, the data showed that more hits occurred with increasing wind speed. Lower wind speeds tended to result in less excitations and excitation of lower frequencies. As wind speed increased, more excitation was seen in the PSD curves which encompassed a broader range of frequencies. This led to more hits across all modes as wind speed increased. Also, the most hits were found to occur when the lighting assemblies were at a 0-degree rotation.

Between the two luminaire types, more mode 1 range hits were seen with the incandescent luminaires for the instance of using mode 2 frequency bands. This would indicate the incandescent

fixtures would be more likely to incite a mode 1 response. It is not indicative that either luminaire type would excite any HMIP type in any mode. Mode 1 excitation involves larger deformations resulting in larger stresses in the pole. Vibration gives lower deformations and stresses as the mode increases. Larger stresses can lead to fatigue cracking at fatigue prone details such as the hand hole at the base of the poles; therefore, it is beneficial to limit excitations in lower modes, specifically mode 1.

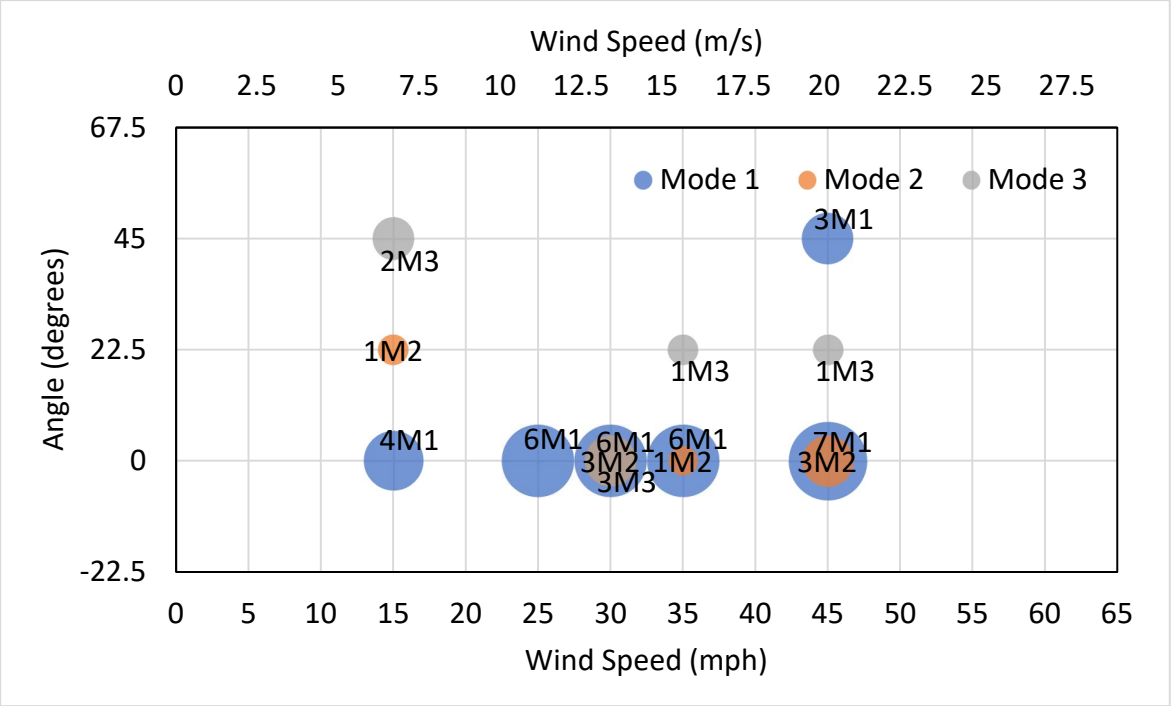

(a)

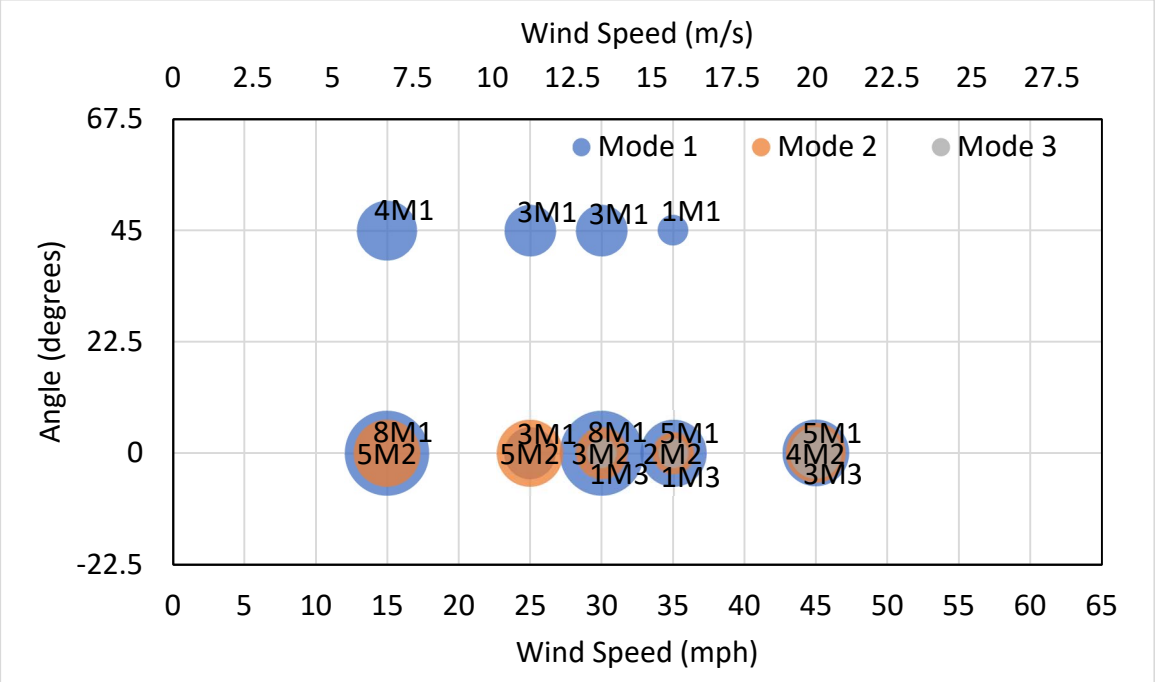
Wind Speed (m/s)
0 2.5 5 7.5 10 12.5 15 17.5 20 22.5 25 27.5
67.5
45
22.5
0
-22.5
Angle (degrees)
Mode 1
Mode 2
Mode 3
4M1
3M1 3M1 1M1
8M1
5M2
3M1 8M1 5M1
5M2 3M2 2M2
1M3 1M3
5M1
4M2
3M3
0 5 10 15 20 25 30 35 40 45 50 55 60 65
Wind Speed (mph)

(b)

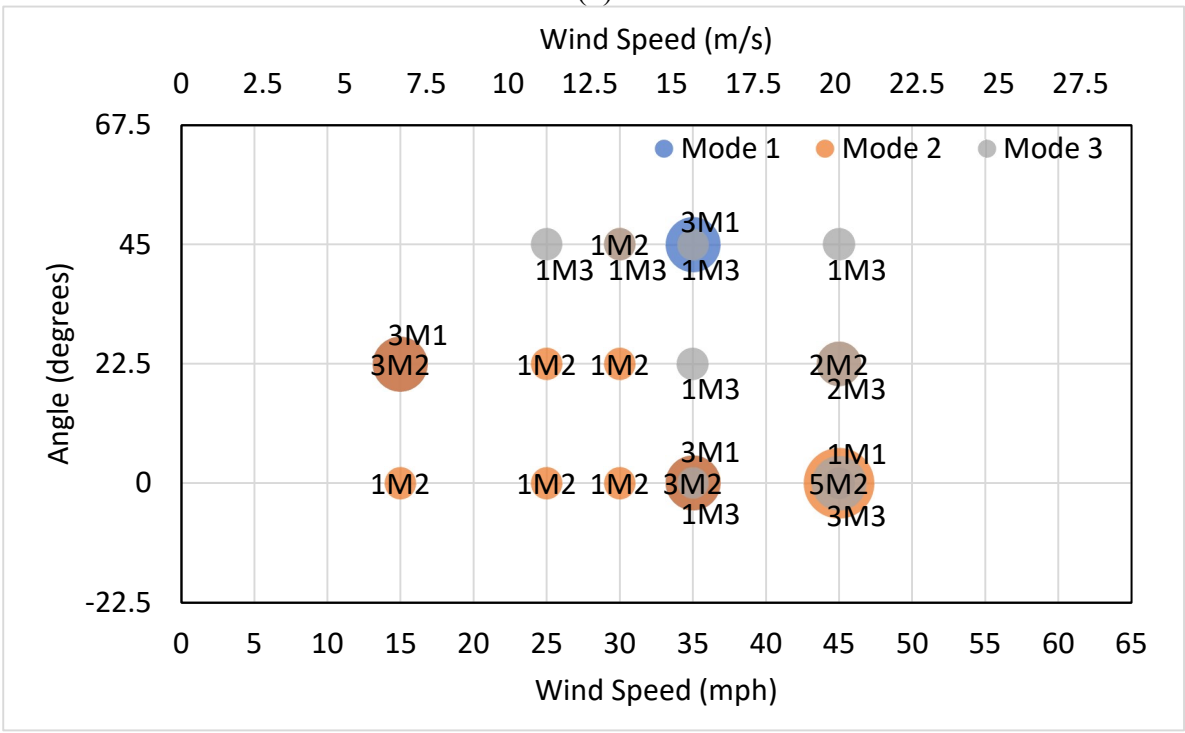
Wind Speed (m/s)
0 2.5 5 7.5 10 12.5 15 17.5 20 22.5 25 27.5
67.5
45
22.5
0
-22.5
Angle (degrees)
Mode 1
Mode 2
Mode 3
3M1
1M2
1M3 1M3 1M3
1M3
3M1
3M2
1M2 1M2
1M3
2M2
2M3
3M1
1M2
1M2 1M2 3M2
1M3
1M1
5M2
3M3
0 5 10 15 20 25 30 35 40 45 50 55 60 65
Wind Speed (mph)

(c)

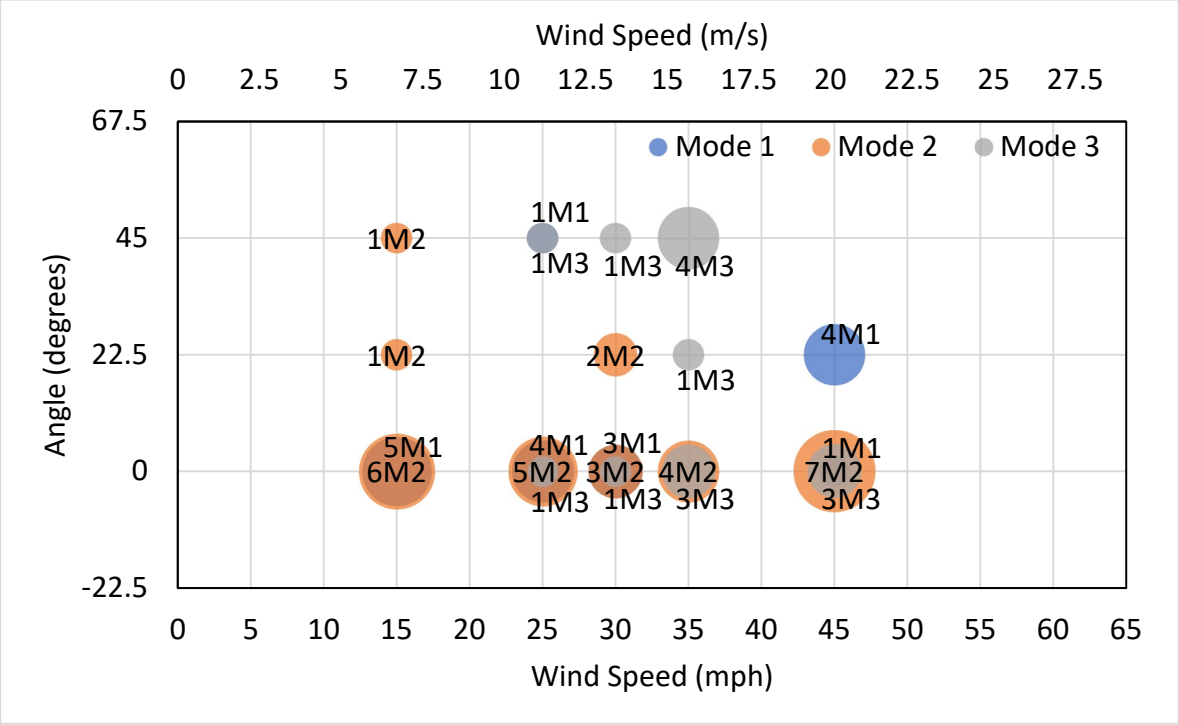

(d)

Figure 15: Peak Hit Comparison Bubble Charts: (a) 4 Incandescent (Mode 2 Fixed Range) (b) 3 Incandescent (Mode 2 Fixed Range) (c) 4 LED (Mode 2 Fixed Range) (d) 3 LED (Mode 2 Fixed Range)

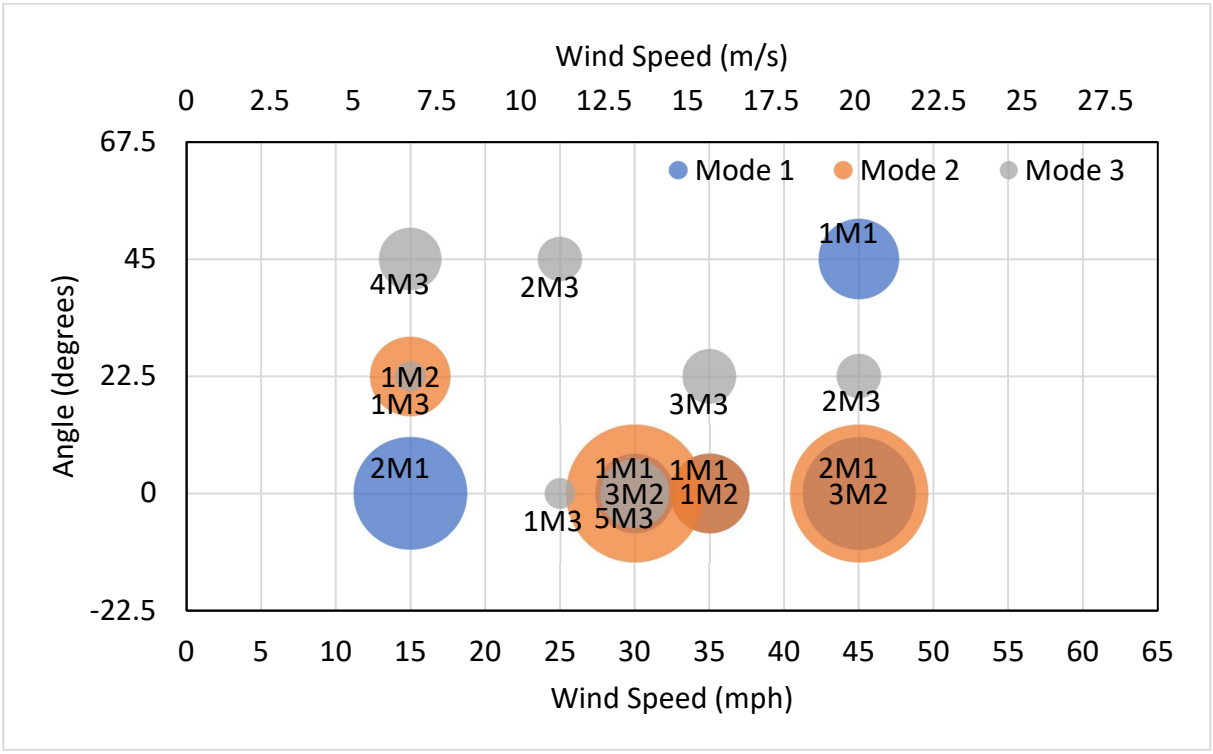
Wind Speed (m/s)
0 2.5 5 7.5 10 12.5 15 17.5 20 22.5 25 27.5
67.5
45
22.5
0
-22.5
Angle (degrees)
Mode 1
Mode 2
Mode 3
4M3
2M3
1M1
1M2
1M3
3M3
2M3
2M1
1M1
3M2
1M3
5M3
1M1
1M2
2M1
3M2
0 5 10 15 20 25 30 35 40 45 50 55 60 65
Wind Speed (mph)

(a)

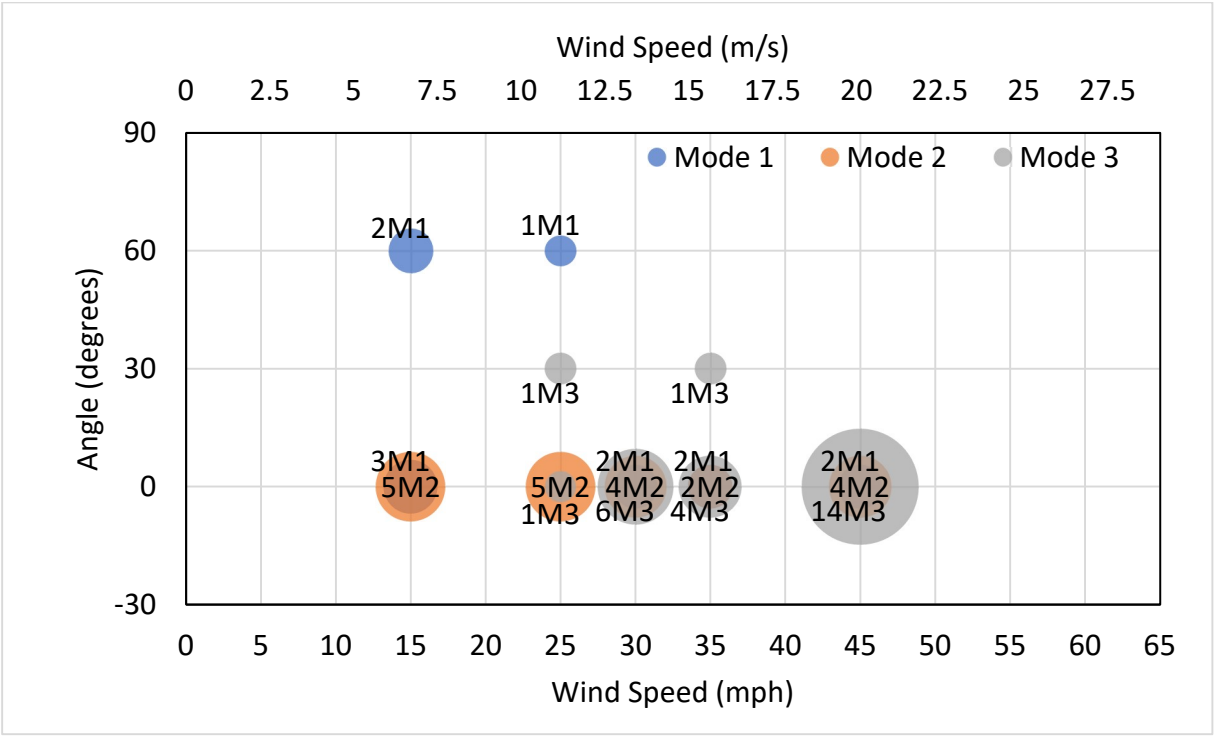
Wind Speed (m/s)
0 2.5 5 7.5 10 12.5 15 17.5 20 22.5 25 27.5
90
60
30
0
-30
Angle (degrees)
Mode 1
Mode 2
Mode 3
2M1
1M1
1M3
1M3
3M1
5M2
5M2
1M3
2M1
4M2
6M3
2M1
2M2
4M3
2M1
4M2
14M3
0 5 10 15 20 25 30 35 40 45 50 55 60 65
Wind Speed (mph)

(b)

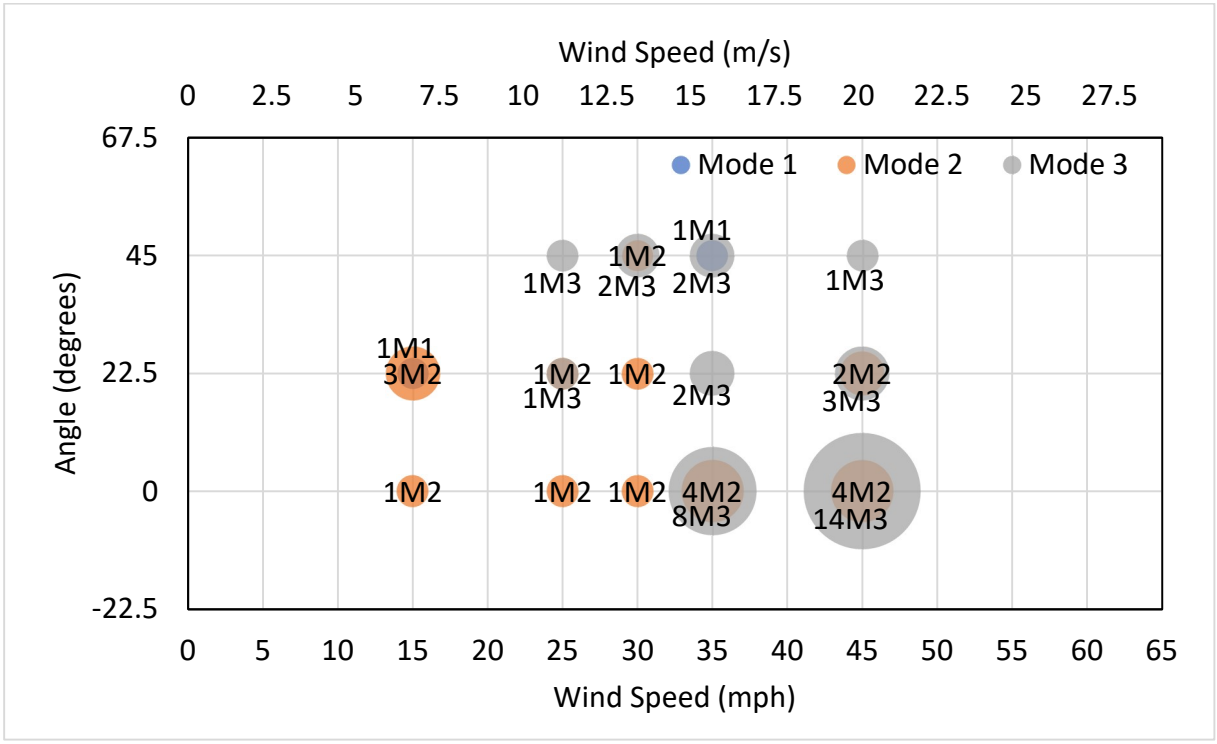

(c)

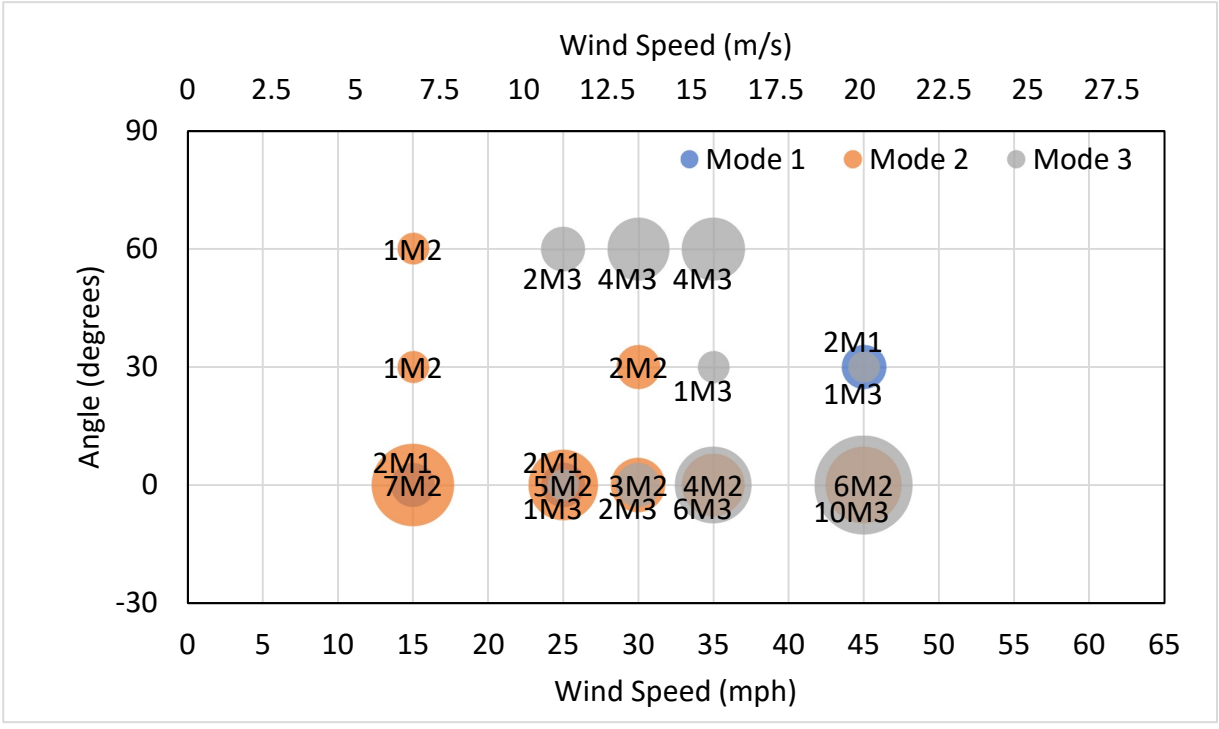

(d)

Figure 16: Peak Hit Comparison Bubble Charts using ±10% of each natural frequency: (a) 4 Incandescent (b) 3 Incandescent (c) 4 LED (d) 3 LED

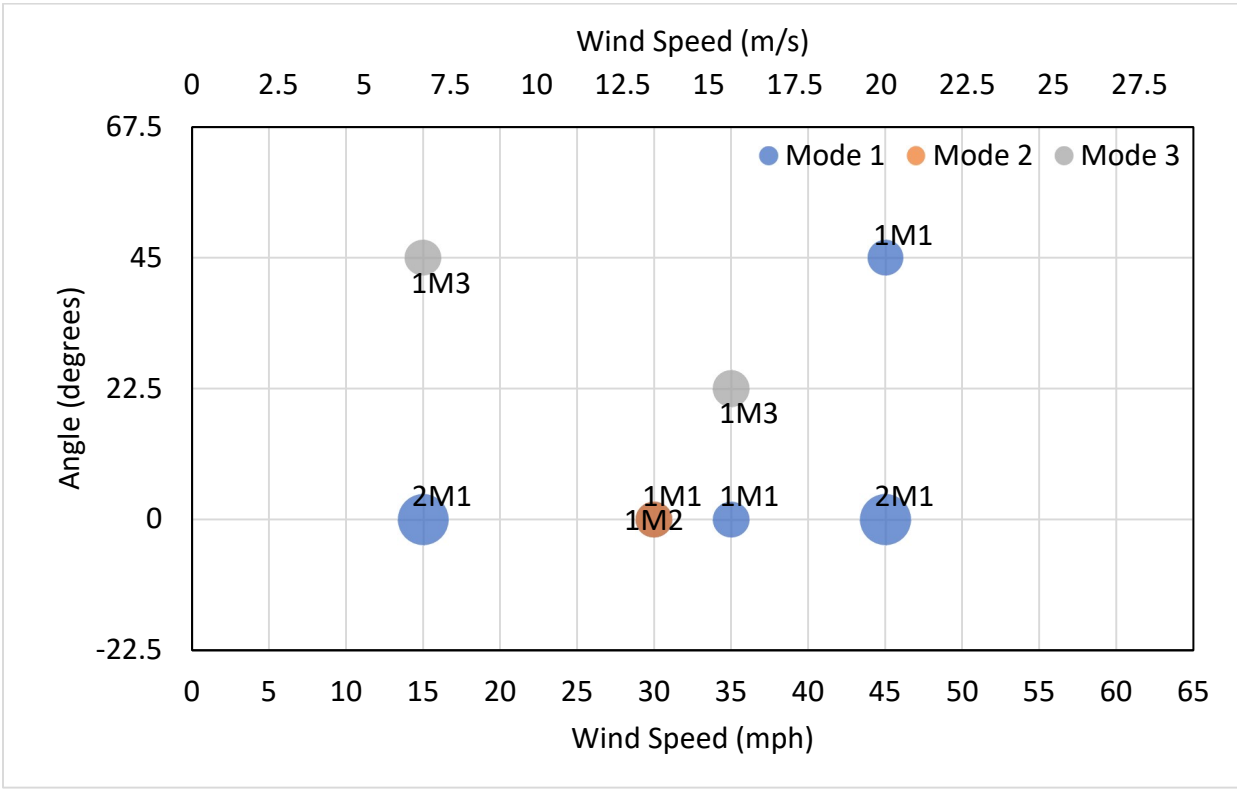
Wind Speed (m/s)
0 2.5 5 7.5 10 12.5 15 17.5 20 22.5 25 27.5
67.5
45
22.5
0
-22.5
Angle (degrees)
Mode 1
Mode 2
Mode 3
1M1
1M3
1M3
2M1
1M1
1M2
1M1
2M1
0 5 10 15 20 25 30 35 40 45 50 55 60 65
Wind Speed (mph)

(a)

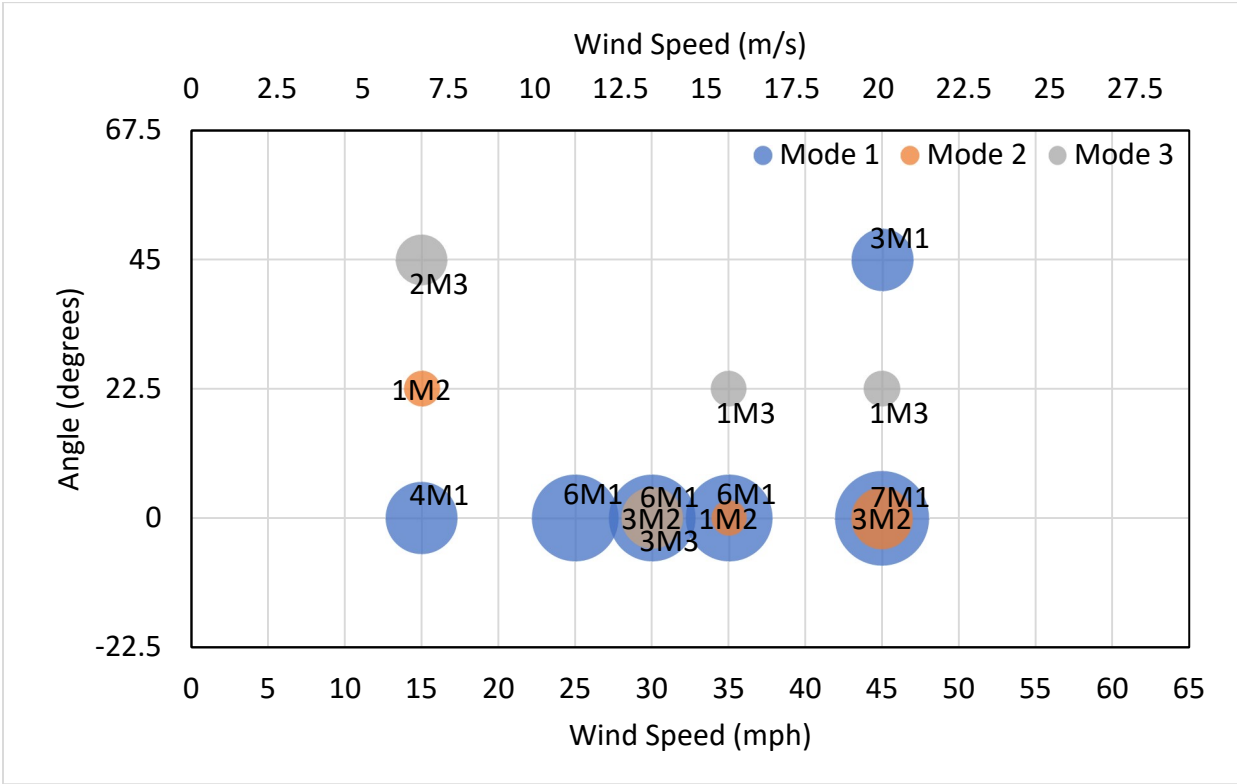
Wind Speed (m/s)
0 2.5 5 7.5 10 12.5 15 17.5 20 22.5 25 27.5
67.5
45
22.5
0
-22.5
Angle (degrees)
Mode 1
Mode 2
Mode 3
3M1
2M3
1M2
1M3
1M3
4M1
6M1
6M1
3M2
3M3
6M1
1M2
7M1
3M2
0 5 10 15 20 25 30 35 40 45 50 55 60 65
Wind Speed (mph)

(b)

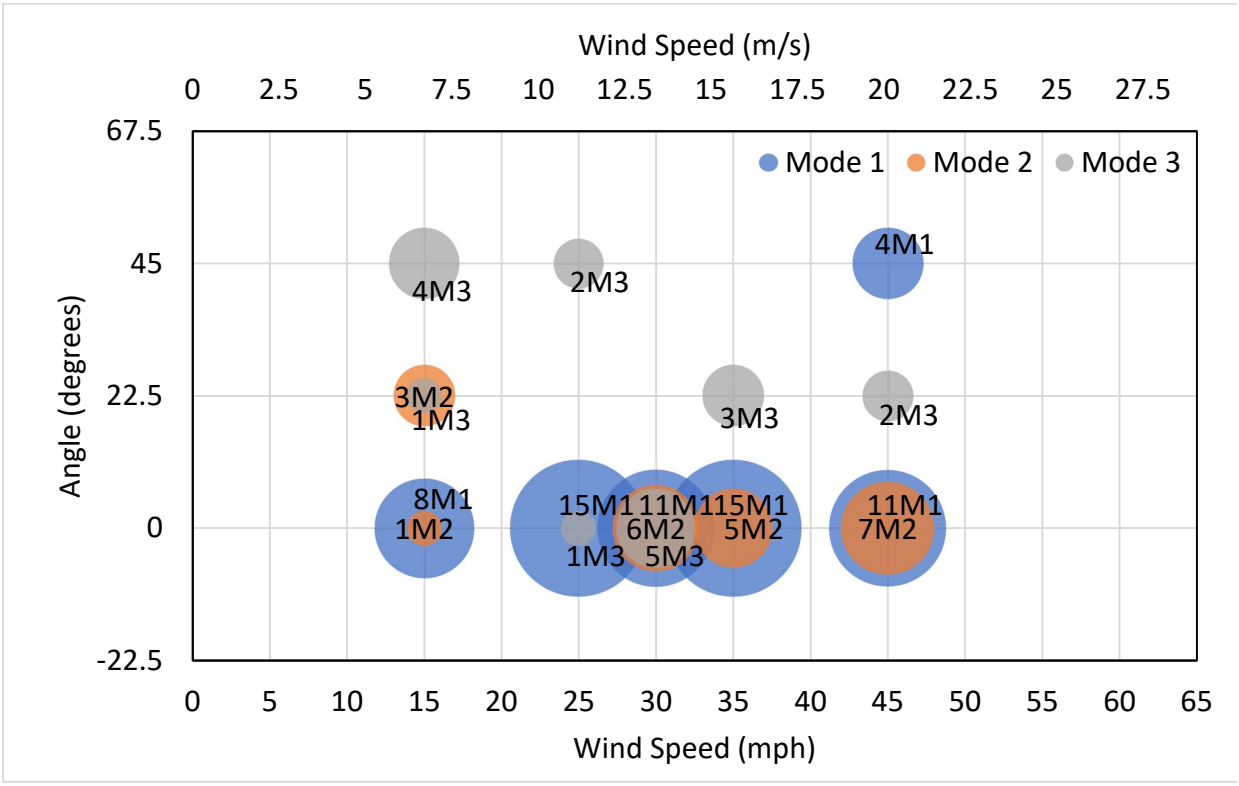

(c)

Figure 17: Peak Hit Comparison Bubble Charts for 4 Incandescent Fixture Configuration using (a) ±10% of Mode 1 (b) ±10% of Mode 2 (c) ±10% of Mode 3

CONCLUSIONS AND FUTURE WORK

5.1 Conclusions

This thesis describes a study on the susceptibility of high mast poles with various light fixture configurations to vortex shedding (lock-in behavior) under various wind speeds and directions. The study utilized a computation fluid dynamics (CFD) modeling approach, in which force time-histories were extracted to determine the frequency of the wind loading on the light fixture assemblies, and compared with the natural frequency of HMIP structures used in Kansas +/- 10%. This comparison facilitated a "hit count" for vortex shedding susceptibility for different light fixture combinations (3 LEDs, 4 LEDs, 3 Incandescents, and 4 Incandescents). The study has led to the following conclusions:

1. There was no clear indication that LED luminaires might incite a greater response than incandescent luminaires in the first mode. This finding is in contrast to a hypothesis that arose after observations of high-amplitude deformations observed in the wind event of February 2019, which appeared to largely affect structures with LED fixtures.
2. A greater number of Mode 1 hits were observed in models with incandescent luminaires than for LED luminaires when the +/-10% natural frequency bandwidth was based on the Mode 2 natural frequency. This finding indicates that incandescent fixtures are more likely to correspond with a Mode 1 response.
3. The number of hits in any frequency range generally increased with the wind speed, indicating greater potential for lock-in behavior under vortex shedding with increasing wind speed.
4. Cases in which the wind direction was straight-on (0-deg angle with the fixture) corresponded with more frequency range hits than the other wind directions for the three

and four fixture configurations. Overall, the results were found to be dependent on wind direction.

5. The results showed susceptibility of both light fixture types to vortex shedding lock-in behavior across the first three natural modes. There was no identifiable trend that selecting one luminaire type over another could decrease susceptibility to lock-in behavior.

5.2 Future Work

The following recommendations for future work are provided:

1. Models should be created and analyzed for a larger range of wind speeds, particularly higher speeds.
2. Additional common luminaire geometries should be considered and included in a suite of models.
3. Three-dimensional models of the luminaires and lowering ring assemblies should be developed to capture the influence of geometry changes along the depth.
4. Fluid-structure interaction models should be developed such that realistic influence of structural deformations of deformations in the lowering ring and pole can be considered in tandem with the fluids analysis.
5. Existing HMIP structures with different luminaire types should be instrumented to determine real responses and compared with the numerical predictions presented in this document.
6. Establish a connection between the PSD magnitude, level of force, and “hits” identified in the data to gauge the likelihood of large deformations due to vortex shedding.

7. Explore the use of vibration dampening devices on HMIPs to mitigate the effects of wind-induced vibrations from phenomenon like vortex shedding. This could be done through field testing. CFD modeling could also be utilized, more specifically for geometry altering methods.

Overall, this research has advanced the start-of-the-art surrounding the behavior of high mast illumination poles under wind loading, and specifically considered the influence of light fixture selection, orientation with respect to wind direction, and wind speed, constituting a novel and important contribution to the field. Additionally, the techniques used for analysis of the data are considered to be novel and have not been applied to this problem before to our knowledge.

Given that the research did not reveal clear differences in susceptibility to vortex shedding between the light fixtures studied, we recommend that solutions for damping high-amplitude responses in HMIP structures be developed and implemented.

REFERENCES

AASHTO. (2001). *Standard Specifications for Structural Support for Highway Signs, Luminaries, and Traffic Signals.* Washington DC: American Association of State Highway and Transportation Officials.

Ahearn, E. B., & Puckett, J. A. (2010). *Reduction of Wind-Induced Vibrations in High-Mast Light Poles.* Laramie, WY: Wyoming Department of Trasportation; Federal Highway Administration.

American Association of State Highway and Transportation Officials (AASHTO). (2013). *Standard Specifications for Structural Supports for Highway Signs, Luminaires, and Traffic Signals.* Washington DC.

Blevins, R. D. (1990). *Flow Induced Vibrations, 2nd Ed.* Van Nostrand Reinhold.

Caracoglia, L. (2007). *Analysis of Light Pole Vibration in Illinois.* Retrieved from http://cee.uiuc.edu/nsel/proj/luca.htm

Chen, G. (2003). *Signal Mast Arm Failure Investigation. Report RDT 03-010.* Missouri Deprartment of Transportation.

Dassault Systems Simulia (DSS). (2016). *Abaqus/CAE User's Guide.* Dassault Systemes Simulia Corp.

Dexter, R. J. (2004). *Investigation of Cracking of High-Mast LIghting Towers.* Iowa Department of Transportation.

Foley, C. M. (2004). *Structural Analysis of Sign Bridge Structures and Luminaire Supports. Report WHRP 04-03.* Wisconsin Department of Transportation.

Giosan, I. (2005). *Vortex Shedding Induced Loads on Free Standing Structures.* Structural Vortex Shedding Response Estimation Methodology and Finite Element Simulation.

Goode, J. S., & van de Lindt, J. (2007). Development of a Semiprescriptive Selection Procedure for Reliability-Based Fatigue Design of High-Mast Lighting Structural Supports. *Journal of Performance of Constructed Facilities*, 193-206.

Hall, N. E. (2015). *Air Propertiees Definitions*. Retrieved from Glenn Research Center, National Aeronautics and Space Administration (NASA): https://www.gre.nasa.gov/www/k-12/airplane/airprop.html

Lienhard, J. H. (1966). *Synopsis of Lift, Drag, and Vortex Frequency Data for Rigid Cicular Cylinders.* Technical Extension Service.

NASA. (2009). *Reynolds Number*. Retrieved from NASA: https://www.grc.nasa.gov/www/BGH/reynolds.html

Peavy, M. D. (2018). *An Aeroelastic Investigation of Wind Induced Vibrations of High-Mast Poles.* Universite Libre de Bruxelles; Ecole Ploytechnique de Bruxelles.

Phares, B. M., Sarkar, P. P., Wipf, T. J., & Chang, B. (2007). *Development of Fatigue Design Procedures for Slender, Tapered Support Structures for Highway Signs, Luminaries, and Traffic Signals Subjected to Wind-Induced Excitation from Vortex Shedding and Buffeting.* Center for Transportation Research and Education (CTRE).

Rice, J. A., LaFave, J. M., & Mehuys, C. H. (2008). *End Connection Effects on Vortex Shedding Susceptibility of Welded Aluminum Truss Tubular Web Members.* American Society of Civil Engineers (ASCE).

APPENDIX A1

A1.1 Time-History of Directional Forces on the Surface in the CFD Simulations

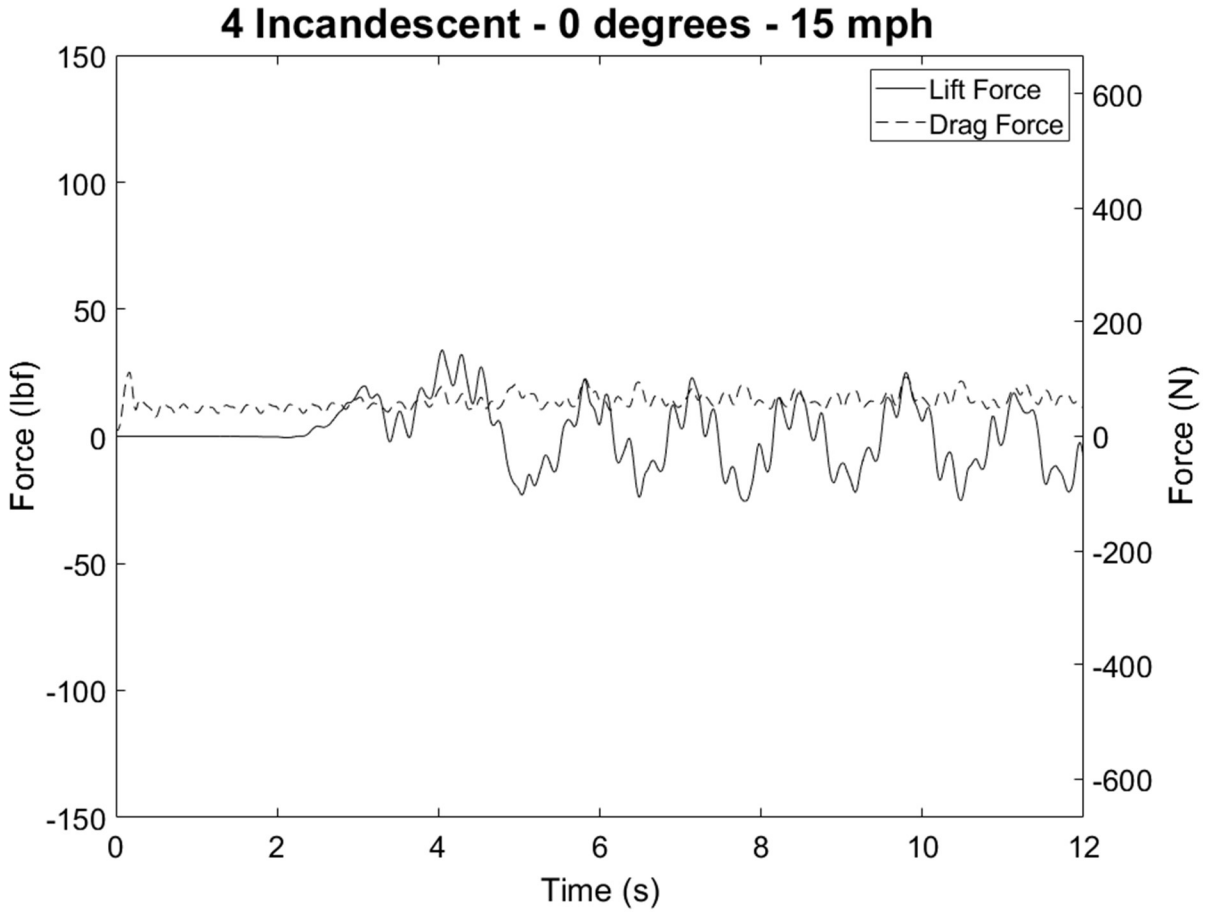

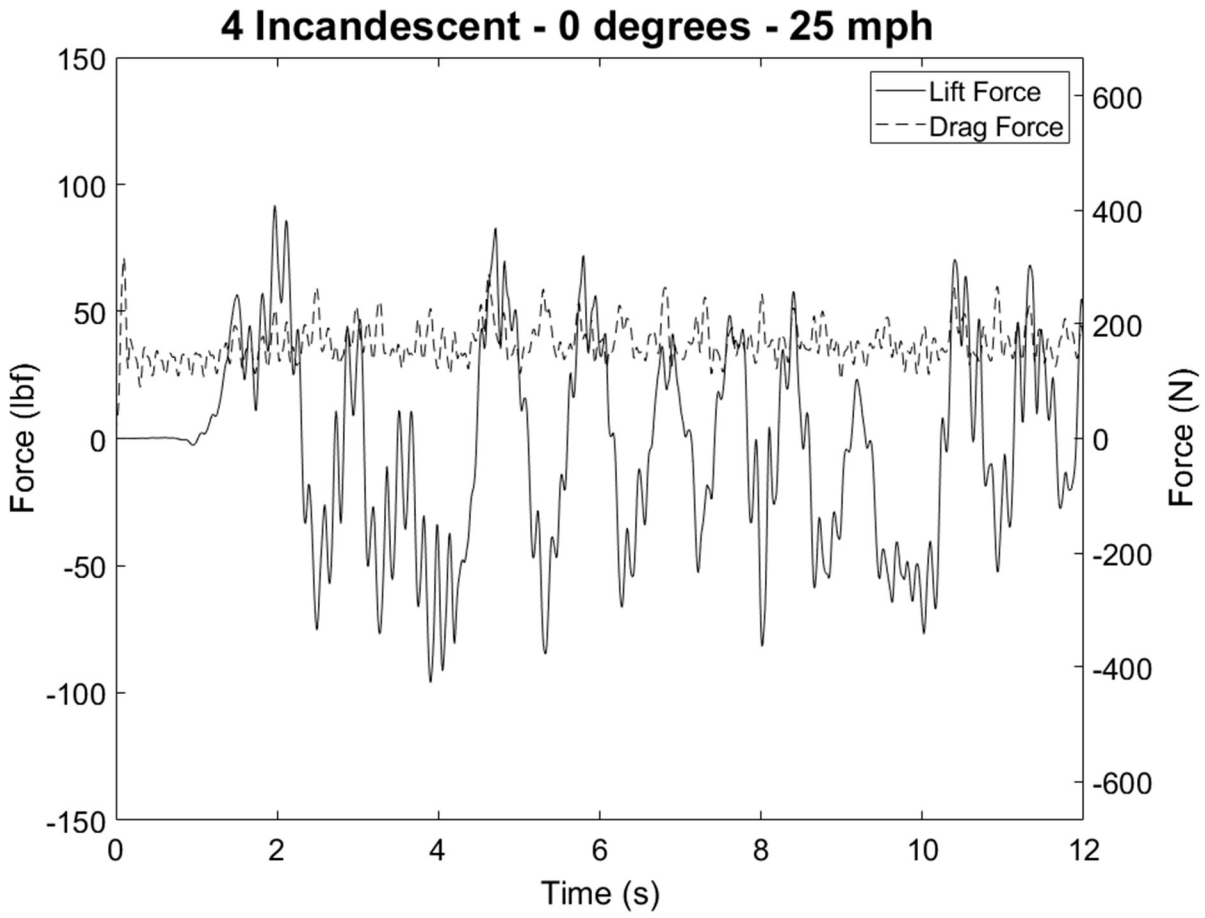
4 Incandescent - 0 degrees - 25 mph
Lift Force
Drag Force
Force (lbf)
Force (N)
Time (s)
150
100
50
0
-50
-100
-150
600
400
200
0
-200
-400
-600
0
2
4
6
8
10
12

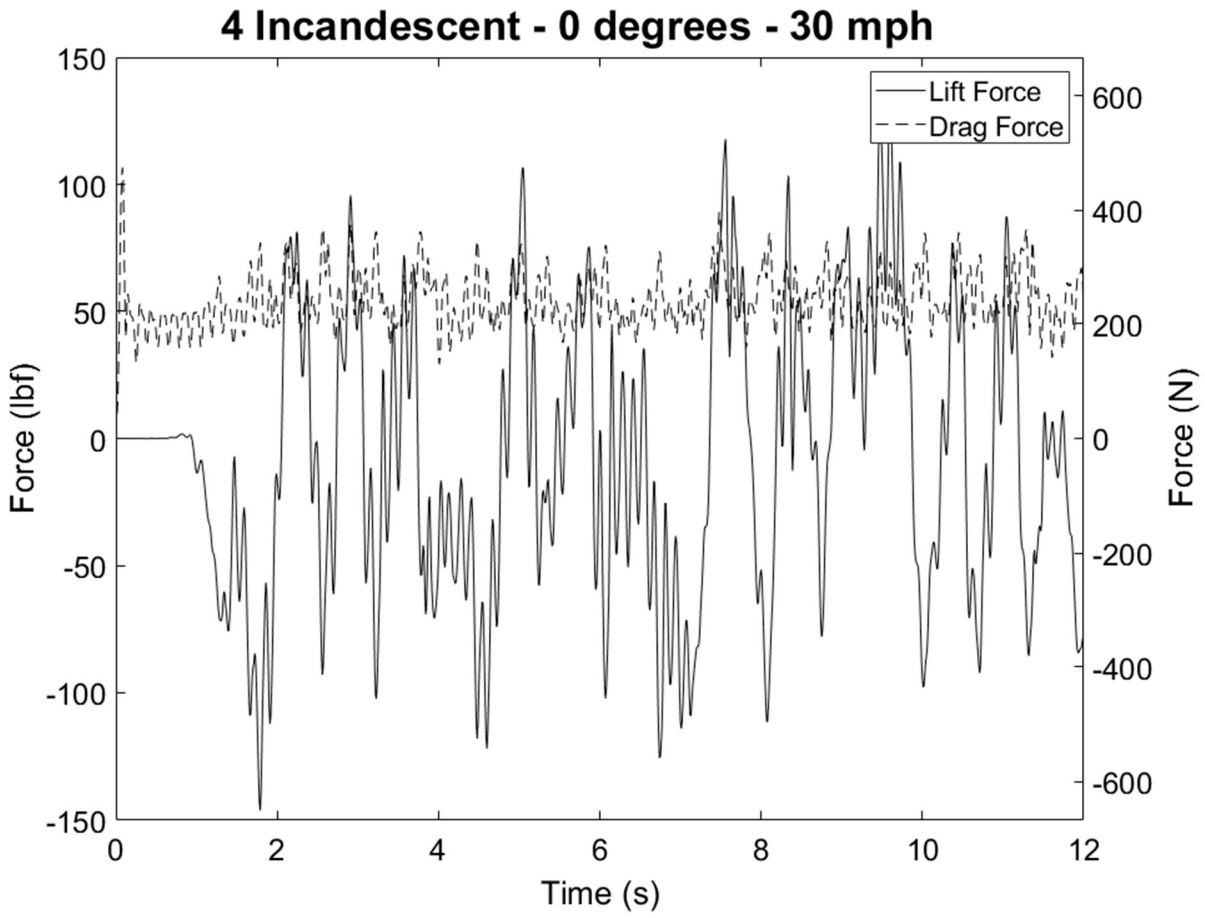
4 Incandescent - 0 degrees - 30 mph
Lift Force
Drag Force
Force (lbf)
Force (N)
Time (s)
150
100
50
0
-50
-100
-150
600
400
200
0
-200
-400
-600
0
2
4
6
8
10
12

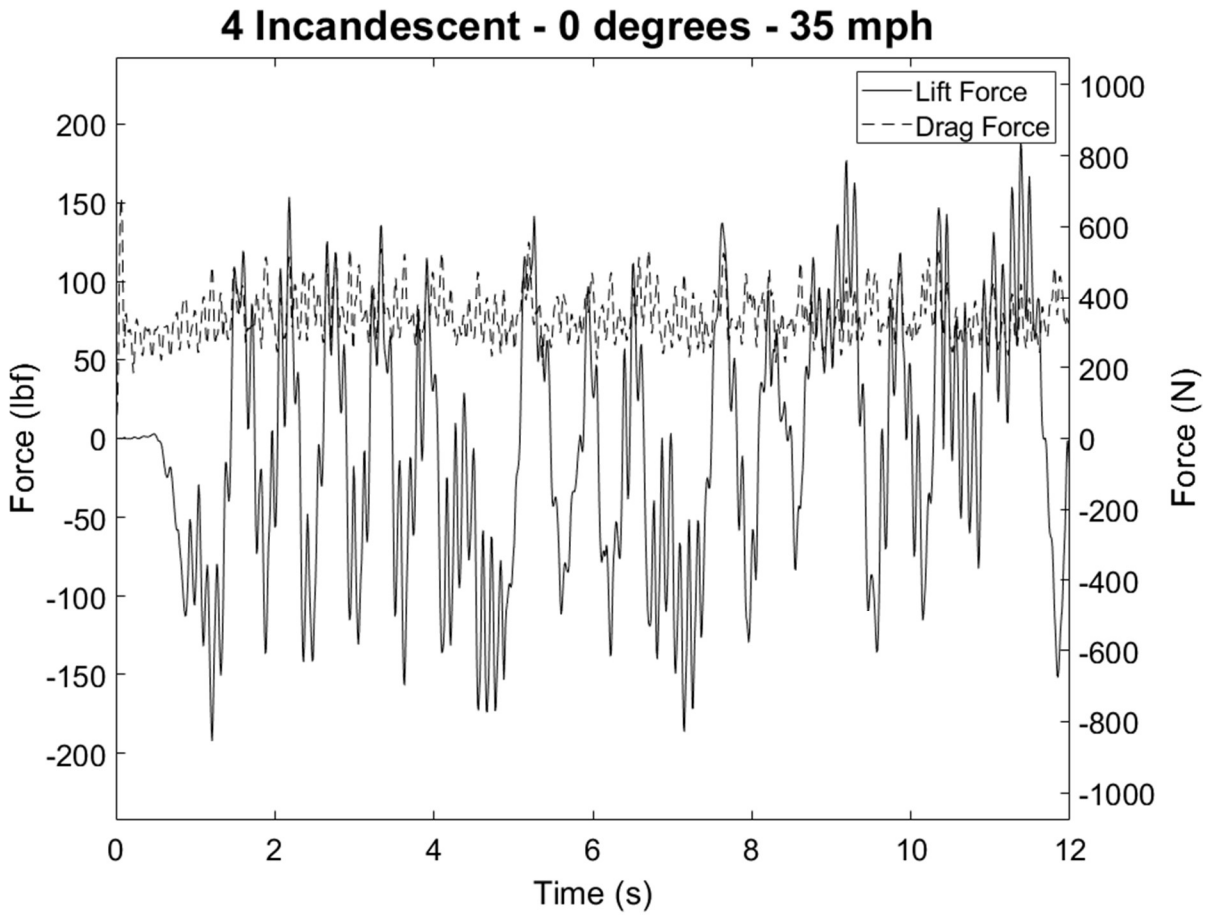
4 Incandescent - 0 degrees - 35 mph
Lift Force
Drag Force
Force (lbf)
Force (N)
Time (s)
200
150
100
50
0
-50
-100
-150
-200
1000
800
600
400
200
0
-200
-400
-600
-800
-1000
0
2
4
6
8
10
12

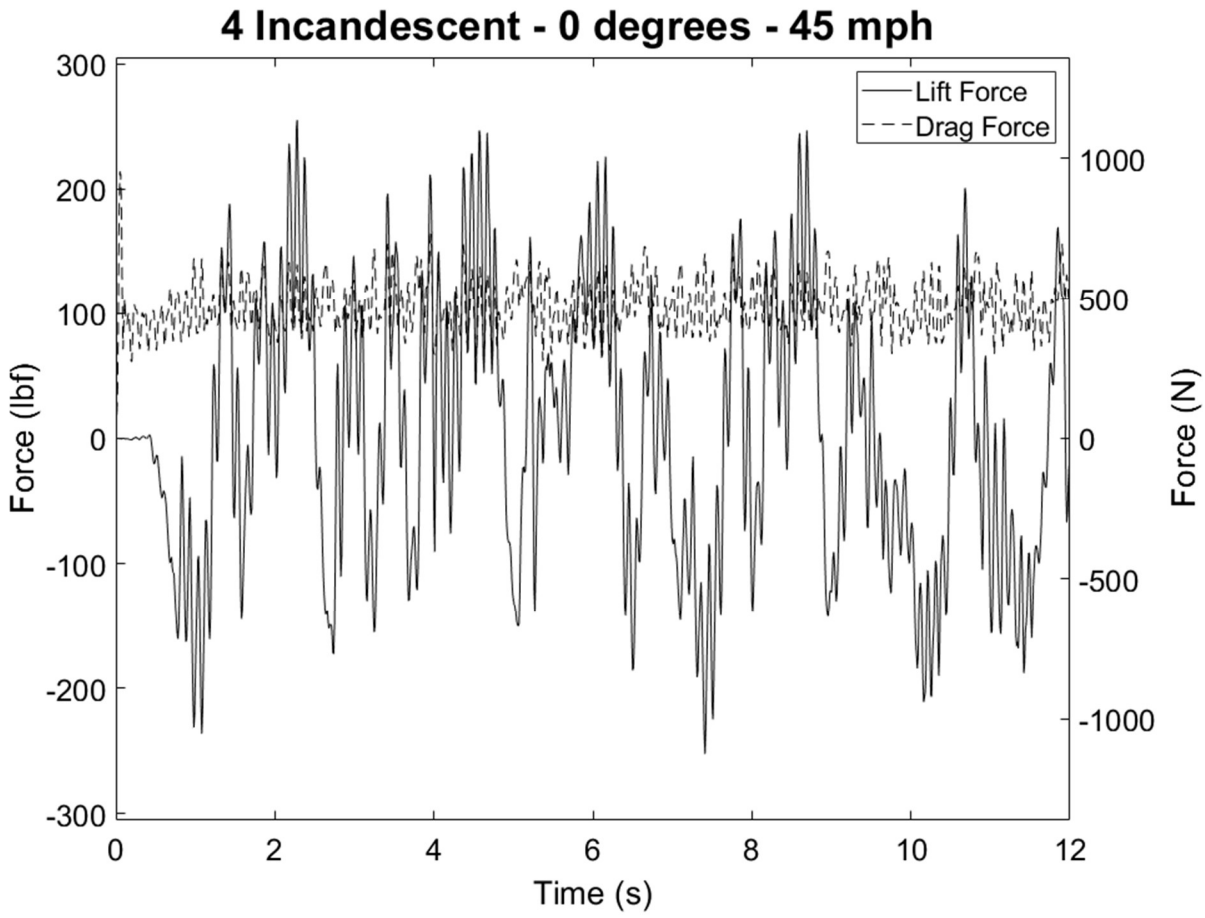
4 Incandescent - 0 degrees - 45 mph
Lift Force
Drag Force
Force (lbf)
Force (N)
Time (s)
300
200
100
0
-100
-200
-300
1000
500
0
-500
-1000
0
2
4
6
8
10
12

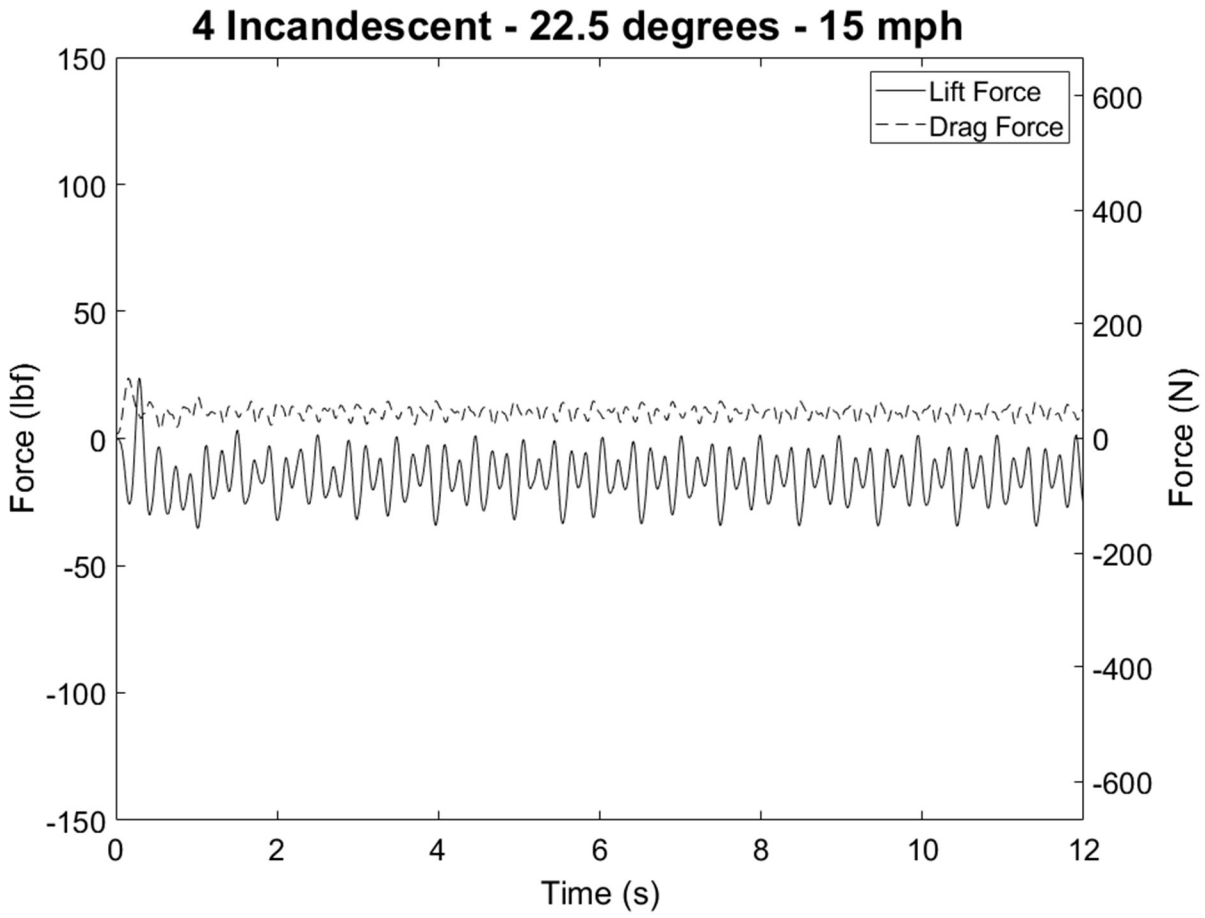
4 Incandescent - 22.5 degrees - 15 mph
Lift Force
Drag Force
Force (lbf)
Force (N)
Time (s)
150
100
50
0
-50
-100
-150
600
400
200
0
-200
-400
-600
0
2
4
6
8
10
12

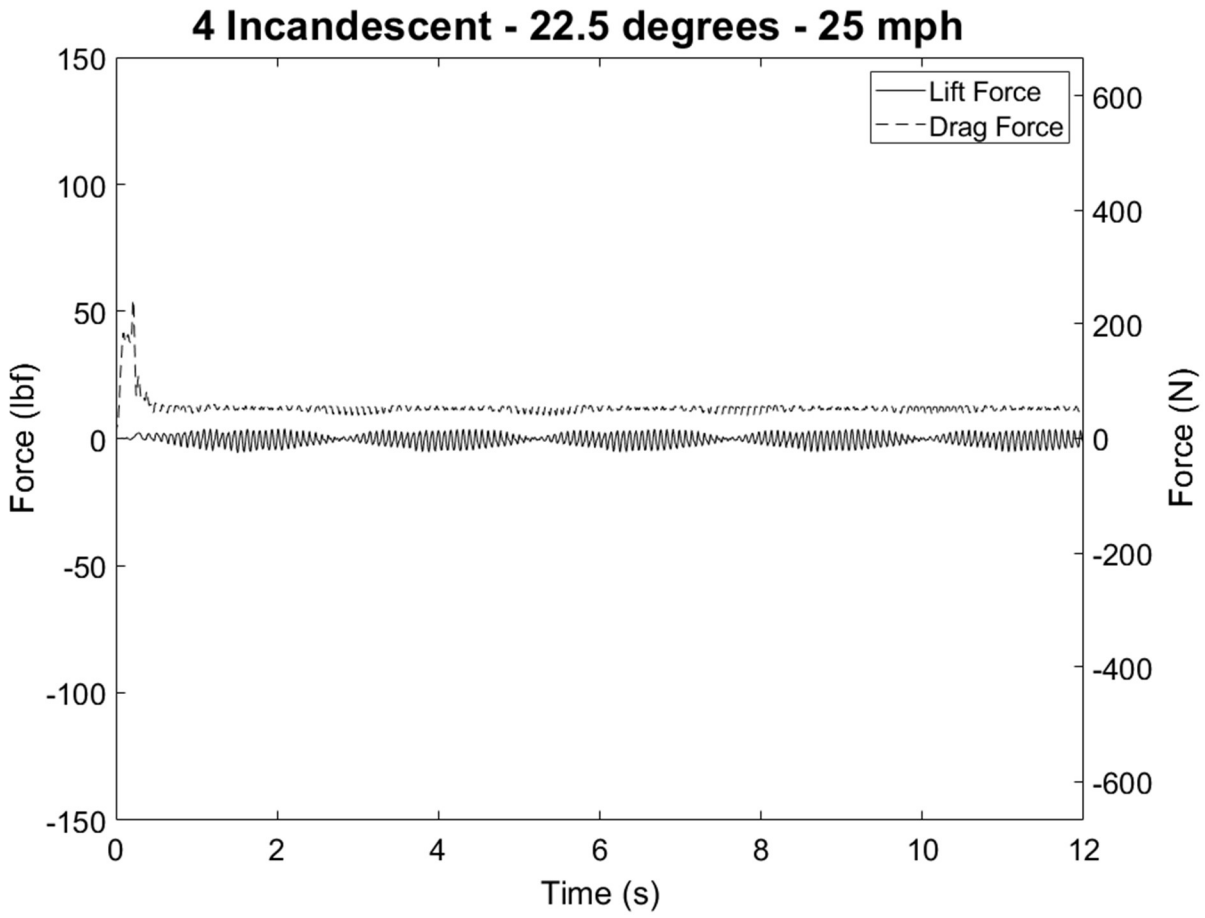
4 Incandescent - 22.5 degrees - 25 mph
Lift Force
Drag Force
Force (lbf)
Force (N)
Time (s)
150
100
50
0
-50
-100
-150
600
400
200
0
-200
-400
-600
0
2
4
6
8
10
12

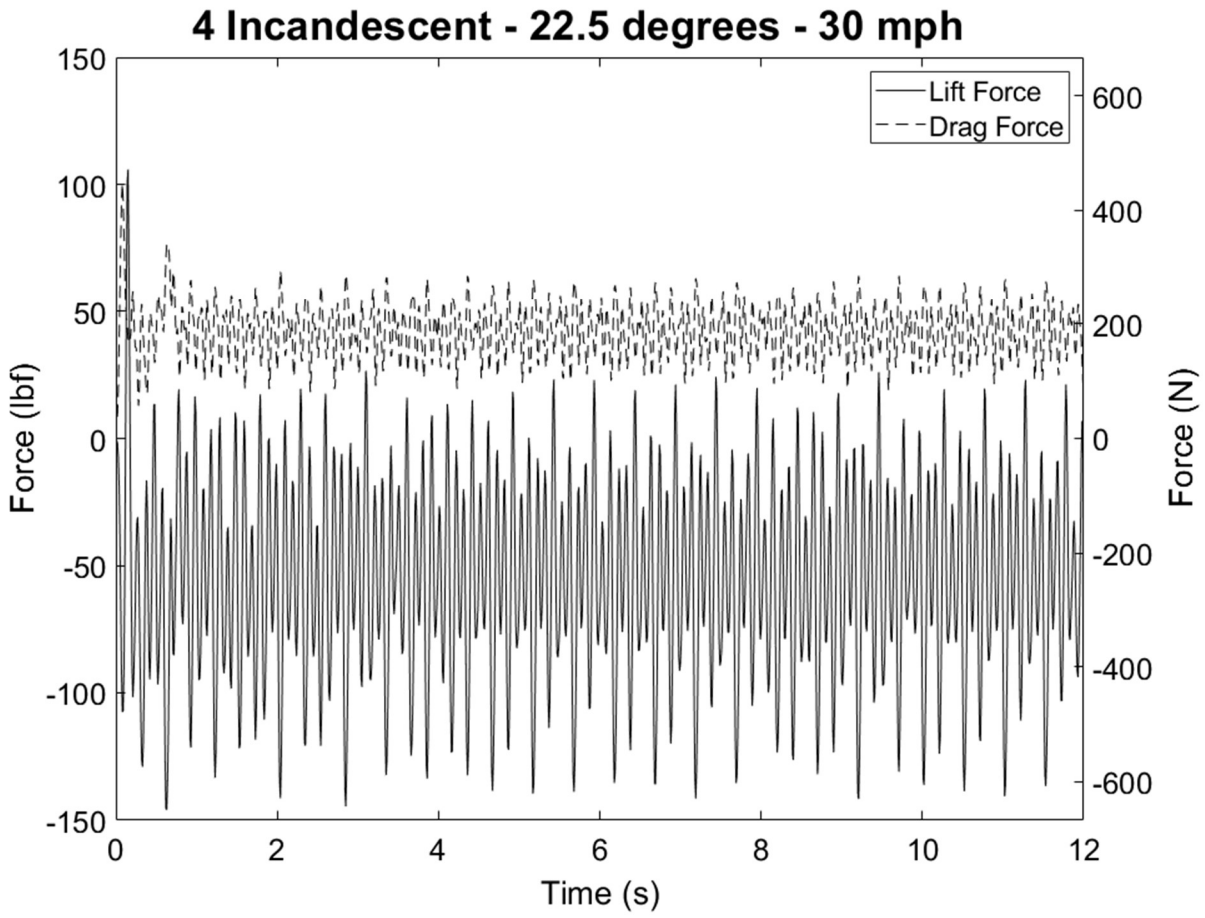
4 Incandescent - 22.5 degrees - 30 mph
Lift Force
Drag Force
Force (lbf)
Force (N)
Time (s)
150
100
50
0
-50
-100
-150
600
400
200
0
-200
-400
-600
0
2
4
6
8
10
12

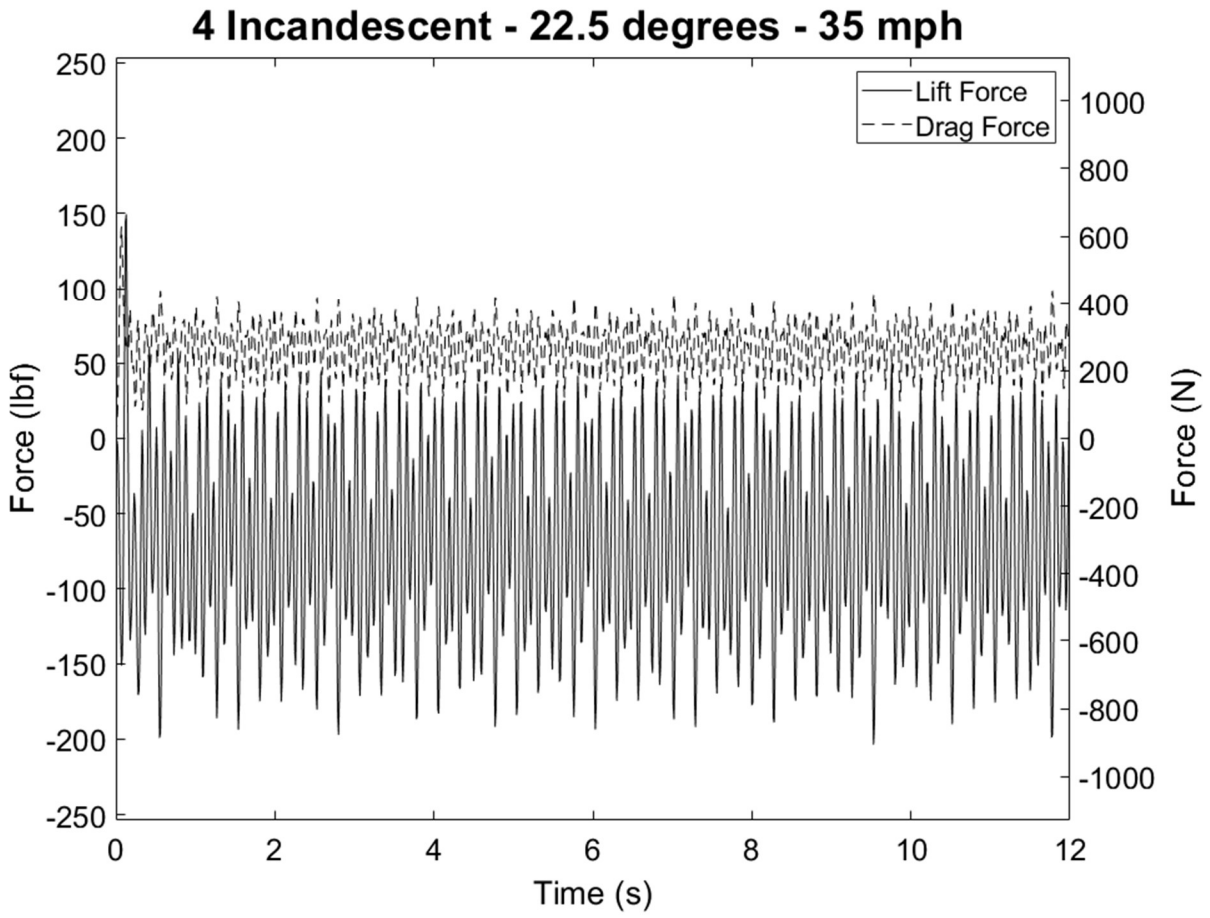
4 Incandescent - 22.5 degrees - 35 mph
Lift Force
Drag Force
Force (lbf)
Force (N)
Time (s)
250
200
150
100
50
0
-50
-100
-150
-200
-250
1000
800
600
400
200
0
-200
-400
-600
-800
-1000
0
2
4
6
8
10
12

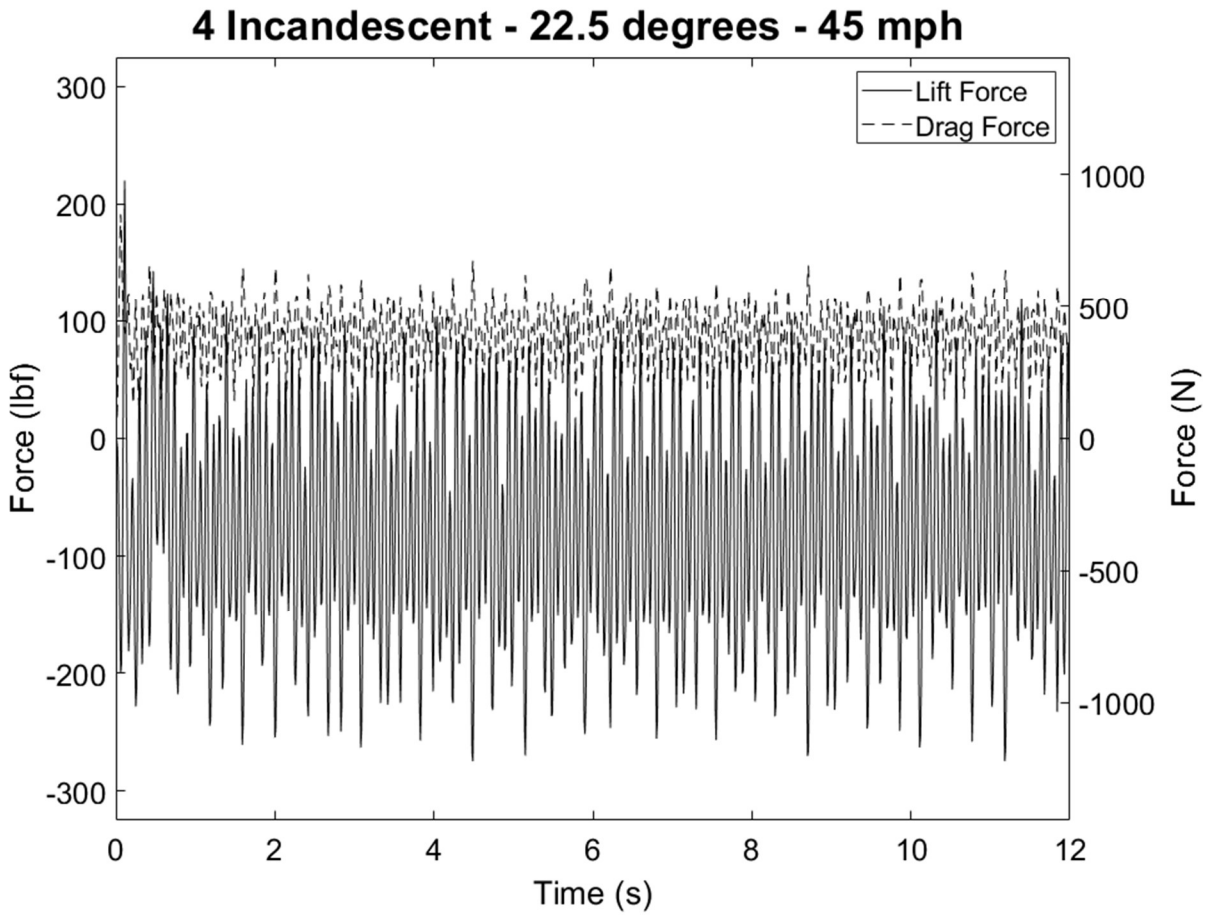
4 Incandescent - 22.5 degrees - 45 mph
Lift Force
Drag Force
Force (lbf)
Force (N)
Time (s)
300
200
100
0
-100
-200
-300
1000
500
0
-500
-1000
0
2
4
6
8
10
12

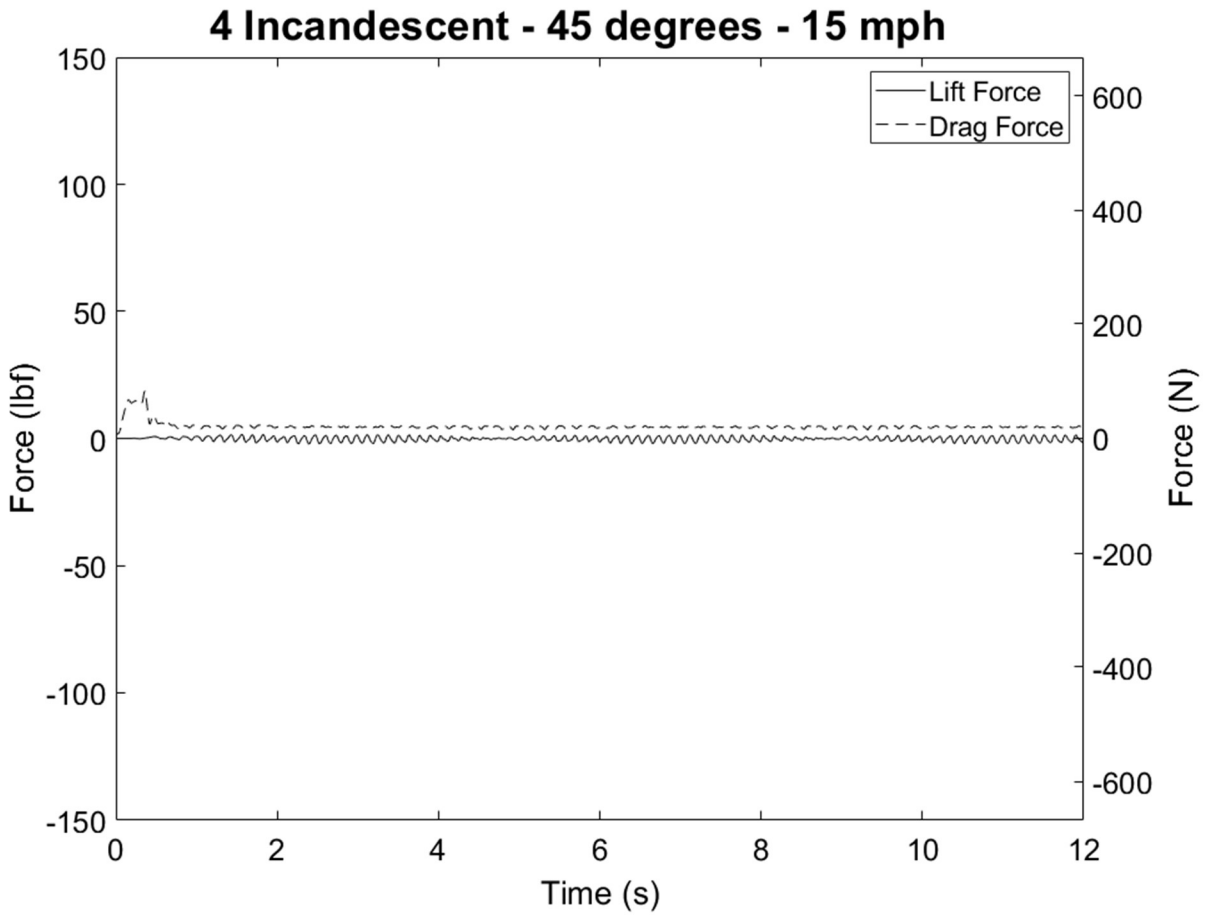
4 Incandescent - 45 degrees - 15 mph
Lift Force
Drag Force
Force (lbf)
Force (N)
Time (s)
150
100
50
0
-50
-100
-150
600
400
200
0
-200
-400
-600
0
2
4
6
8
10
12

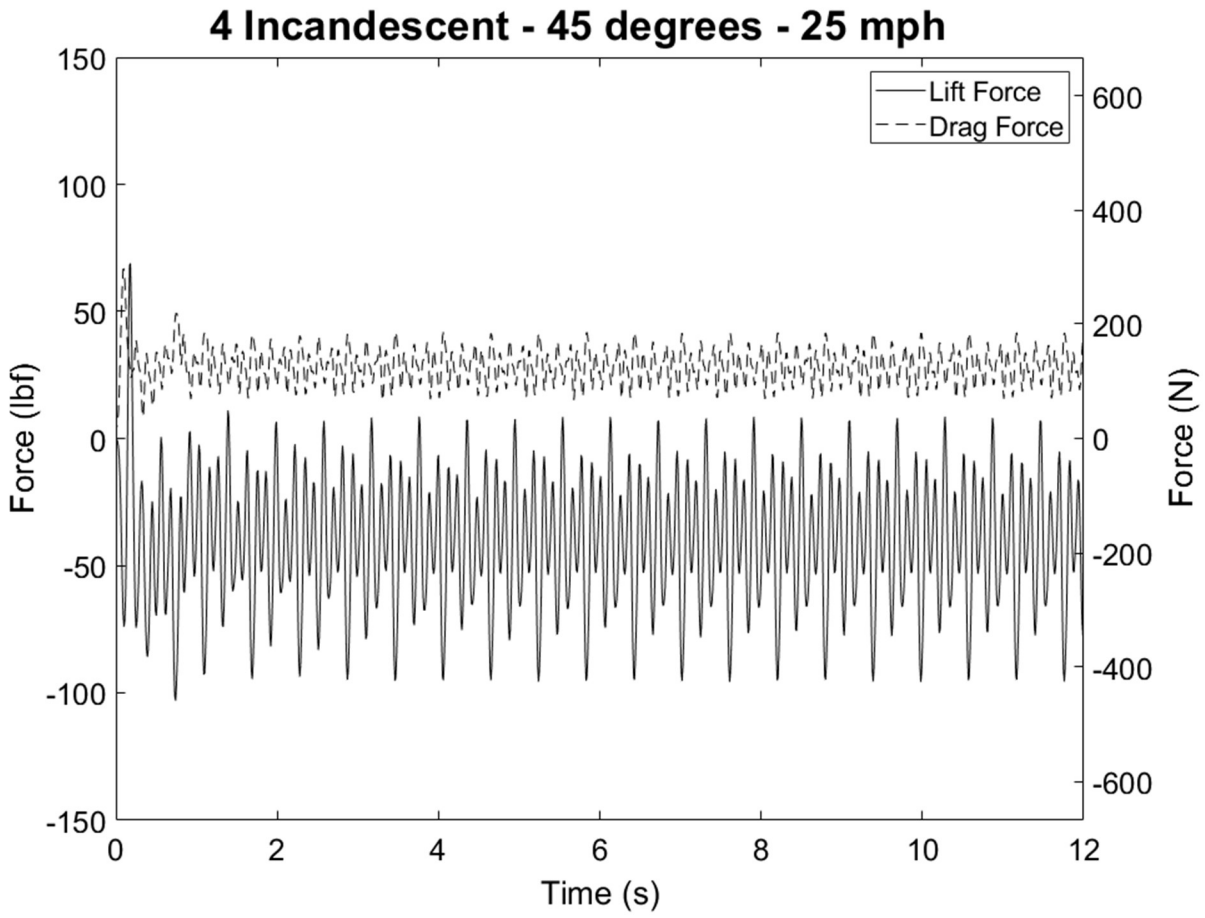
4 Incandescent - 45 degrees - 25 mph
Lift Force
Drag Force
Force (lbf)
Force (N)
Time (s)
150
100
50
0
-50
-100
-150
600
400
200
0
-200
-400
-600
0
2
4
6
8
10
12

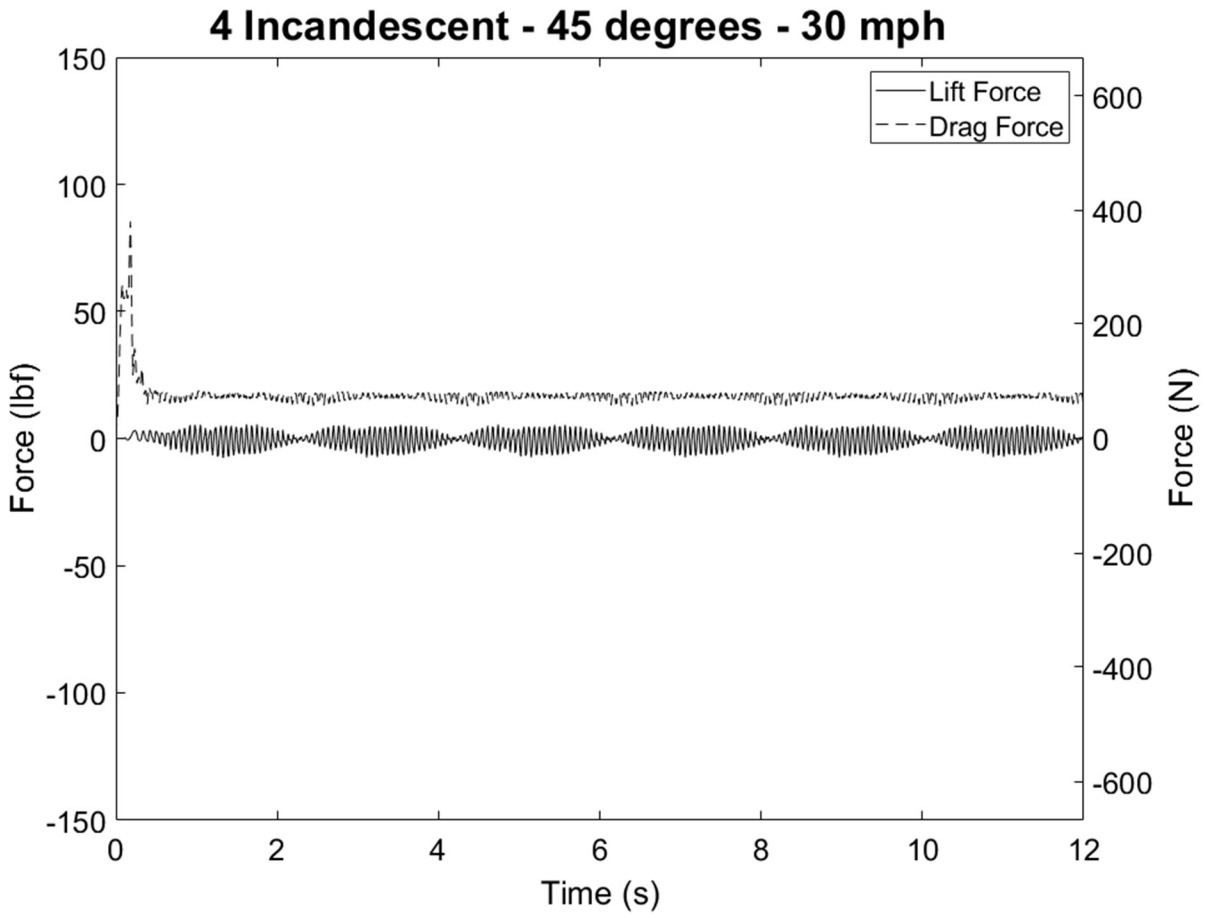
4 Incandescent - 45 degrees - 30 mph
Lift Force
Drag Force
Force (lbf)
Force (N)
Time (s)
150
100
50
0
-50
-100
-150
600
400
200
0
-200
-400
-600
0
2
4
6
8
10
12

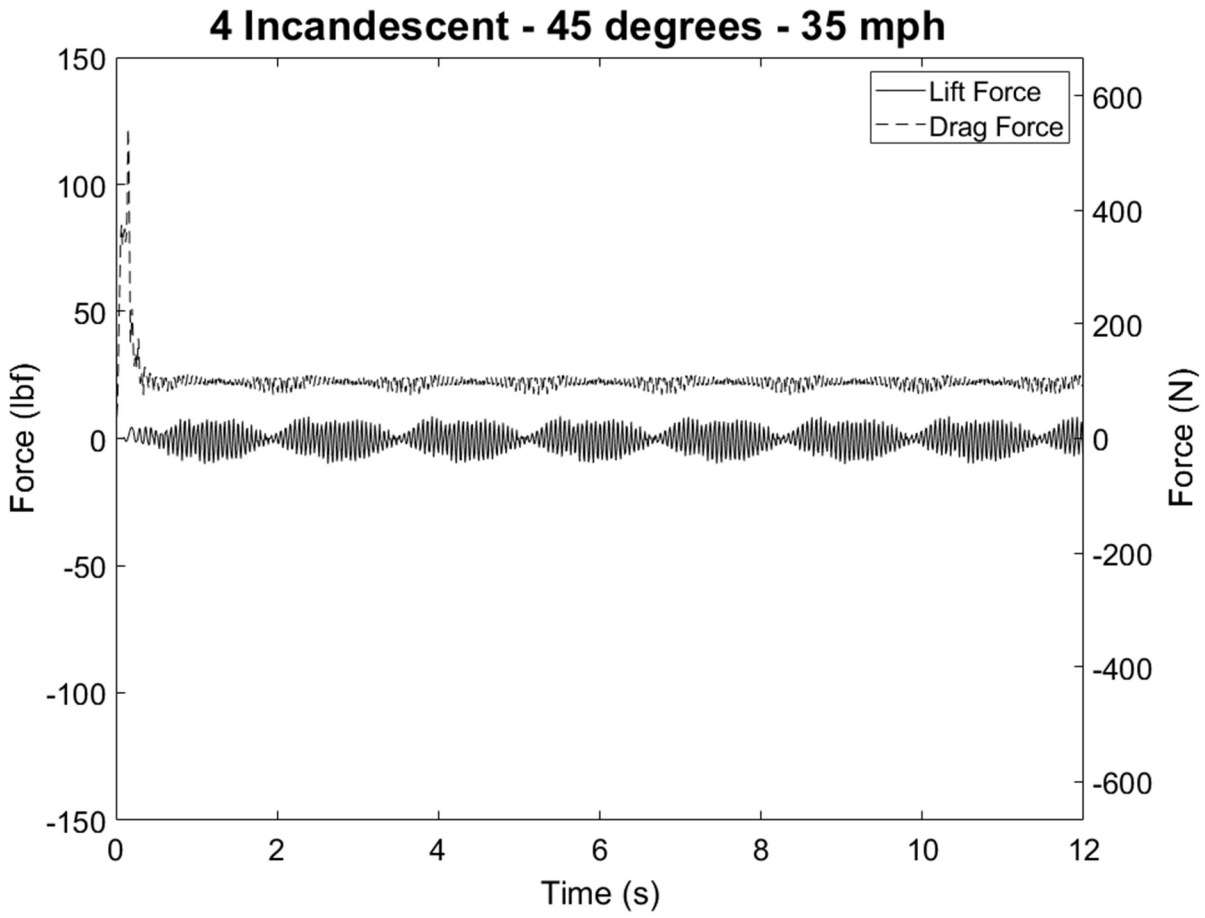
4 Incandescent - 45 degrees - 35 mph
Lift Force
Drag Force
Force (lbf)
Force (N)
Time (s)
150
100
50
0
-50
-100
-150
600
400
200
0
-200
-400
-600
0
2
4
6
8
10
12

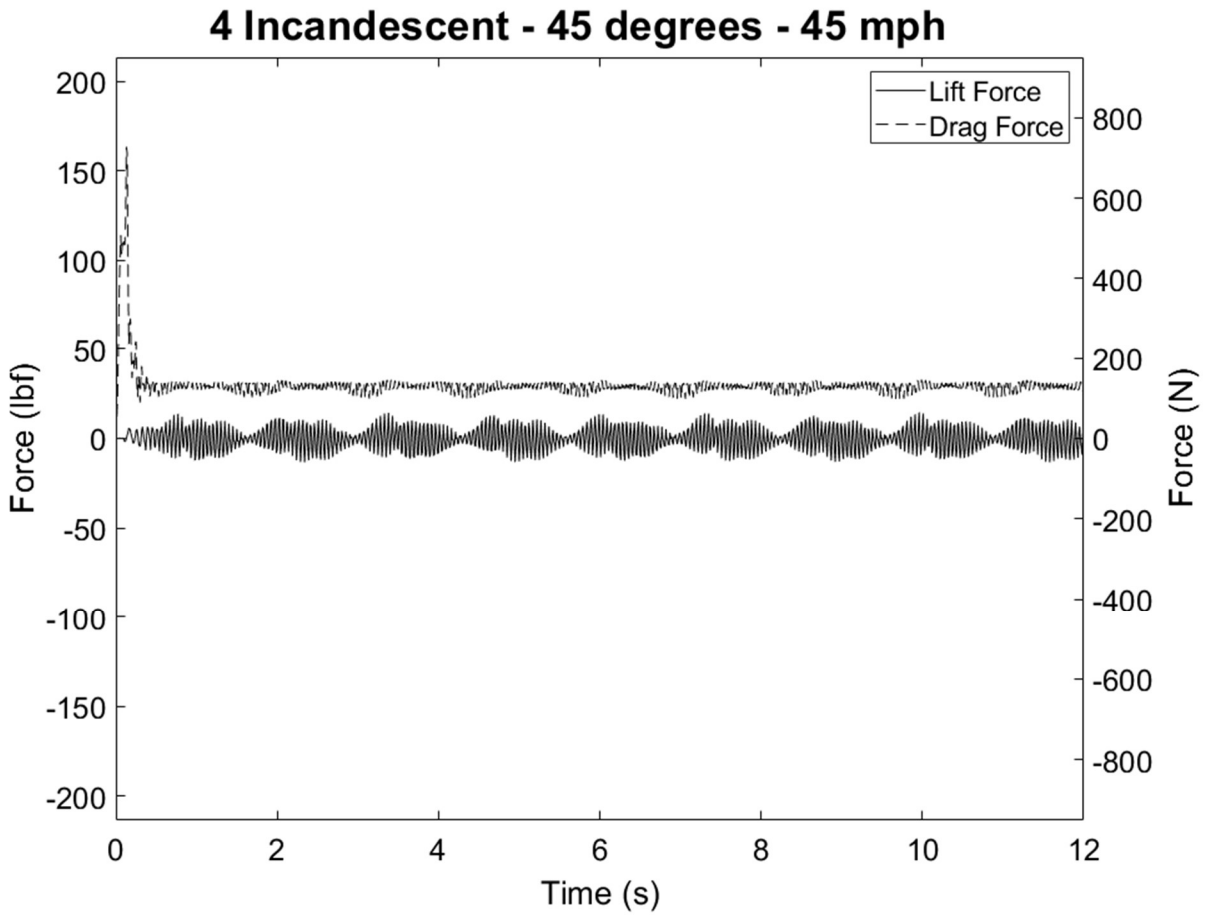
4 Incandescent - 45 degrees - 45 mph
Lift Force
Drag Force
Force (lbf)
Force (N)
Time (s)
200
150
100
50
0
-50
-100
-150
-200
800
600
400
200
0
-200
-400
-600
-800
0
2
4
6
8
10
12

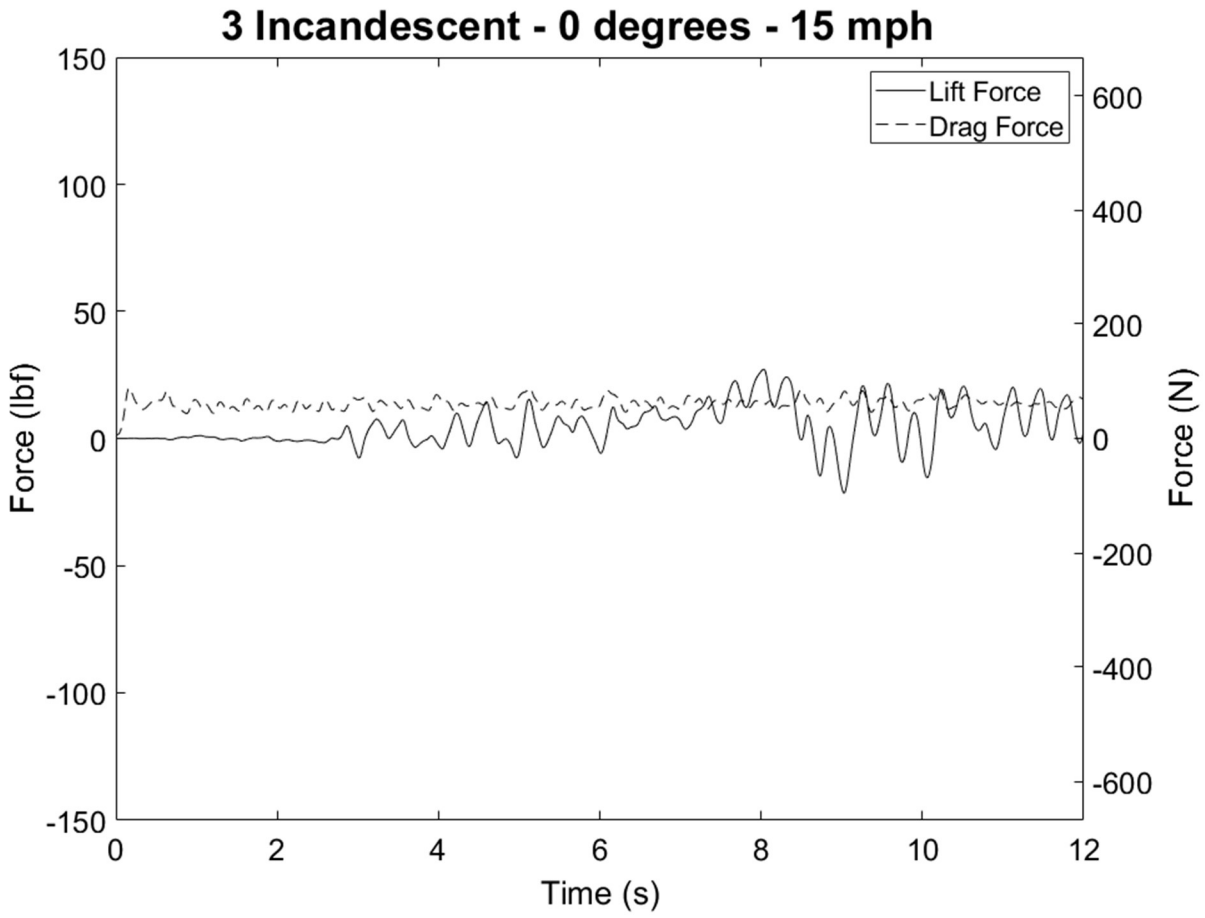
3 Incandescent - 0 degrees - 15 mph
Lift Force
Drag Force
Force (lbf)
Force (N)
Time (s)
150
100
50
0
-50
-100
-150
600
400
200
0
-200
-400
-600
0
2
4
6
8
10
12

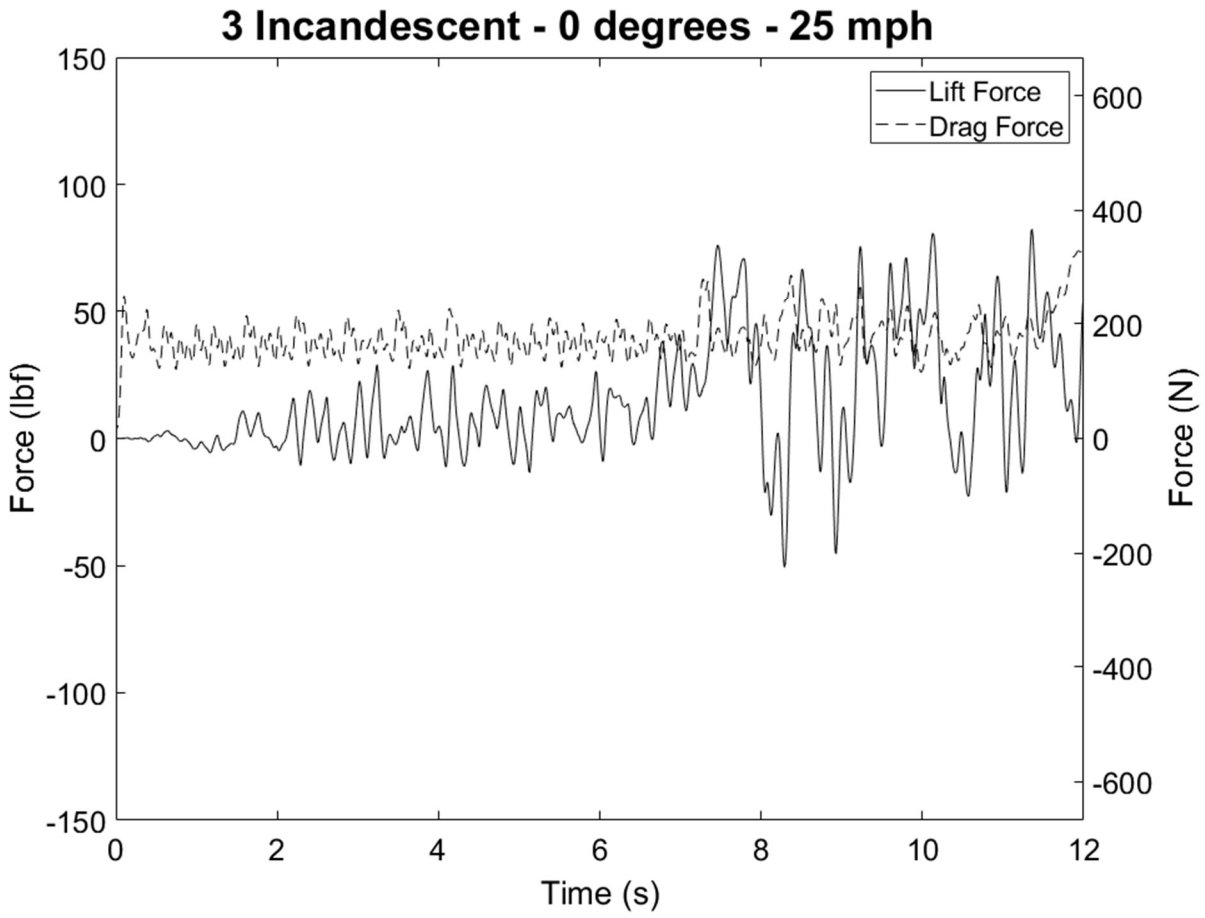
3 Incandescent - 0 degrees - 25 mph
Lift Force
Drag Force
Force (lbf)
Force (N)
Time (s)
150
100
50
0
-50
-100
-150
600
400
200
0
-200
-400
-600
0
2
4
6
8
10
12

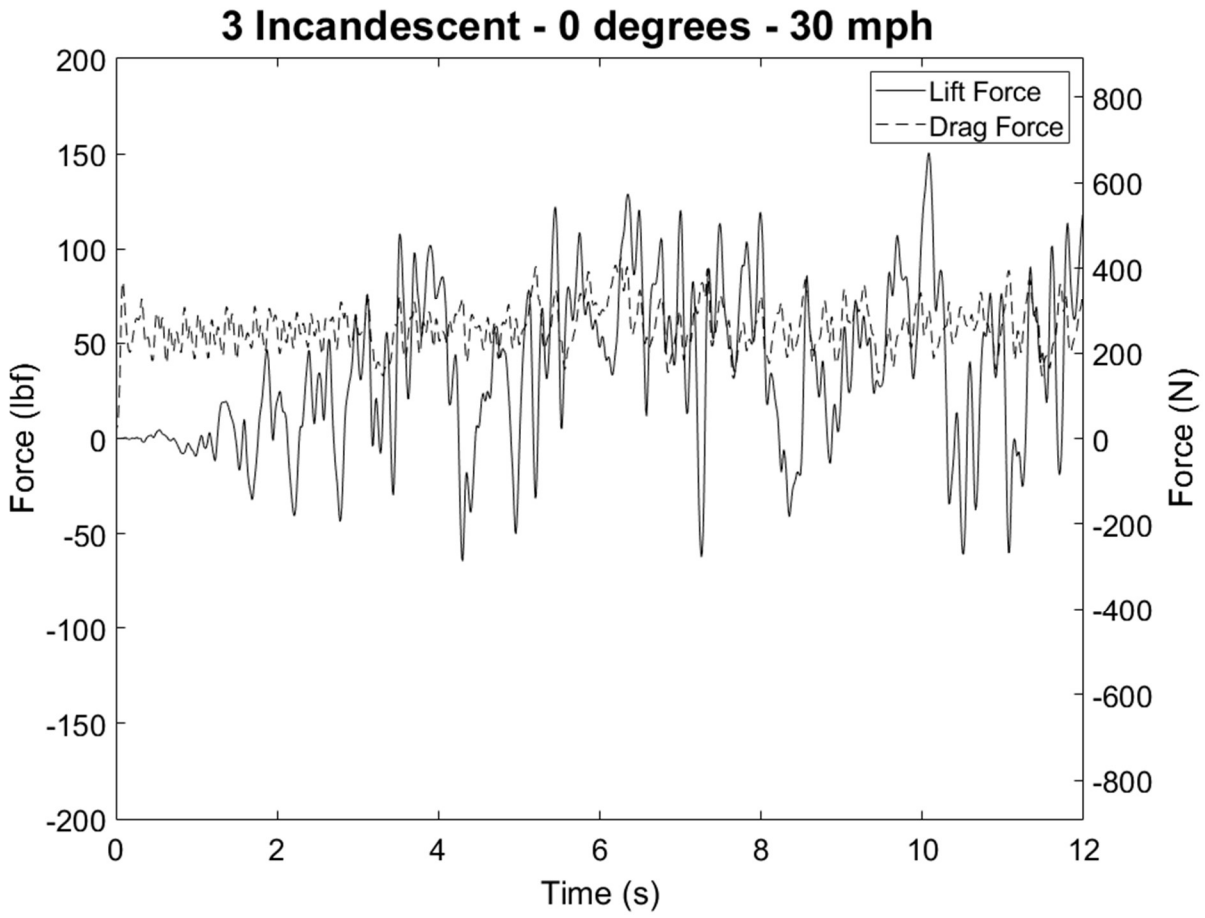
3 Incandescent - 0 degrees - 30 mph
Lift Force
Drag Force
Force (lbf)
Force (N)
Time (s)
200
150
100
50
0
-50
-100
-150
-200
800
600
400
200
0
-200
-400
-600
-800
0
2
4
6
8
10
12

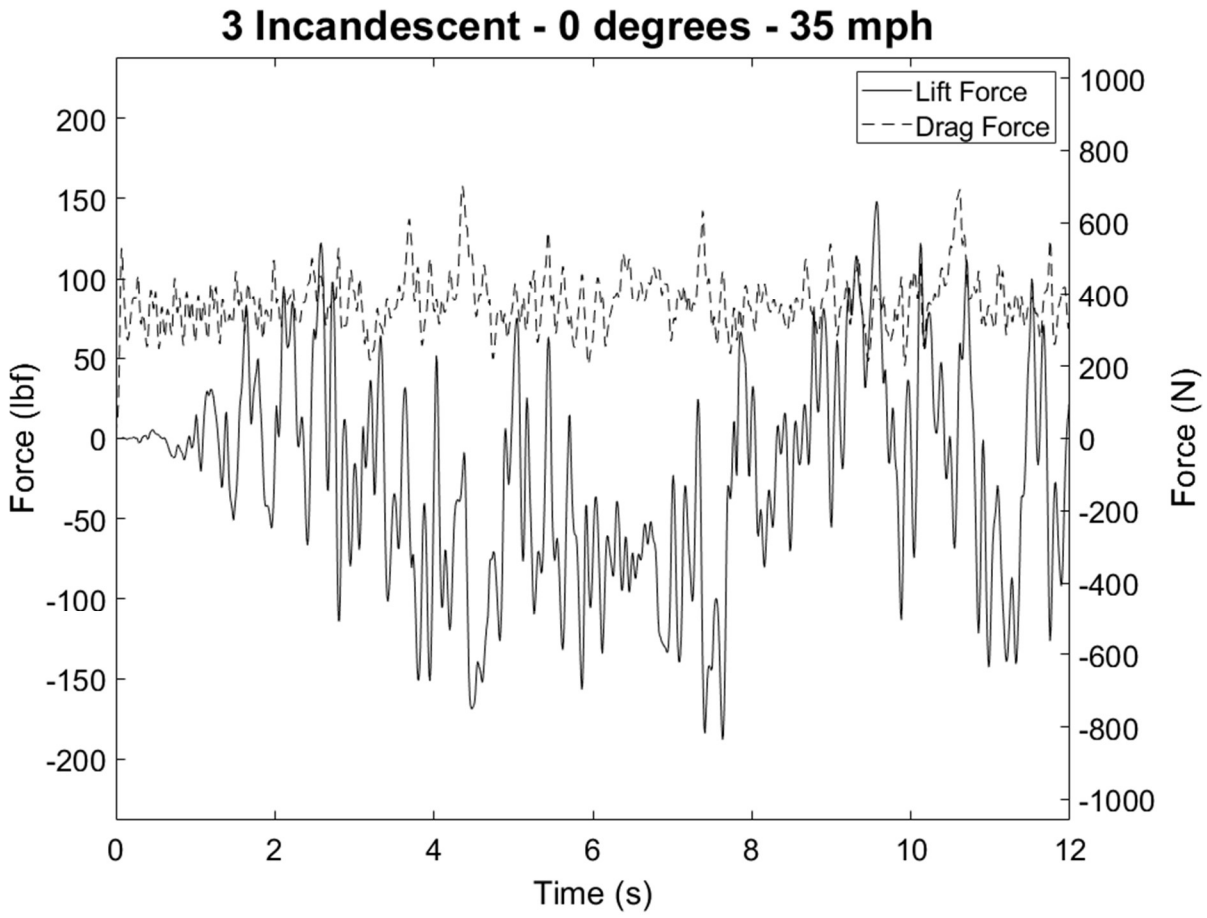
3 Incandescent - 0 degrees - 35 mph
Lift Force
Drag Force
Force (lbf)
Force (N)
Time (s)
200
150
100
50
0
-50
-100
-150
-200
1000
800
600
400
200
0
-200
-400
-600
-800
-1000
0
2
4
6
8
10
12

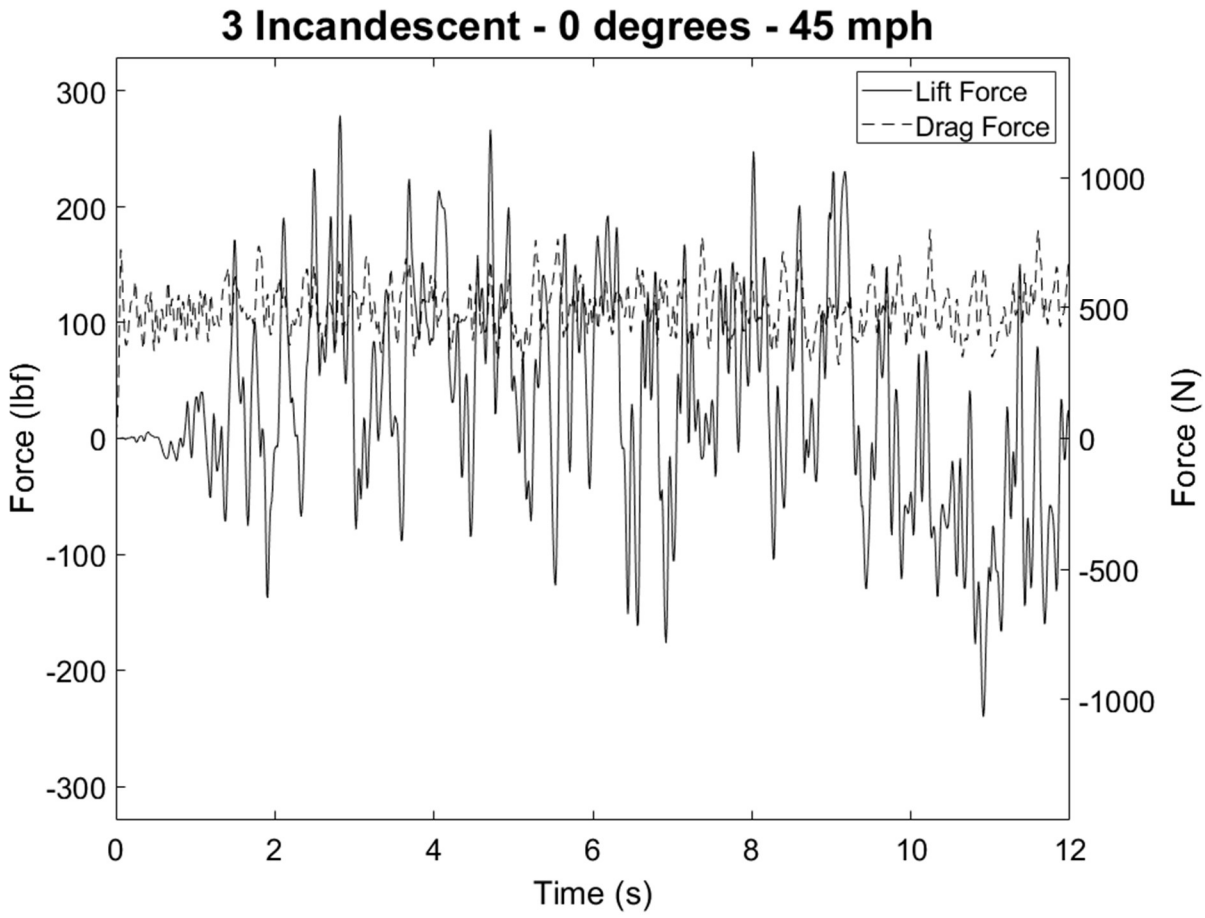
3 Incandescent - 0 degrees - 45 mph
Lift Force
Drag Force
Force (lbf)
Force (N)
Time (s)
300
200
100
0
-100
-200
-300
1000
500
0
-500
-1000
0
2
4
6
8
10
12

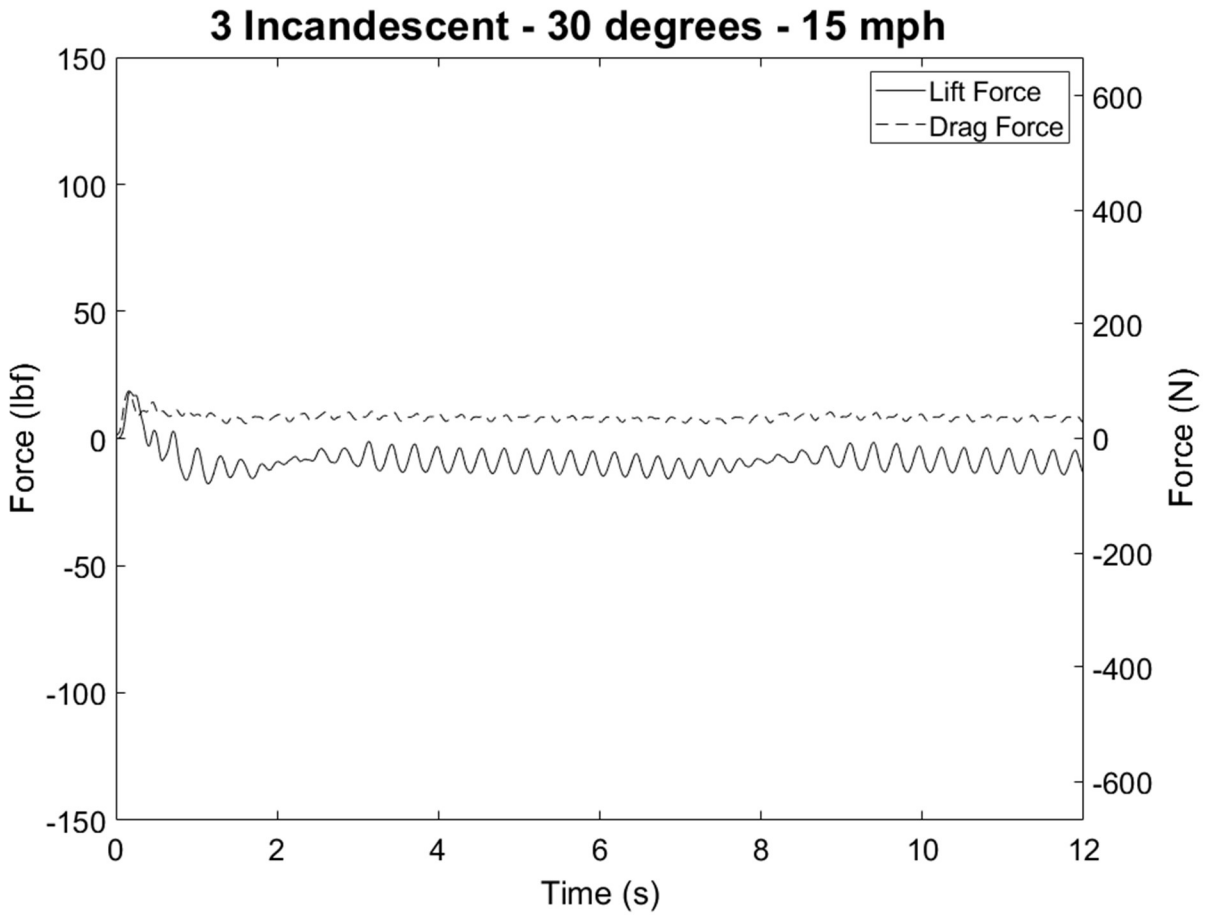
3 Incandescent - 30 degrees - 15 mph
Lift Force
Drag Force
Force (lbf)
Force (N)
Time (s)
150
100
50
0
-50
-100
-150
600
400
200
0
-200
-400
-600
0
2
4
6
8
10
12

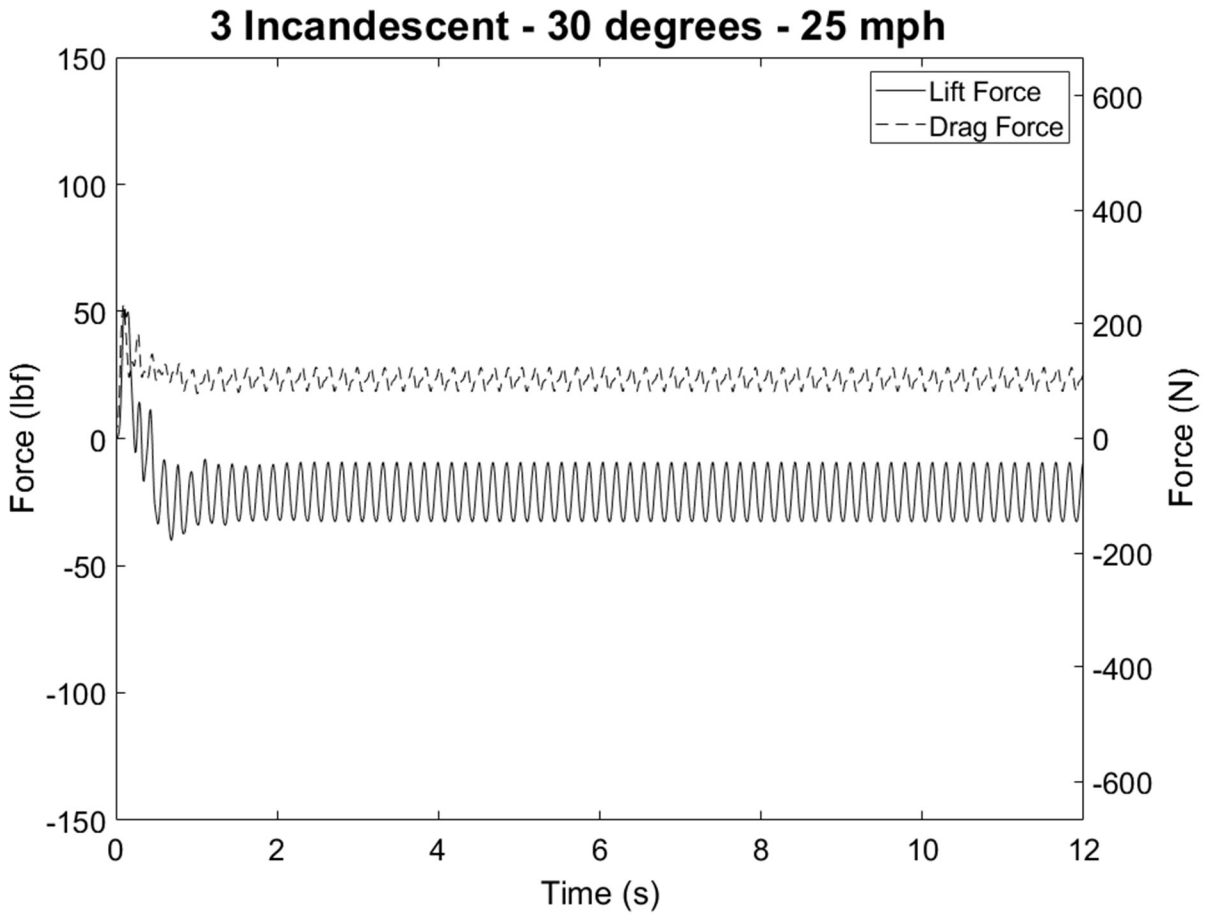
3 Incandescent - 30 degrees - 25 mph
Lift Force
Drag Force
Force (lbf)
Force (N)
Time (s)
150
100
50
0
-50
-100
-150
600
400
200
0
-200
-400
-600
0
2
4
6
8
10
12

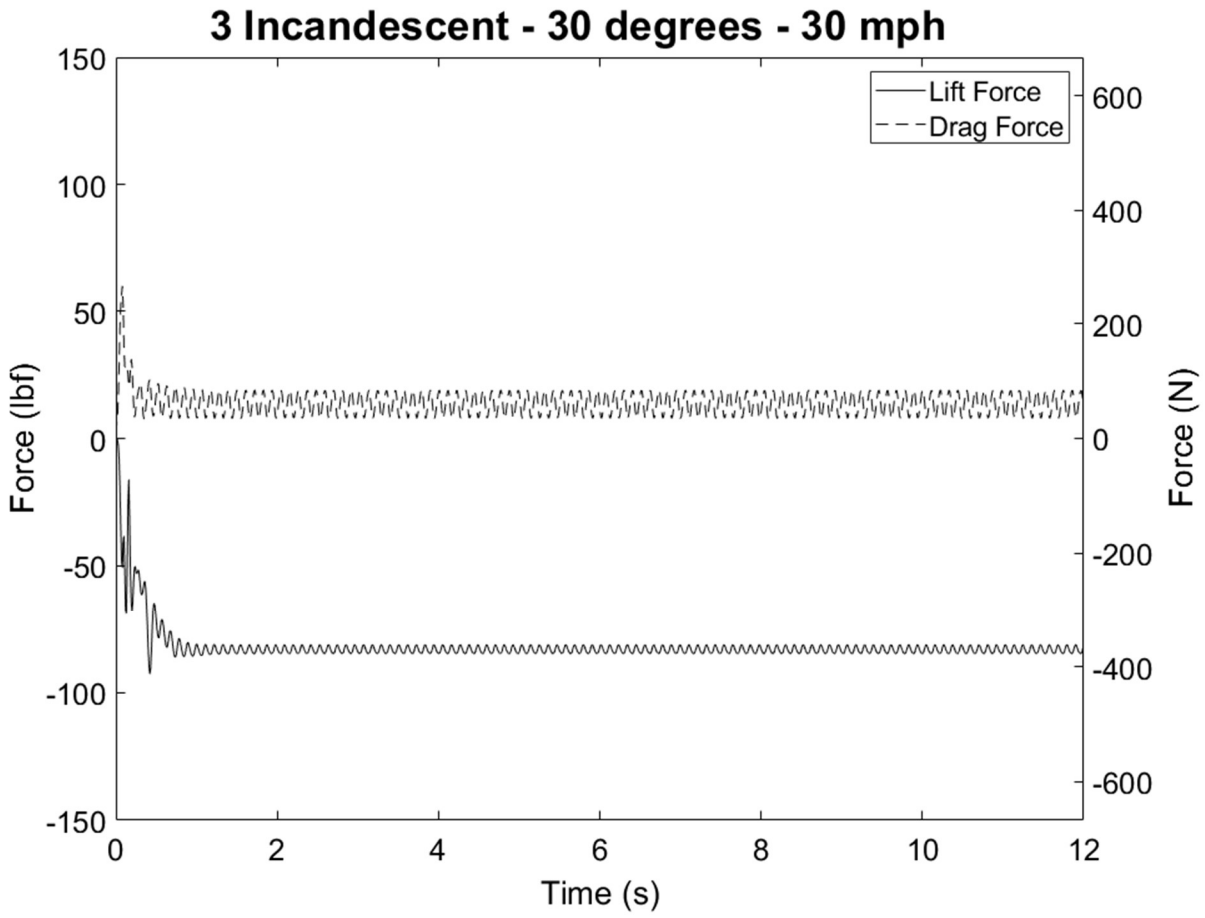
3 Incandescent - 30 degrees - 30 mph
Lift Force
Drag Force
Force (lbf)
Force (N)
Time (s)
150
100
50
0
-50
-100
-150
600
400
200
0
-200
-400
-600
0
2
4
6
8
10
12

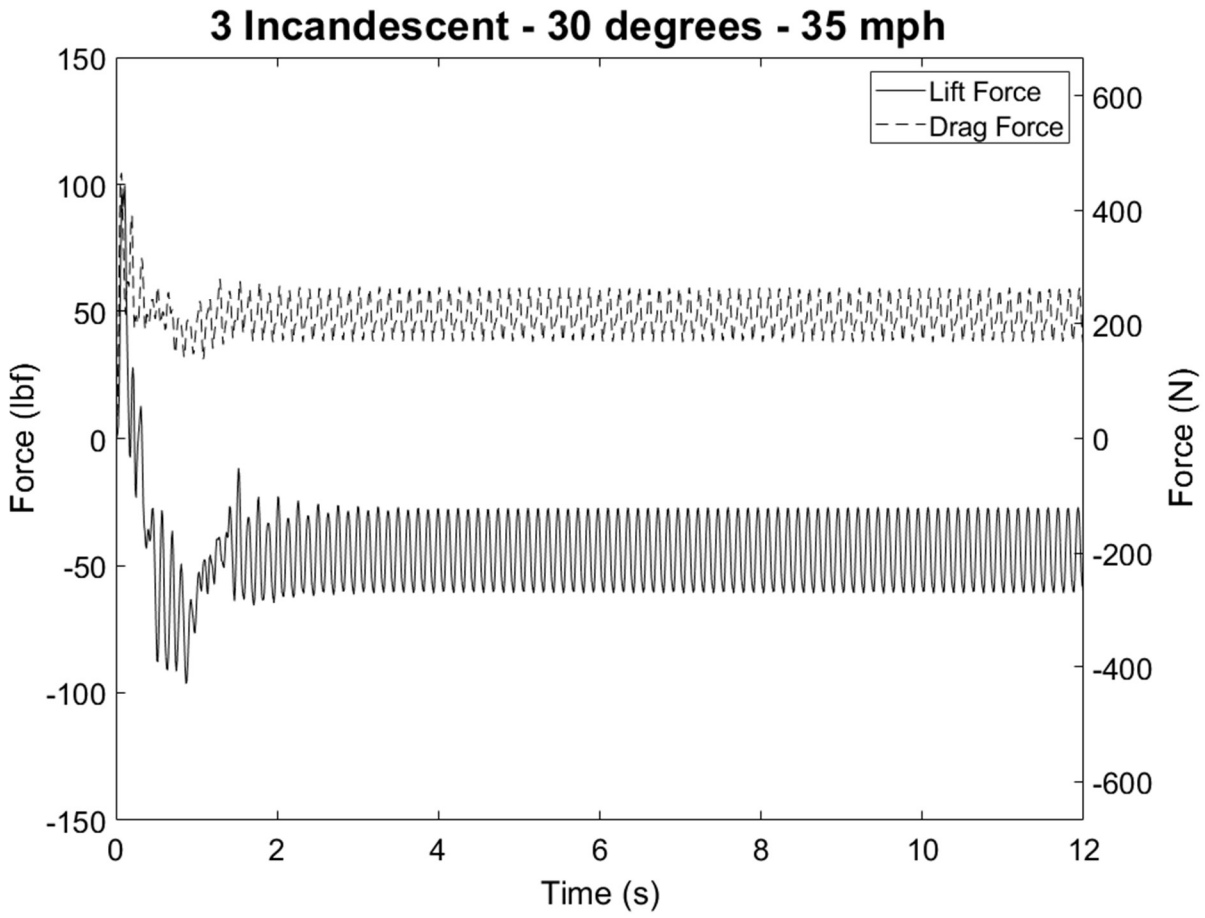
3 Incandescent - 30 degrees - 35 mph
Lift Force
Drag Force
Force (lbf)
Force (N)
Time (s)
150
100
50
0
-50
-100
-150
600
400
200
0
-200
-400
-600
0
2
4
6
8
10
12

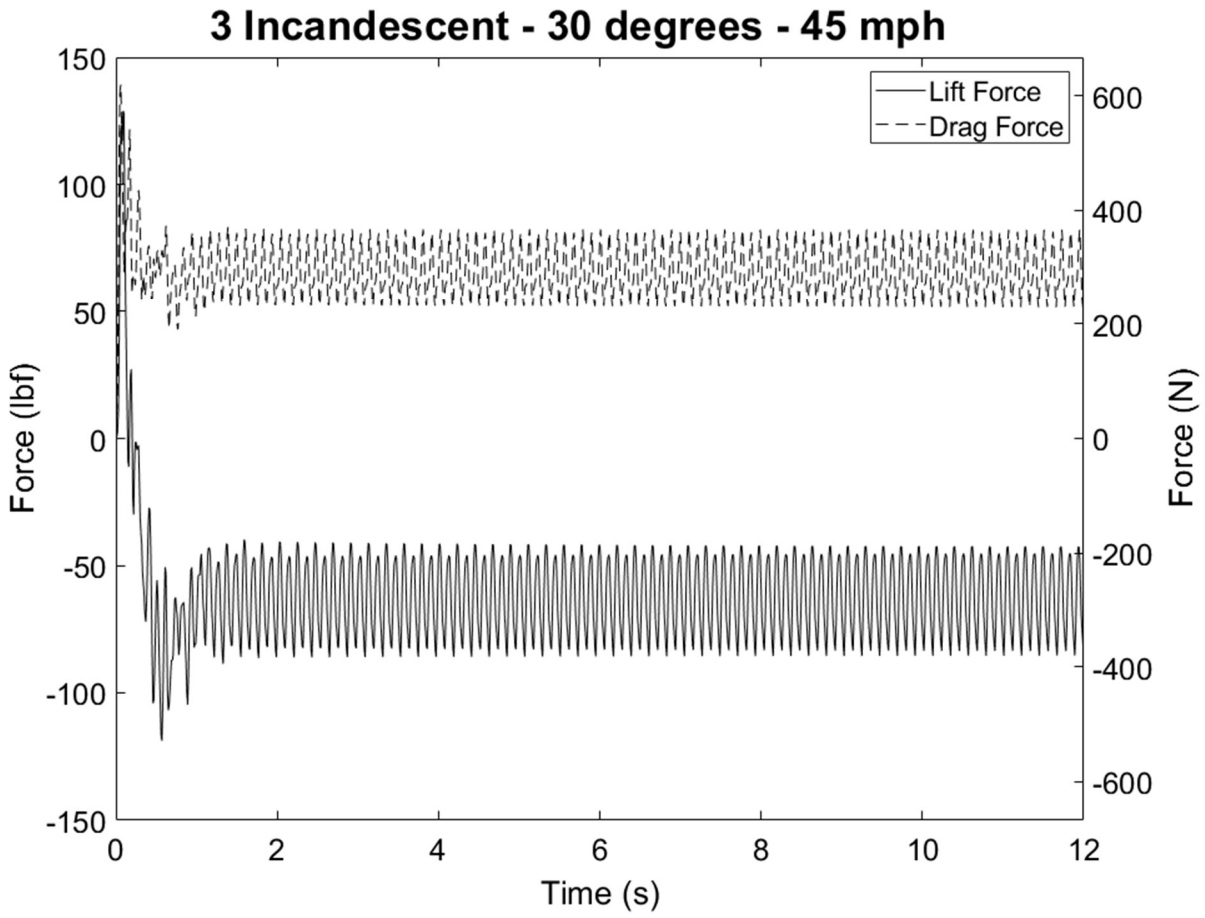
3 Incandescent - 30 degrees - 45 mph
Lift Force
Drag Force
Force (lbf)
Force (N)
Time (s)
150
100
50
0
-50
-100
-150
600
400
200
0
-200
-400
-600
0
2
4
6
8
10
12

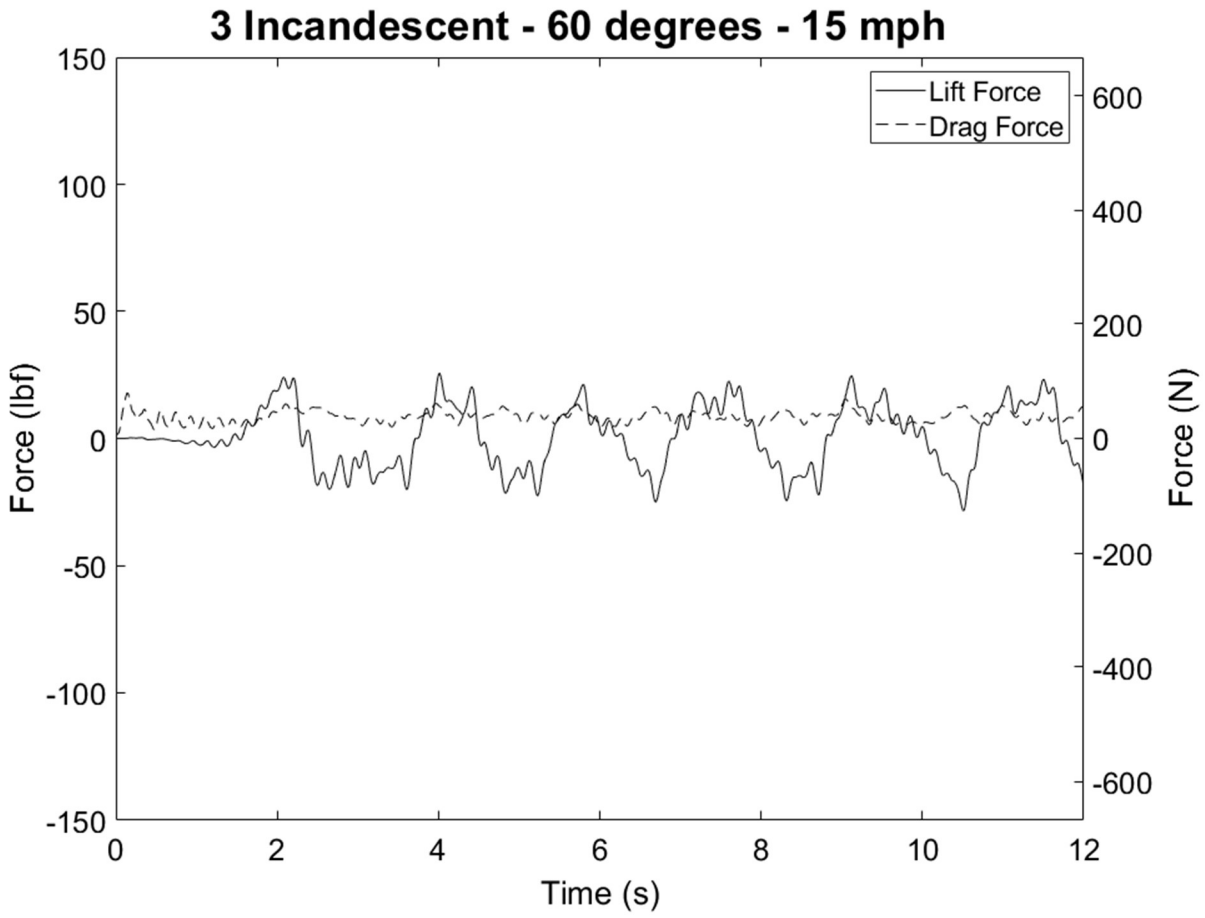
3 Incandescent - 60 degrees - 15 mph
Lift Force
Drag Force
Force (lbf)
Force (N)
Time (s)
150
100
50
0
-50
-100
-150
600
400
200
0
-200
-400
-600
0
2
4
6
8
10
12

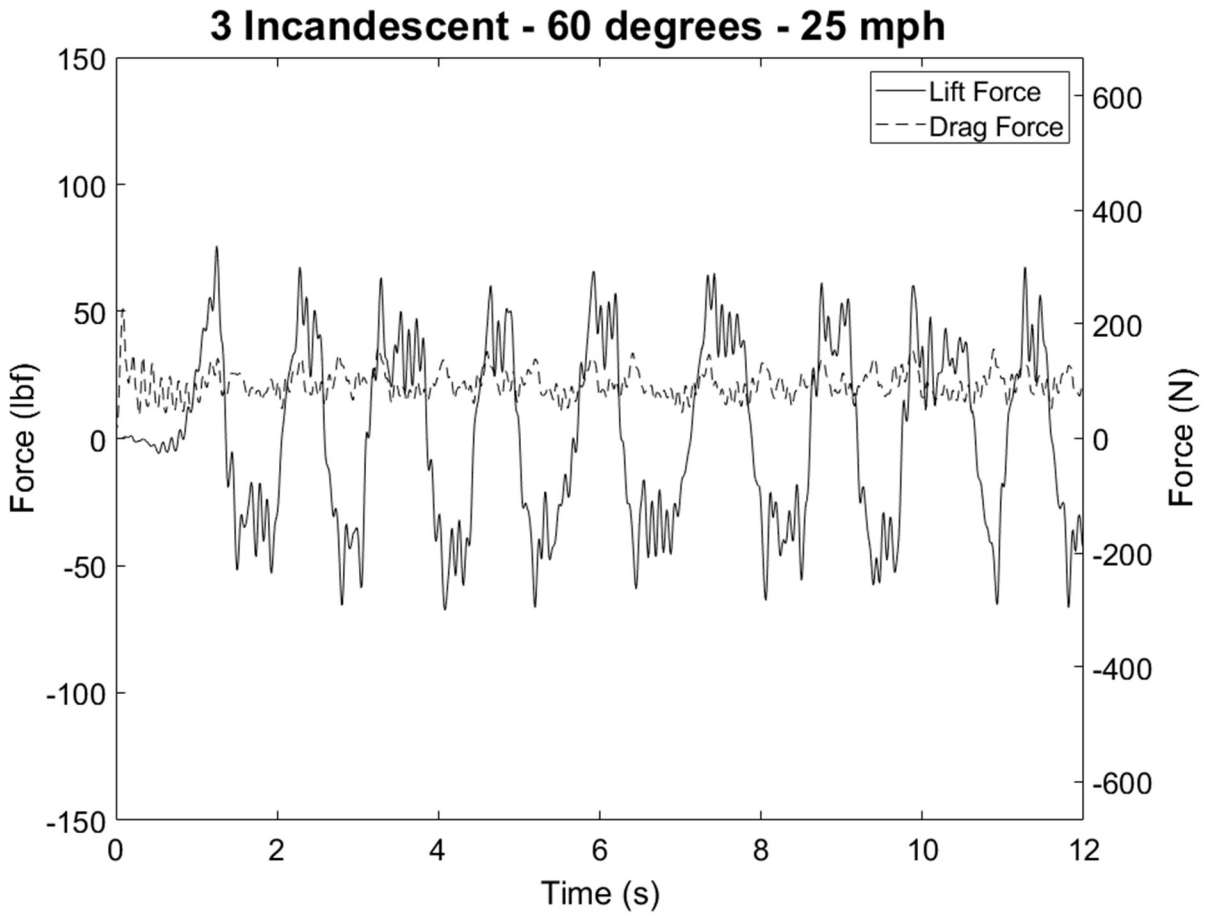
3 Incandescent - 60 degrees - 25 mph
Lift Force
Drag Force
Force (lbf)
Force (N)
Time (s)
150
100
50
0
-50
-100
-150
600
400
200
0
-200
-400
-600
0
2
4
6
8
10
12

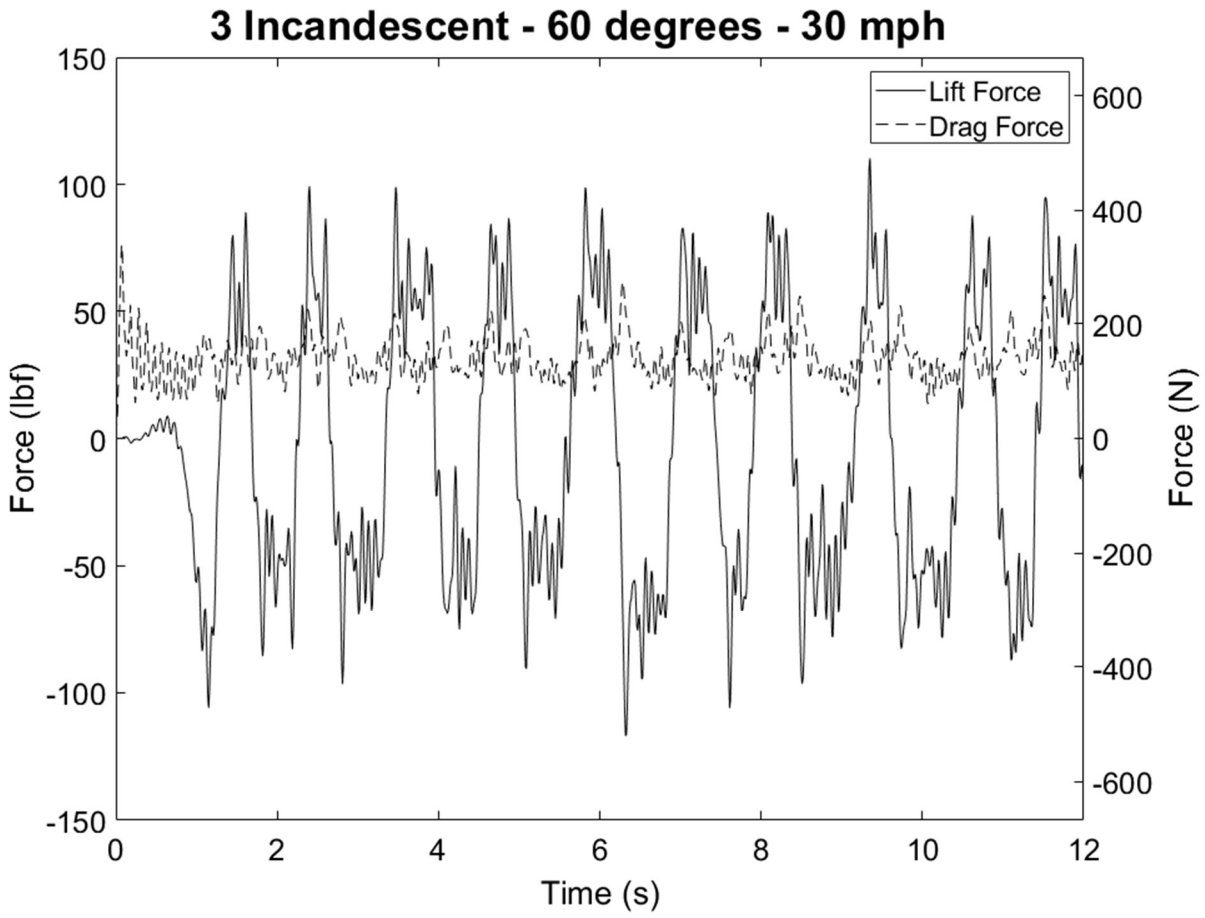
3 Incandescent - 60 degrees - 30 mph
Lift Force
Drag Force
Force (lbf)
Force (N)
Time (s)
150
100
50
0
-50
-100
-150
600
400
200
0
-200
-400
-600
0
2
4
6
8
10
12

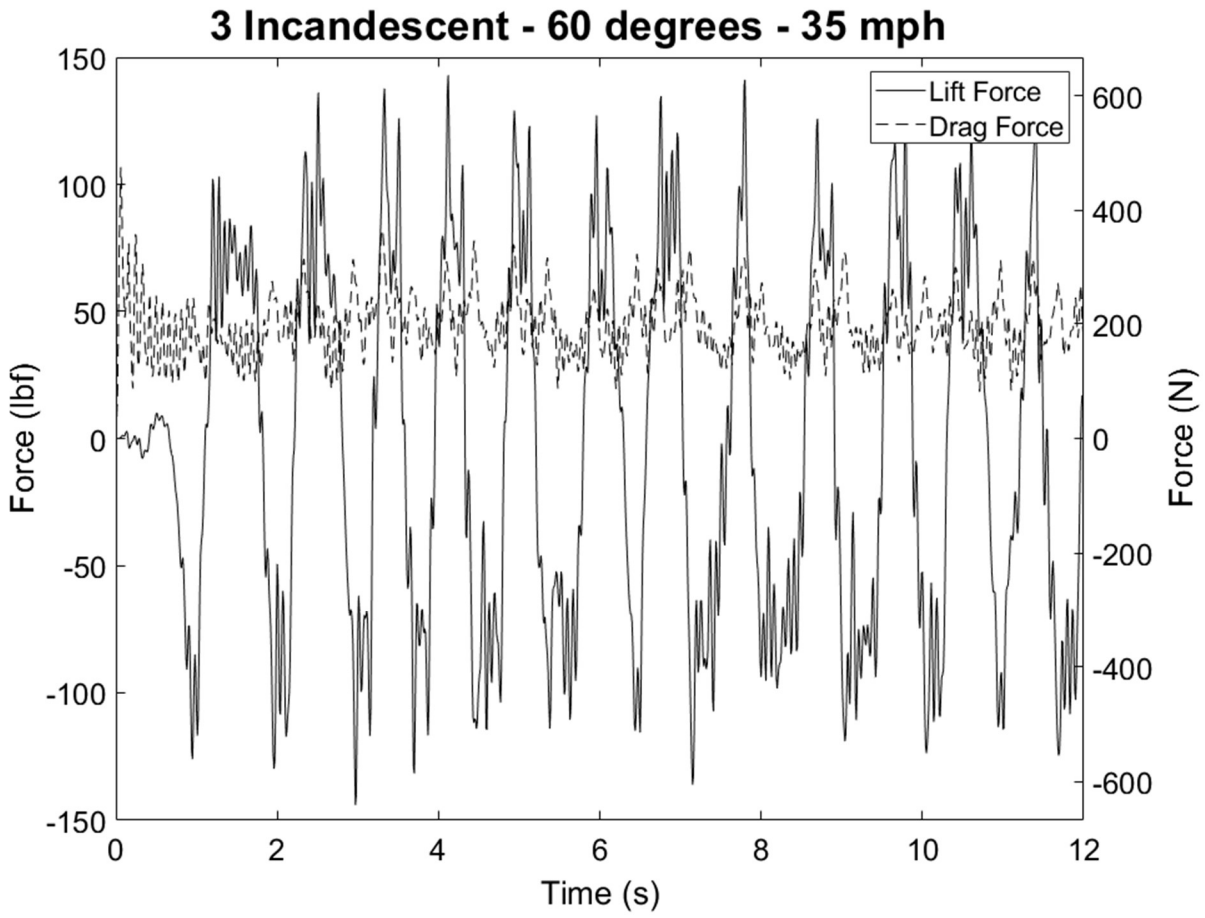
3 Incandescent - 60 degrees - 35 mph
Lift Force
Drag Force
Force (lbf)
Force (N)
Time (s)
150
100
50
0
-50
-100
-150
600
400
200
0
-200
-400
-600
0
2
4
6
8
10
12

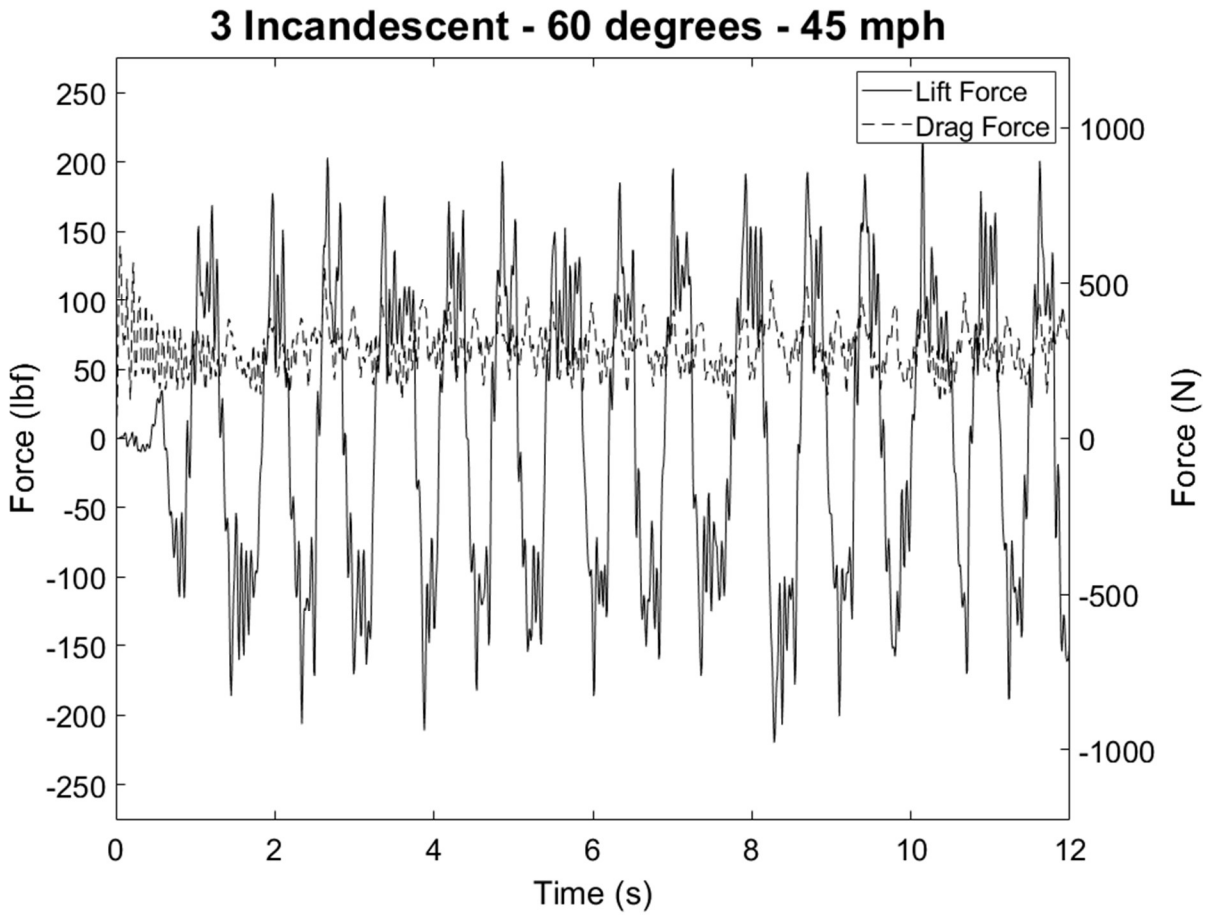
3 Incandescent - 60 degrees - 45 mph
Lift Force
Drag Force
Force (lbf)
Force (N)
Time (s)
250
200
150
100
50
0
-50
-100
-150
-200
-250
1000
500
0
-500
-1000
0
2
4
6
8
10
12

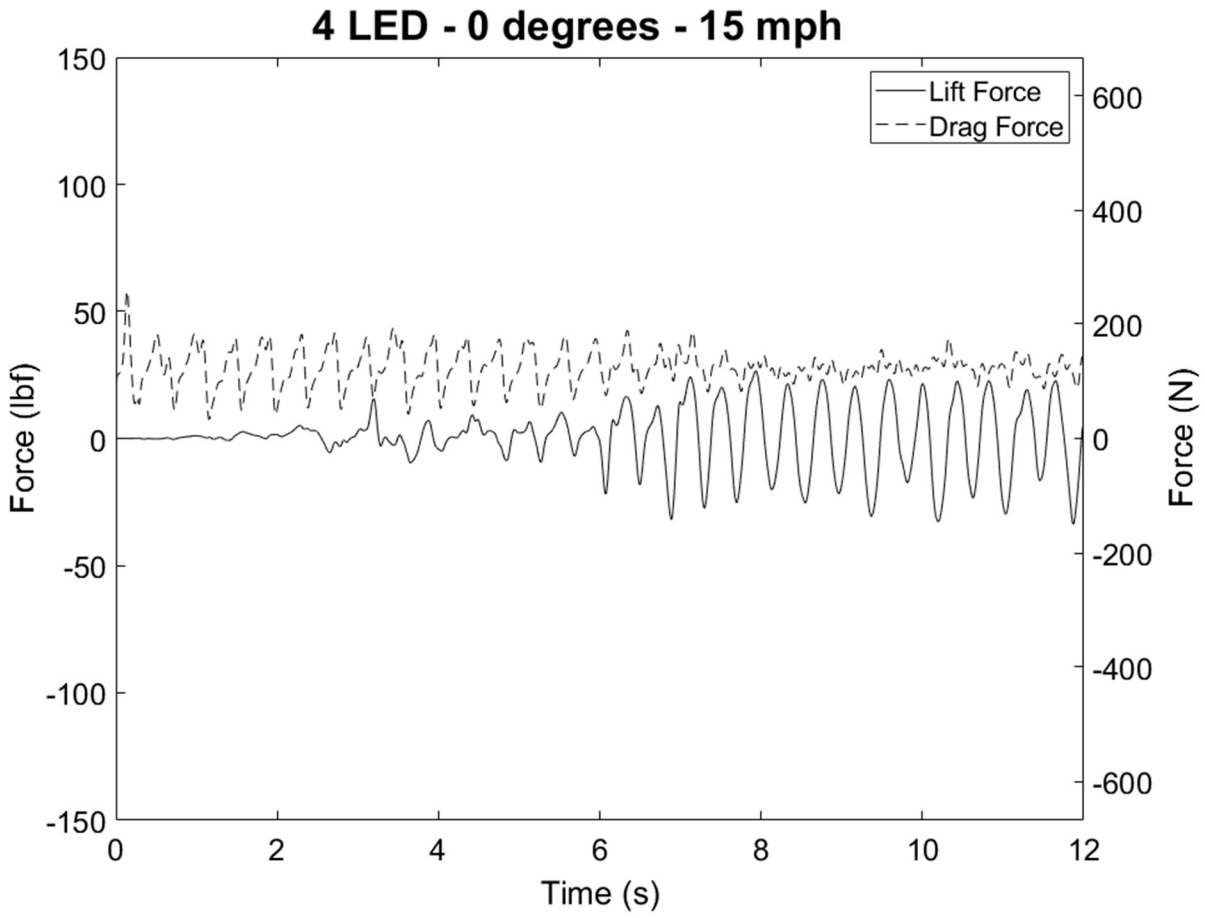
4 LED - 0 degrees - 15 mph
Lift Force
Drag Force
Force (lbf)
Force (N)
Time (s)
150
100
50
0
-50
-100
-150
600
400
200
0
-200
-400
-600
0
2
4
6
8
10
12

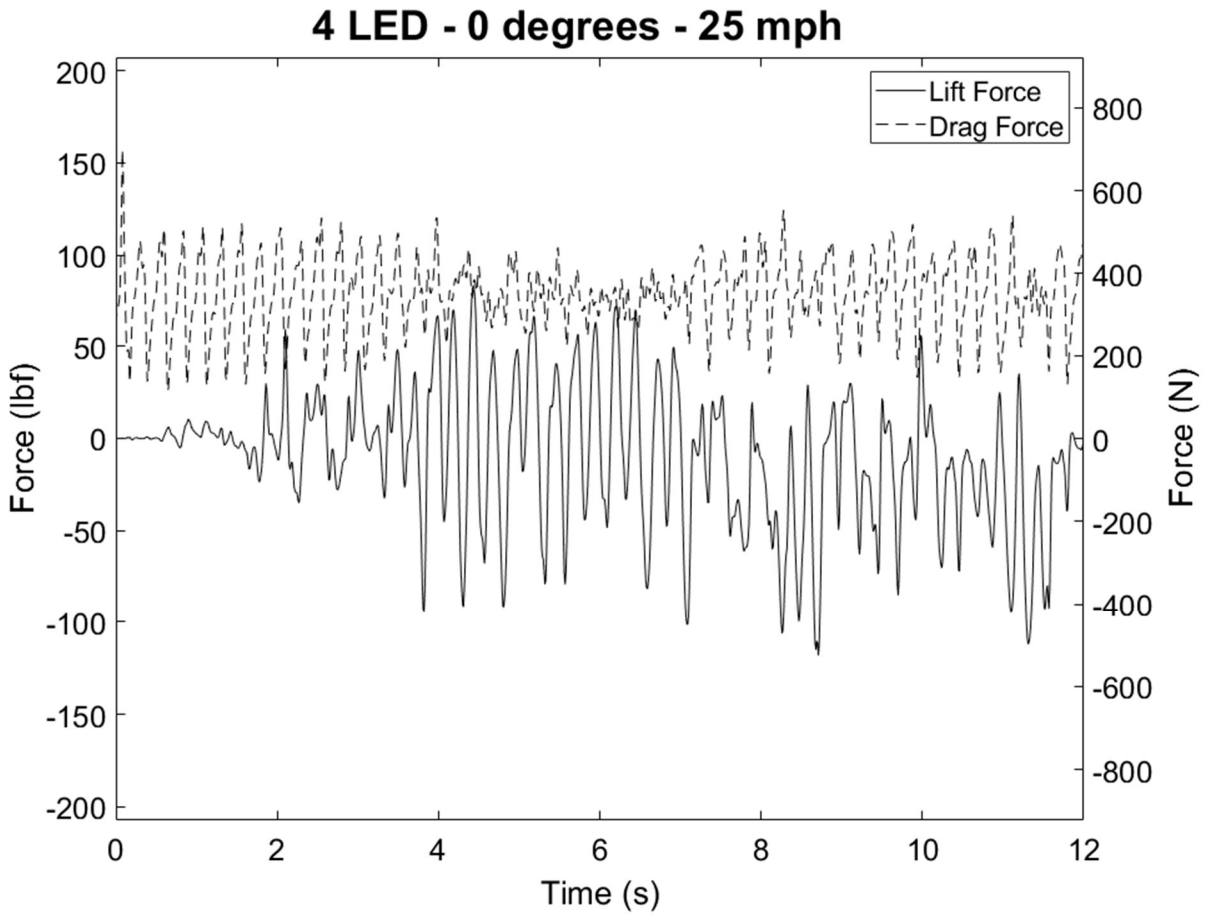
4 LED - 0 degrees - 25 mph
Lift Force
Drag Force
Force (lbf)
Force (N)
Time (s)
200
150
100
50
0
-50
-100
-150
-200
800
600
400
200
0
-200
-400
-600
-800
0
2
4
6
8
10
12

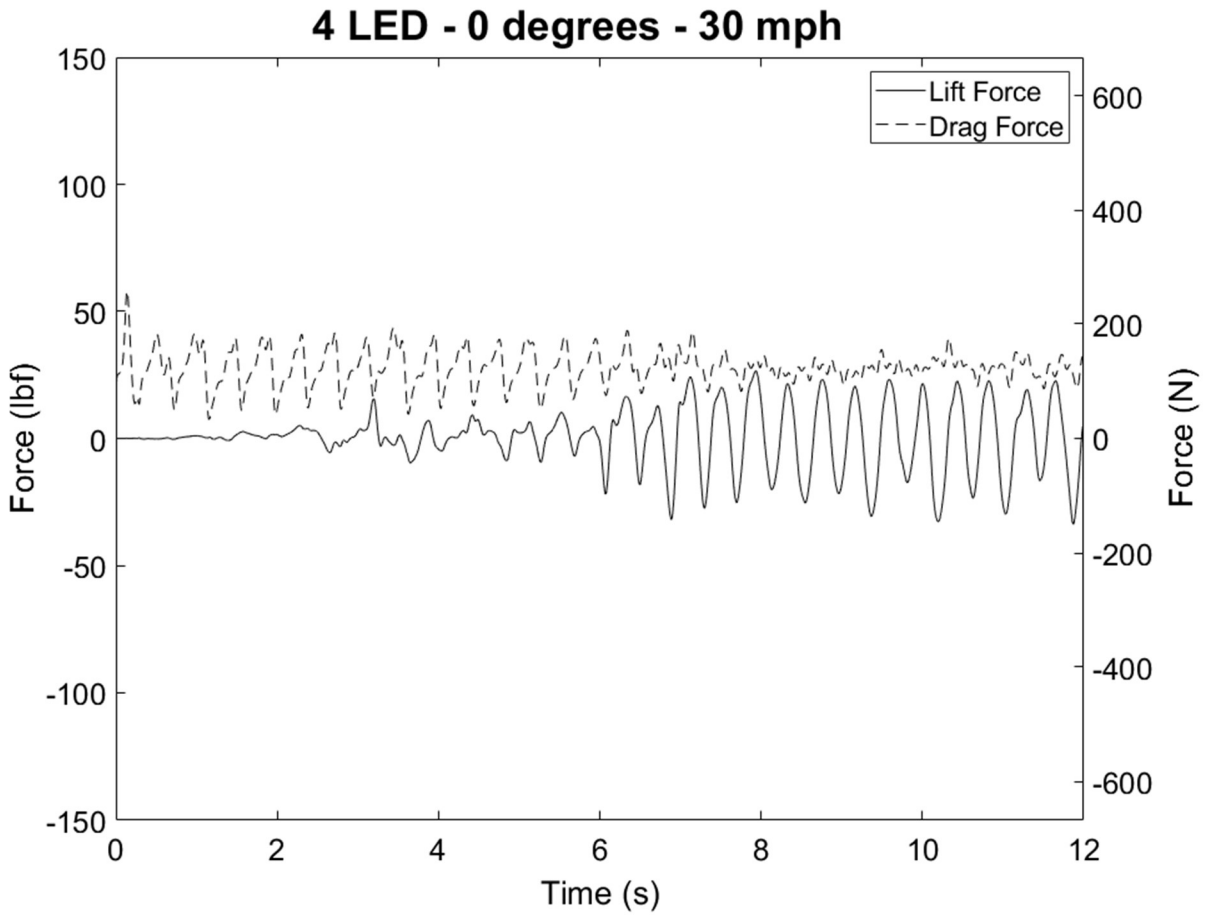
4 LED - 0 degrees - 30 mph
Lift Force
Drag Force
Force (lbf)
Force (N)
Time (s)
150
100
50
0
-50
-100
-150
600
400
200
0
-200
-400
-600
0
2
4
6
8
10
12

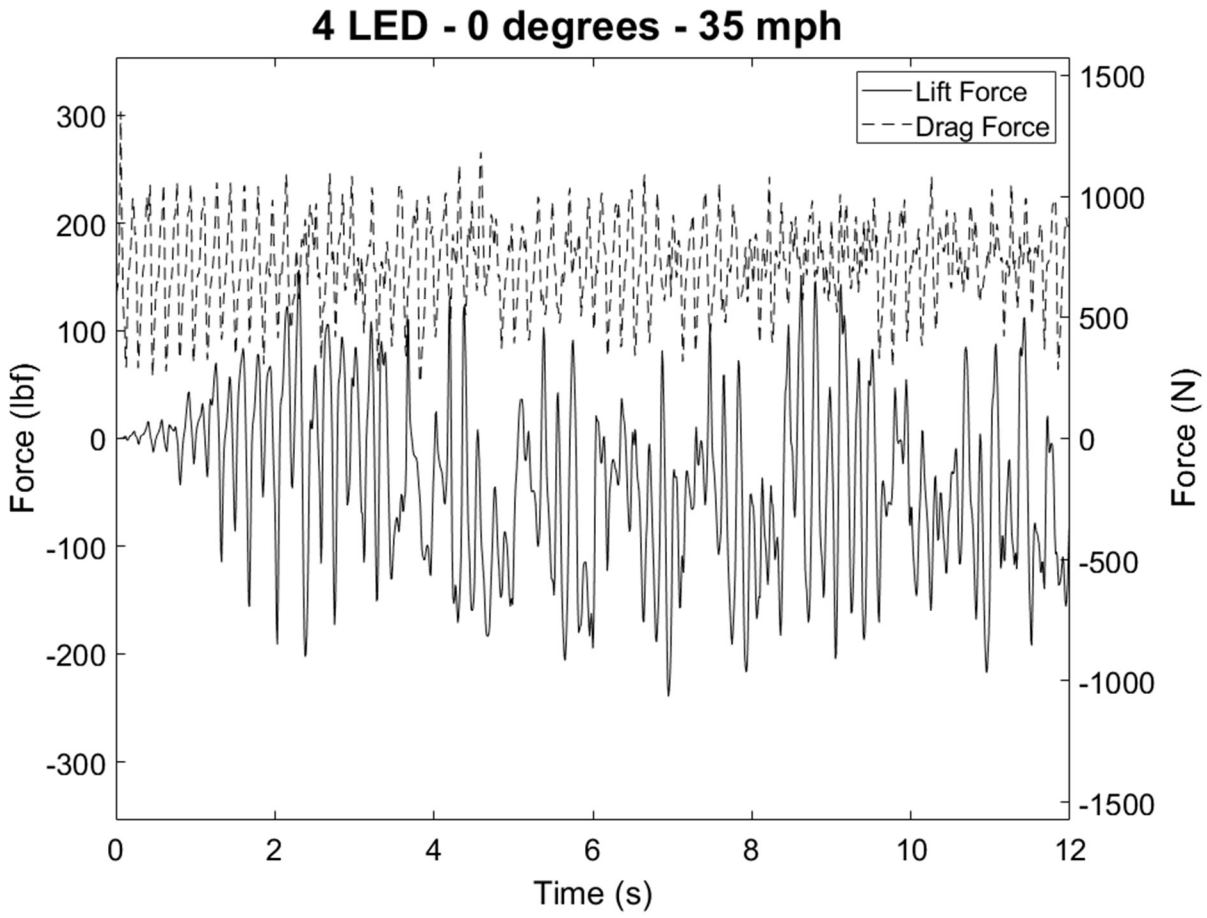
4 LED - 0 degrees - 35 mph
Lift Force
Drag Force
Force (lbf)
Force (N)
Time (s)
300
200
100
0
-100
-200
-300
1500
1000
500
0
-500
-1000
-1500
0
2
4
6
8
10
12

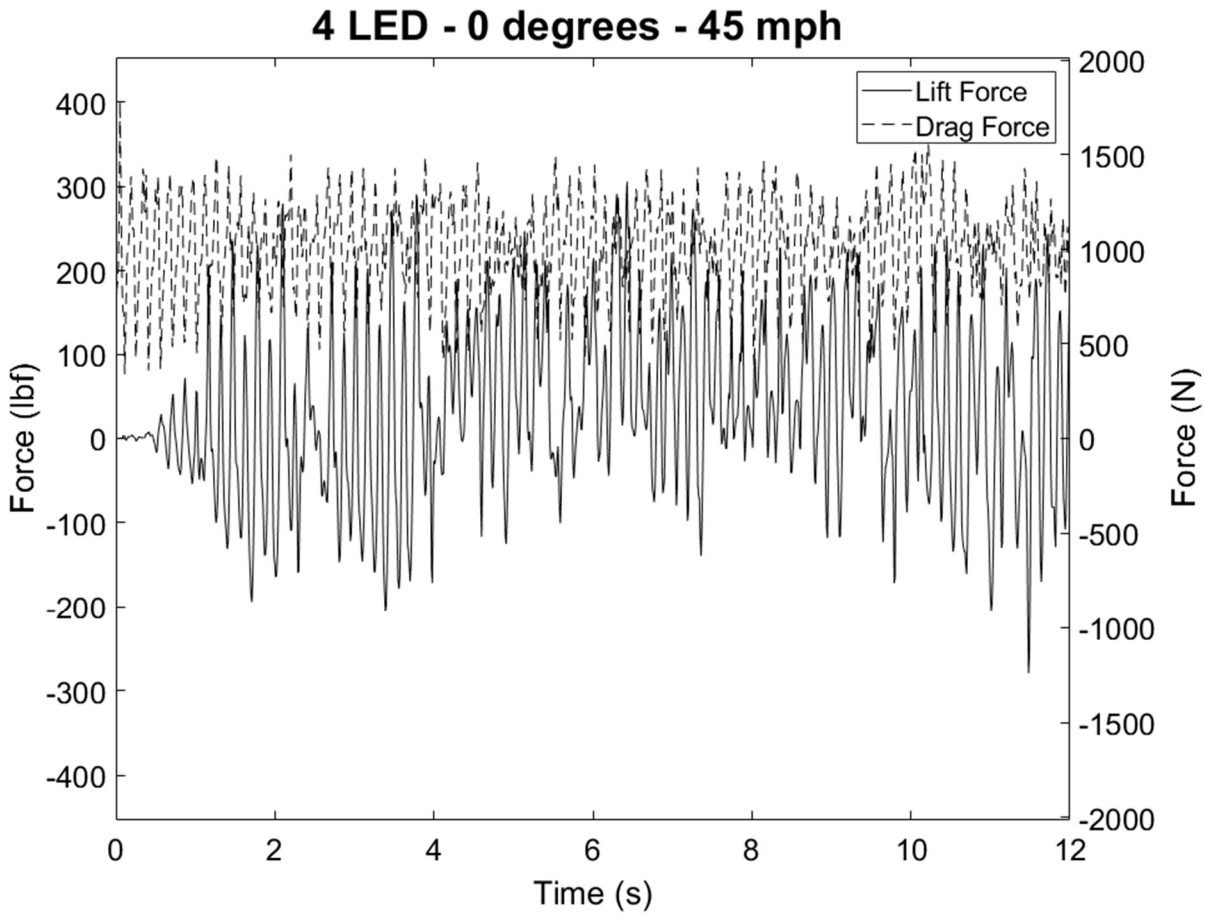
4 LED - 0 degrees - 45 mph
Lift Force
Drag Force
Force (lbf)
Force (N)
Time (s)
400
300
200
100
0
-100
-200
-300
-400
2000
1500
1000
500
0
-500
-1000
-1500
-2000
0
2
4
6
8
10
12

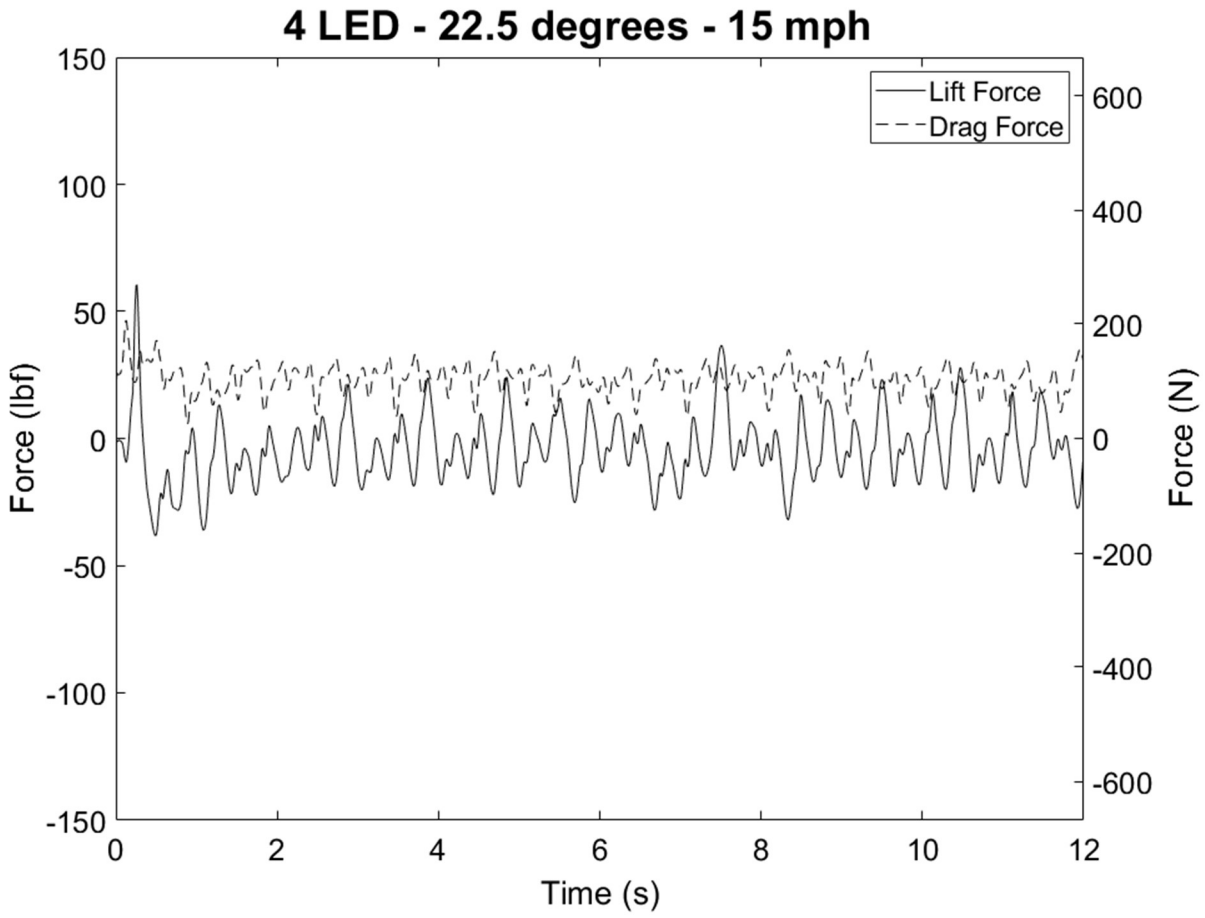
4 LED - 22.5 degrees - 15 mph
Lift Force
Drag Force
Force (lbf)
Force (N)
Time (s)
150
100
50
0
-50
-100
-150
600
400
200
0
-200
-400
-600
0
2
4
6
8
10
12

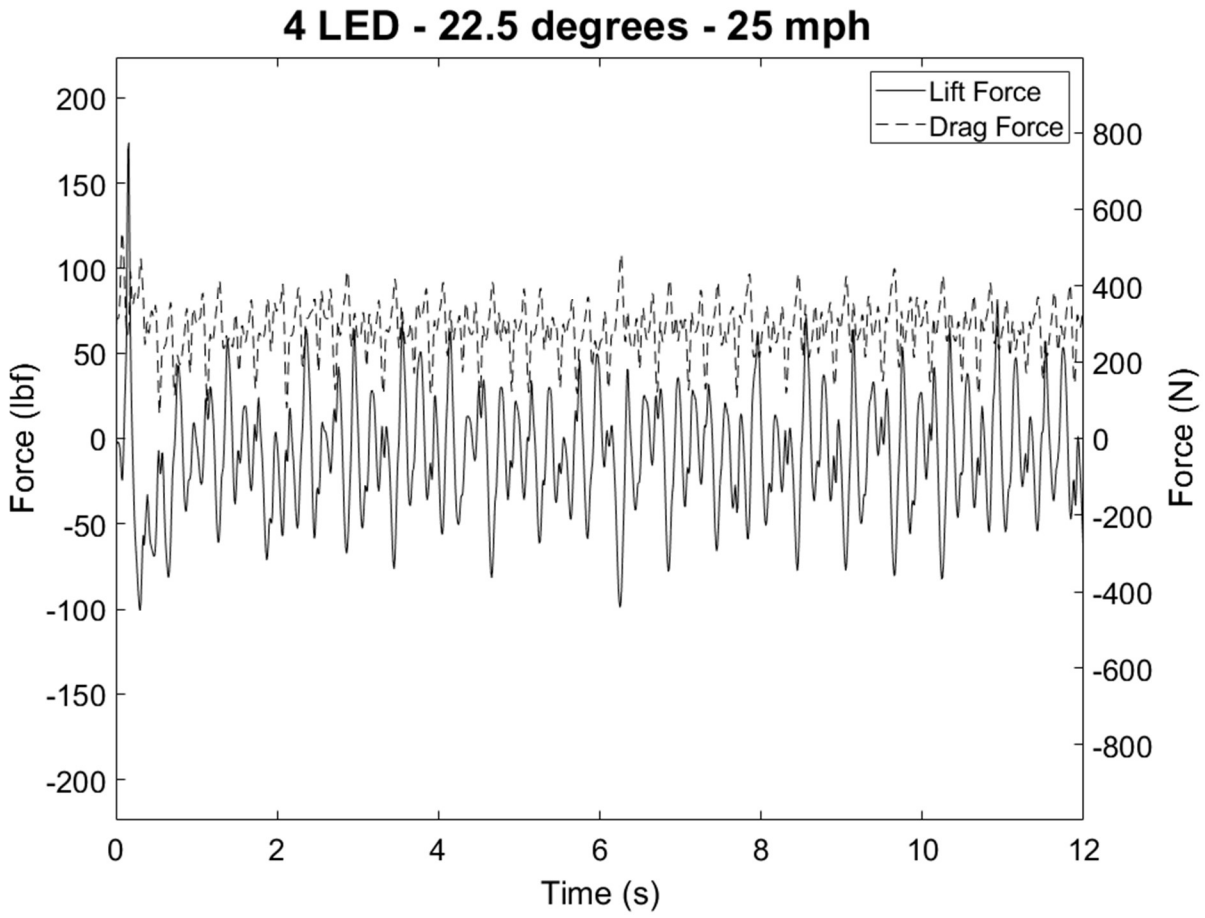
4 LED - 22.5 degrees - 25 mph
Lift Force
Drag Force
Force (lbf)
Force (N)
Time (s)
200
150
100
50
0
-50
-100
-150
-200
800
600
400
200
0
-200
-400
-600
-800
0
2
4
6
8
10
12

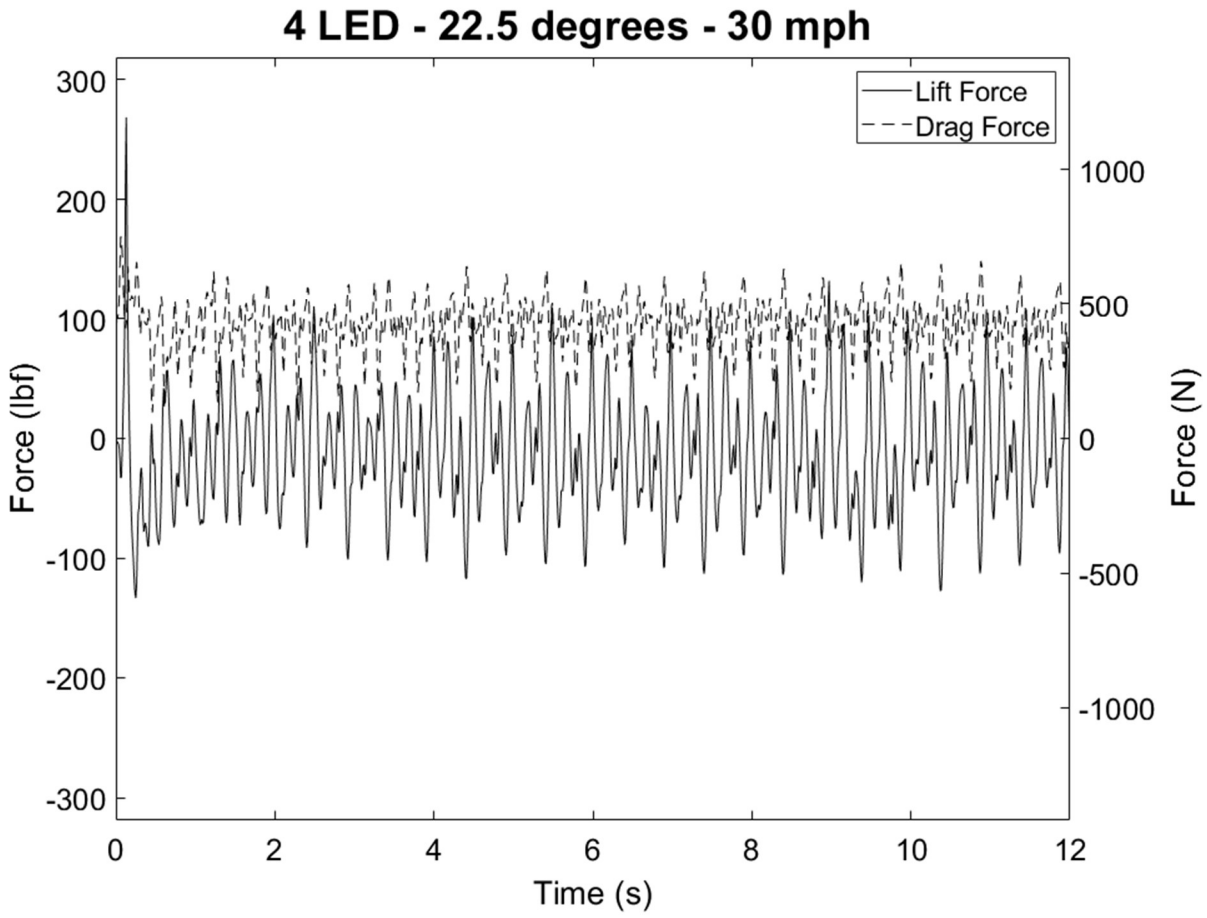
4 LED - 22.5 degrees - 30 mph
Lift Force
Drag Force
Force (lbf)
Force (N)
Time (s)
300
200
100
0
-100
-200
-300
1000
500
0
-500
-1000
0
2
4
6
8
10
12

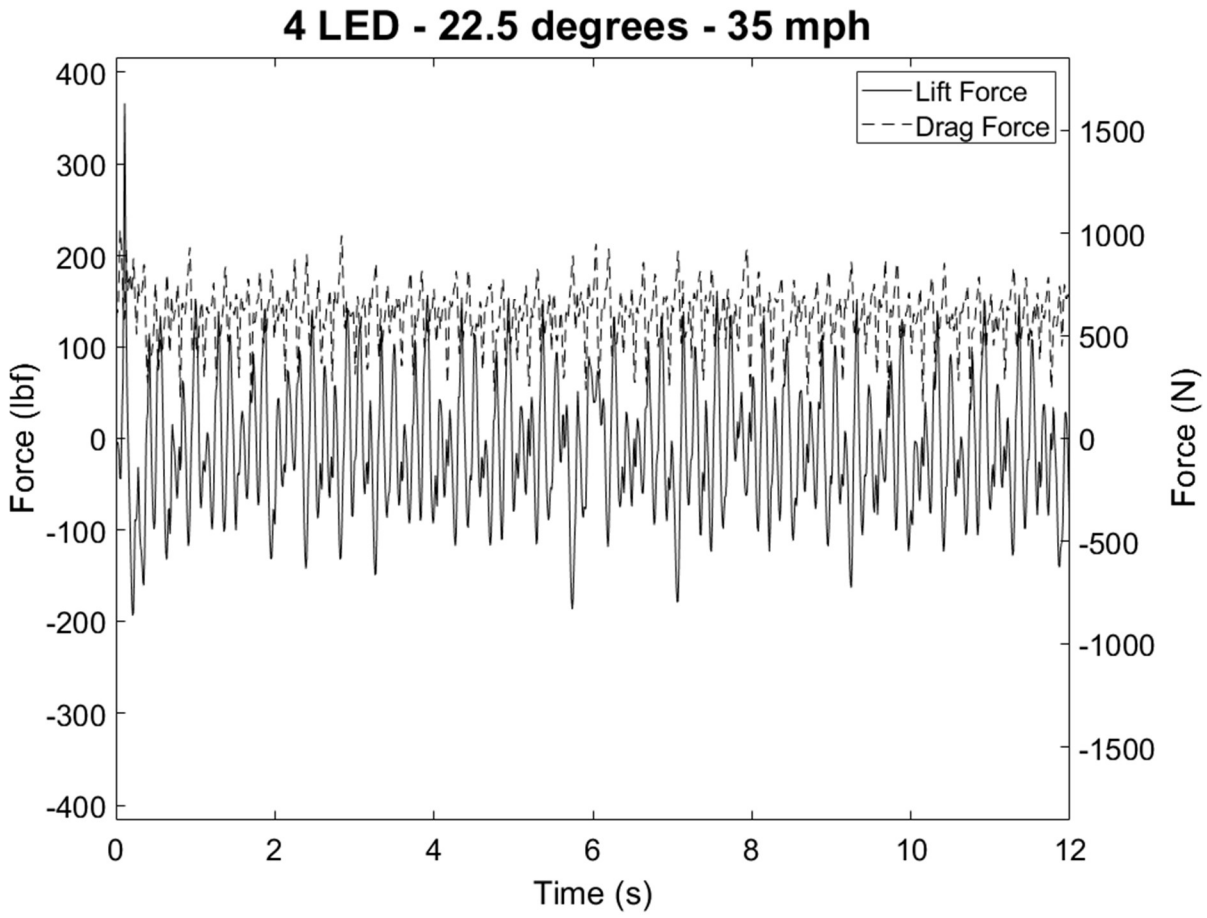
4 LED - 22.5 degrees - 35 mph
Lift Force
Drag Force
Force (lbf)
Force (N)
Time (s)
400
300
200
100
0
-100
-200
-300
-400
1500
1000
500
0
-500
-1000
-1500
0
2
4
6
8
10
12

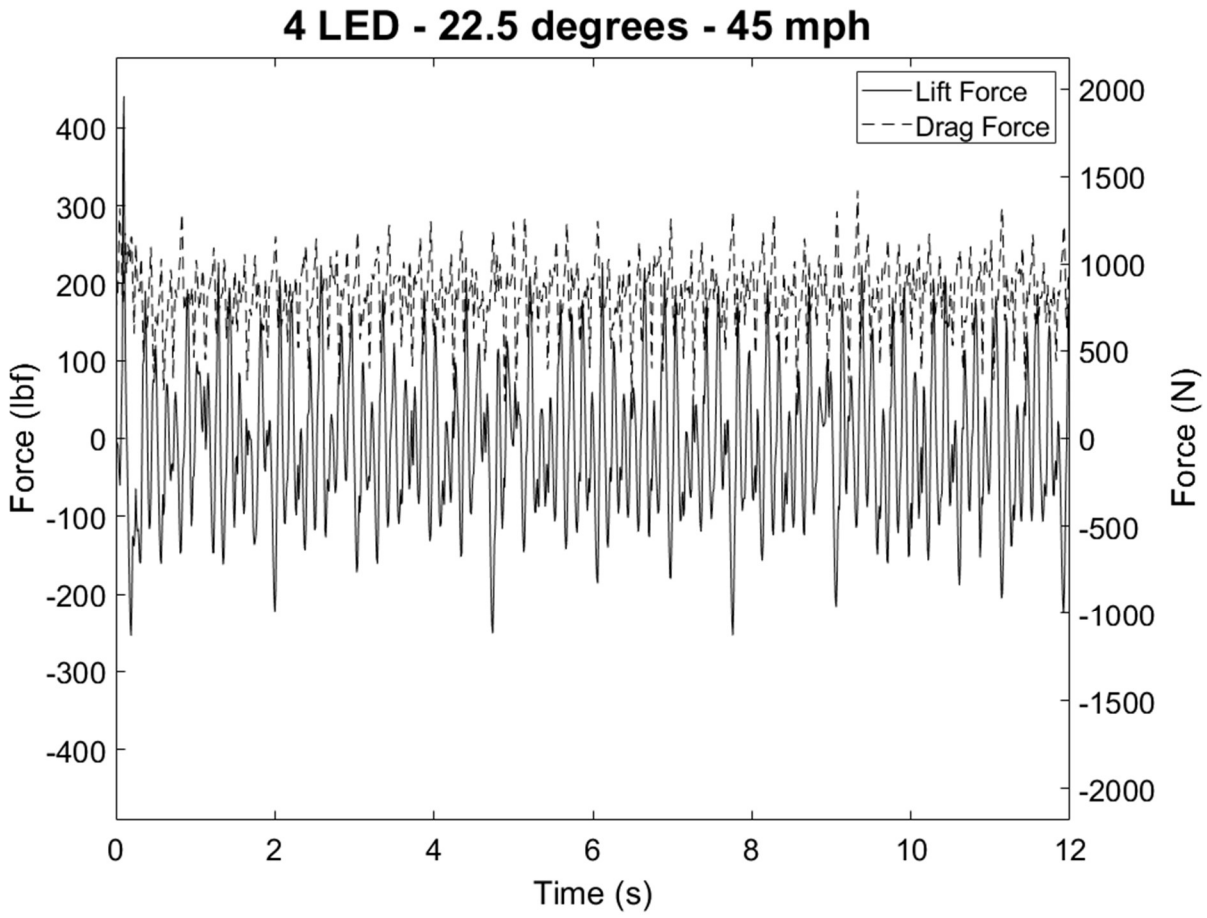
4 LED - 22.5 degrees - 45 mph
Lift Force
Drag Force
Force (lbf)
Force (N)
Time (s)
400
300
200
100
0
-100
-200
-300
-400
2000
1500
1000
500
0
-500
-1000
-1500
-2000
0
2
4
6
8
10
12

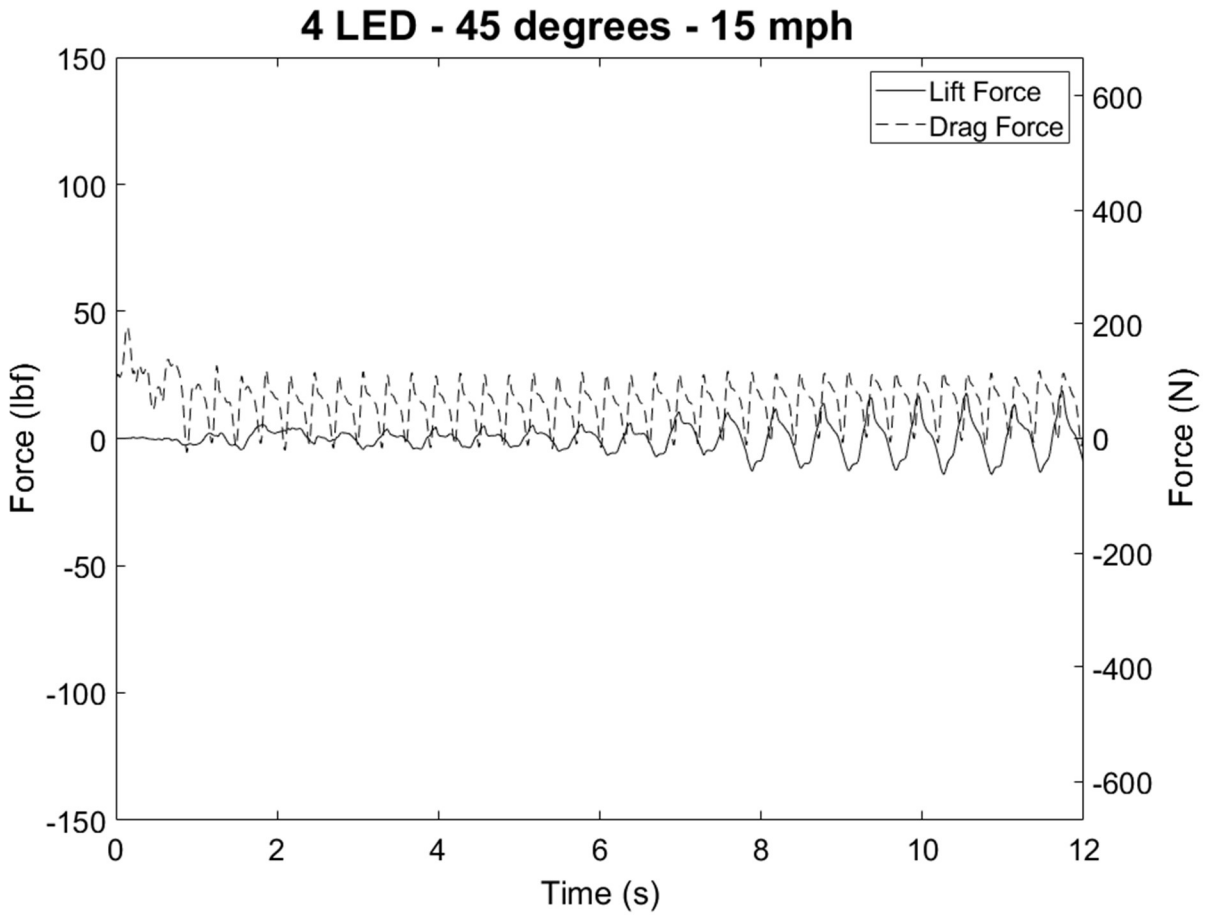
4 LED - 45 degrees - 15 mph
Lift Force
Drag Force
Force (lbf)
Force (N)
Time (s)
150
100
50
0
-50
-100
-150
600
400
200
0
-200
-400
-600
0
2
4
6
8
10
12

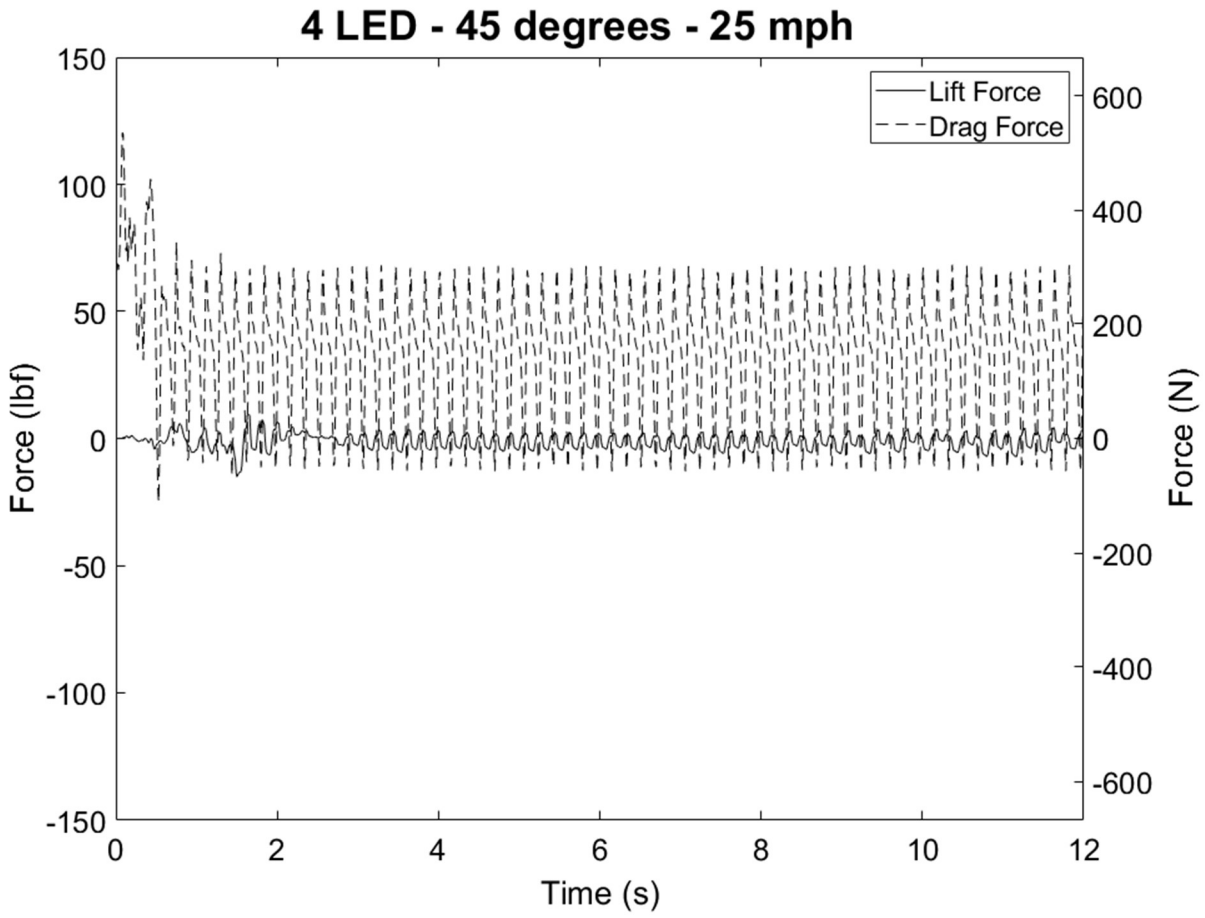
4 LED - 45 degrees - 25 mph
Lift Force
Drag Force
Force (lbf)
Force (N)
Time (s)
150
100
50
0
-50
-100
-150
600
400
200
0
-200
-400
-600
0
2
4
6
8
10
12

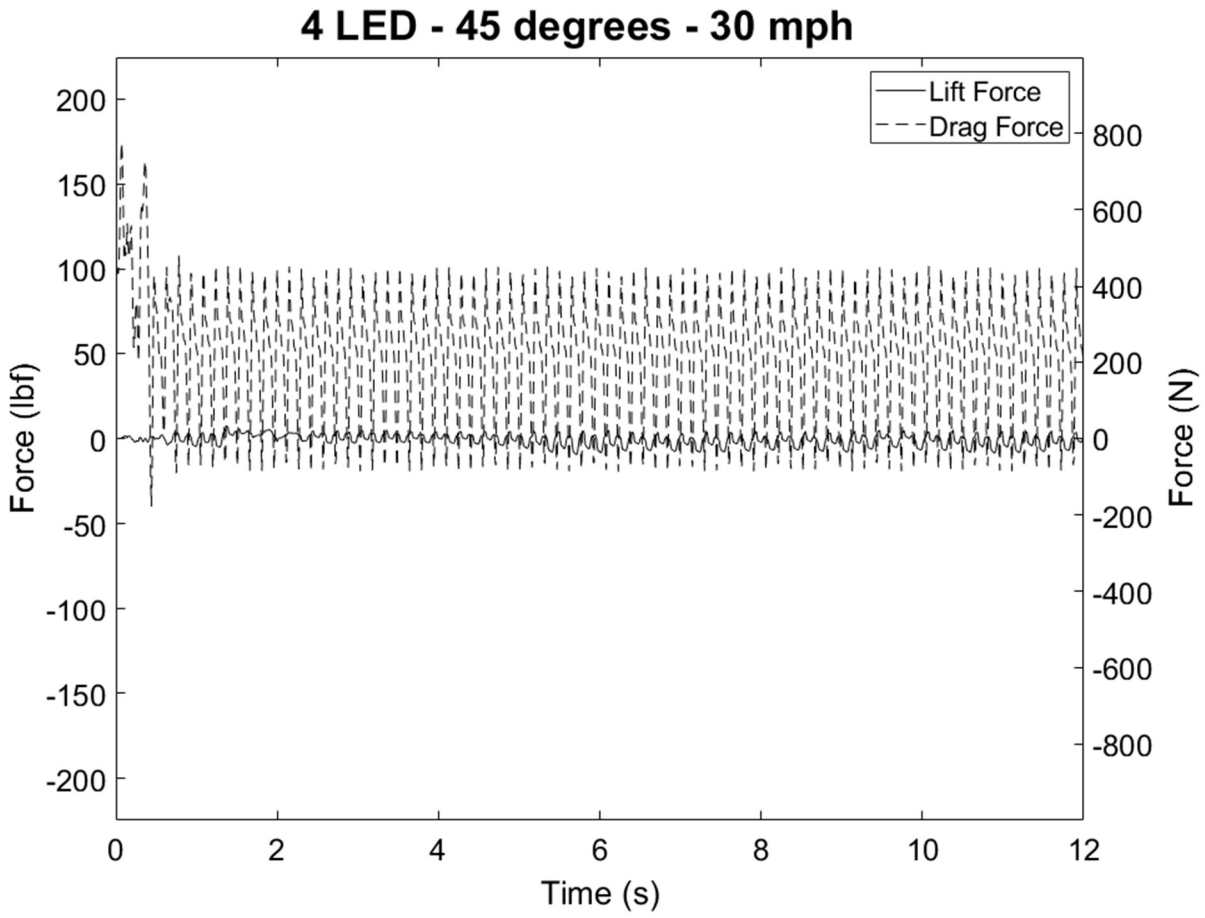
4 LED - 45 degrees - 30 mph
Lift Force
Drag Force
Force (lbf)
Force (N)
Time (s)
200
150
100
50
0
-50
-100
-150
-200
800
600
400
200
0
-200
-400
-600
-800
0
2
4
6
8
10
12

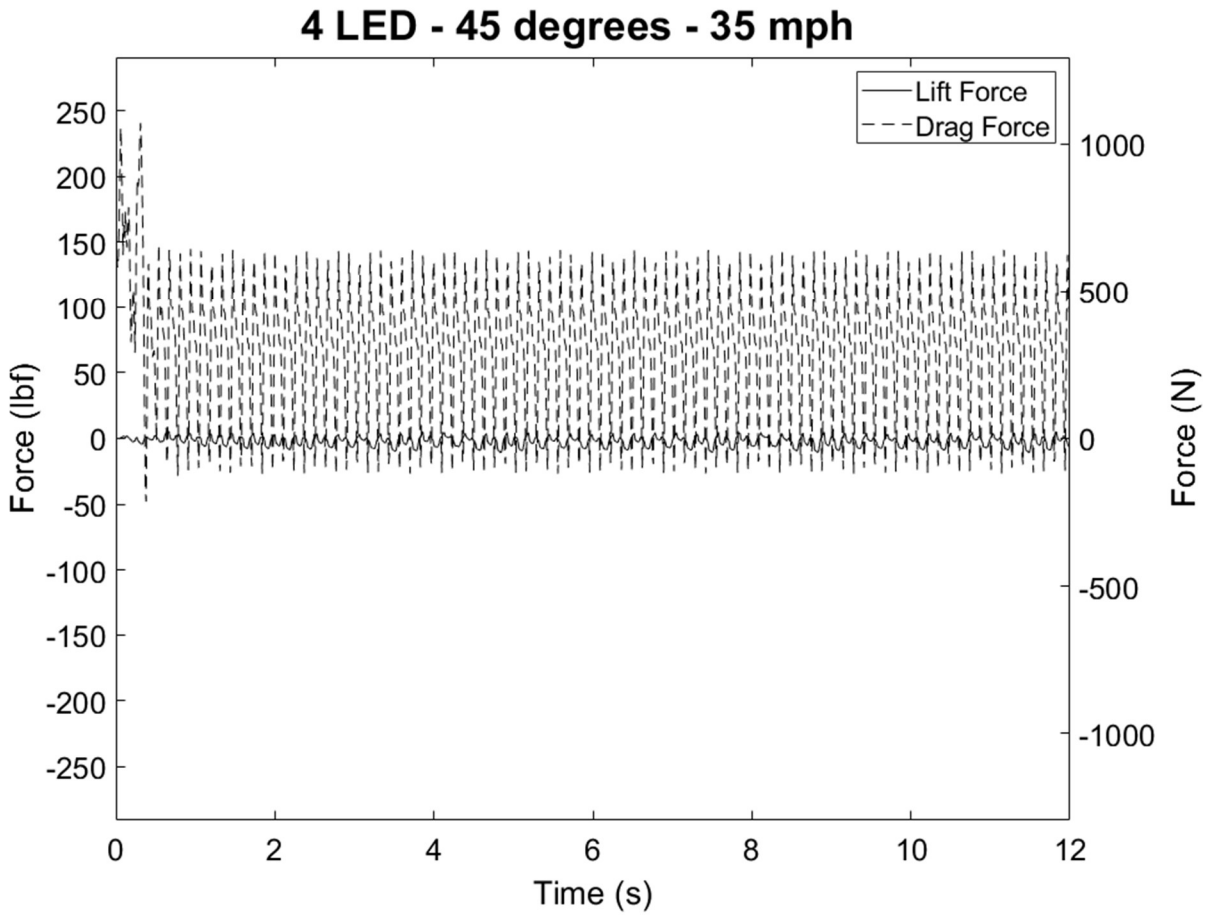
4 LED - 45 degrees - 35 mph
Lift Force
Drag Force
Force (lbf)
Force (N)
Time (s)
250
200
150
100
50
0
-50
-100
-150
-200
-250
1000
500
0
-500
-1000
0
2
4
6
8
10
12

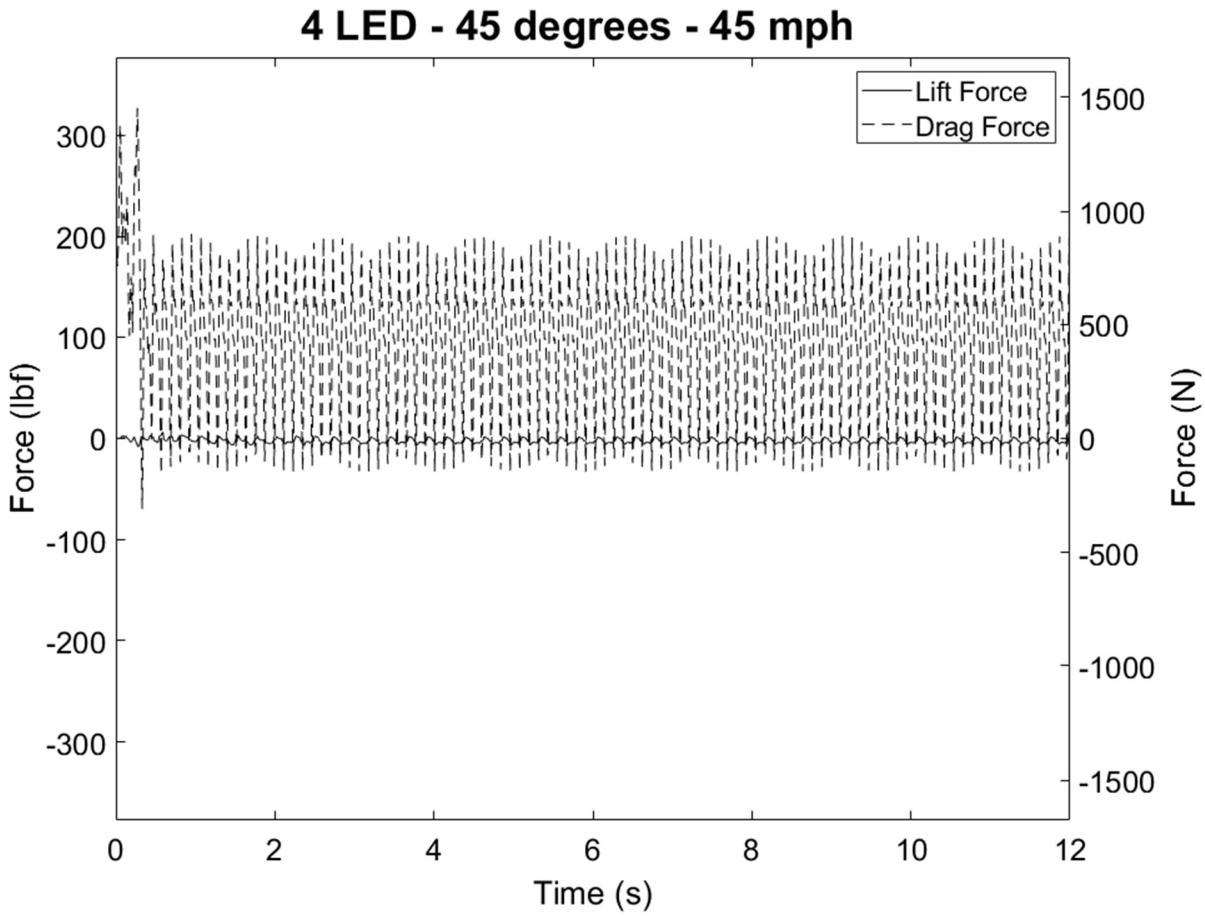
4 LED - 45 degrees - 45 mph
Lift Force
Drag Force
Force (lbf)
Force (N)
Time (s)
300
200
100
0
-100
-200
-300
1500
1000
500
0
-500
-1000
-1500
0
2
4
6
8
10
12

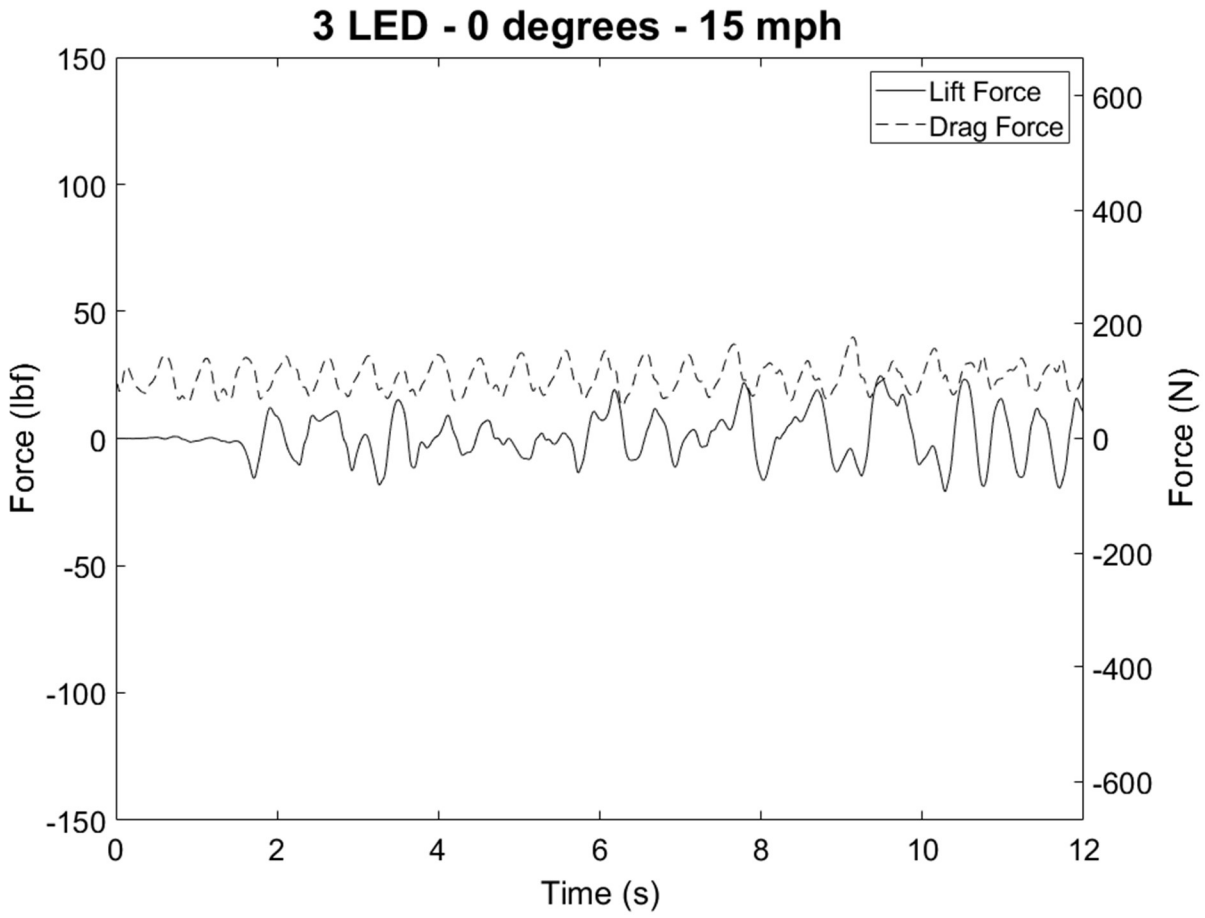
3 LED - 0 degrees - 15 mph
Lift Force
Drag Force
Force (lbf)
Force (N)
Time (s)
150
100
50
0
-50
-100
-150
600
400
200
0
-200
-400
-600
0
2
4
6
8
10
12

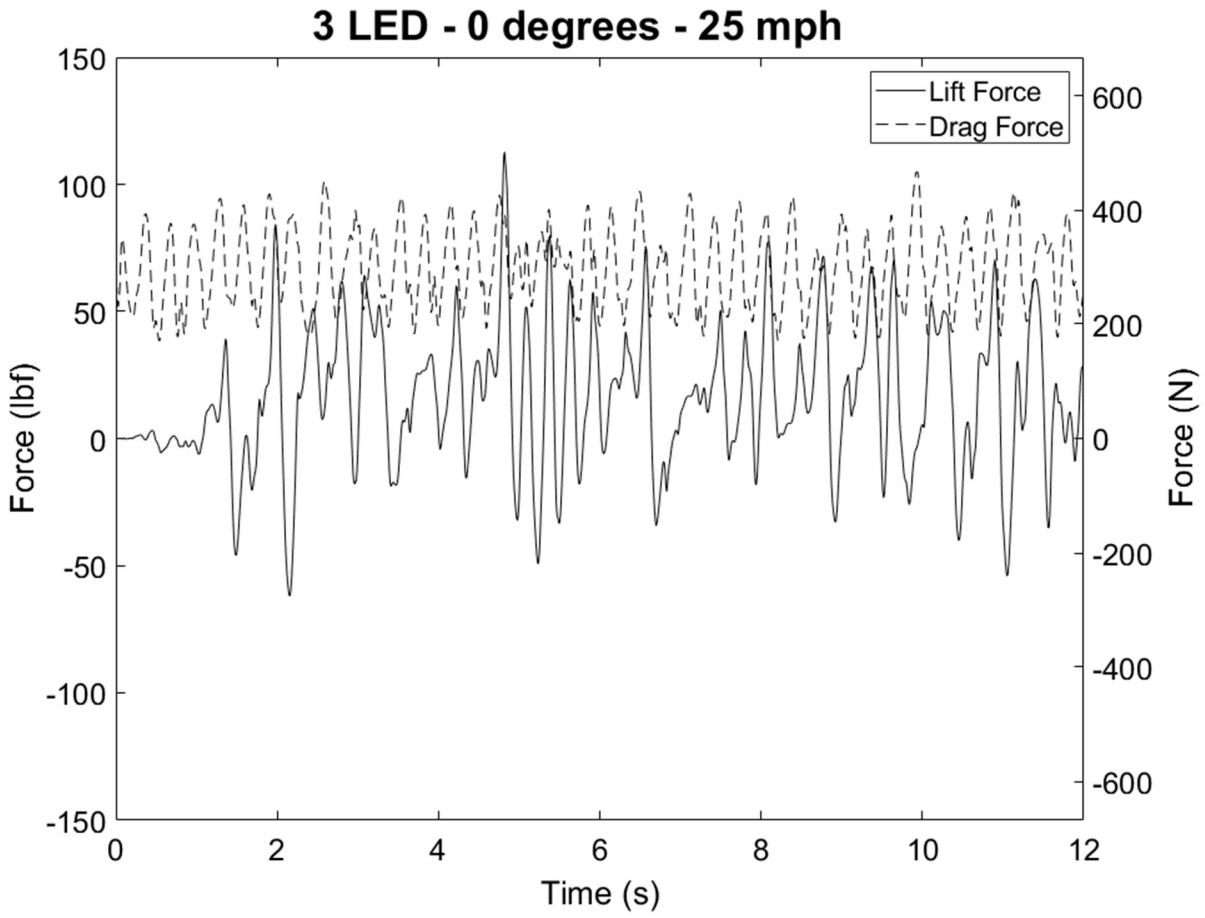
3 LED - 0 degrees - 25 mph
Lift Force
Drag Force
Force (lbf)
Force (N)
Time (s)
150
100
50
0
-50
-100
-150
600
400
200
0
-200
-400
-600
0
2
4
6
8
10
12

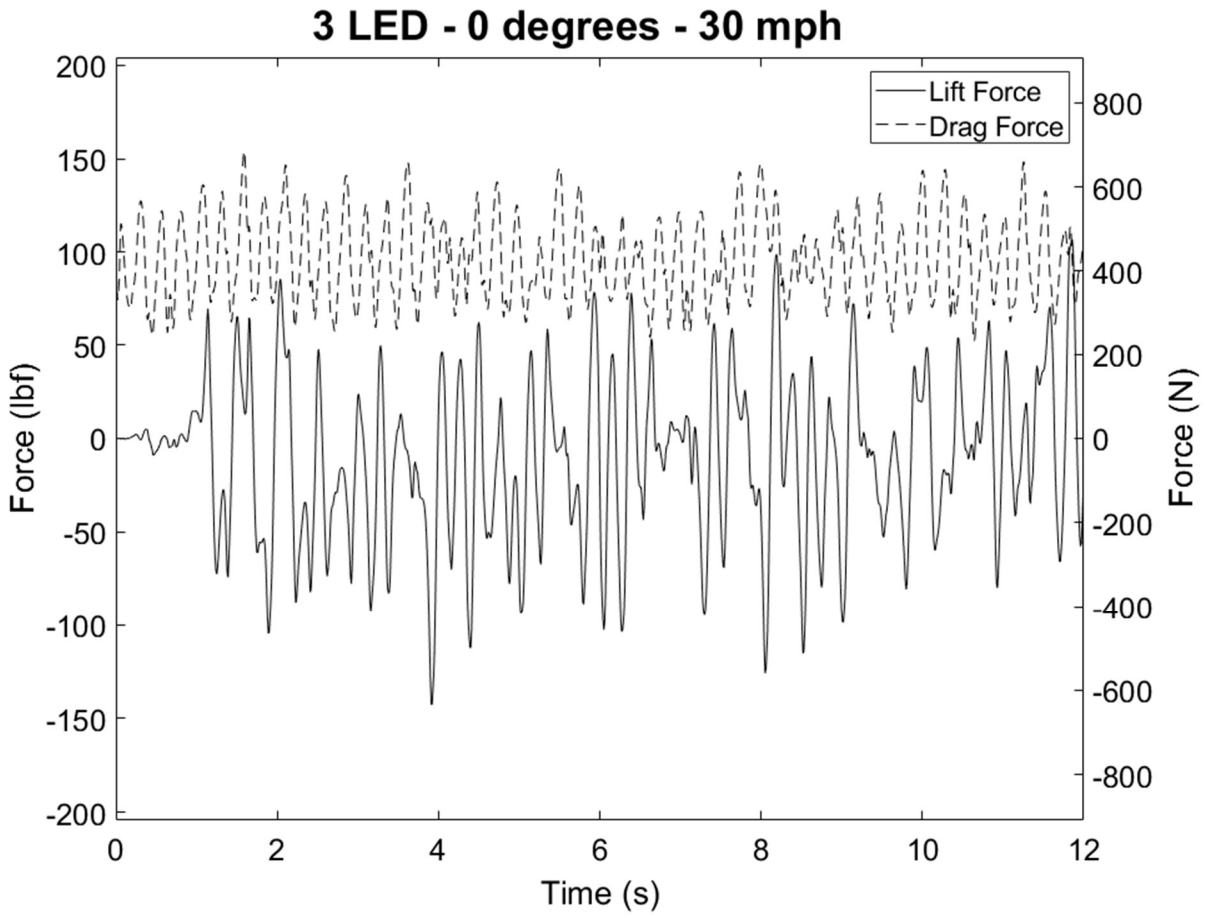
3 LED - 0 degrees - 30 mph
Lift Force
Drag Force
Force (lbf)
Force (N)
Time (s)
200
150
100
50
0
-50
-100
-150
-200
800
600
400
200
0
-200
-400
-600
-800
0
2
4
6
8
10
12

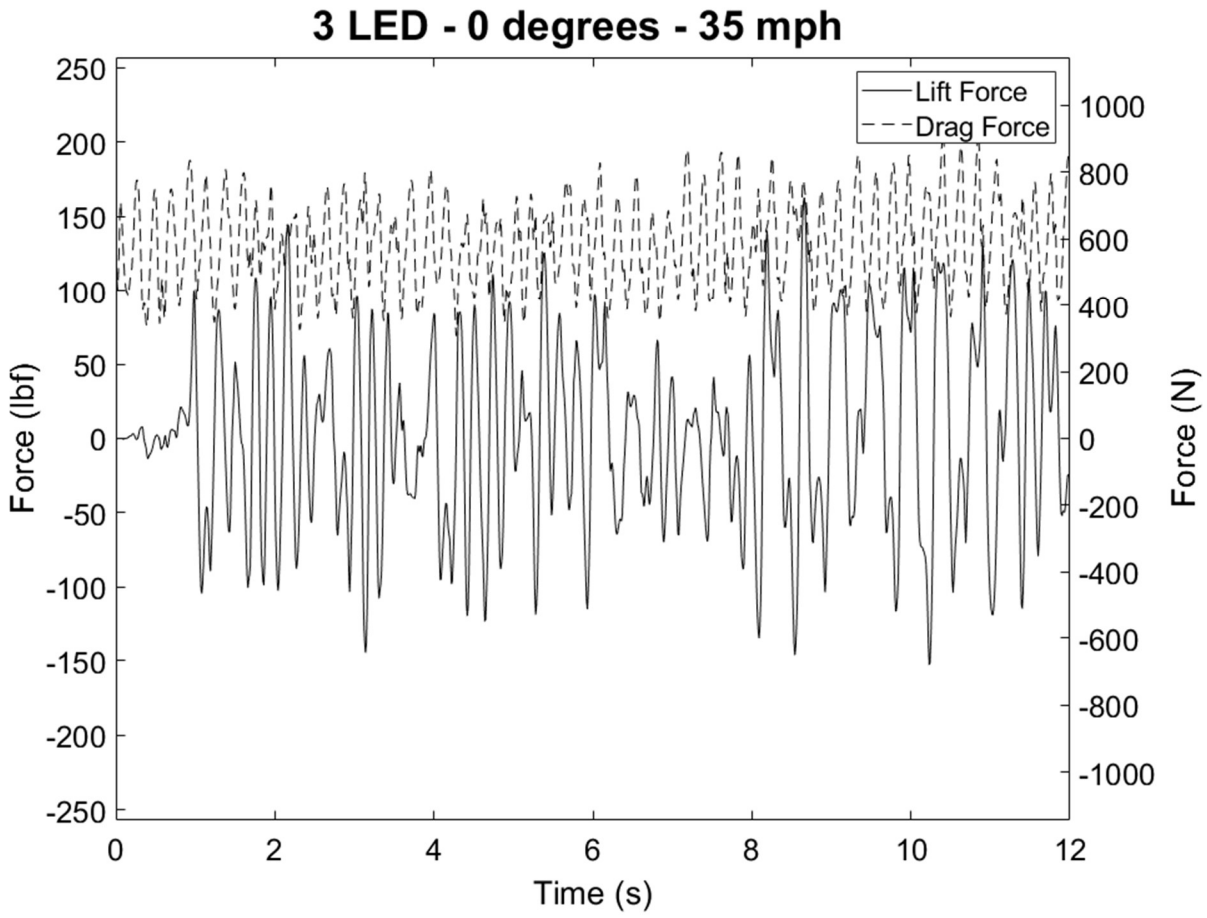
3 LED - 0 degrees - 35 mph
Lift Force
Drag Force
Force (lbf)
Force (N)
Time (s)
250
200
150
100
50
0
-50
-100
-150
-200
-250
1000
800
600
400
200
0
-200
-400
-600
-800
-1000
0
2
4
6
8
10
12

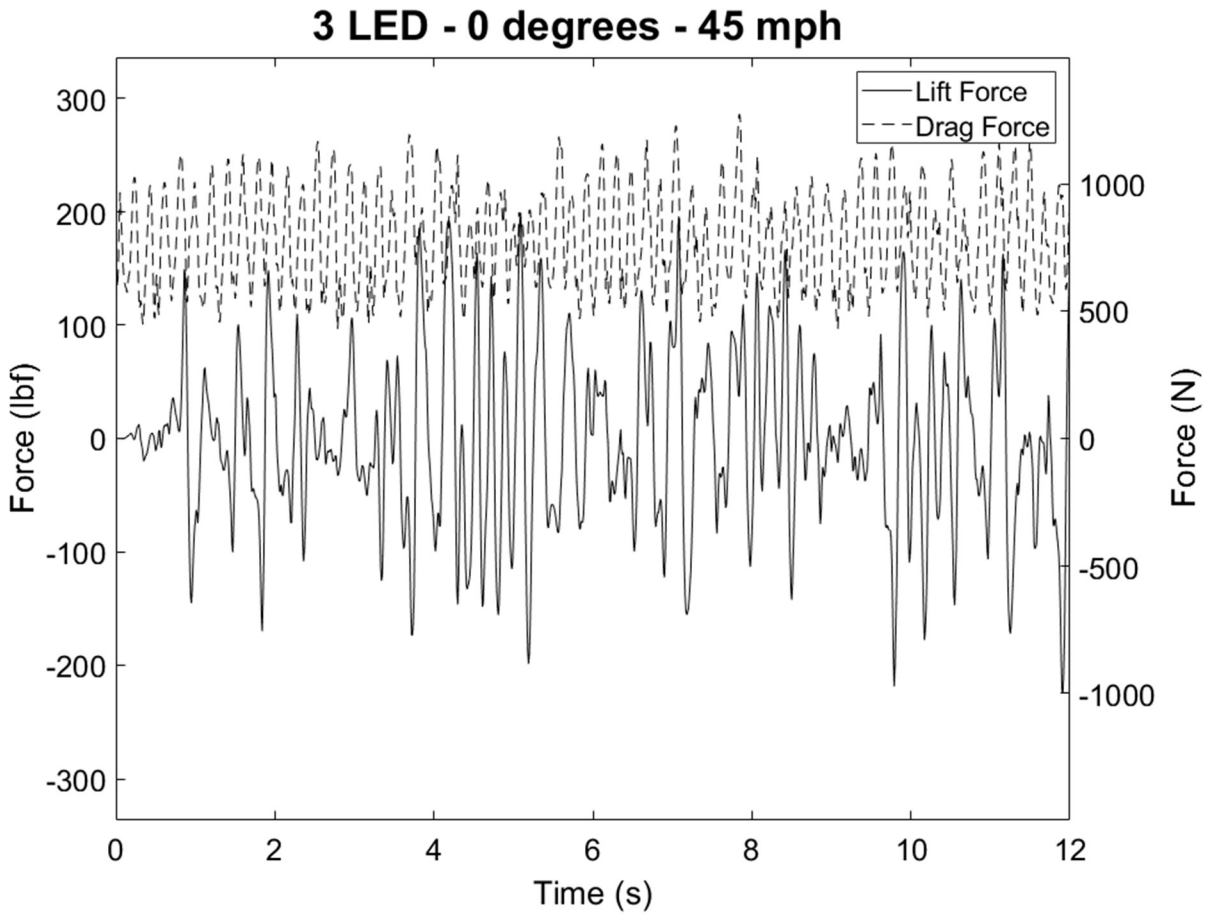
3 LED - 0 degrees - 45 mph
Lift Force
Drag Force
Force (lbf)
Force (N)
Time (s)
300
200
100
0
-100
-200
-300
1000
500
0
-500
-1000
0
2
4
6
8
10
12

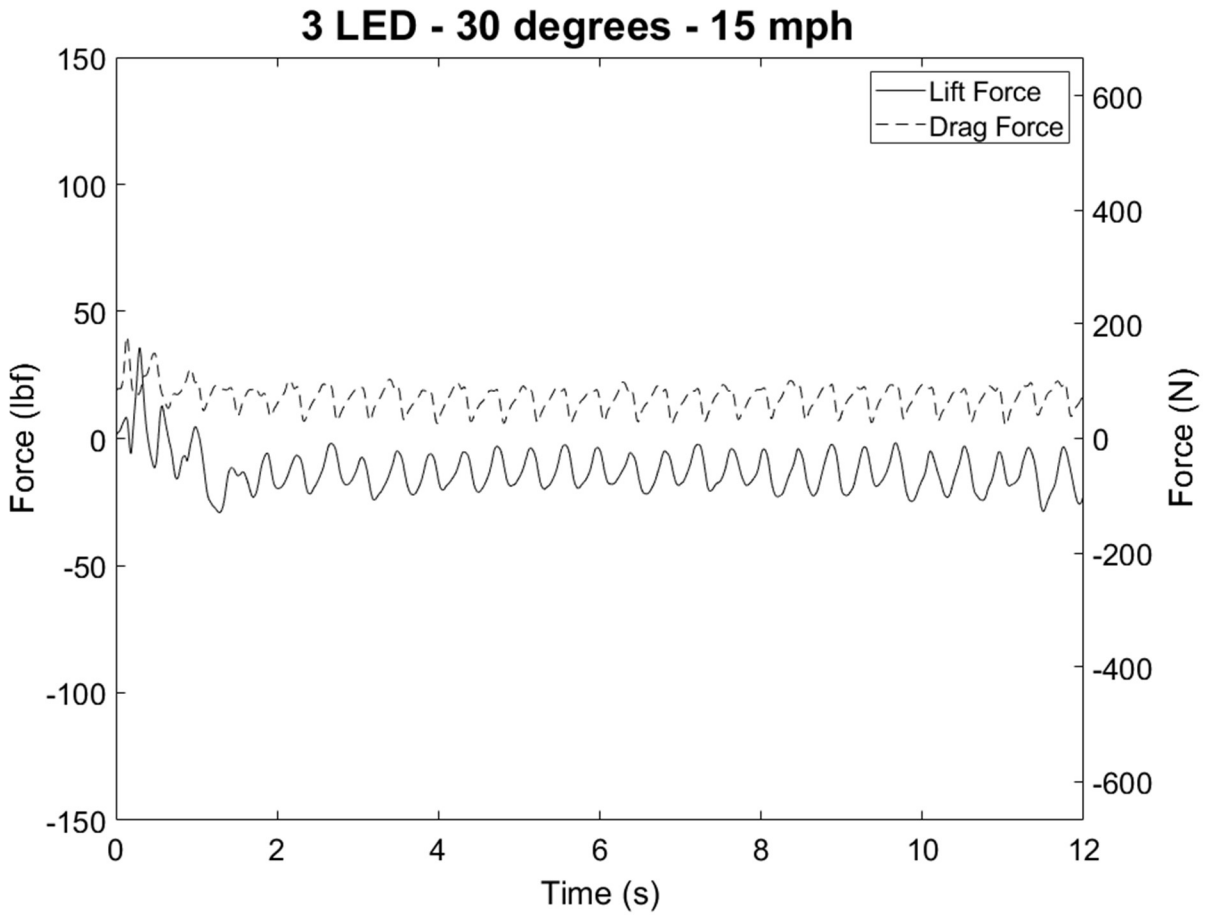
3 LED - 30 degrees - 15 mph
Lift Force
Drag Force
Force (lbf)
Force (N)
Time (s)
150
100
50
0
-50
-100
-150
600
400
200
0
-200
-400
-600
0
2
4
6
8
10
12

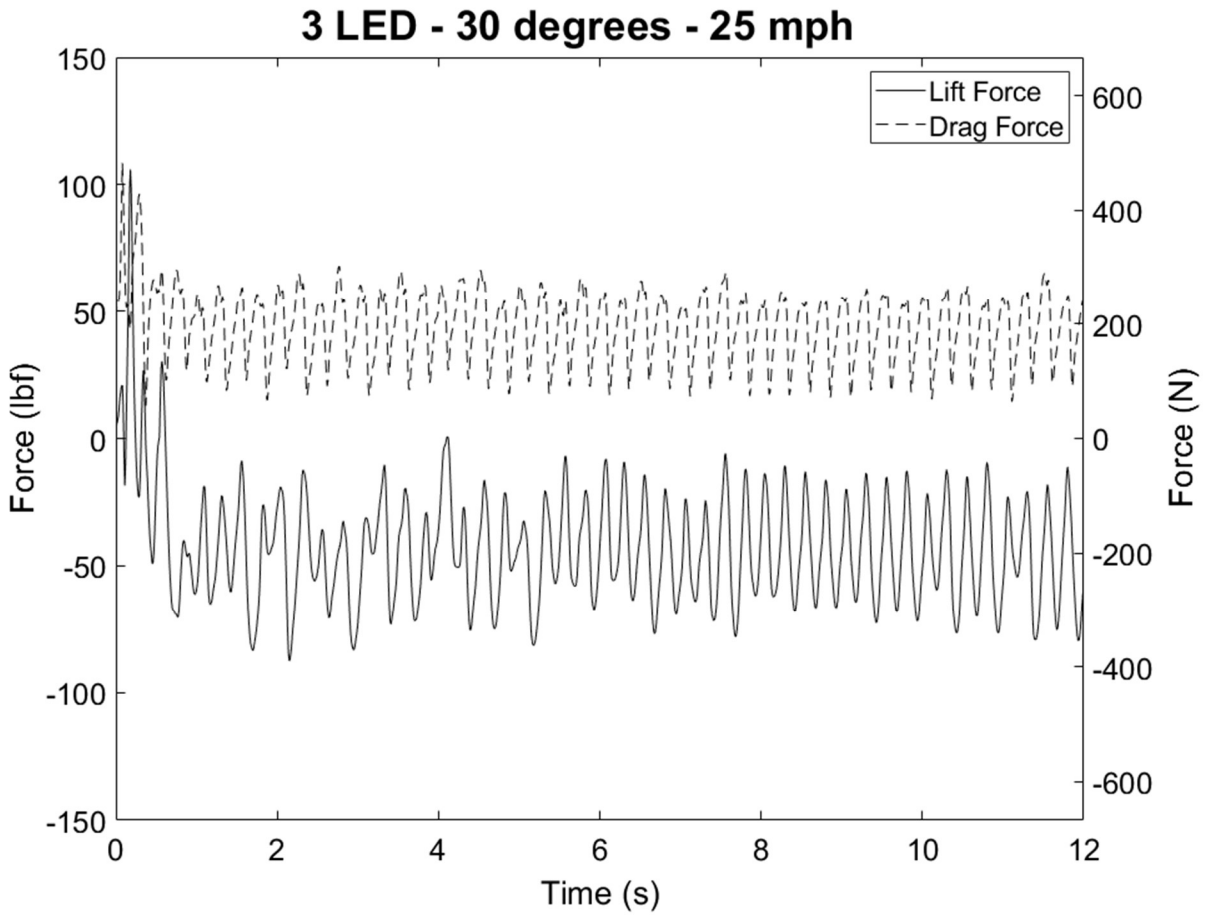
3 LED - 30 degrees - 25 mph
Lift Force
Drag Force
Force (lbf)
Force (N)
Time (s)
150
100
50
0
-50
-100
-150
600
400
200
0
-200
-400
-600
0
2
4
6
8
10
12

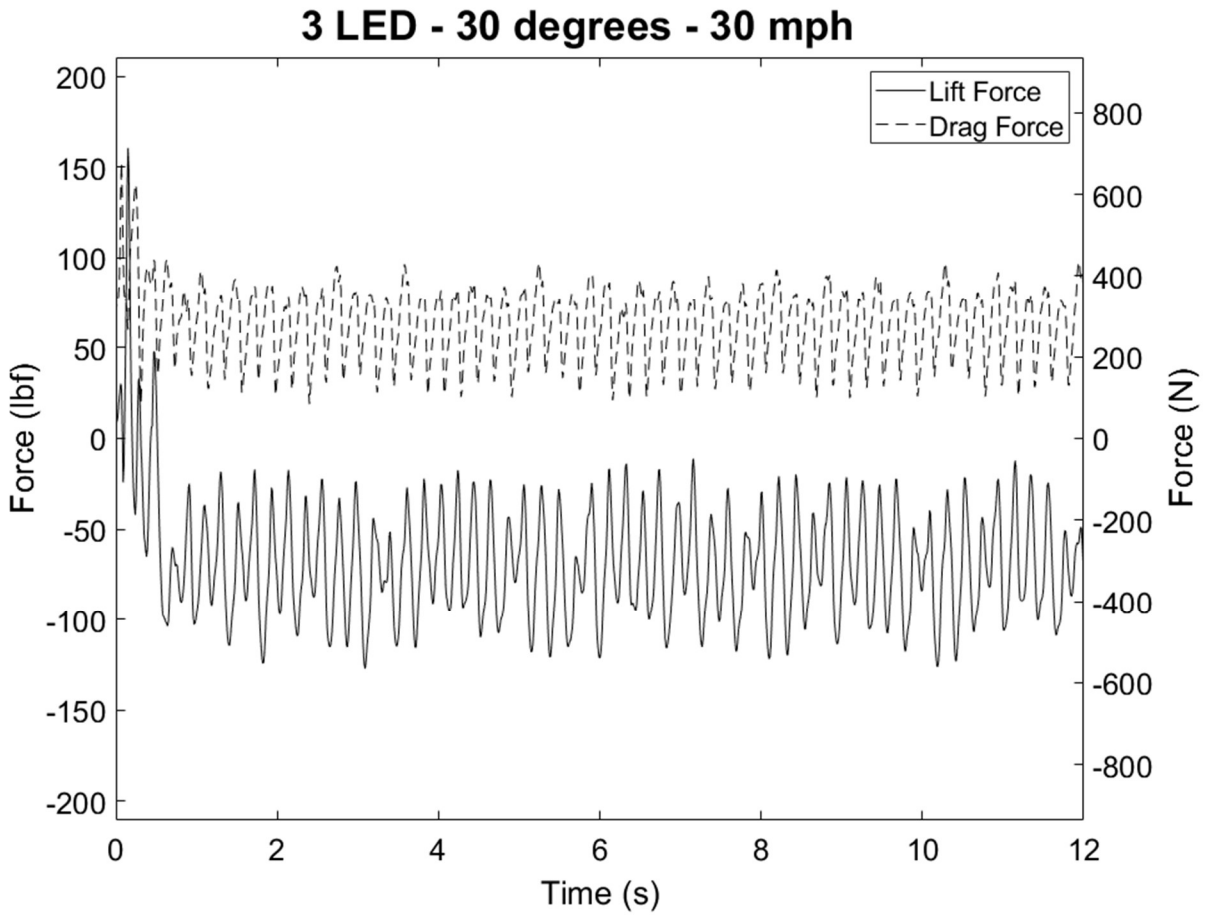
3 LED - 30 degrees - 30 mph
Lift Force
Drag Force
Force (lbf)
Force (N)
Time (s)
200
150
100
50
0
-50
-100
-150
-200
800
600
400
200
0
-200
-400
-600
-800
0
2
4
6
8
10
12

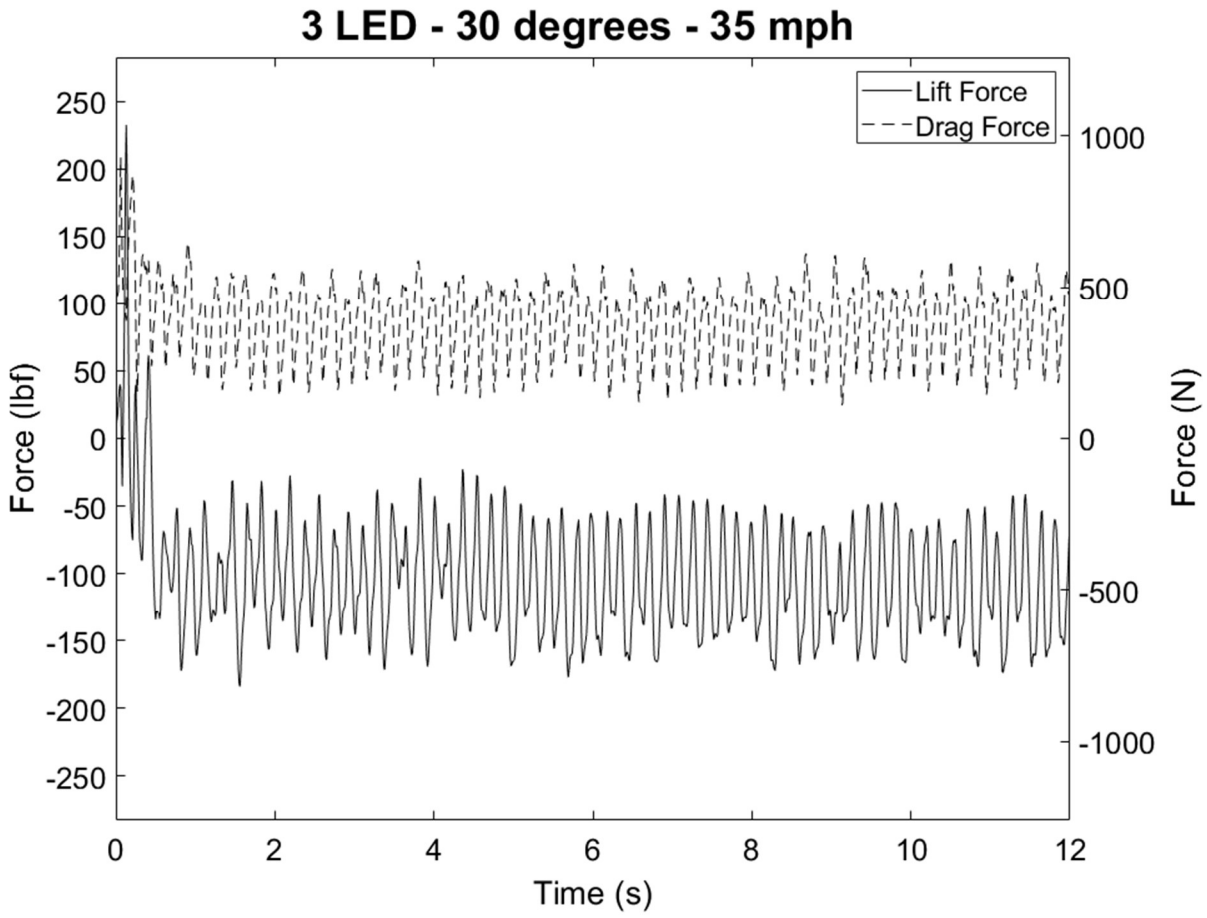
3 LED - 30 degrees - 35 mph
Lift Force
Drag Force
Force (lbf)
Force (N)
Time (s)
250
200
150
100
50
0
-50
-100
-150
-200
-250
1000
500
0
-500
-1000
0
2
4
6
8
10
12

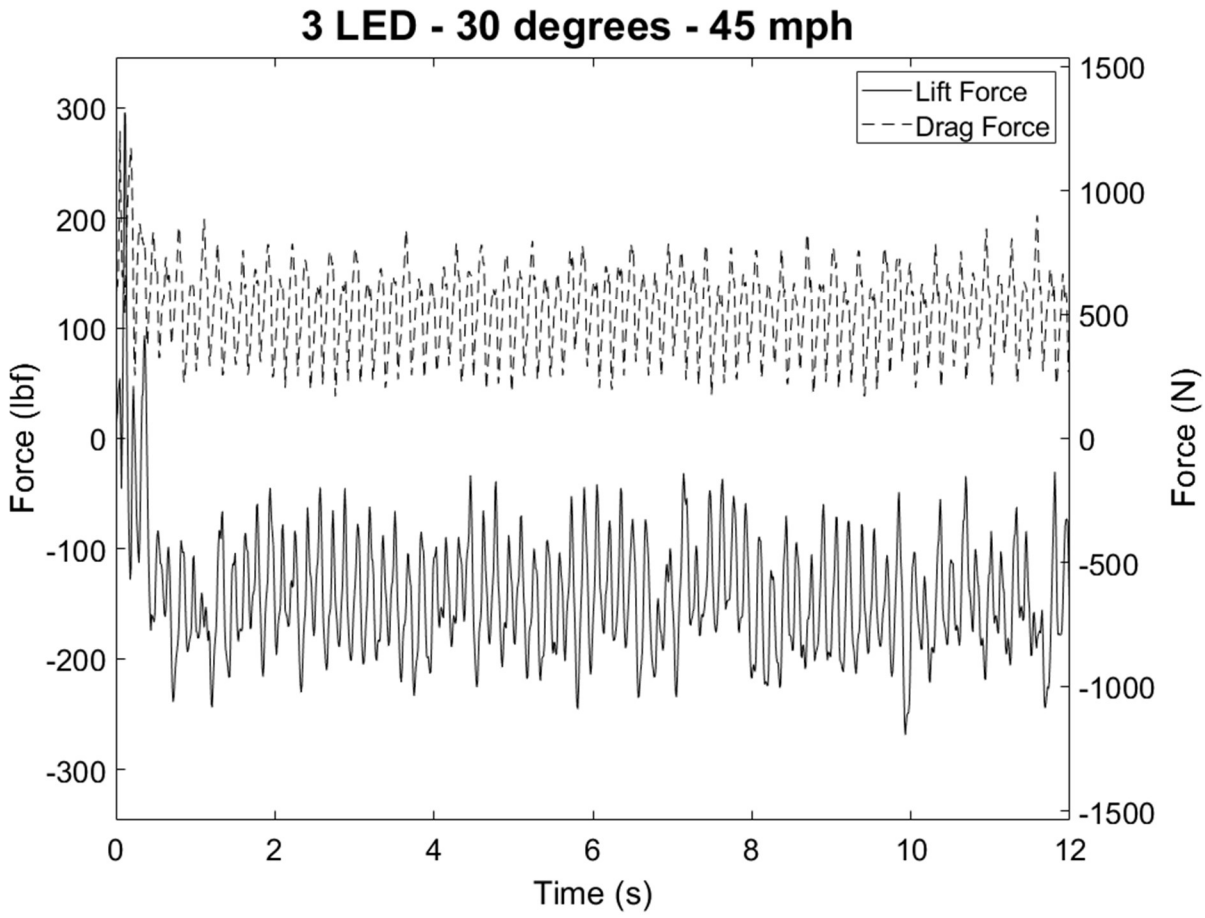
3 LED - 30 degrees - 45 mph
Lift Force
Drag Force
Force (lbf)
Force (N)
Time (s)
300
200
100
0
-100
-200
-300
1500
1000
500
0
-500
-1000
-1500
0
2
4
6
8
10
12

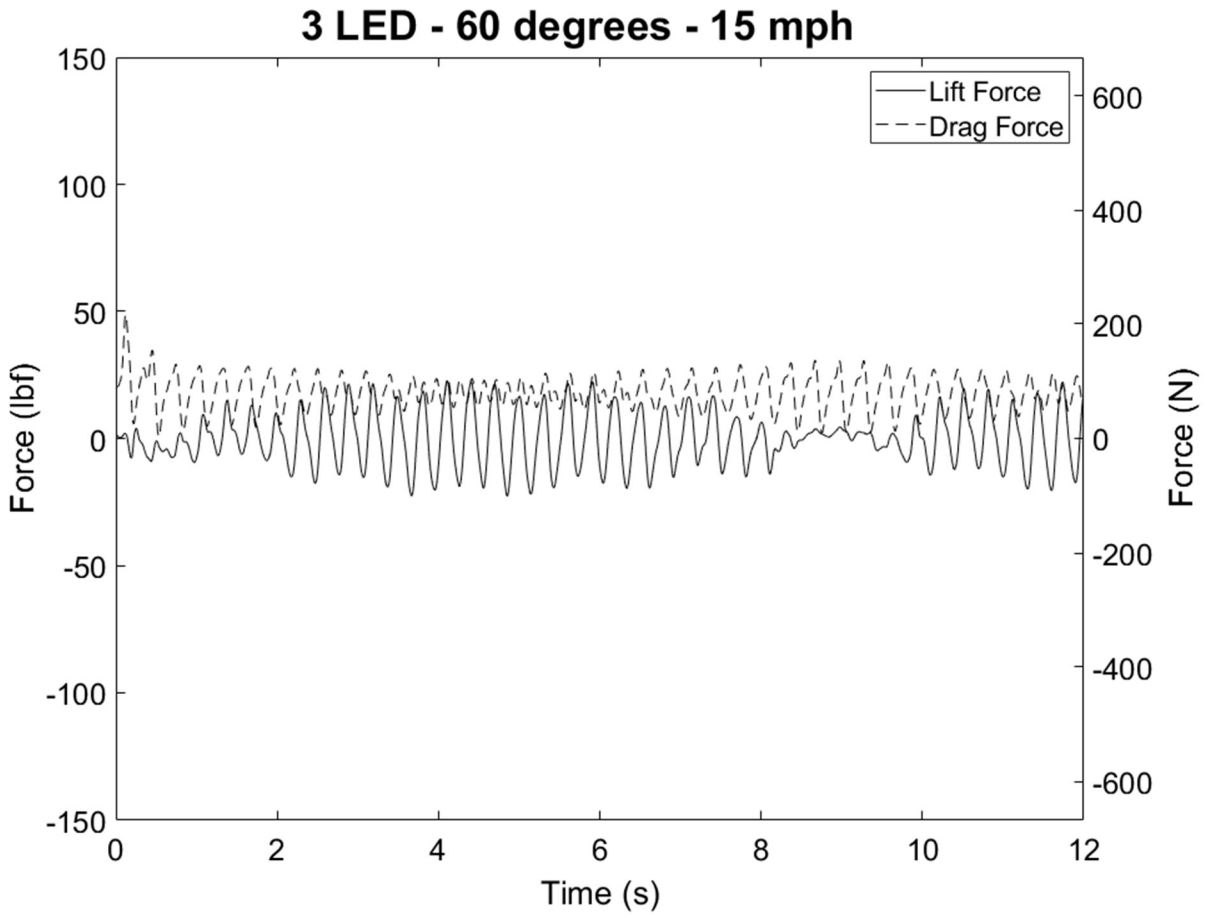
3 LED - 60 degrees - 15 mph
Lift Force
Drag Force
Force (lbf)
Force (N)
Time (s)
150
100
50
0
-50
-100
-150
600
400
200
0
-200
-400
-600
0
2
4
6
8
10
12

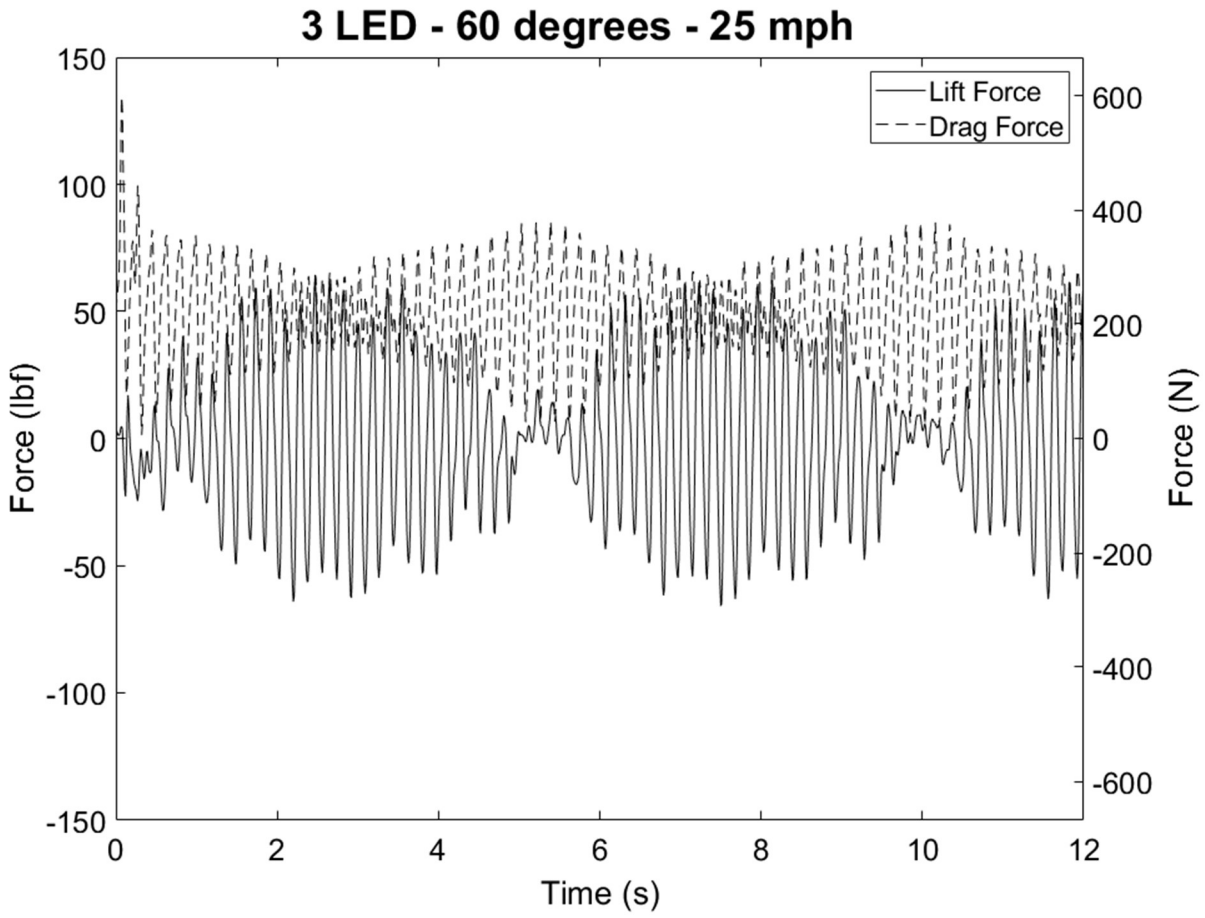
3 LED - 60 degrees - 25 mph
Lift Force
Drag Force
Force (lbf)
Force (N)
Time (s)
150
100
50
0
-50
-100
-150
600
400
200
0
-200
-400
-600
0
2
4
6
8
10
12

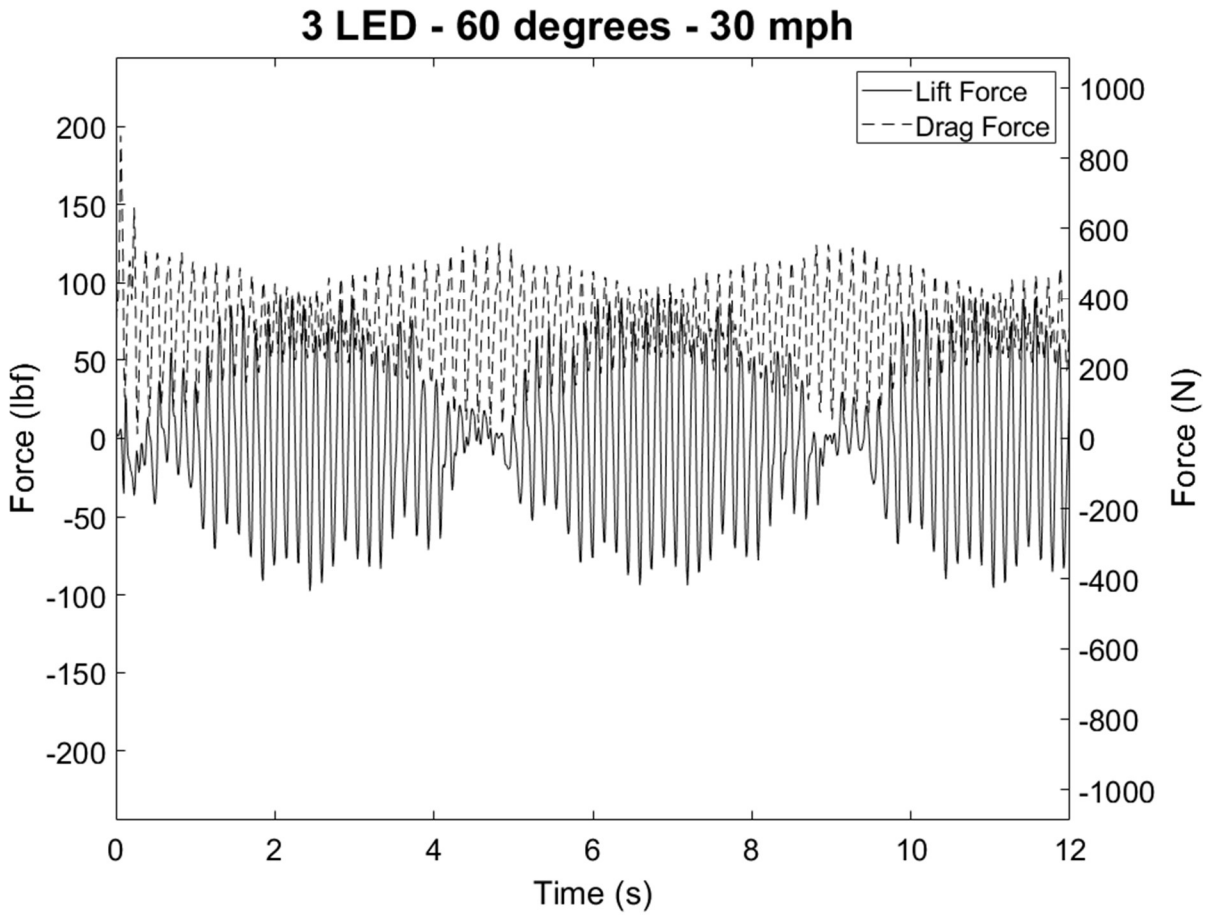
3 LED - 60 degrees - 30 mph
Lift Force
Drag Force
Force (lbf)
Force (N)
Time (s)
200
150
100
50
0
-50
-100
-150
-200
1000
800
600
400
200
0
-200
-400
-600
-800
-1000
0
2
4
6
8
10
12

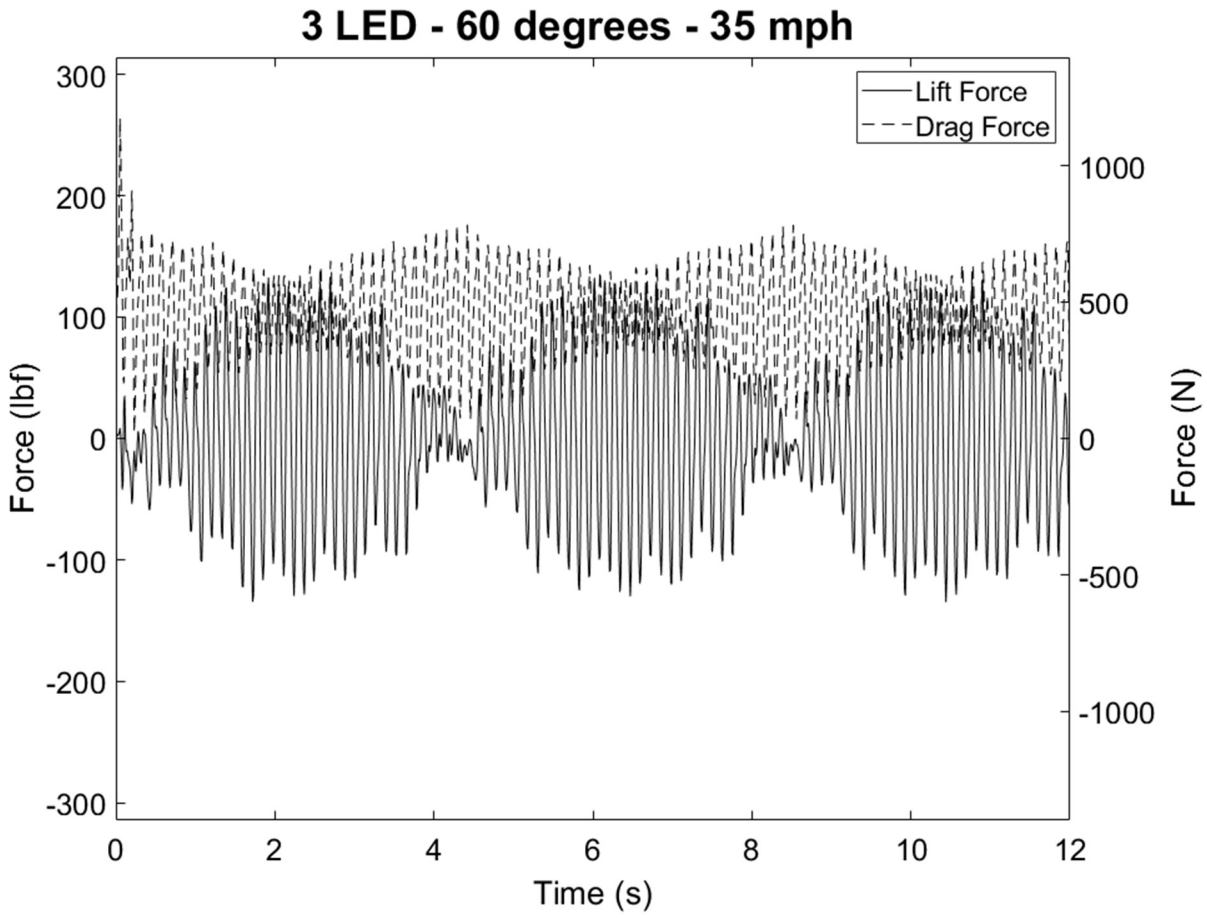
3 LED - 60 degrees - 35 mph
Lift Force
Drag Force
Force (lbf)
Force (N)
Time (s)
300
200
100
0
-100
-200
-300
1000
500
0
-500
-1000
0
2
4
6
8
10
12

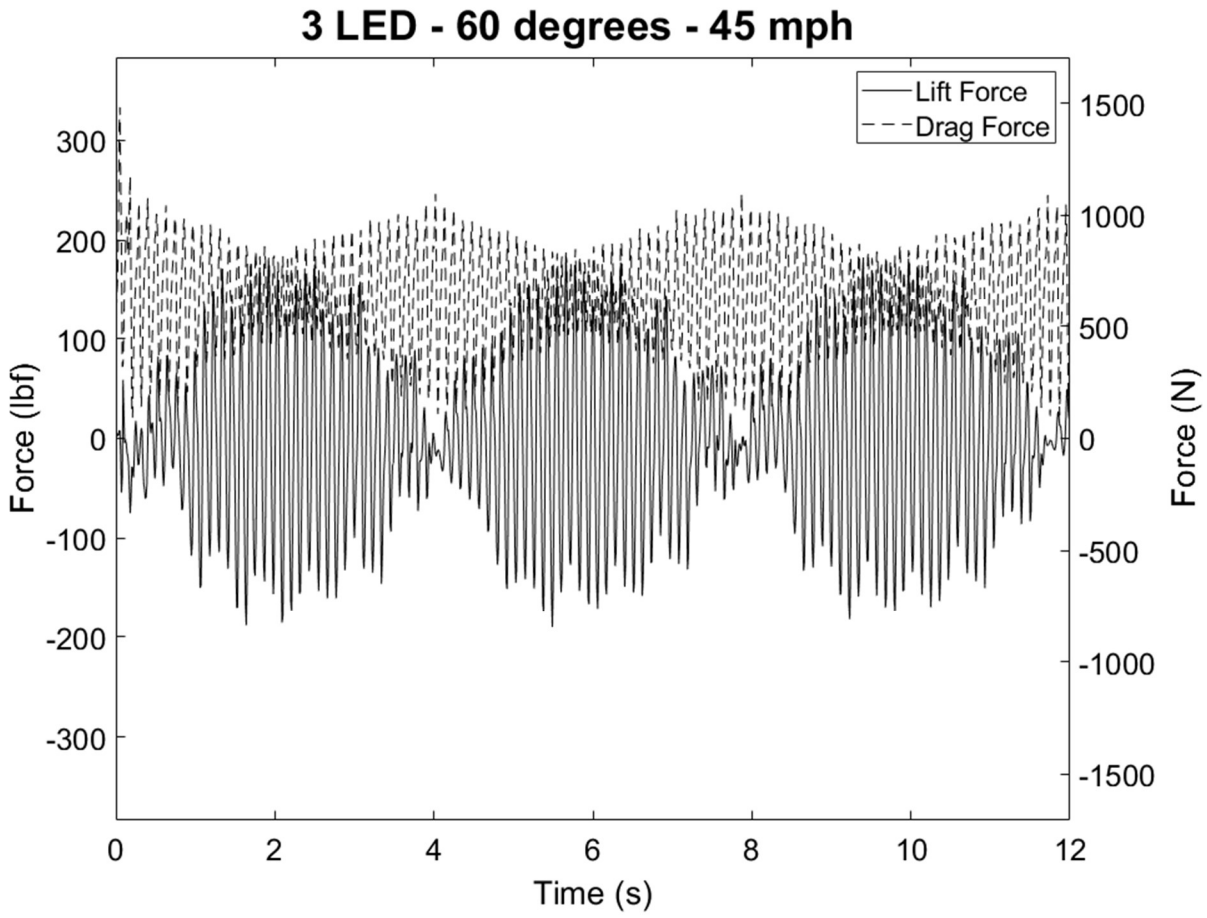
3 LED - 60 degrees - 45 mph
Lift Force
Drag Force
Force (lbf)
Force (N)
Time (s)
300
200
100
0
-100
-200
-300
1500
1000
500
0
-500
-1000
-1500
0
2
4
6
8
10
12

APPENDIX A2

A2.1 Power Spectral Density Plots for Abaqus Simulations

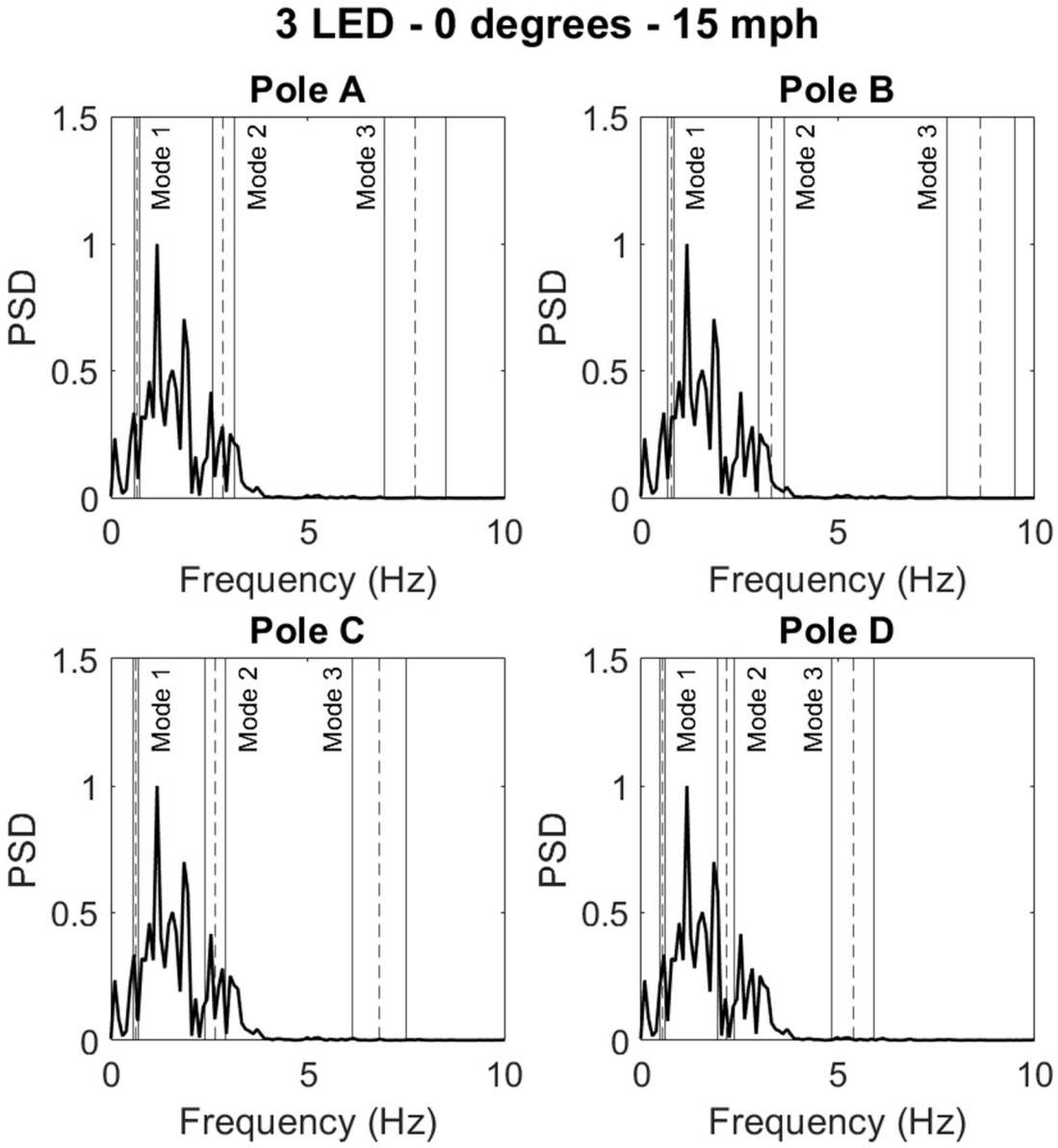

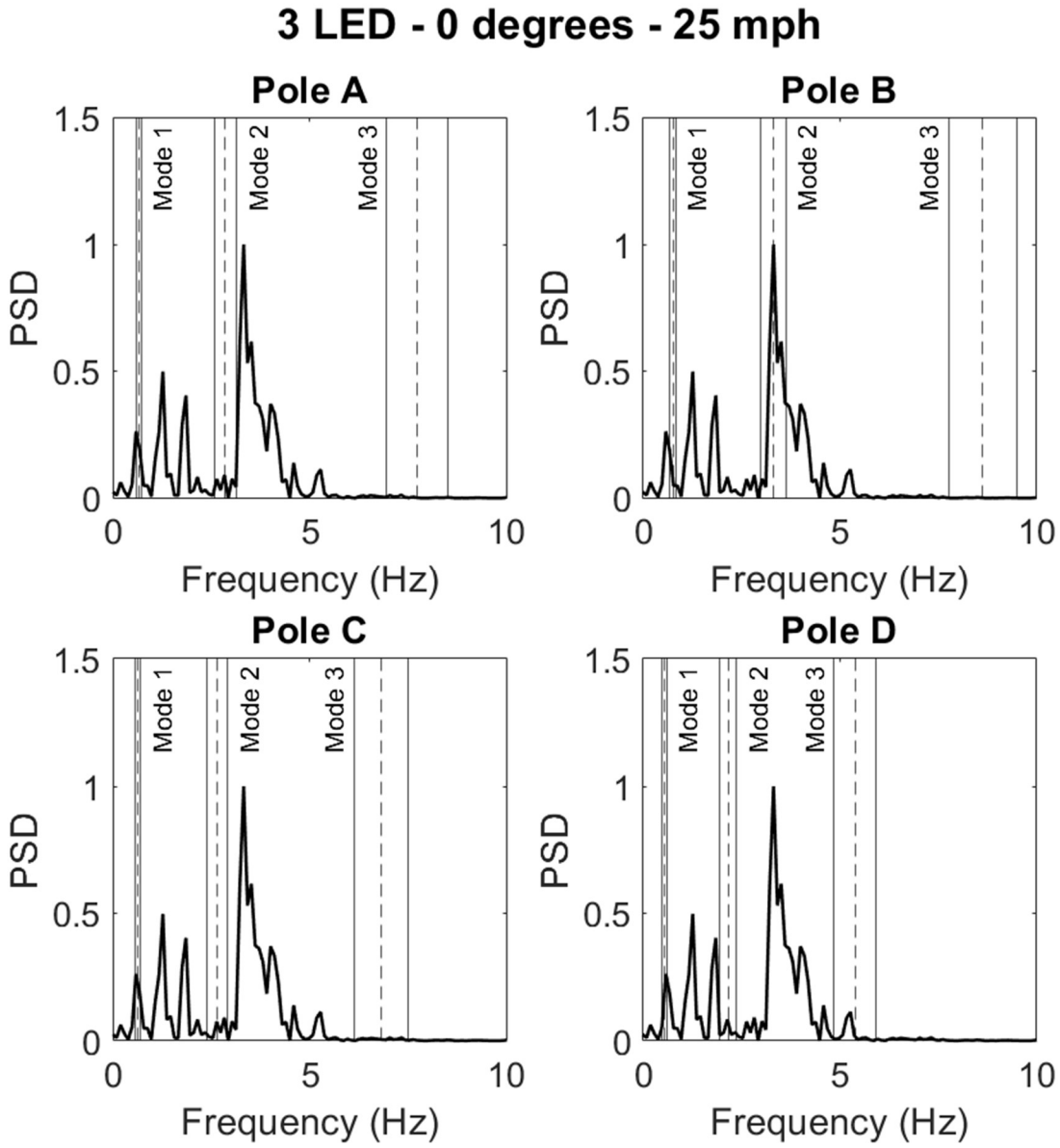
3 LED - 0 degrees - 25 mph
Pole A
Pole B
Pole C
Pole D
Mode 1
Mode 2
Mode 3
PSD
Frequency (Hz)
0
0.5
1
1.5
5
10

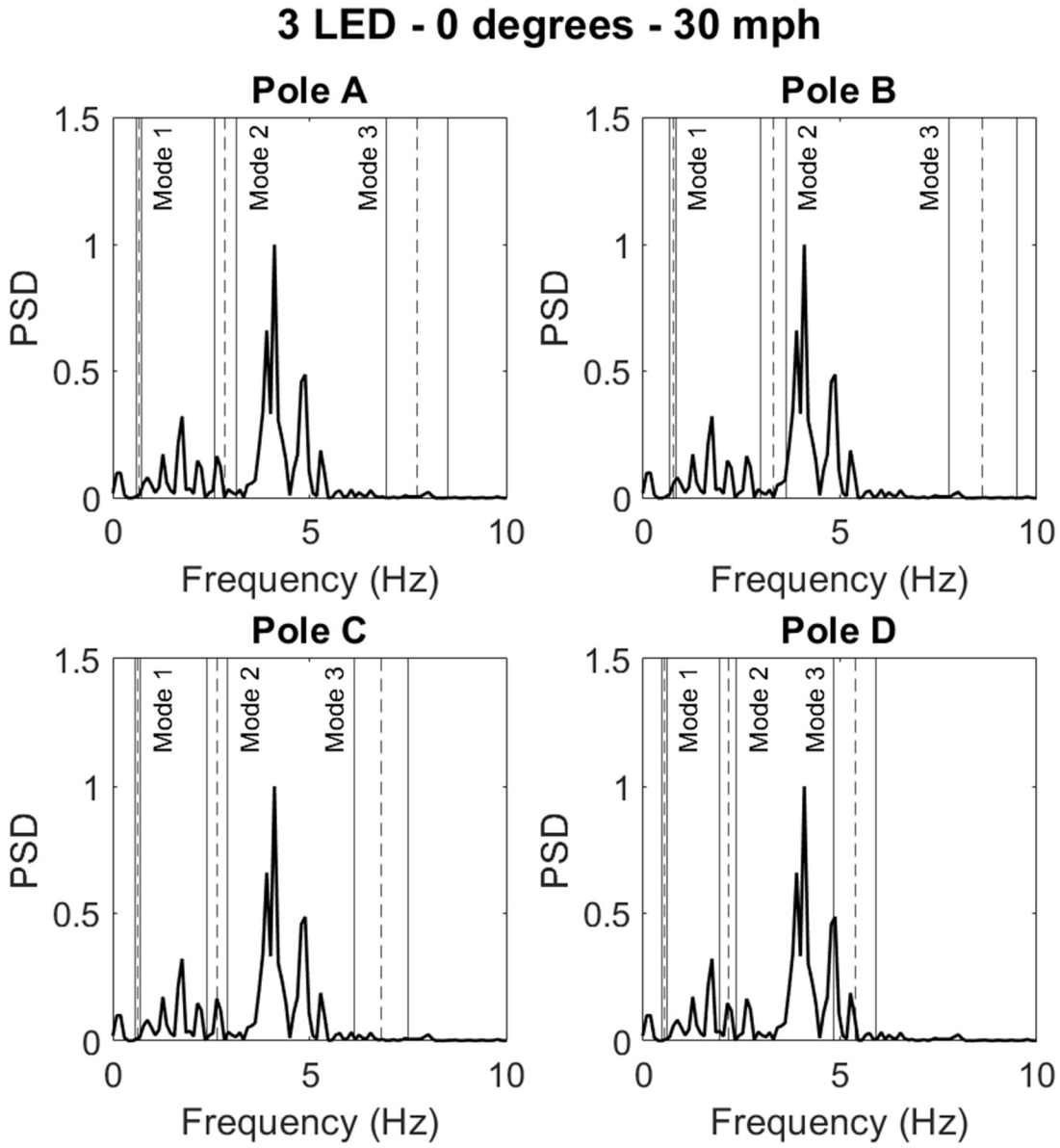
3 LED - 0 degrees - 30 mph
Pole A
Pole B
Pole C
Pole D
Mode 1
Mode 2
Mode 3
PSD
Frequency (Hz)
0
0.5
1
1.5
5
10

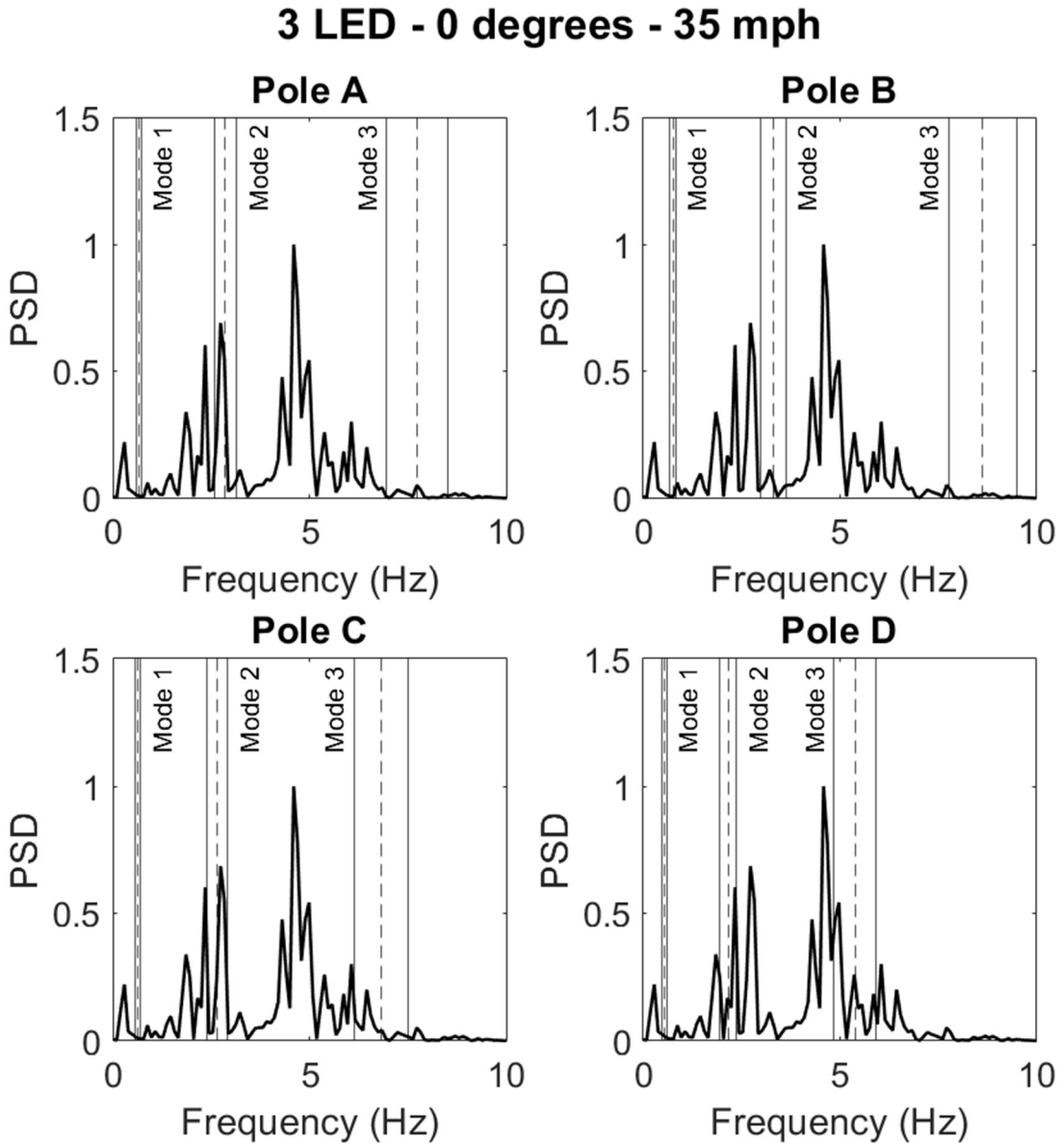
3 LED - 0 degrees - 35 mph
Pole A
Pole B
Pole C
Pole D
Mode 1
Mode 2
Mode 3
PSD
Frequency (Hz)
0
0.5
1
1.5
5
10

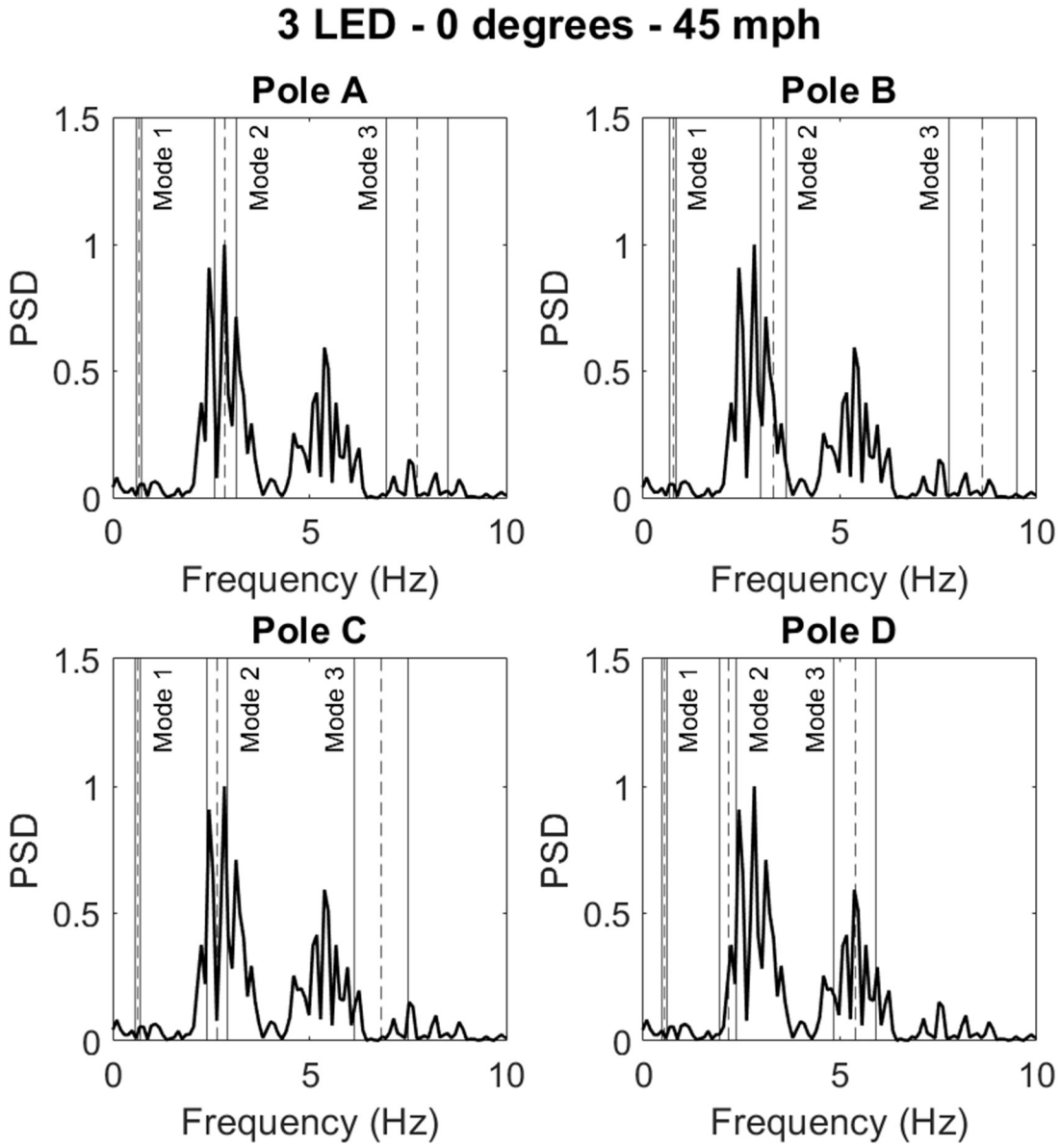
3 LED - 0 degrees - 45 mph
Pole A
Pole B
Pole C
Pole D
Mode 1
Mode 2
Mode 3
PSD
Frequency (Hz)
0
0.5
1
1.5
5
10

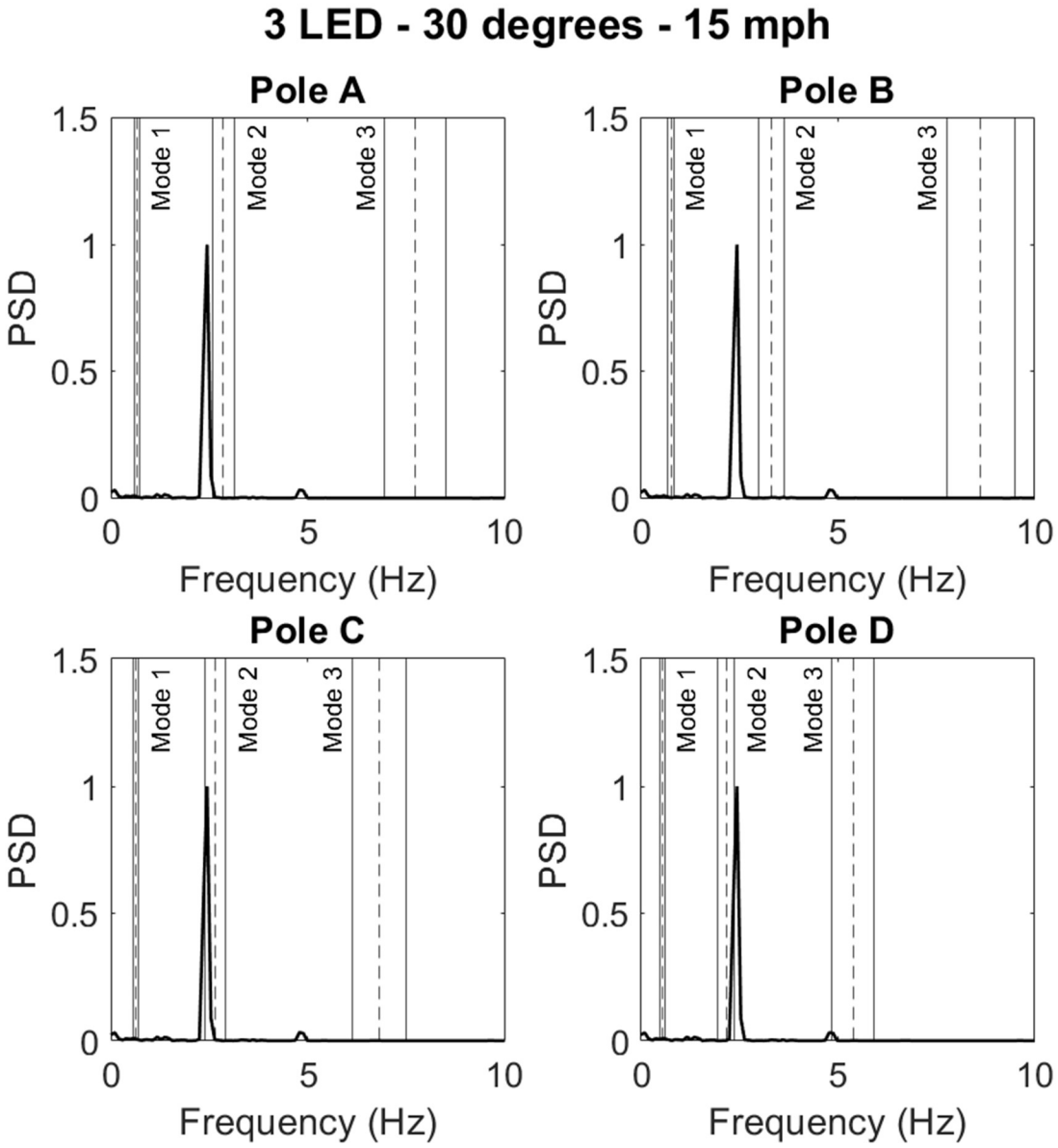
3 LED - 30 degrees - 15 mph
Pole A
Pole B
Pole C
Pole D
Mode 1
Mode 2
Mode 3
PSD
Frequency (Hz)
0
0.5
1
1.5
5
10

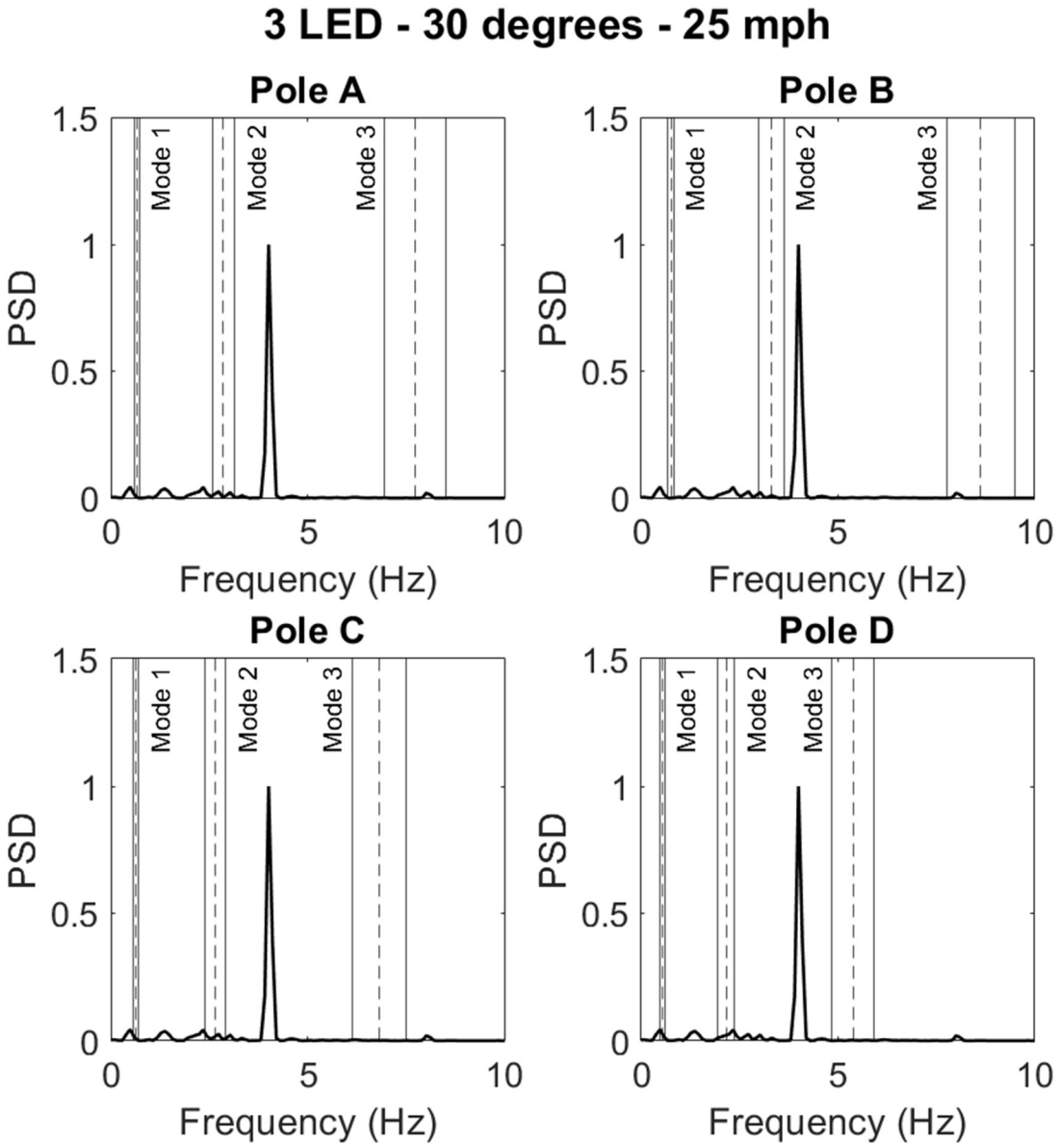
3 LED - 30 degrees - 25 mph
Pole A
Pole B
Pole C
Pole D
Mode 1
Mode 2
Mode 3
PSD
Frequency (Hz)
0
0.5
1
1.5
5
10

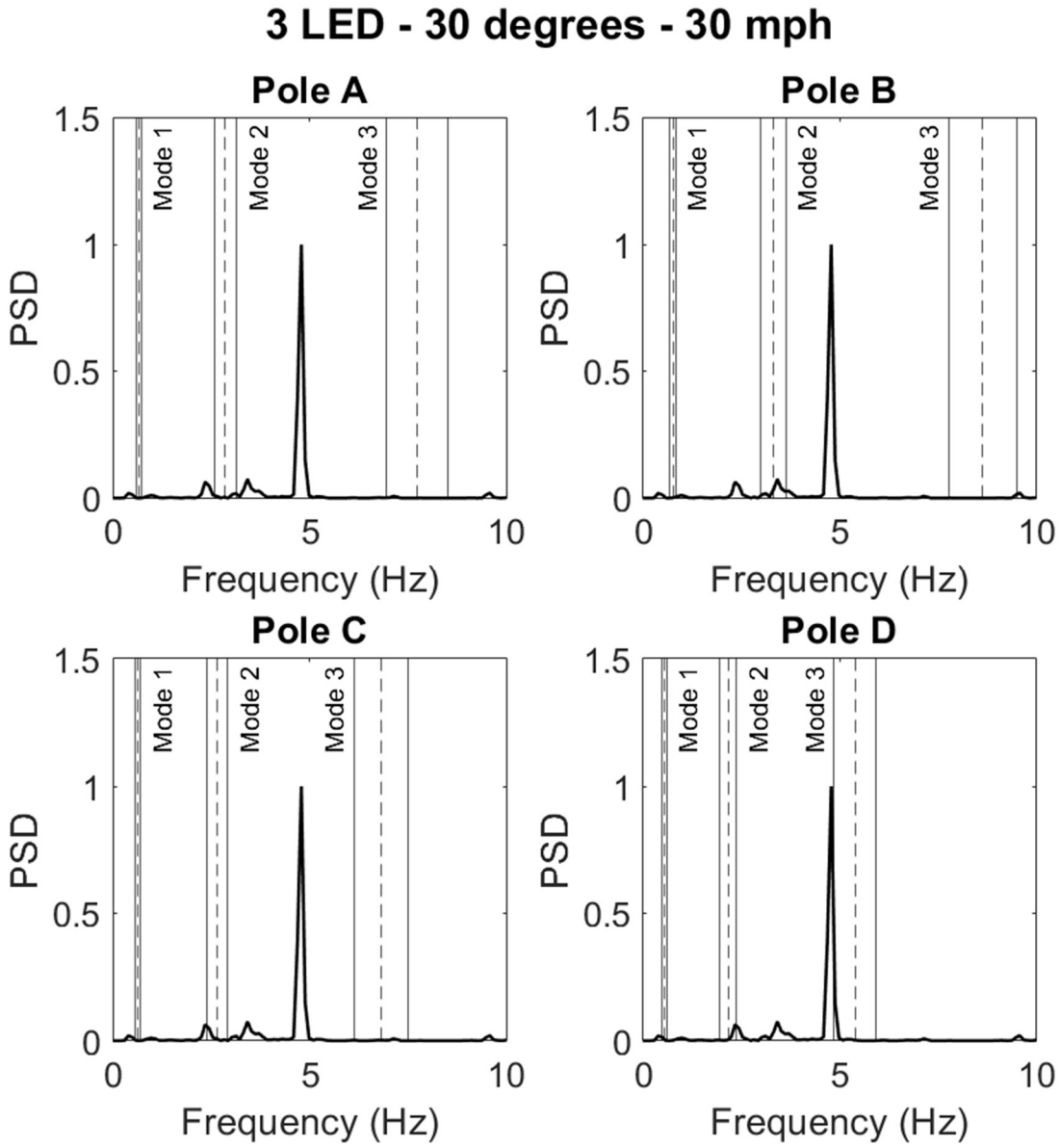
3 LED - 30 degrees - 30 mph
Pole A
Pole B
Pole C
Pole D
Mode 1
Mode 2
Mode 3
PSD
Frequency (Hz)
0
0.5
1
1.5
5
10

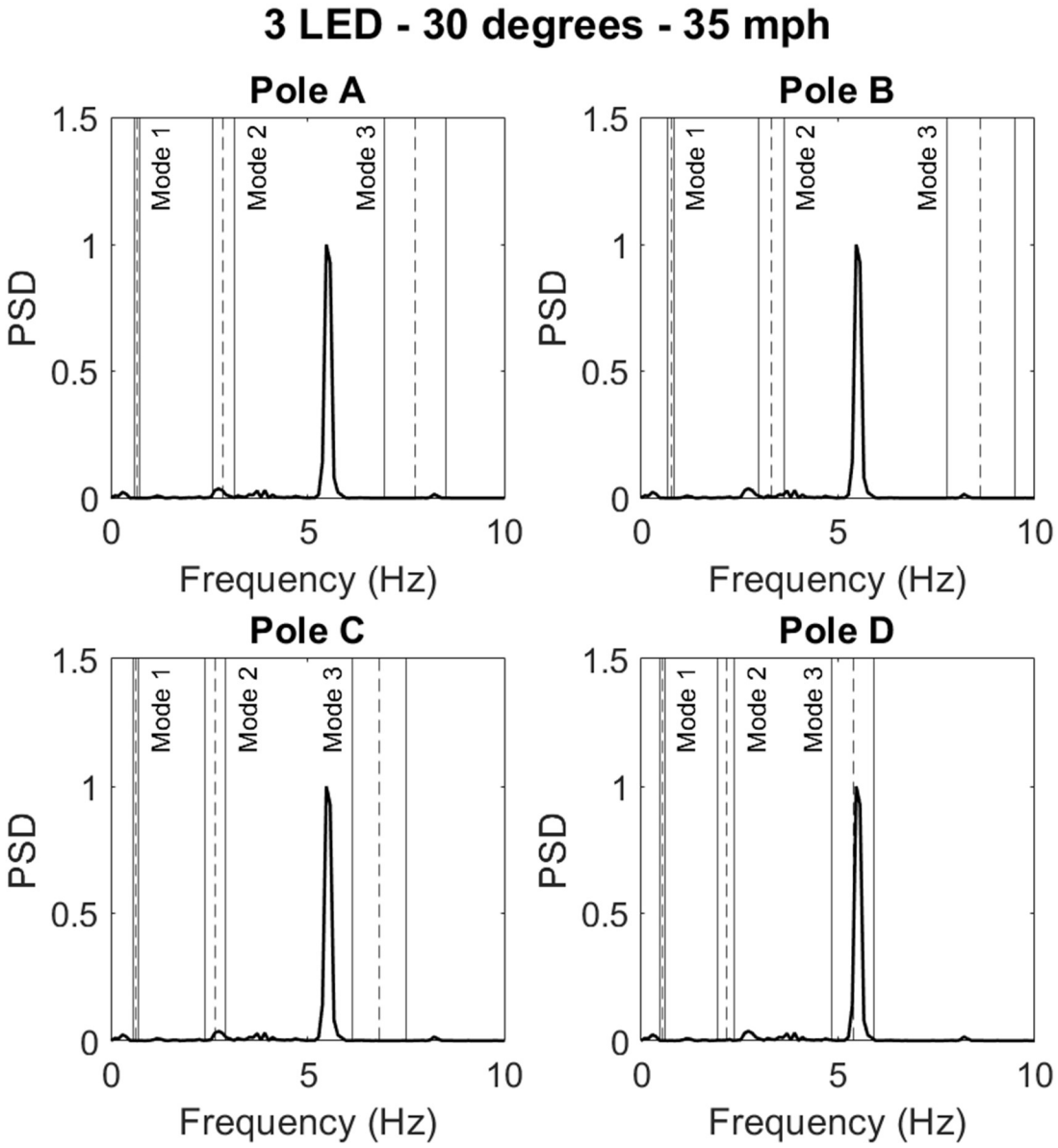
3 LED - 30 degrees - 35 mph
Pole A
Pole B
Pole C
Pole D
Mode 1
Mode 2
Mode 3
PSD
Frequency (Hz)
0
0.5
1
1.5
5
10

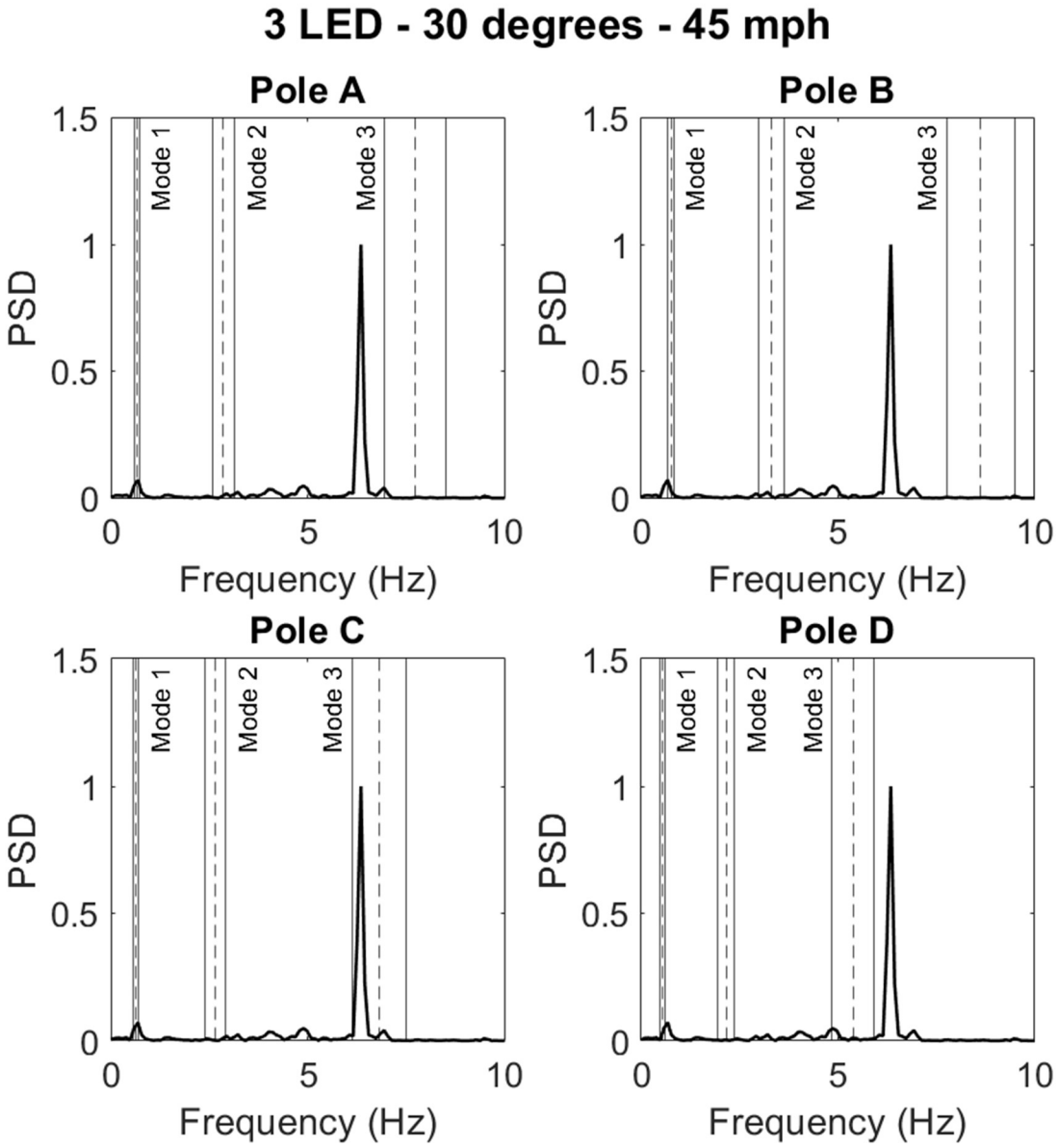
3 LED - 30 degrees - 45 mph
Pole A
Pole B
Pole C
Pole D
Mode 1
Mode 2
Mode 3
PSD
Frequency (Hz)
0
0.5
1
1.5
5
10

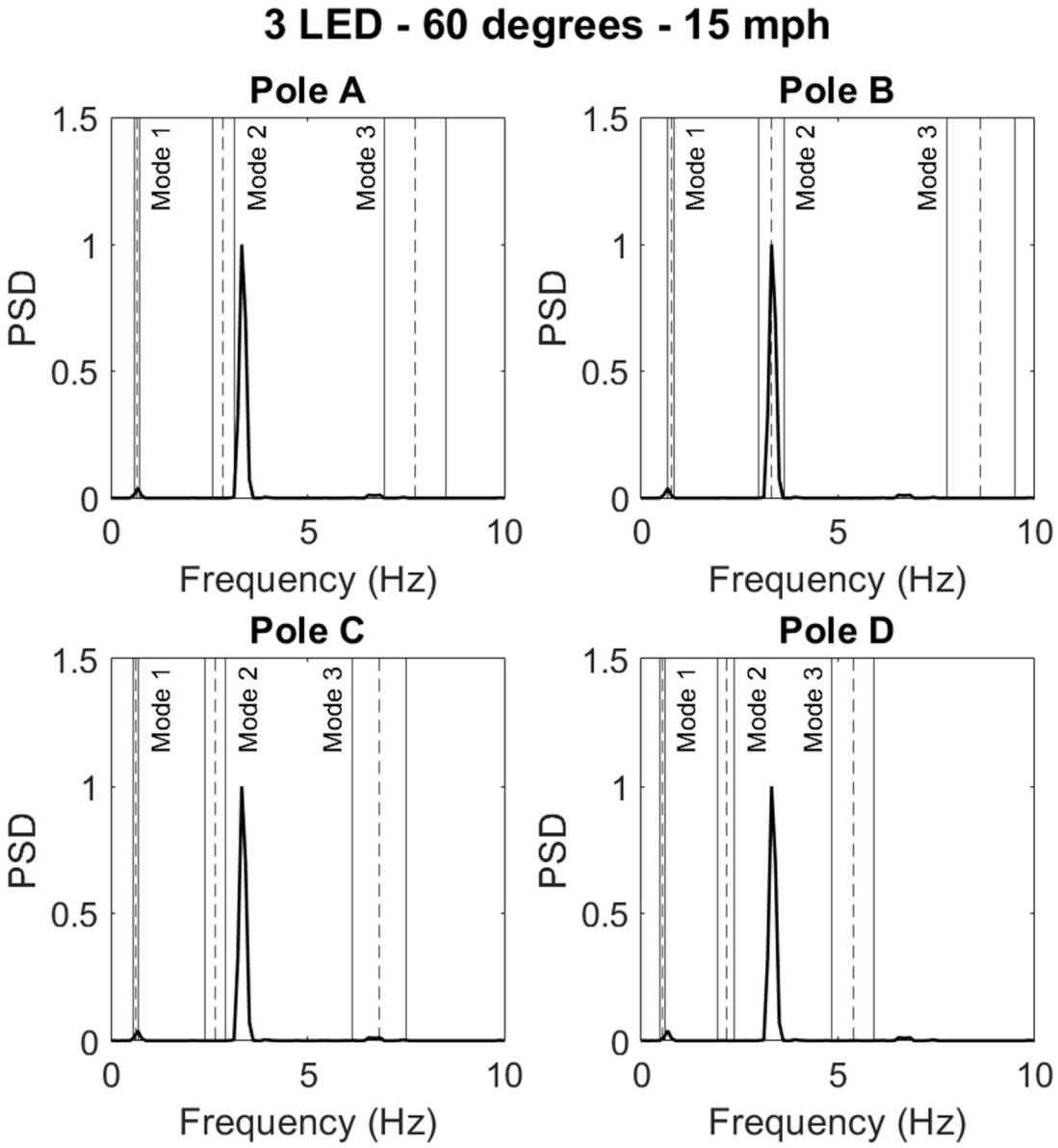
3 LED - 60 degrees - 15 mph
Pole A
Pole B
Pole C
Pole D
Mode 1
Mode 2
Mode 3
PSD
Frequency (Hz)
0
0.5
1
1.5
5
10

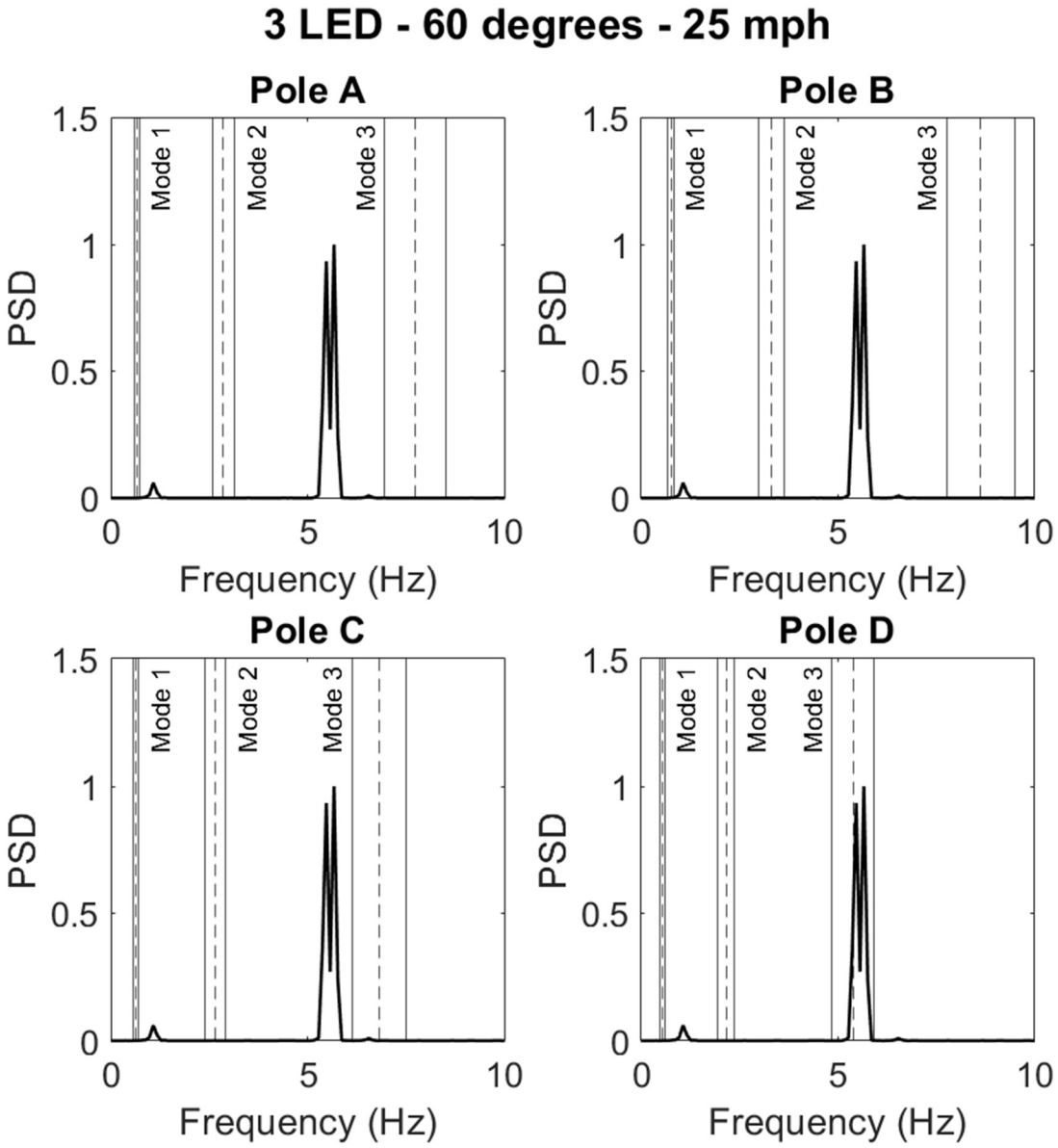
3 LED - 60 degrees - 25 mph
Pole A
Pole B
Pole C
Pole D
Mode 1
Mode 2
Mode 3
PSD
Frequency (Hz)
0
0.5
1
1.5
5
10

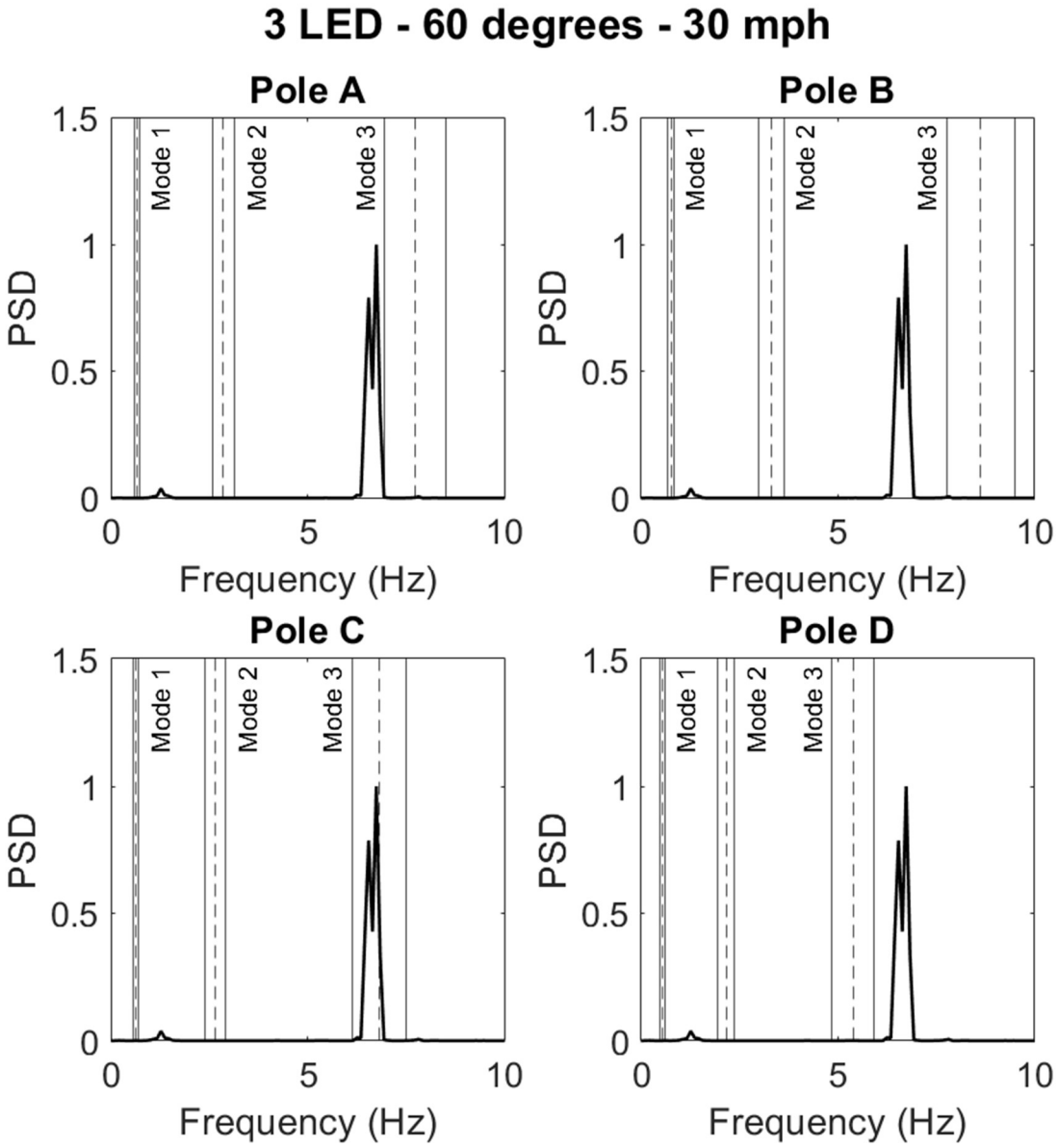
3 LED - 60 degrees - 30 mph
Pole A
Pole B
Pole C
Pole D
Mode 1
Mode 2
Mode 3
PSD
Frequency (Hz)
0
0.5
1
1.5
5
10

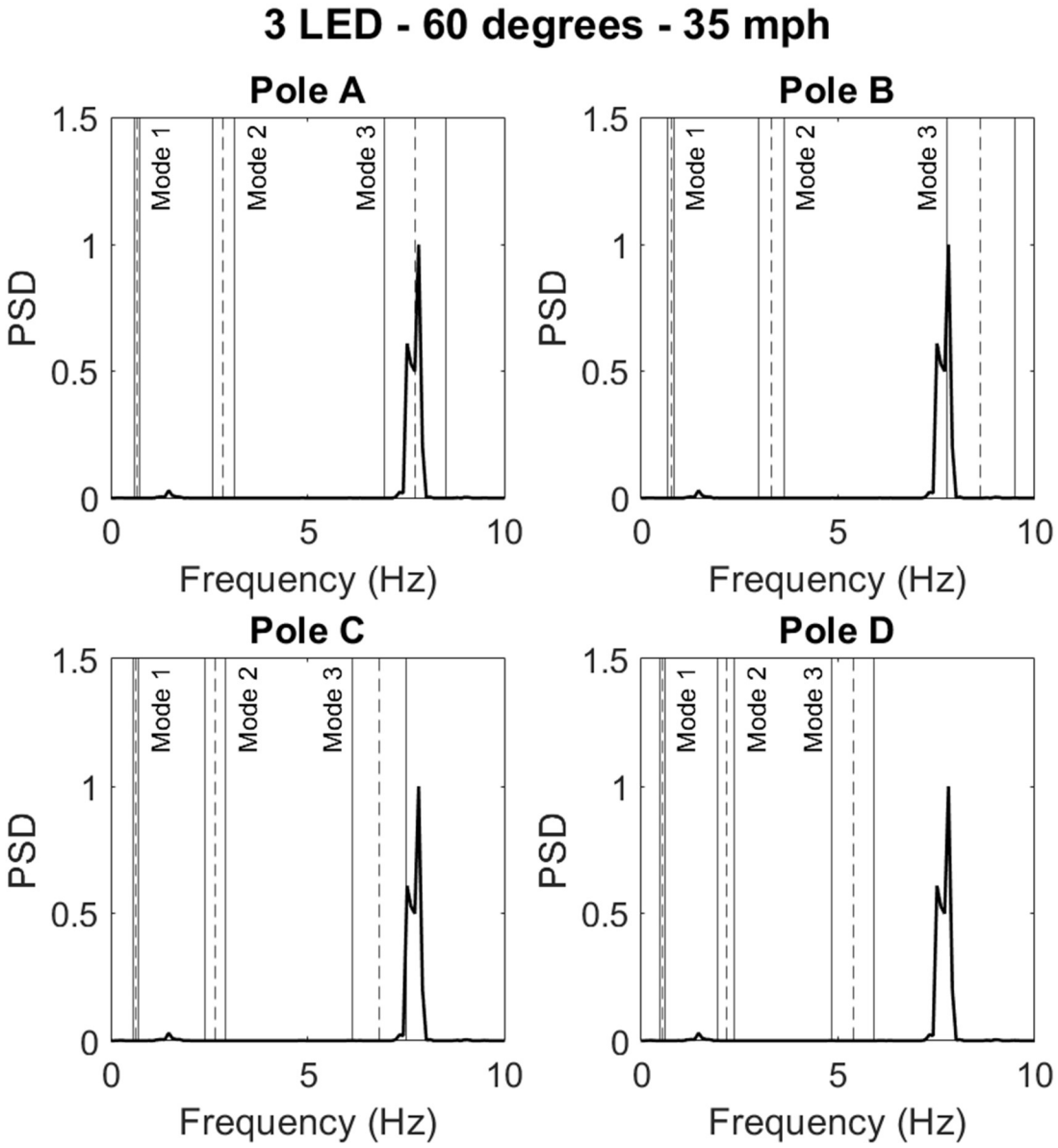
3 LED - 60 degrees - 35 mph
Pole A
Pole B
Pole C
Pole D
Mode 1
Mode 2
Mode 3
PSD
Frequency (Hz)
0
0.5
1
1.5
5
10

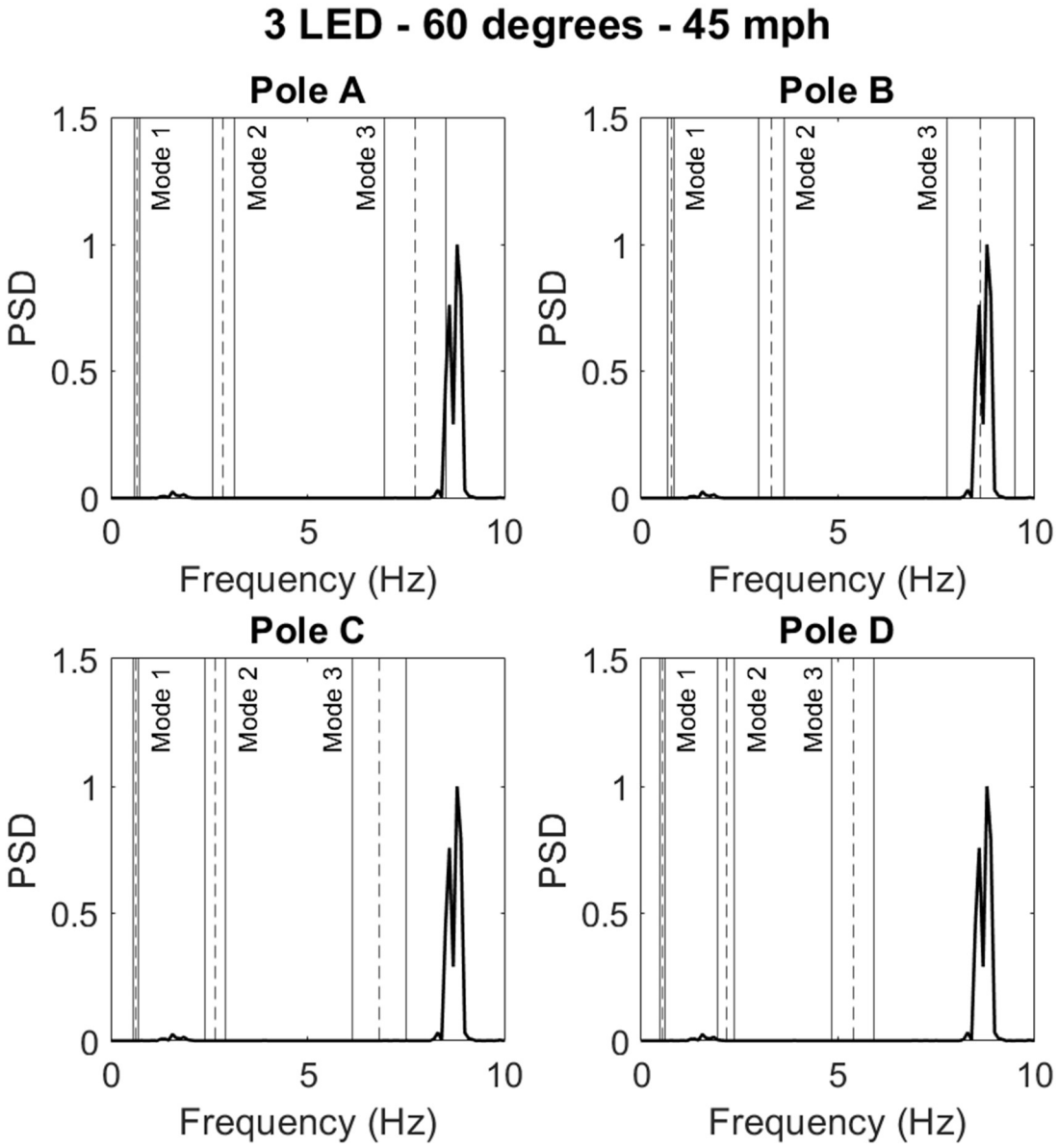
3 LED - 60 degrees - 45 mph
Pole A
Pole B
Pole C
Pole D
Mode 1
Mode 2
Mode 3
PSD
Frequency (Hz)
0
0.5
1
1.5
5
10

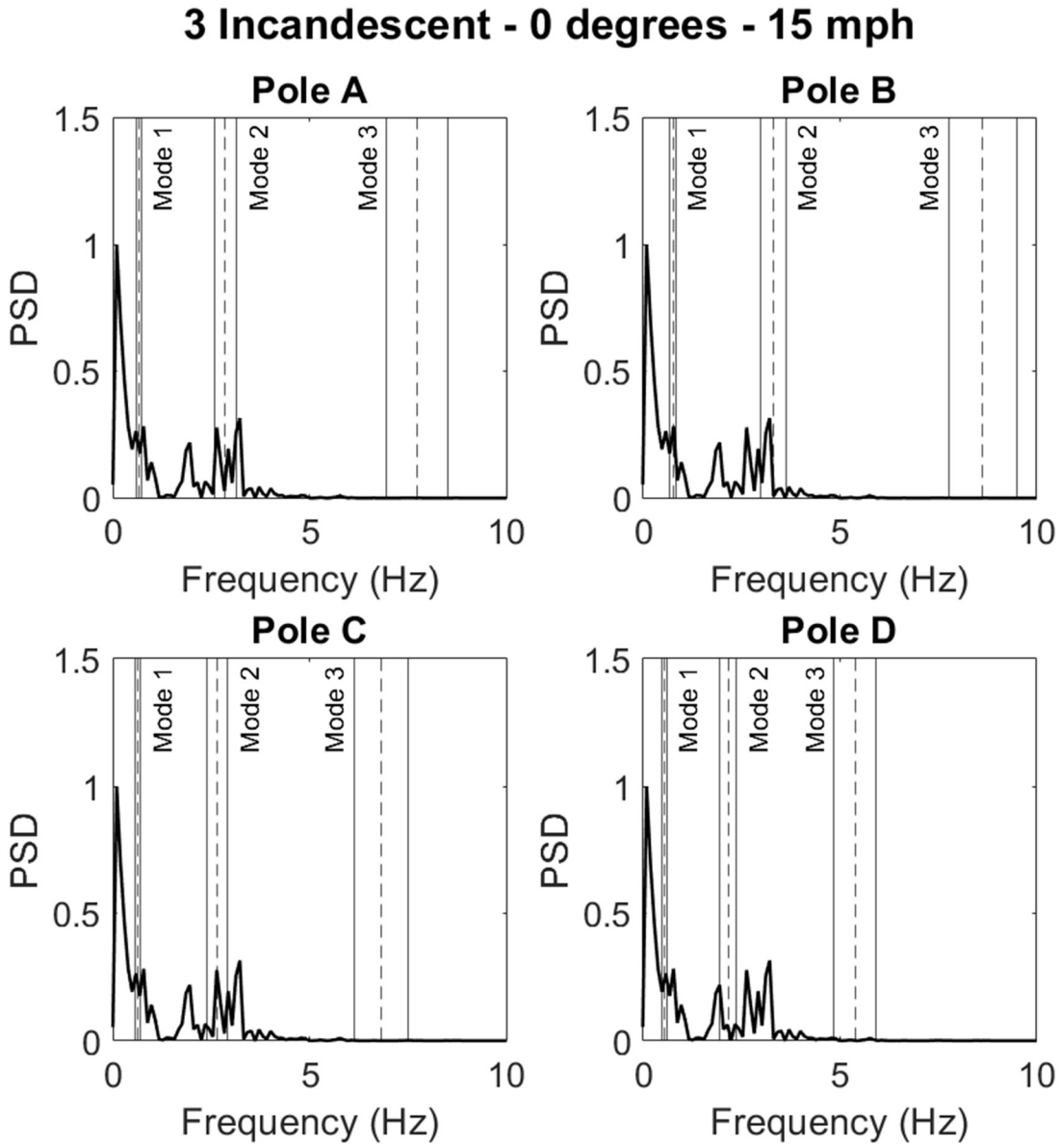
3 Incandescent - 0 degrees - 15 mph
Pole A
Pole B
Pole C
Pole D
Mode 1
Mode 2
Mode 3
PSD
Frequency (Hz)
0
0.5
1
1.5
5
10

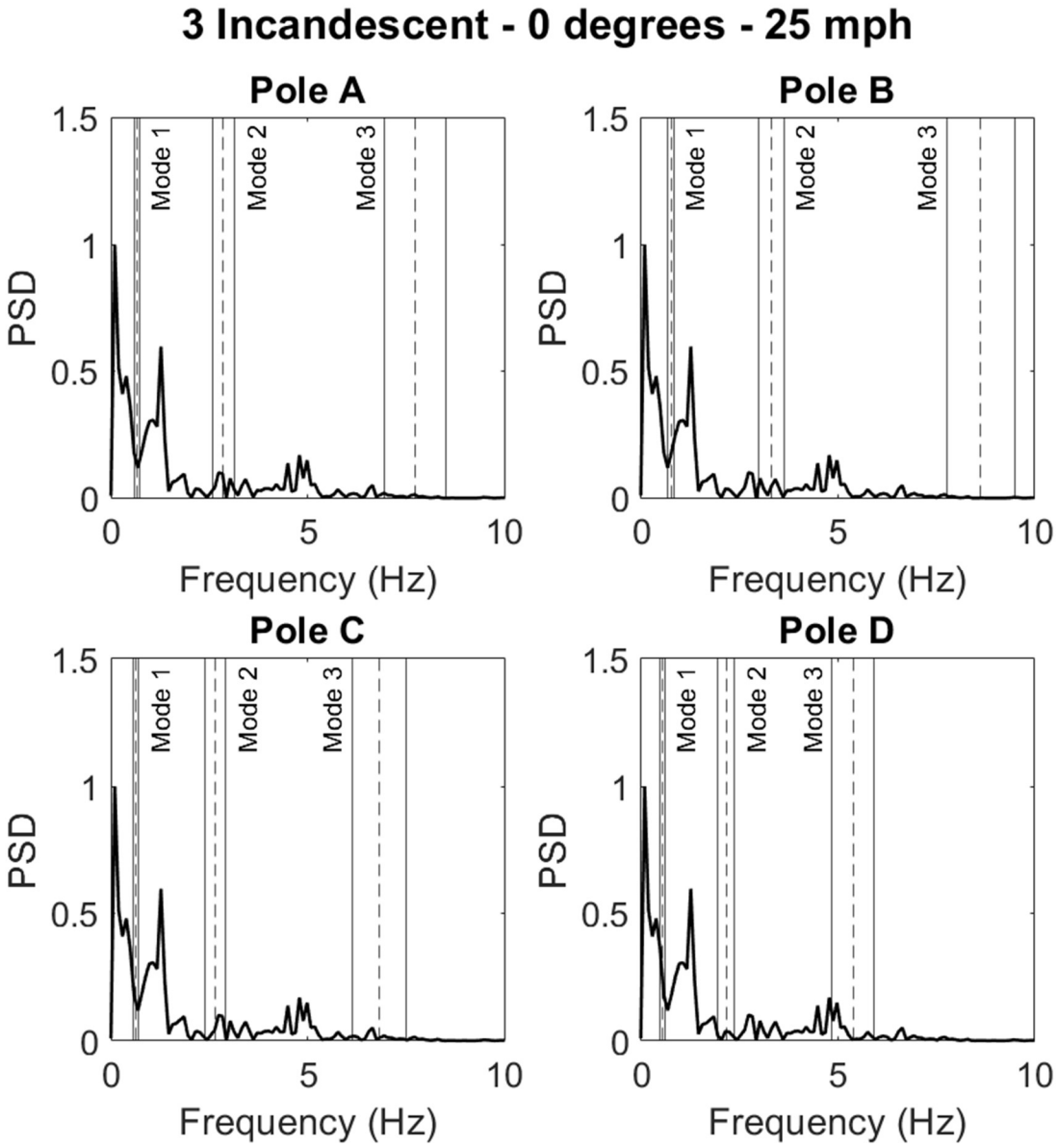
3 Incandescent - 0 degrees - 25 mph
Pole A
Pole B
Pole C
Pole D
Mode 1
Mode 2
Mode 3
PSD
Frequency (Hz)
0
0.5
1
1.5
5
10

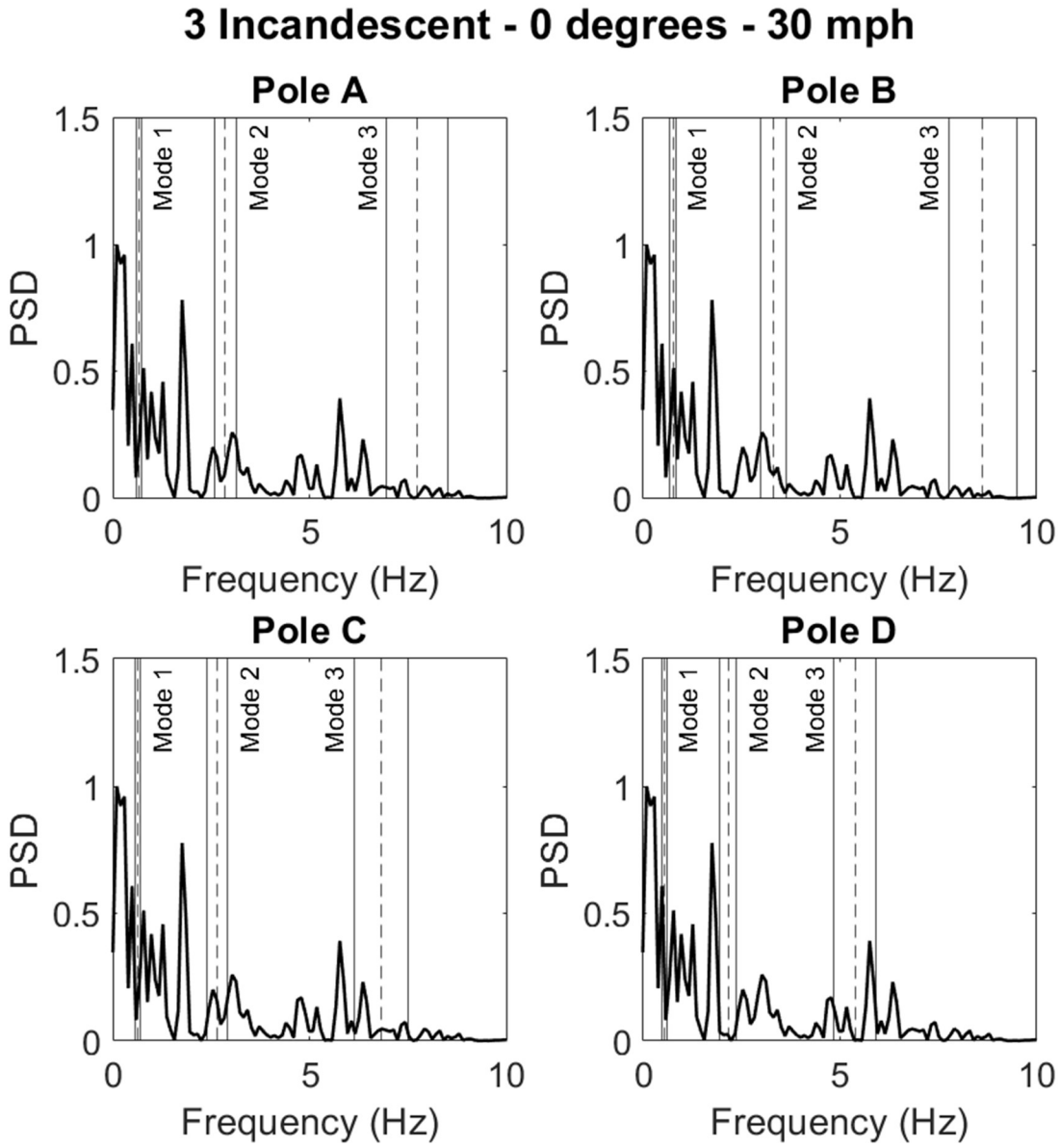
3 Incandescent - 0 degrees - 30 mph
Pole A
Pole B
Pole C
Pole D
Mode 1
Mode 2
Mode 3
PSD
Frequency (Hz)
0
0.5
1
1.5
5
10

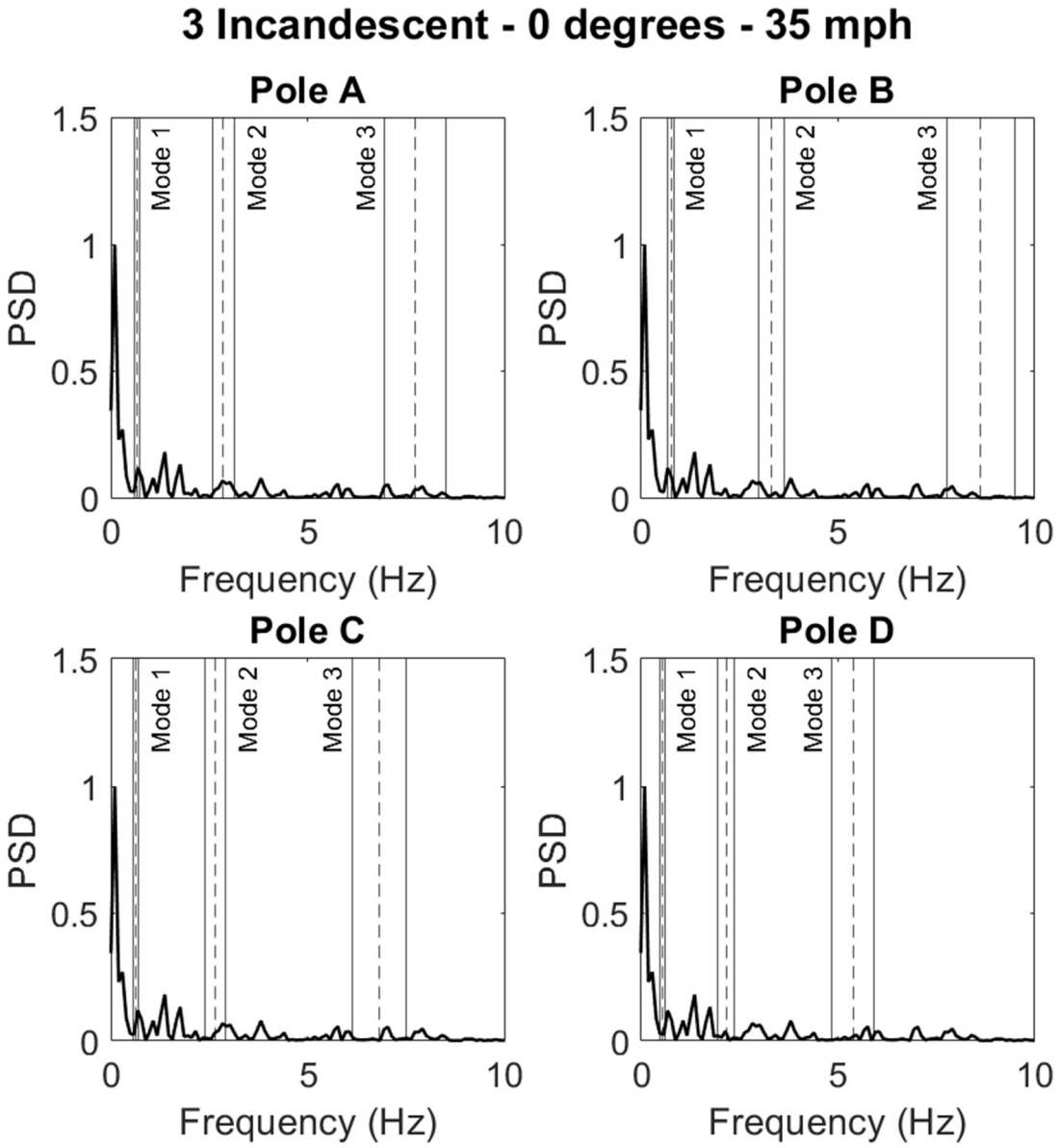
3 Incandescent - 0 degrees - 35 mph
Pole A
Pole B
Pole C
Pole D
Mode 1
Mode 2
Mode 3
PSD
Frequency (Hz)
0
0.5
1
1.5
5
10

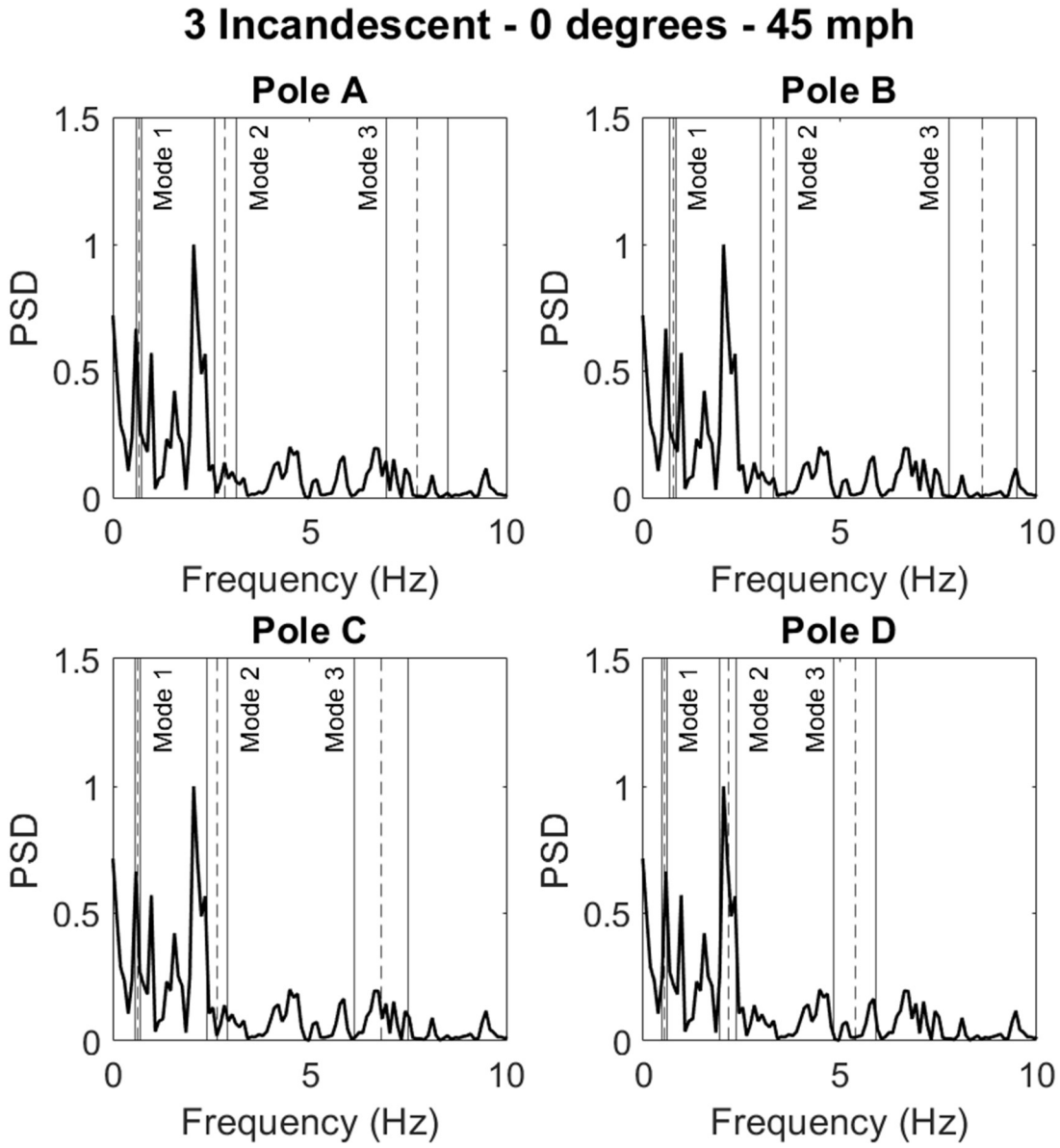
3 Incandescent - 0 degrees - 45 mph
Pole A
Pole B
Pole C
Pole D
Mode 1
Mode 2
Mode 3
PSD
Frequency (Hz)
0
0.5
1
1.5
5
10

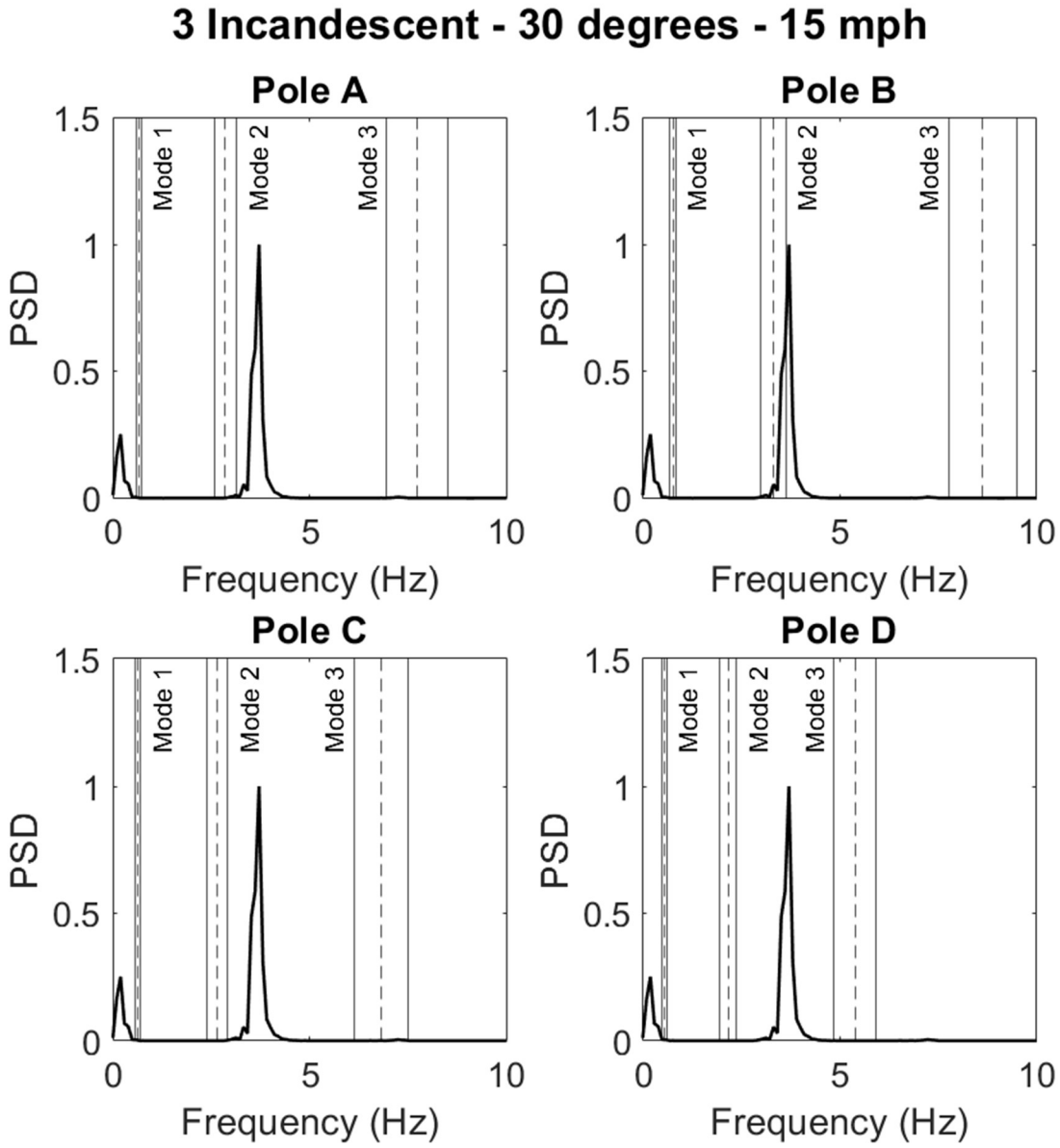
3 Incandescent - 30 degrees - 15 mph
Pole A
Pole B
Pole C
Pole D
Mode 1
Mode 2
Mode 3
PSD
Frequency (Hz)
0
0.5
1
1.5
5
10

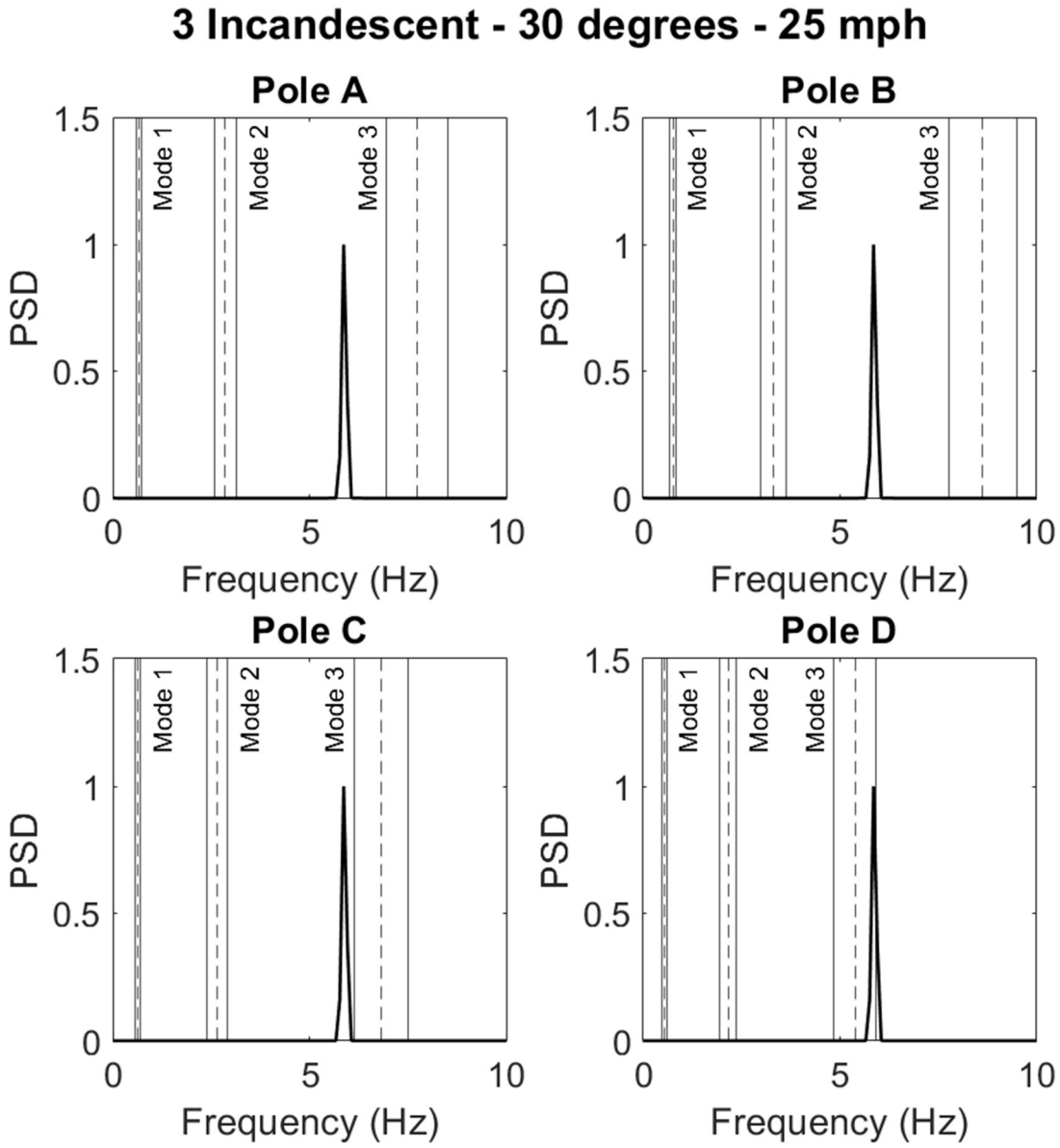
3 Incandescent - 30 degrees - 25 mph
Pole A
Pole B
Pole C
Pole D
Mode 1
Mode 2
Mode 3
PSD
Frequency (Hz)
0
0.5
1
1.5
5
10

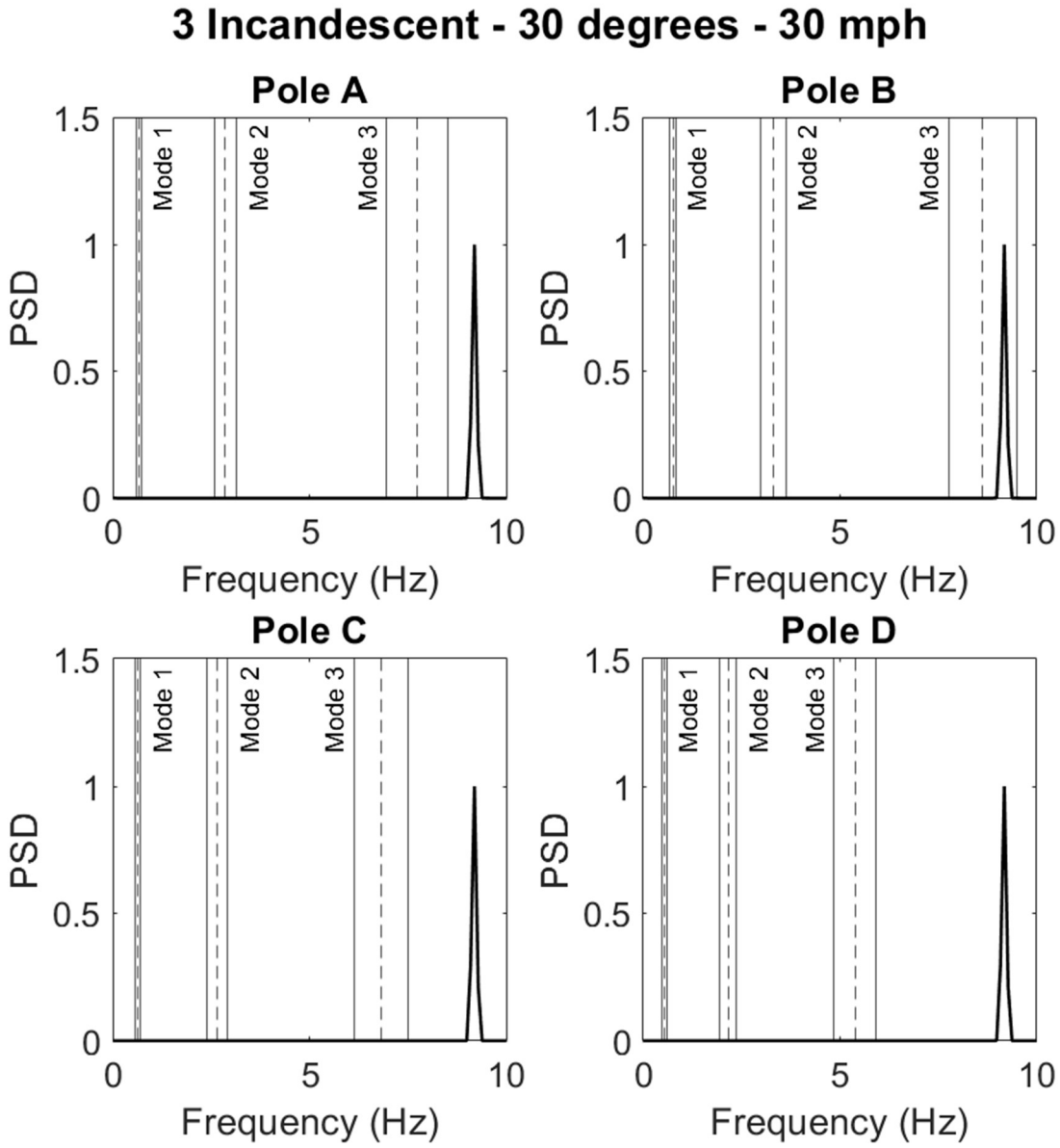
3 Incandescent - 30 degrees - 30 mph
Pole A
Pole B
Pole C
Pole D
Mode 1
Mode 2
Mode 3
PSD
Frequency (Hz)
0
0.5
1
1.5
5
10

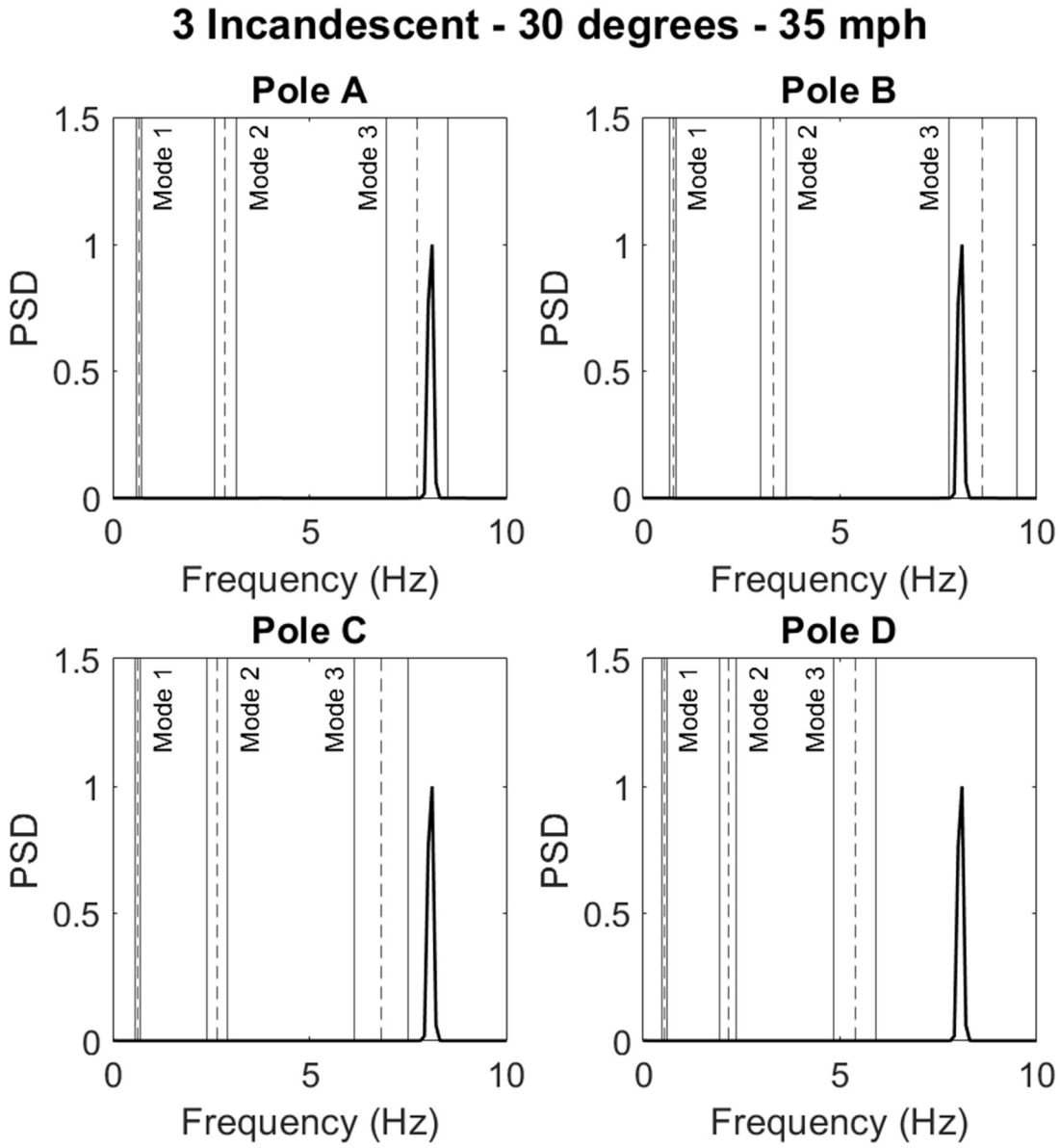
3 Incandescent - 30 degrees - 35 mph
Pole A
Pole B
Pole C
Pole D
Mode 1
Mode 2
Mode 3
PSD
Frequency (Hz)
0
0.5
1
1.5
5
10

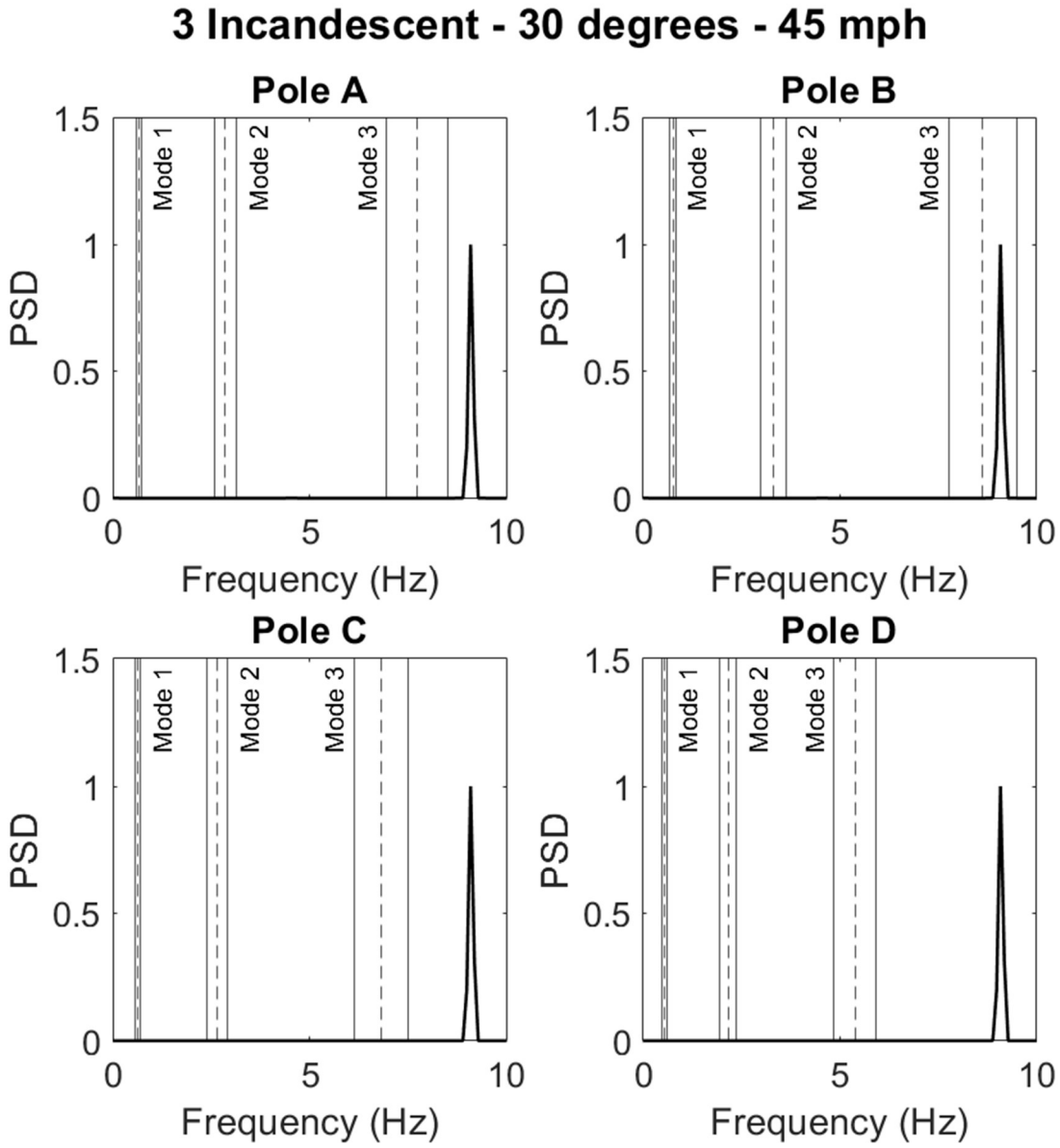
3 Incandescent - 30 degrees - 45 mph
Pole A
Pole B
Pole C
Pole D
Mode 1
Mode 2
Mode 3
PSD
Frequency (Hz)
0
0.5
1
1.5
5
10

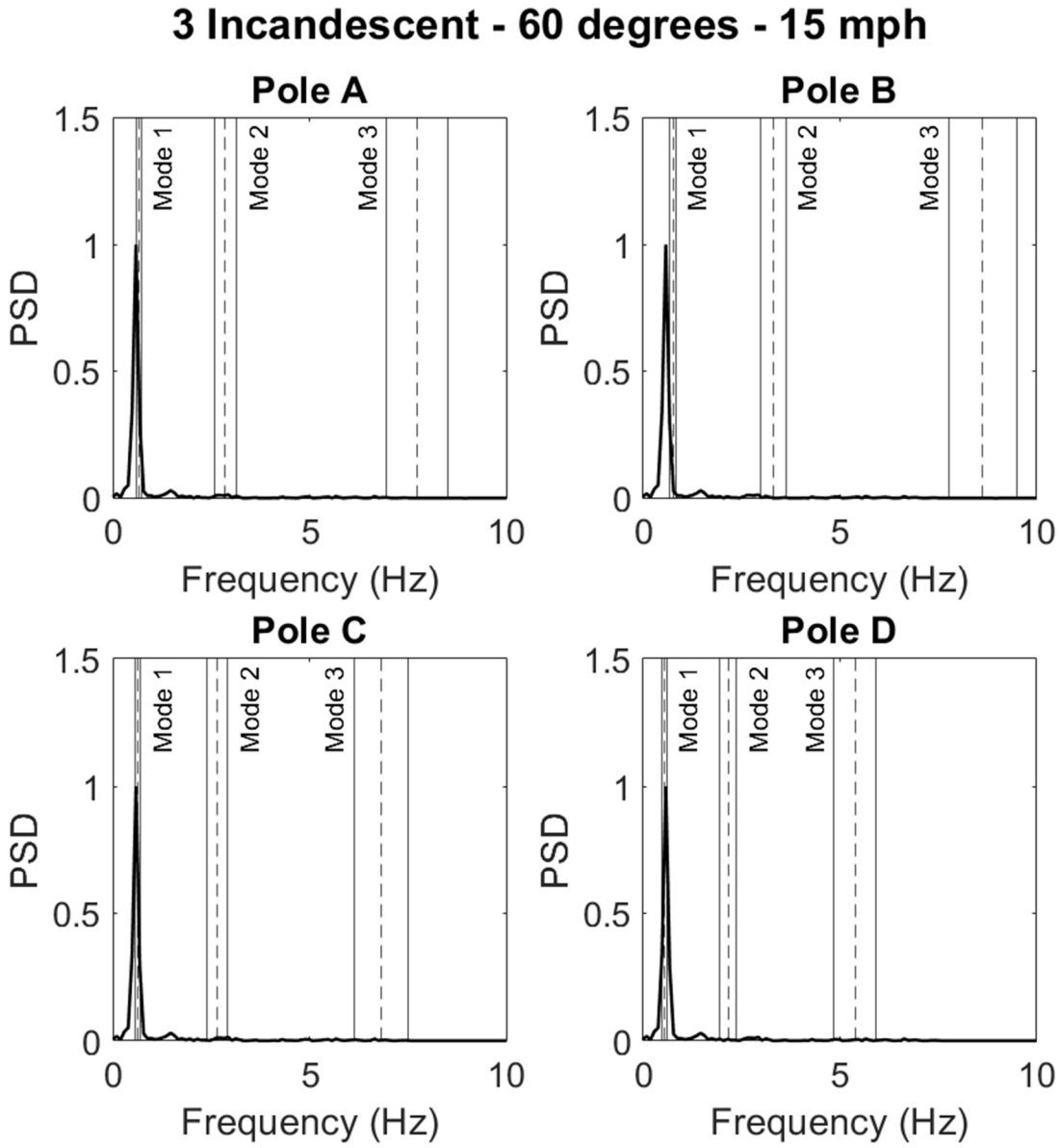
3 Incandescent - 60 degrees - 15 mph
Pole A
Pole B
Pole C
Pole D
Mode 1
Mode 2
Mode 3
PSD
Frequency (Hz)
0
0.5
1
1.5
5
10

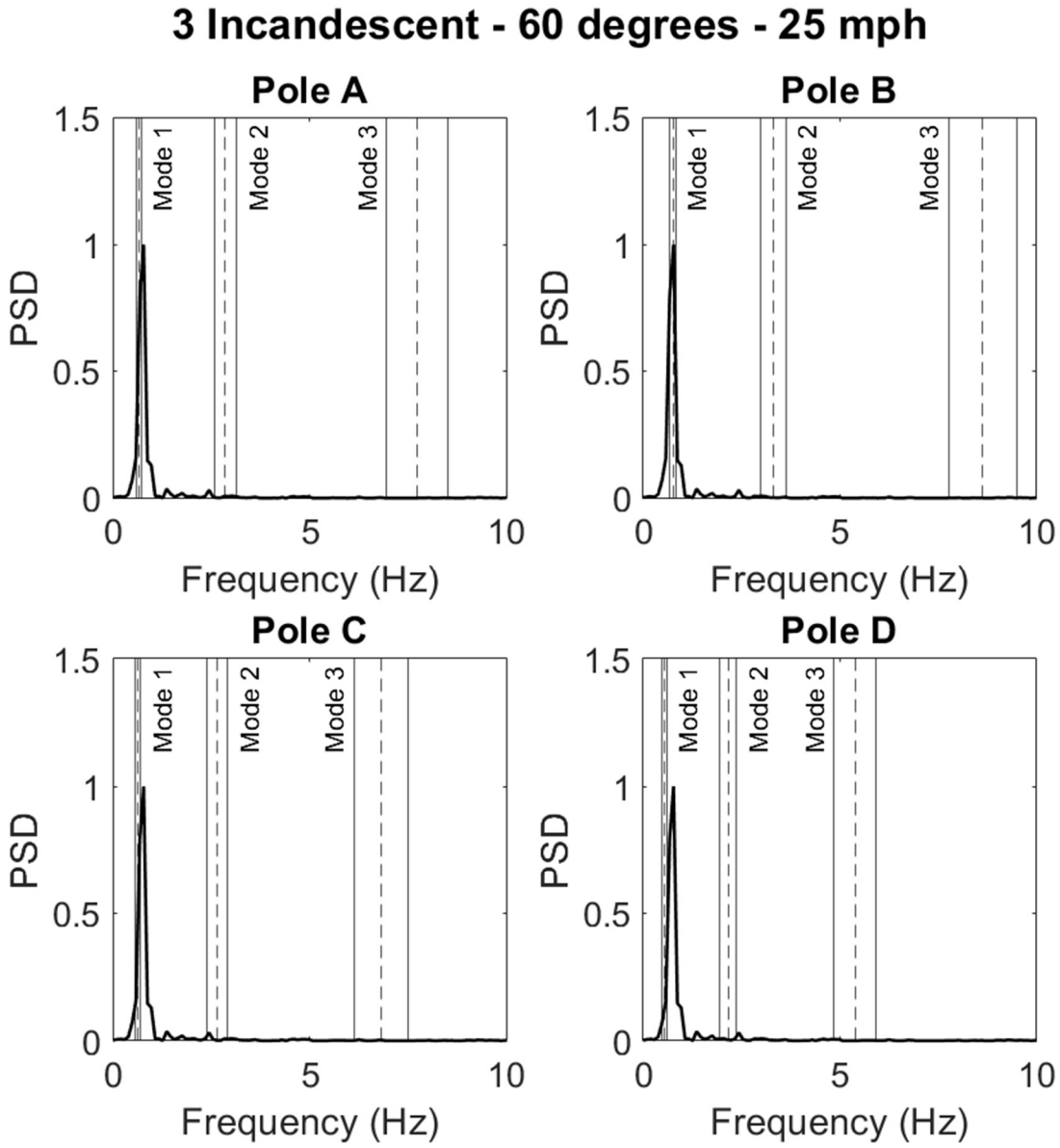
3 Incandescent - 60 degrees - 25 mph
Pole A
Pole B
Pole C
Pole D
Mode 1
Mode 2
Mode 3
PSD
Frequency (Hz)
0
0.5
1
1.5
5
10

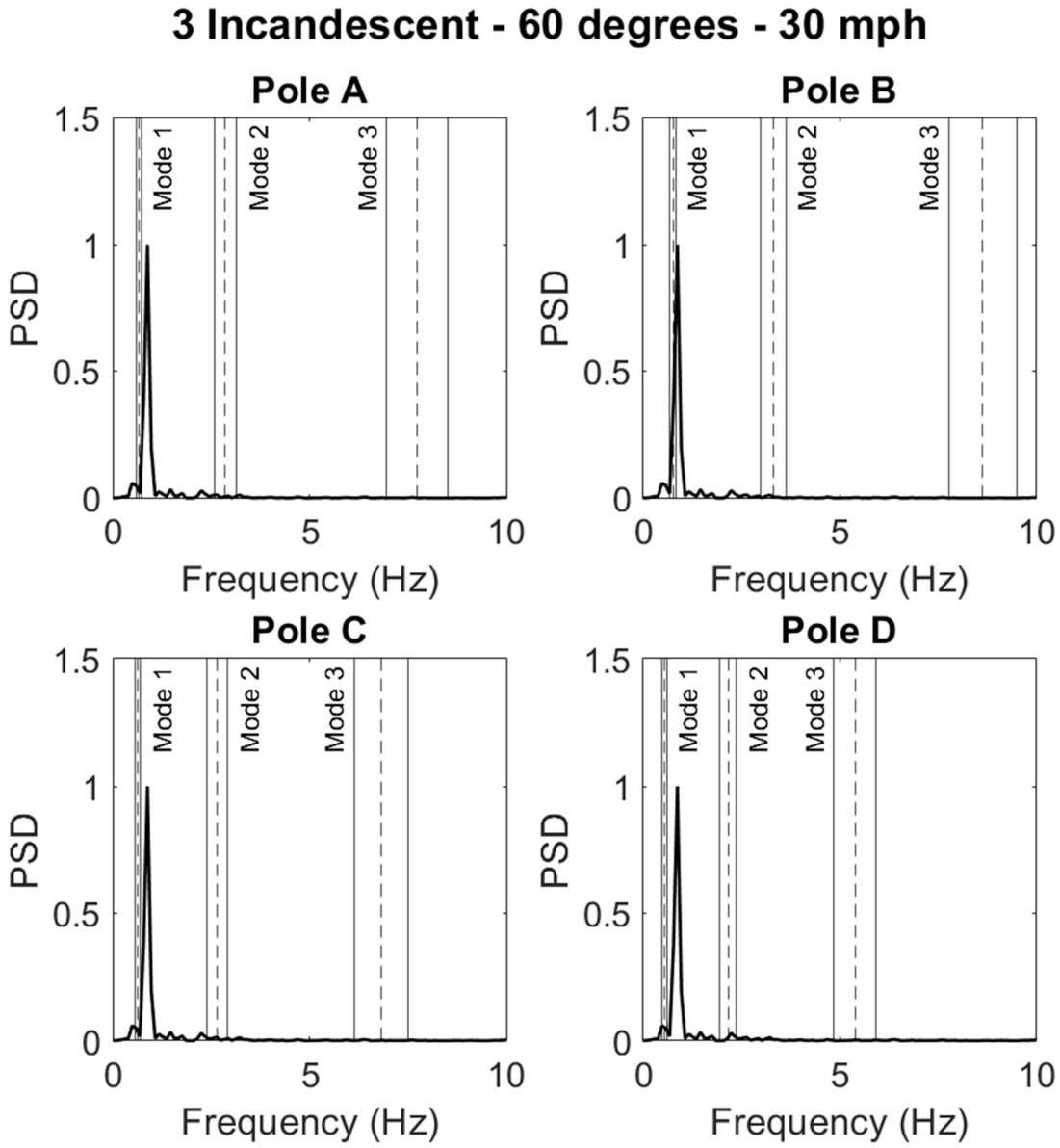
3 Incandescent - 60 degrees - 30 mph
Pole A
Pole B
Pole C
Pole D
PSD
Frequency (Hz)
Mode 1
Mode 2
Mode 3
0
0.5
1
1.5
5
10

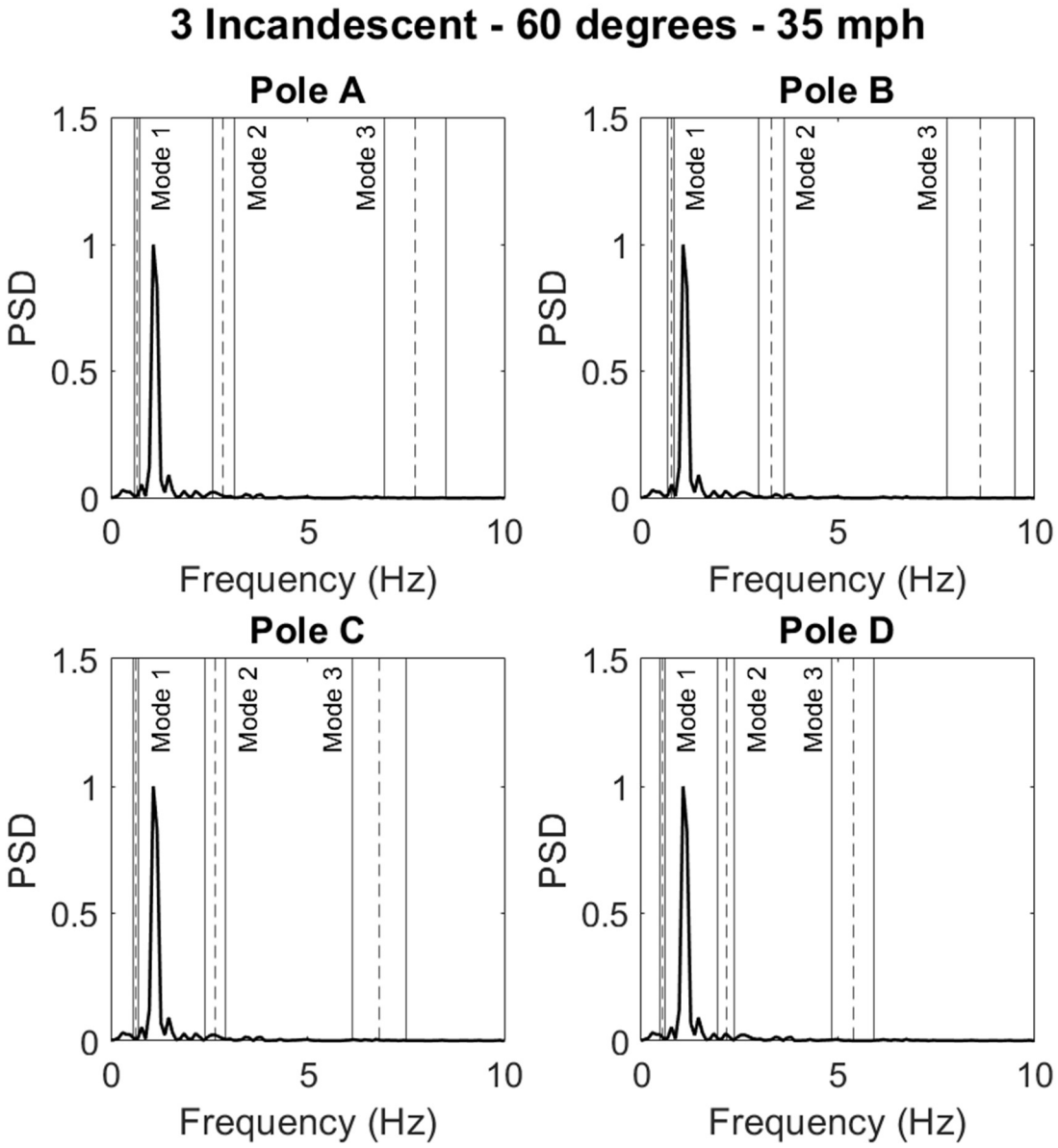
3 Incandescent - 60 degrees - 35 mph
Pole A
Pole B
Pole C
Pole D
Mode 1
Mode 2
Mode 3
PSD
Frequency (Hz)
0
0.5
1
1.5
5
10

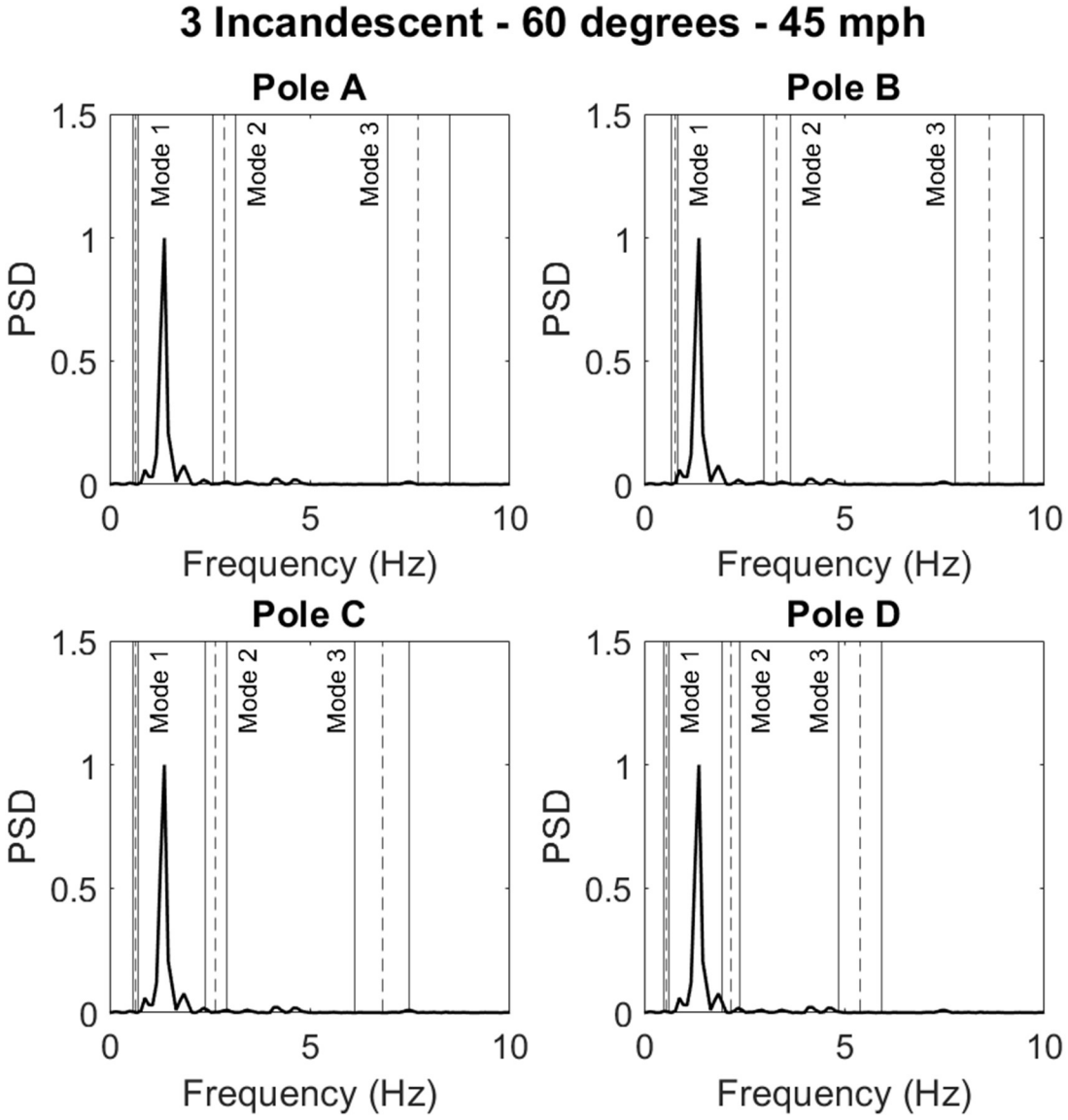
3 Incandescent - 60 degrees - 45 mph
Pole A
Pole B
Pole C
Pole D
Mode 1
Mode 2
Mode 3
PSD
Frequency (Hz)
0
0.5
1
1.5
5
10

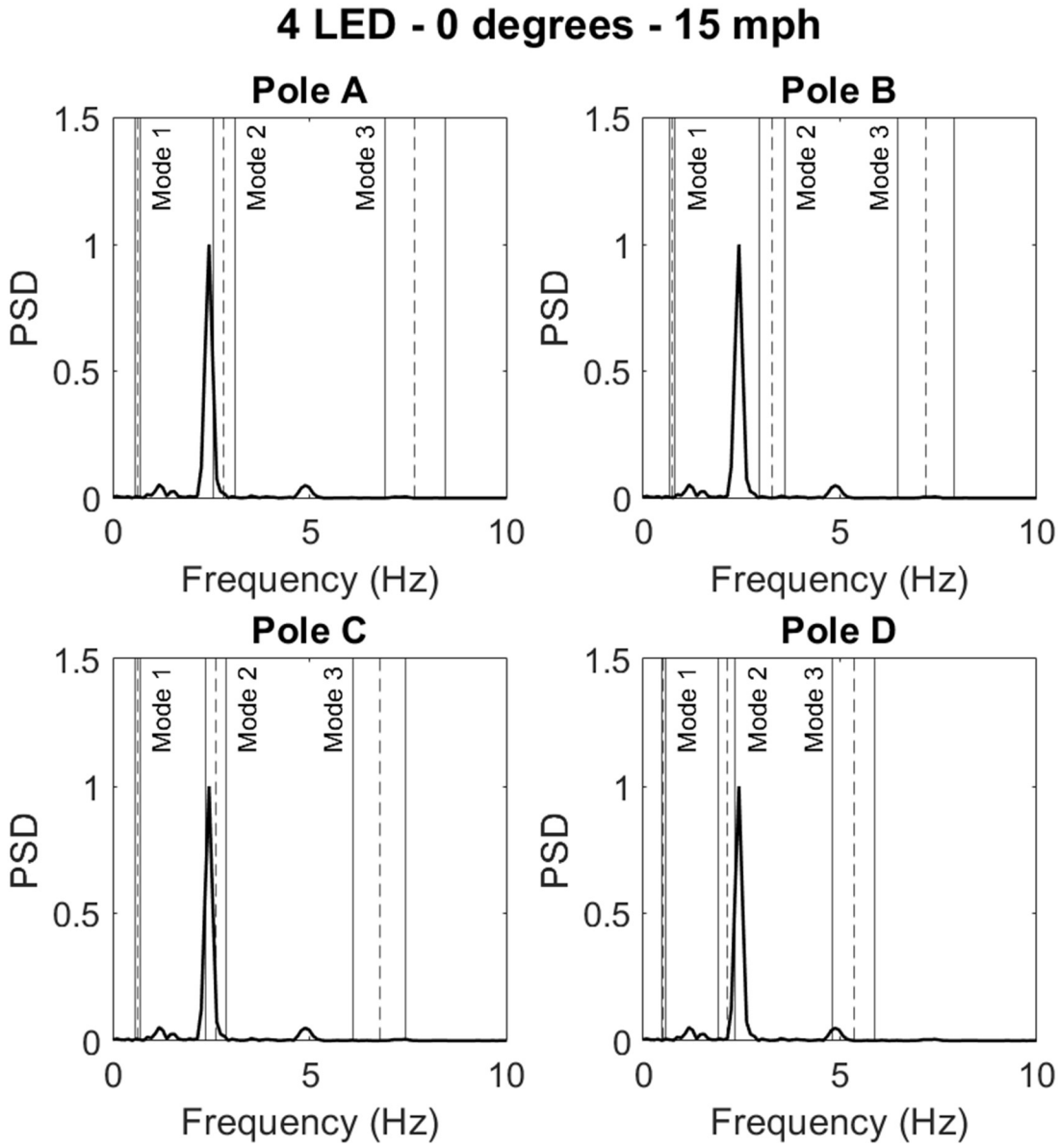
4 LED - 0 degrees - 15 mph
Pole A
Pole B
Pole C
Pole D
Mode 1
Mode 2
Mode 3
PSD
Frequency (Hz)
0
0.5
1
1.5
5
10

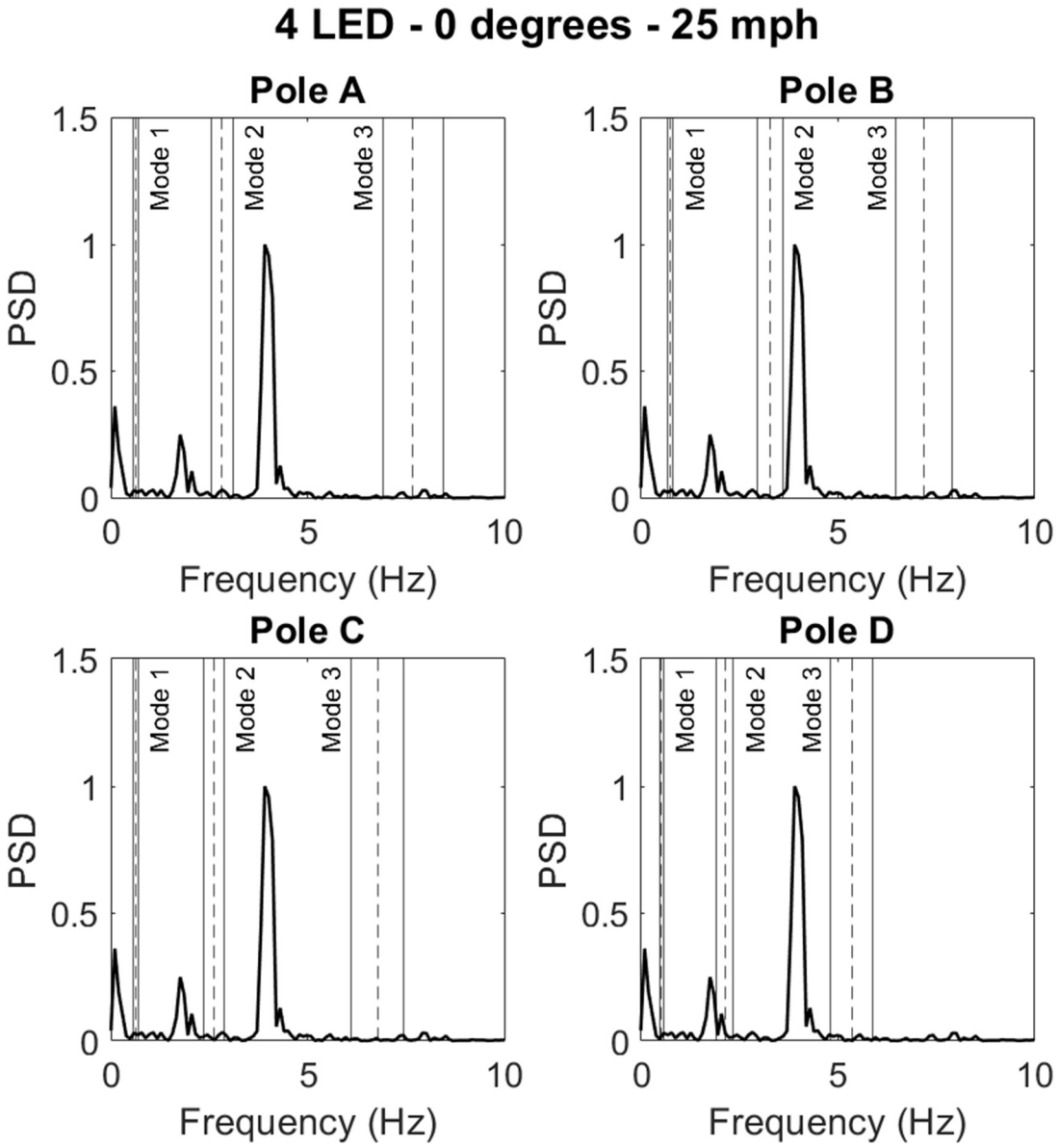
4 LED - 0 degrees - 25 mph
Pole A
Pole B
Pole C
Pole D
Mode 1
Mode 2
Mode 3
PSD
Frequency (Hz)
0
0.5
1
1.5
5
10

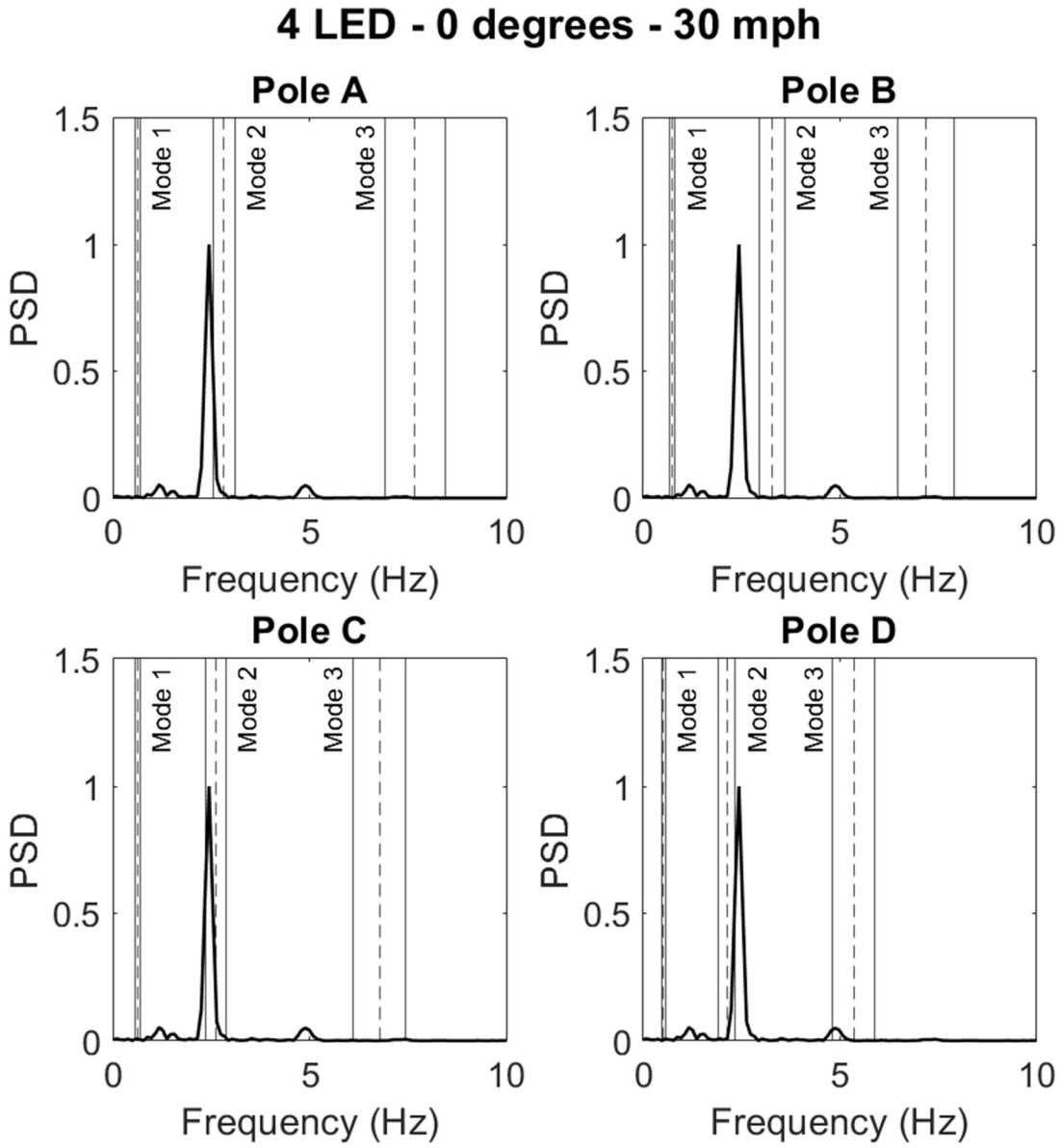
4 LED - 0 degrees - 30 mph
Pole A
Pole B
Pole C
Pole D
Mode 1
Mode 2
Mode 3
PSD
Frequency (Hz)
0
0.5
1
1.5
5
10

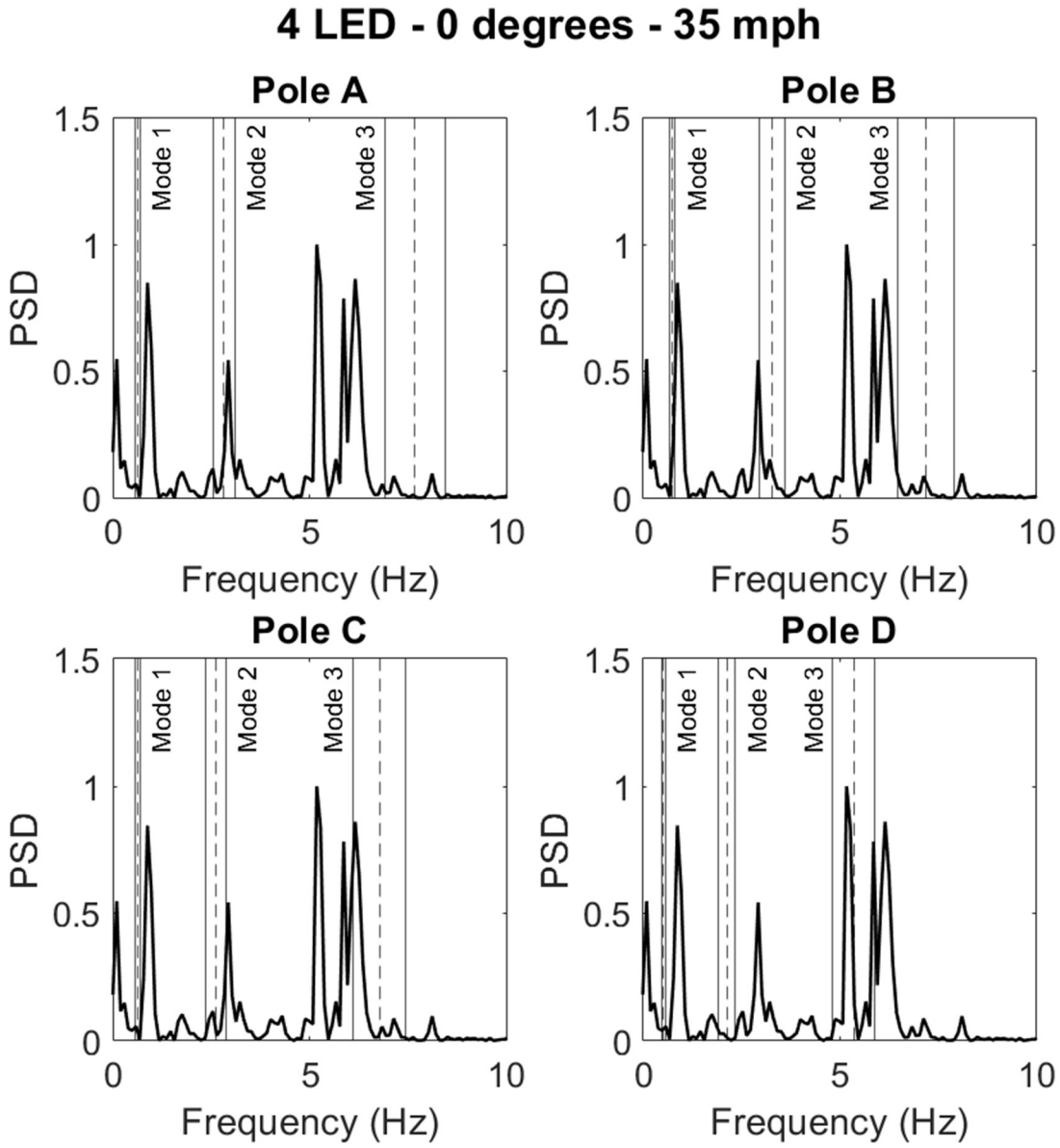
4 LED - 0 degrees - 35 mph
Pole A
Pole B
Pole C
Pole D
Mode 1
Mode 2
Mode 3
PSD
Frequency (Hz)
0
0.5
1
1.5
5
10

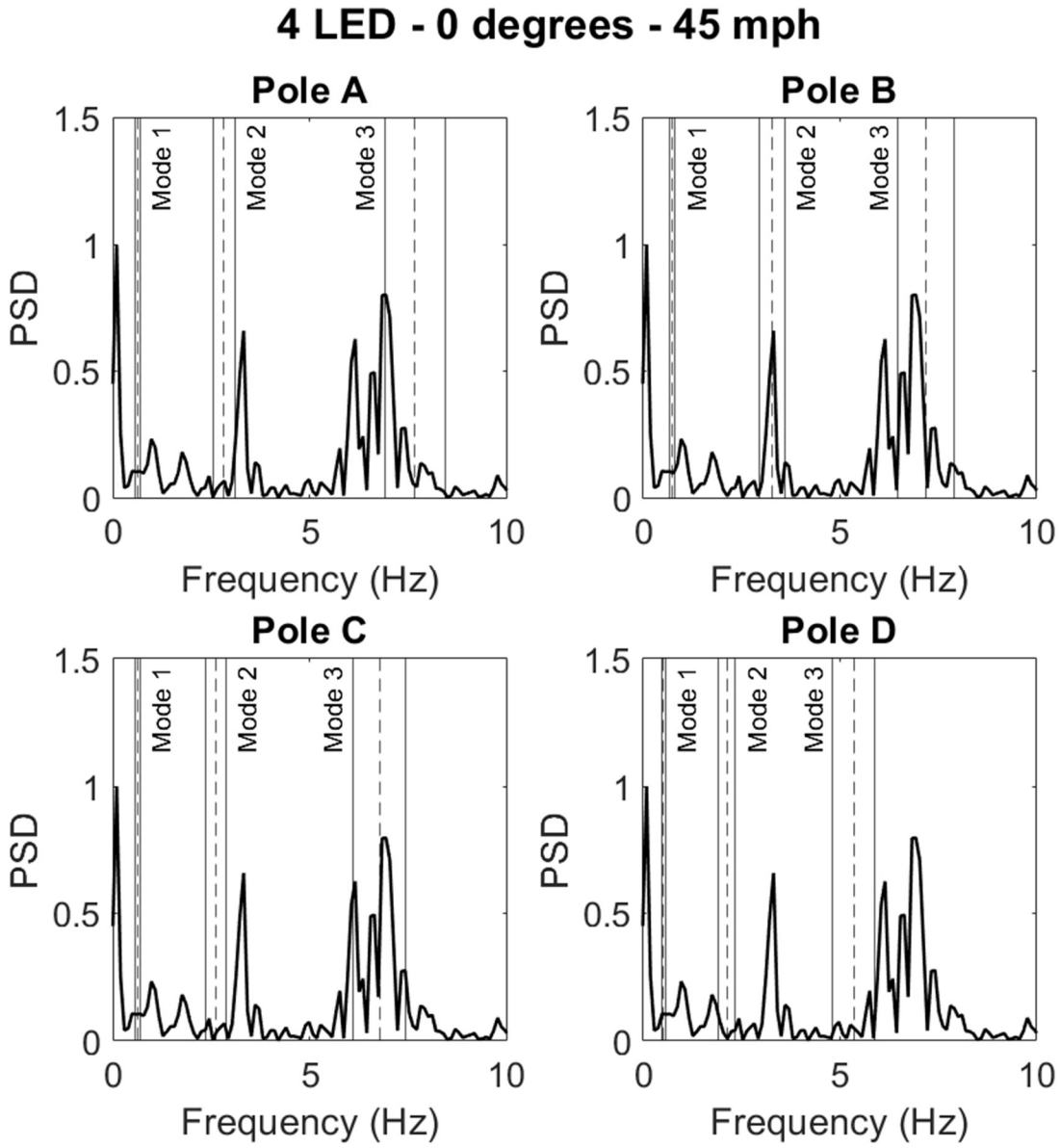
4 LED - 0 degrees - 45 mph
Pole A
Pole B
Pole C
Pole D
Mode 1
Mode 2
Mode 3
PSD
Frequency (Hz)
0
0.5
1
1.5
0
5
10

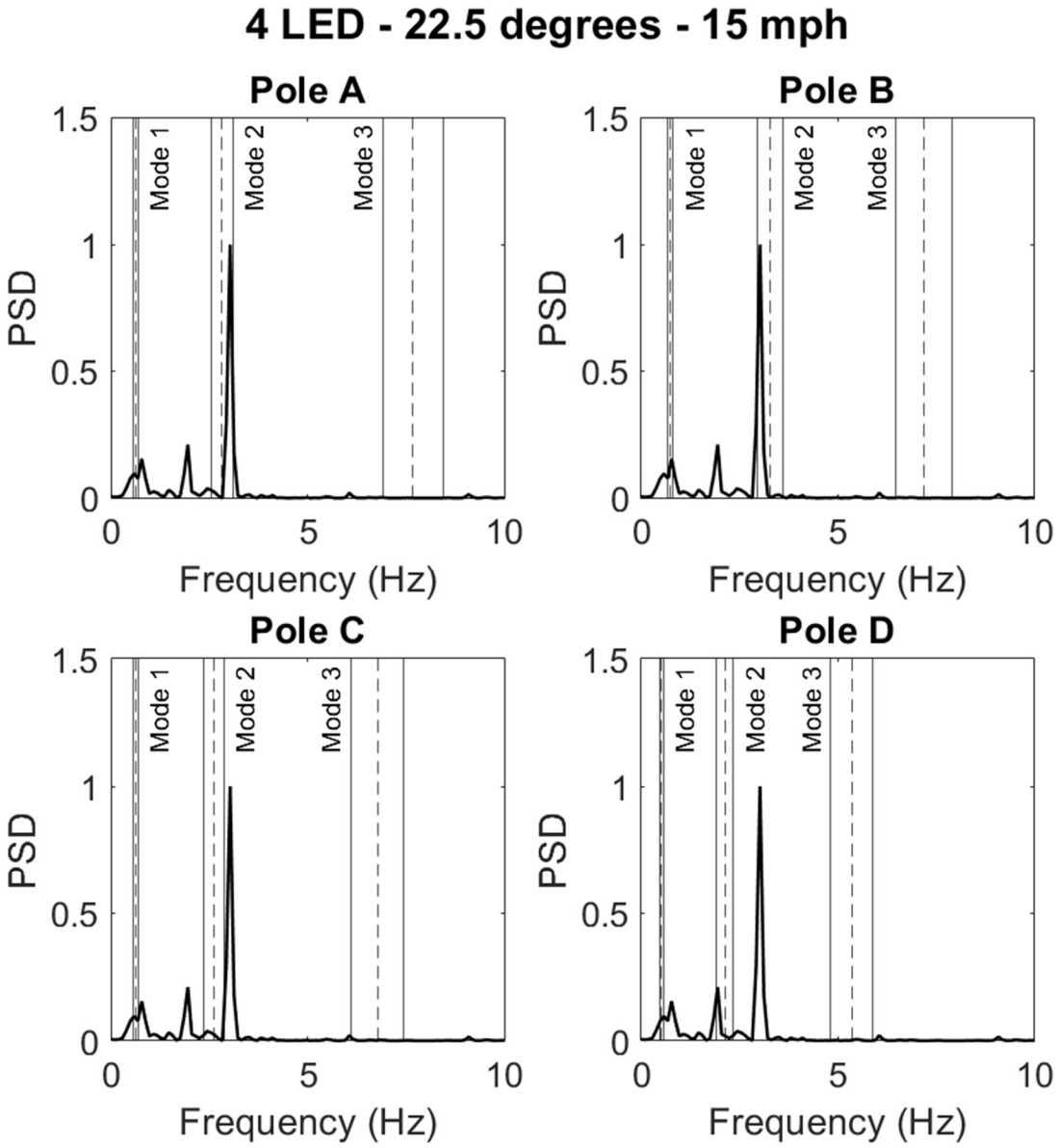
4 LED - 22.5 degrees - 15 mph
Pole A
Pole B
Pole C
Pole D
PSD
Frequency (Hz)
Mode 1
Mode 2
Mode 3
0
0.5
1
1.5
5
10

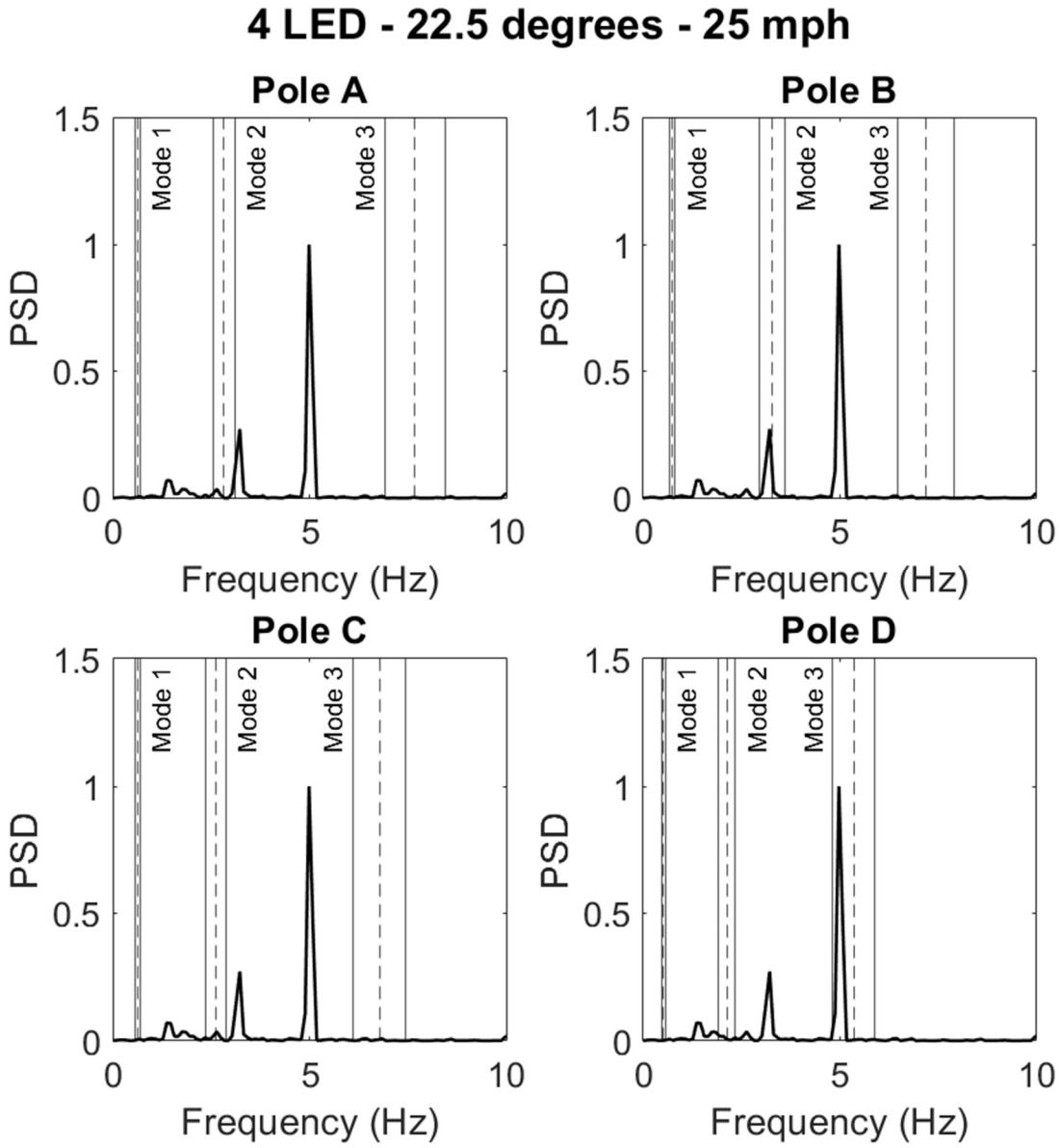
4 LED - 22.5 degrees - 25 mph
Pole A
Pole B
Pole C
Pole D
Mode 1
Mode 2
Mode 3
PSD
Frequency (Hz)
0
0.5
1
1.5
5
10

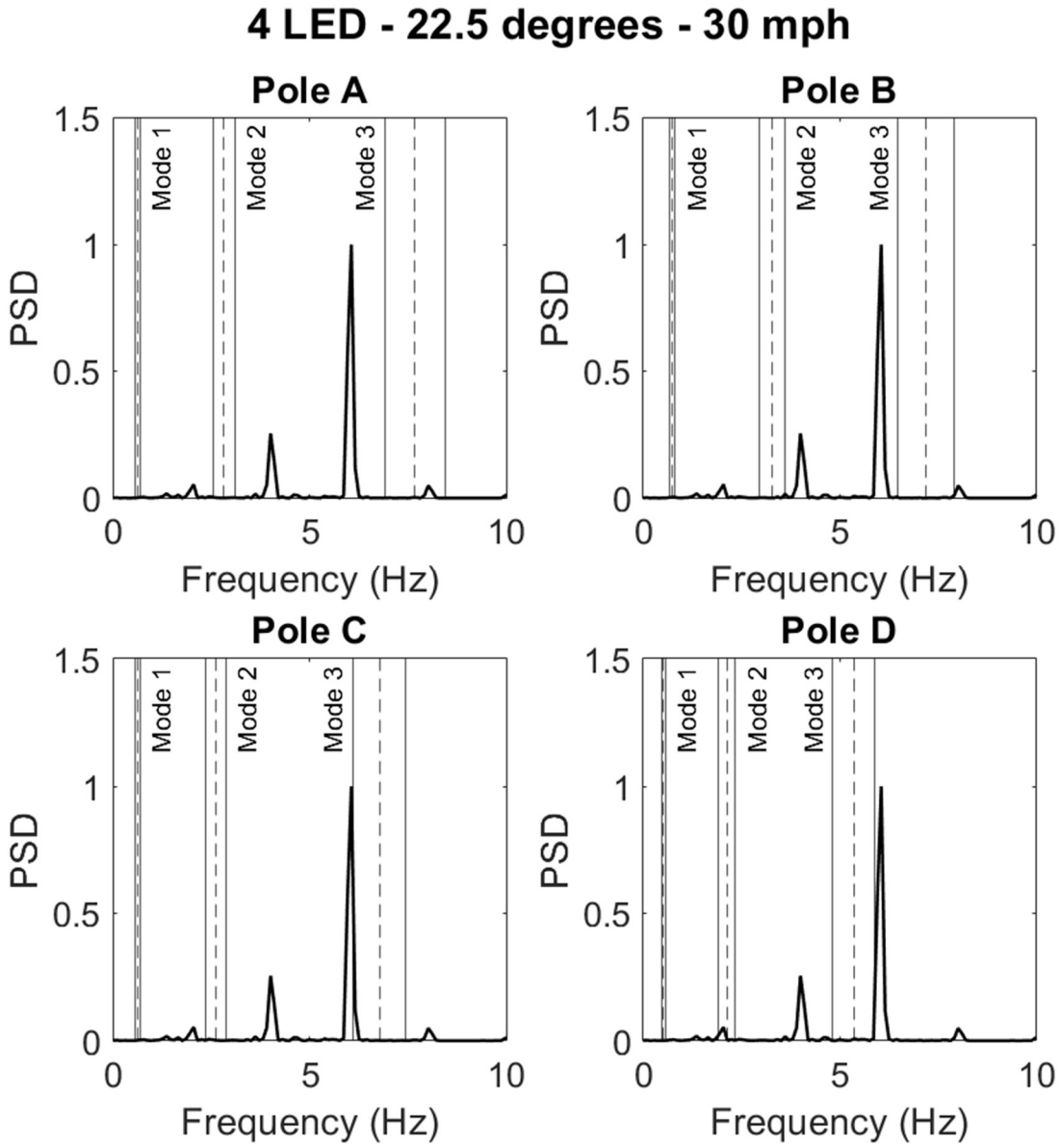
4 LED - 22.5 degrees - 30 mph
Pole A
Pole B
Pole C
Pole D
PSD
Frequency (Hz)
Mode 1
Mode 2
Mode 3
0
0.5
1
1.5
5
10

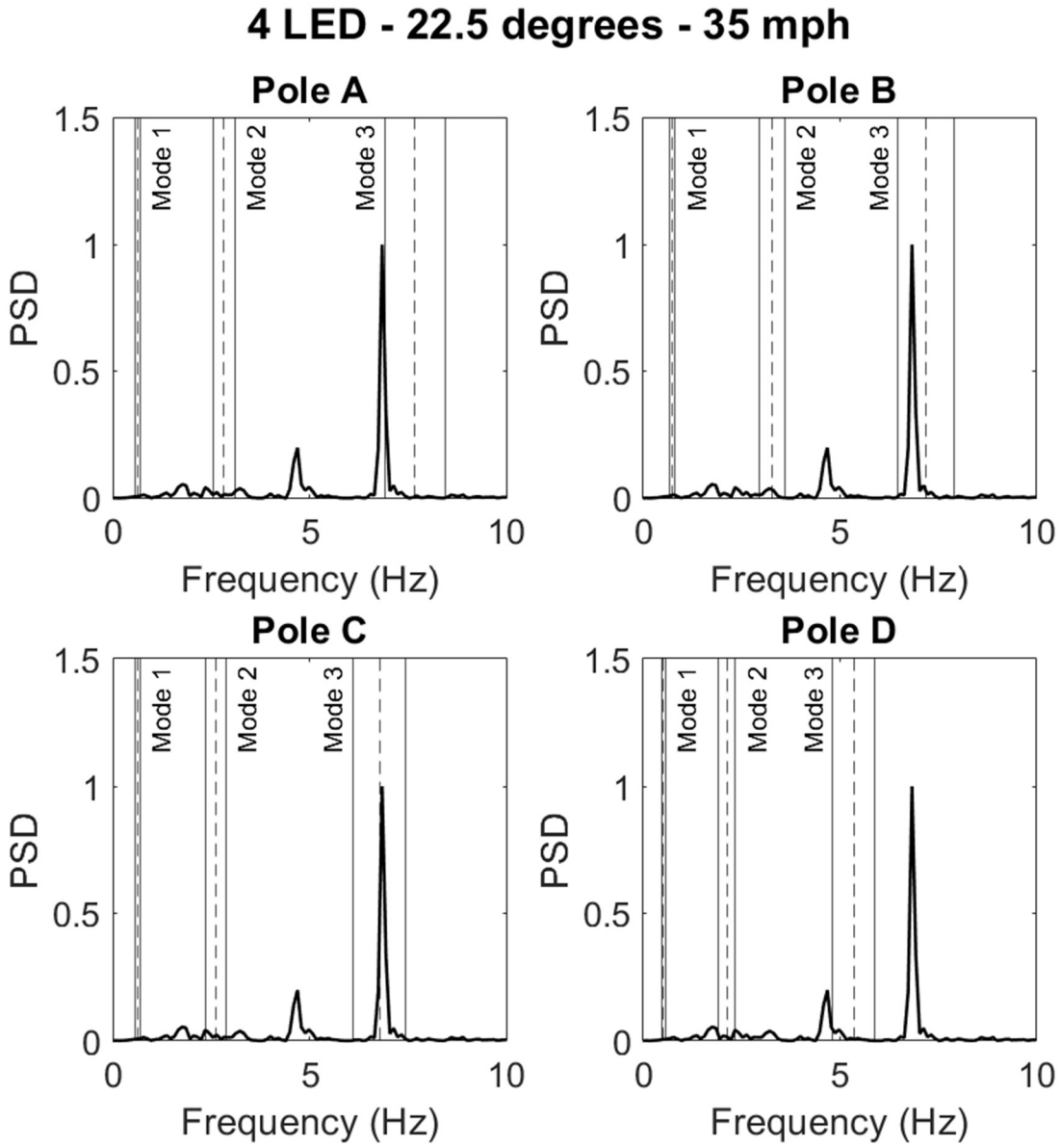
4 LED - 22.5 degrees - 35 mph
Pole A
Pole B
Pole C
Pole D
Mode 1
Mode 2
Mode 3
PSD
Frequency (Hz)
0
0.5
1
1.5
5
10

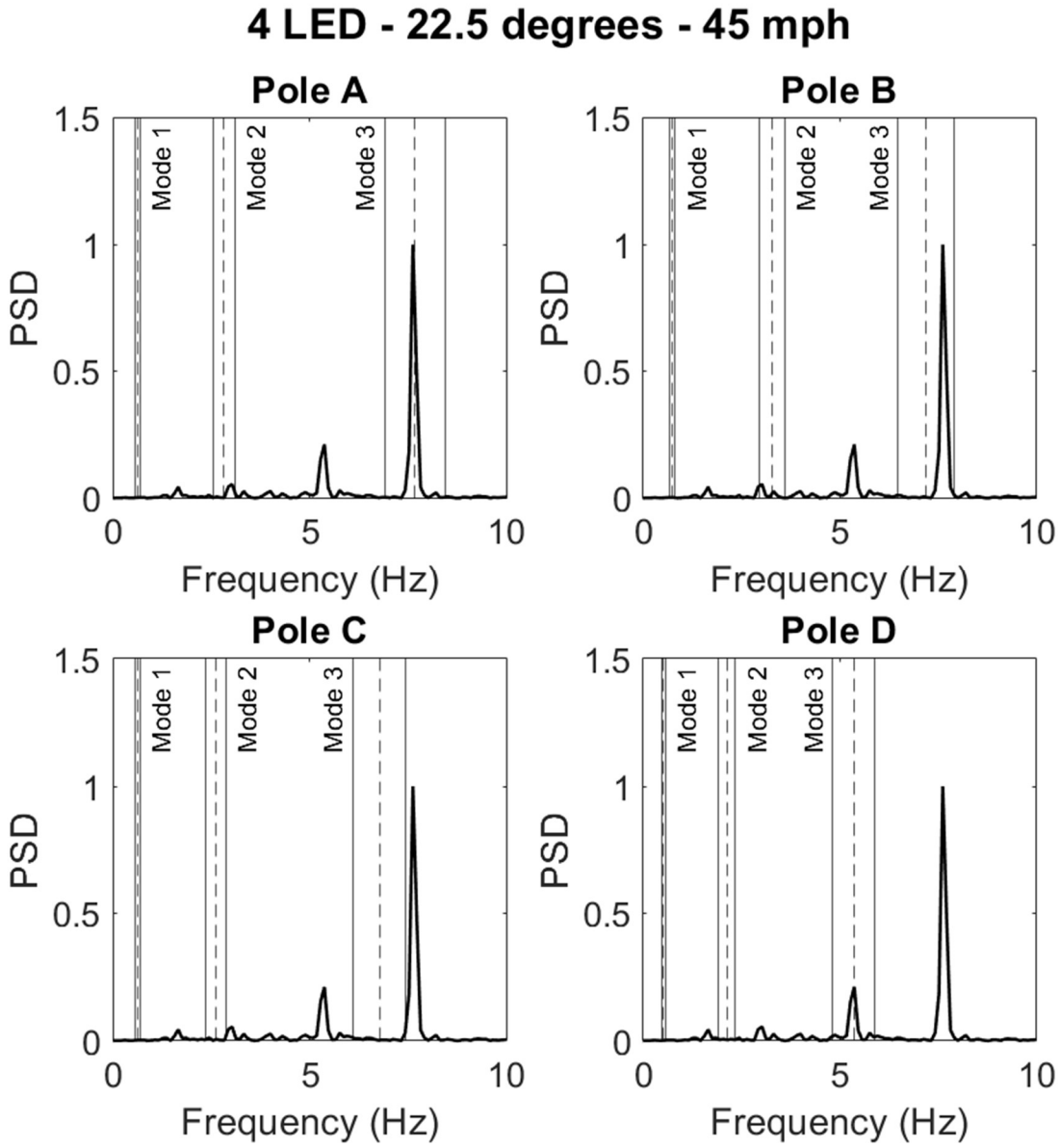
4 LED - 22.5 degrees - 45 mph
Pole A
Pole B
Pole C
Pole D
Mode 1
Mode 2
Mode 3
PSD
Frequency (Hz)
0
0.5
1
1.5
5
10

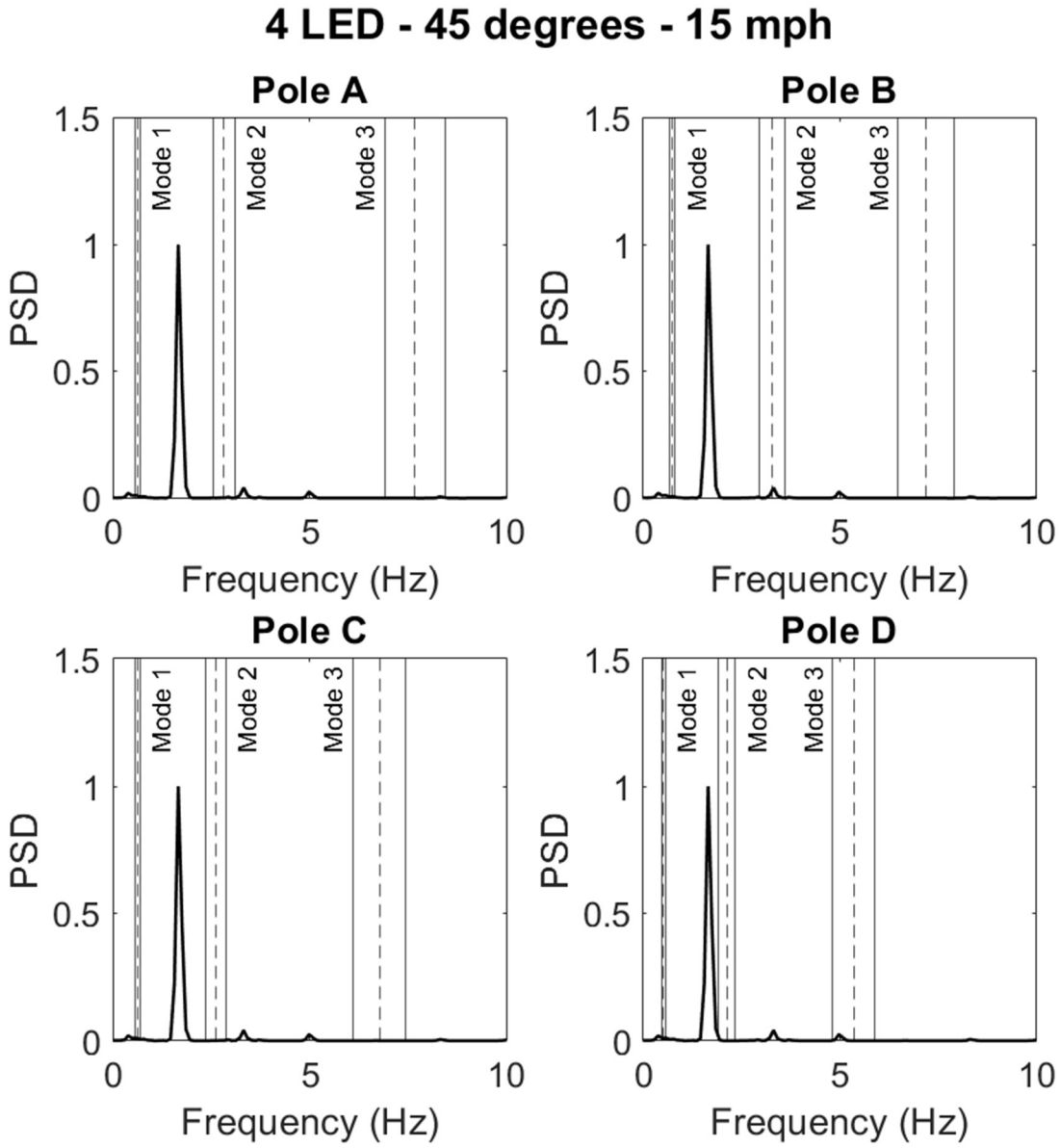
4 LED - 45 degrees - 15 mph
Pole A
Pole B
Pole C
Pole D
Mode 1
Mode 2
Mode 3
PSD
Frequency (Hz)
0
0.5
1
1.5
5
10

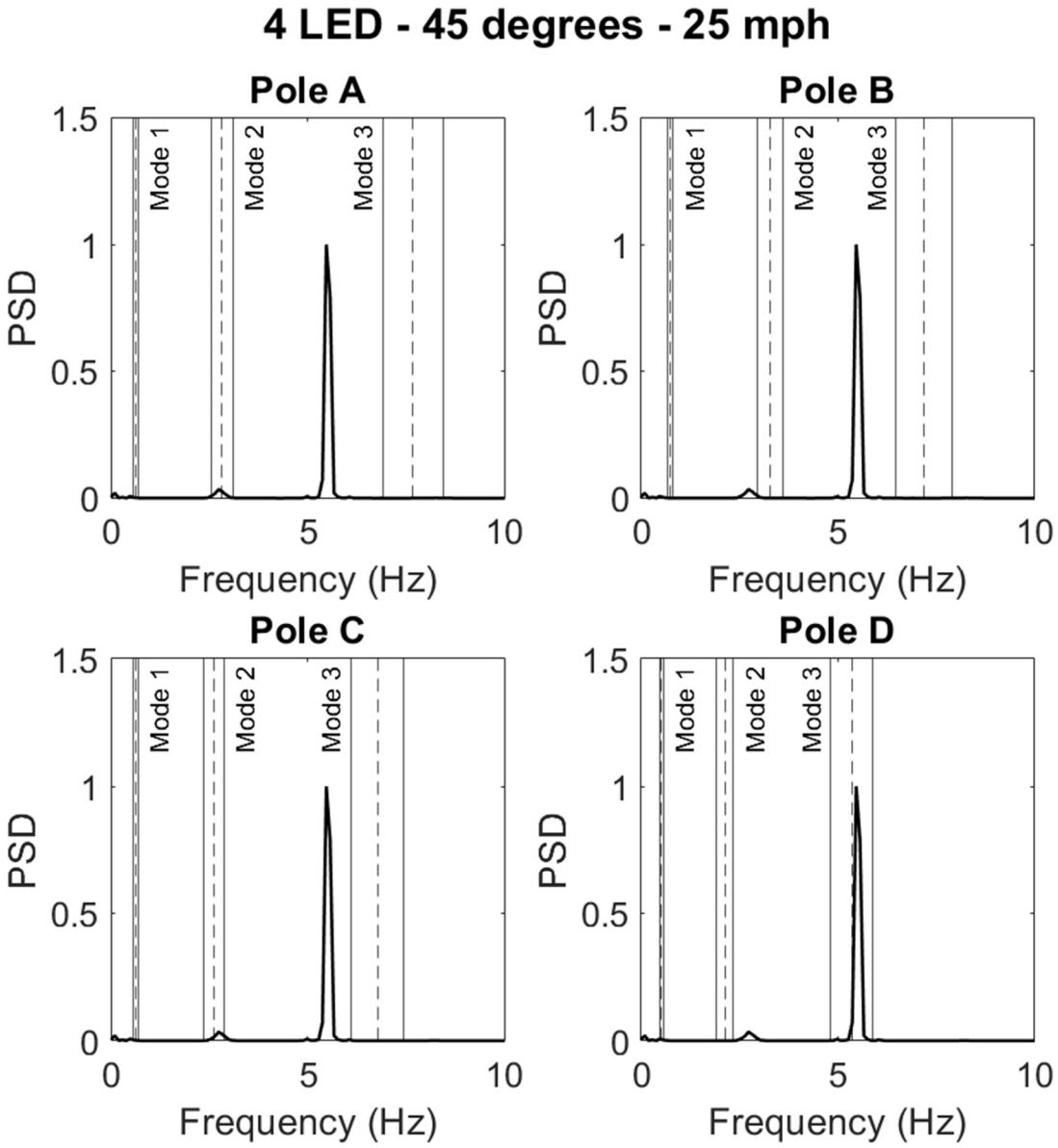
4 LED - 45 degrees - 25 mph
Pole A
Pole B
Pole C
Pole D
Mode 1
Mode 2
Mode 3
PSD
Frequency (Hz)
0
0.5
1
1.5
5
10

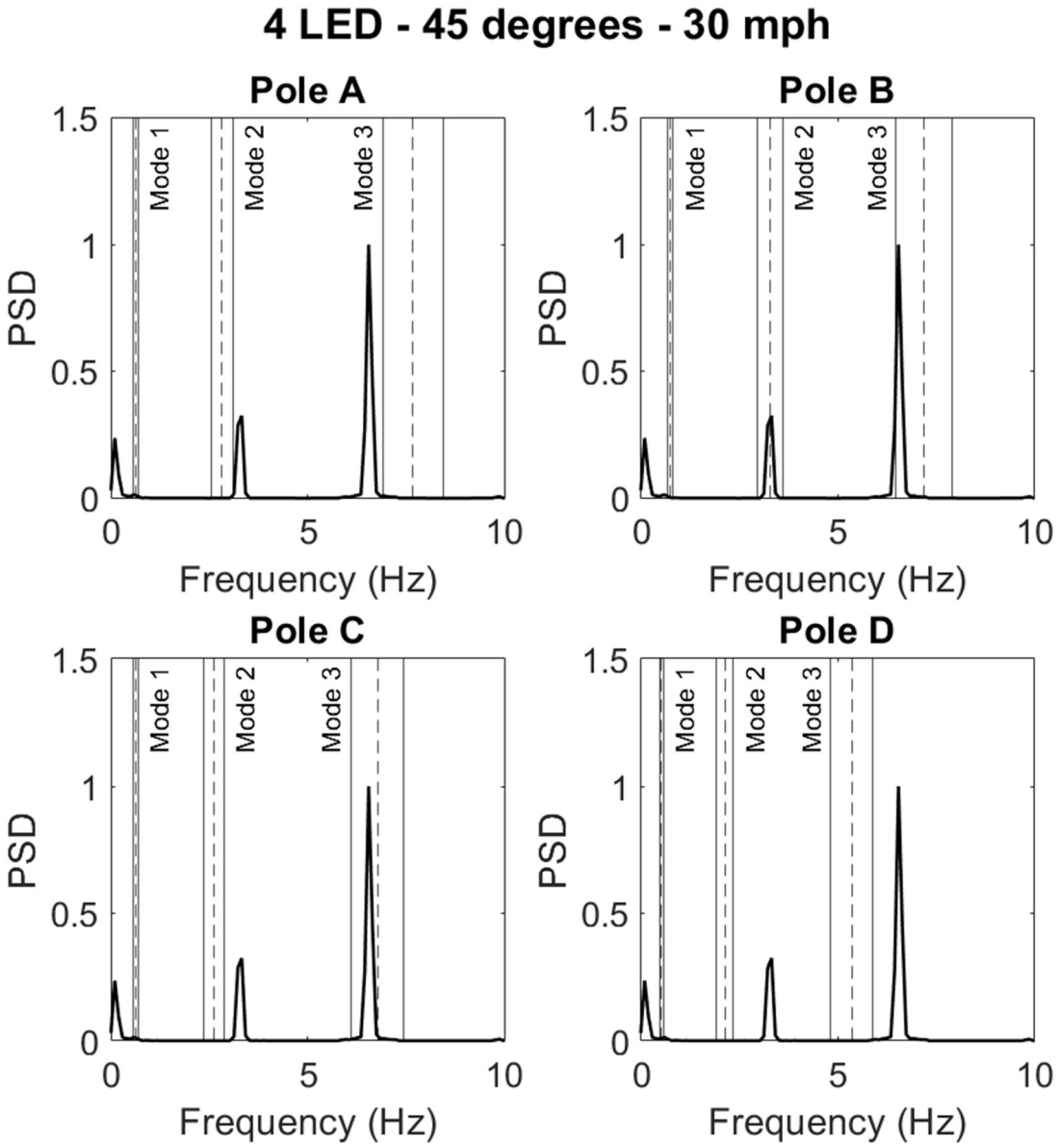
4 LED - 45 degrees - 30 mph
Pole A
Pole B
Pole C
Pole D
Mode 1
Mode 2
Mode 3
PSD
Frequency (Hz)
0
0.5
1
1.5
5
10

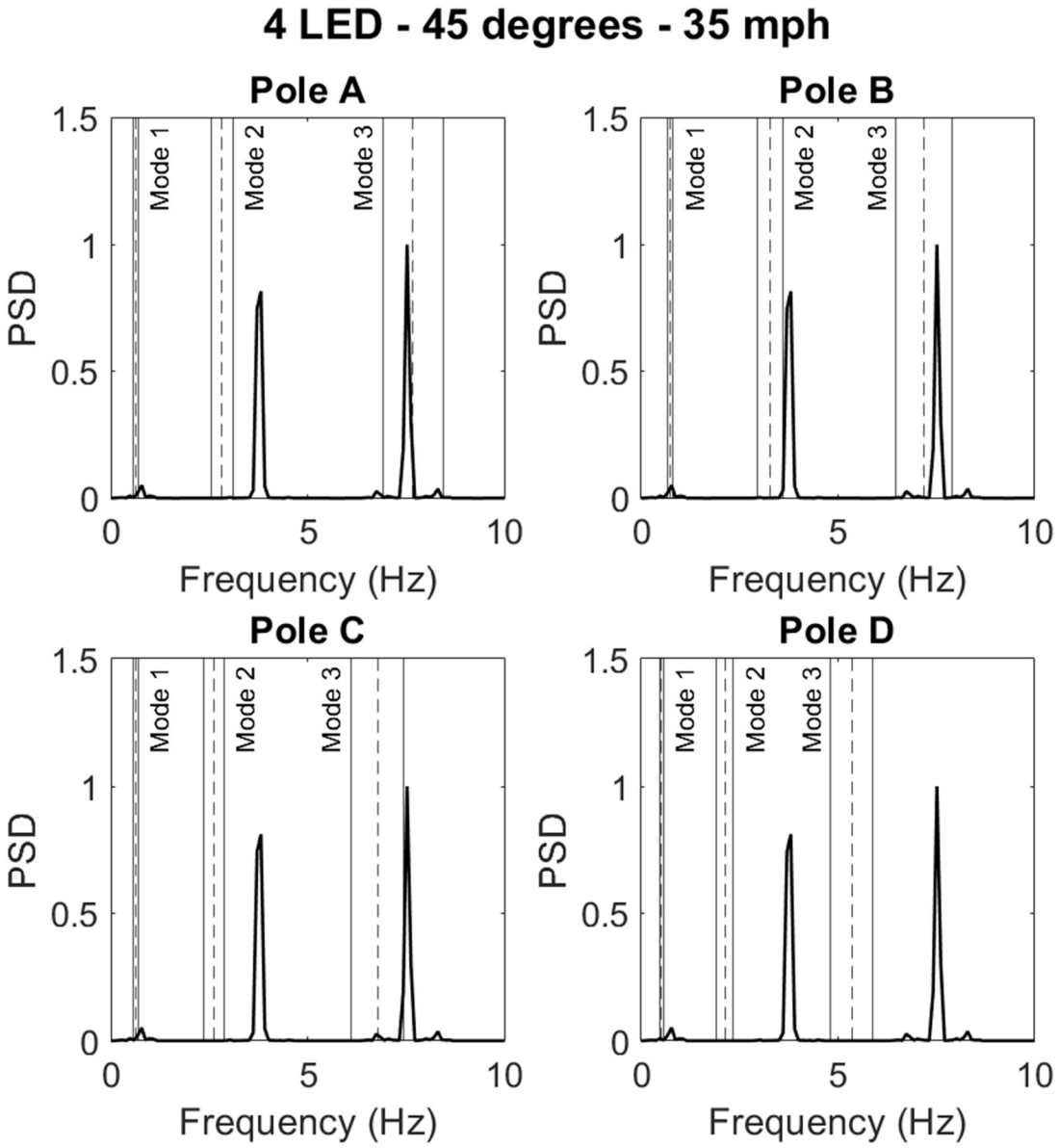
4 LED - 45 degrees - 35 mph
Pole A
Pole B
Pole C
Pole D
Mode 1
Mode 2
Mode 3
PSD
Frequency (Hz)
0
0.5
1
1.5
5
10

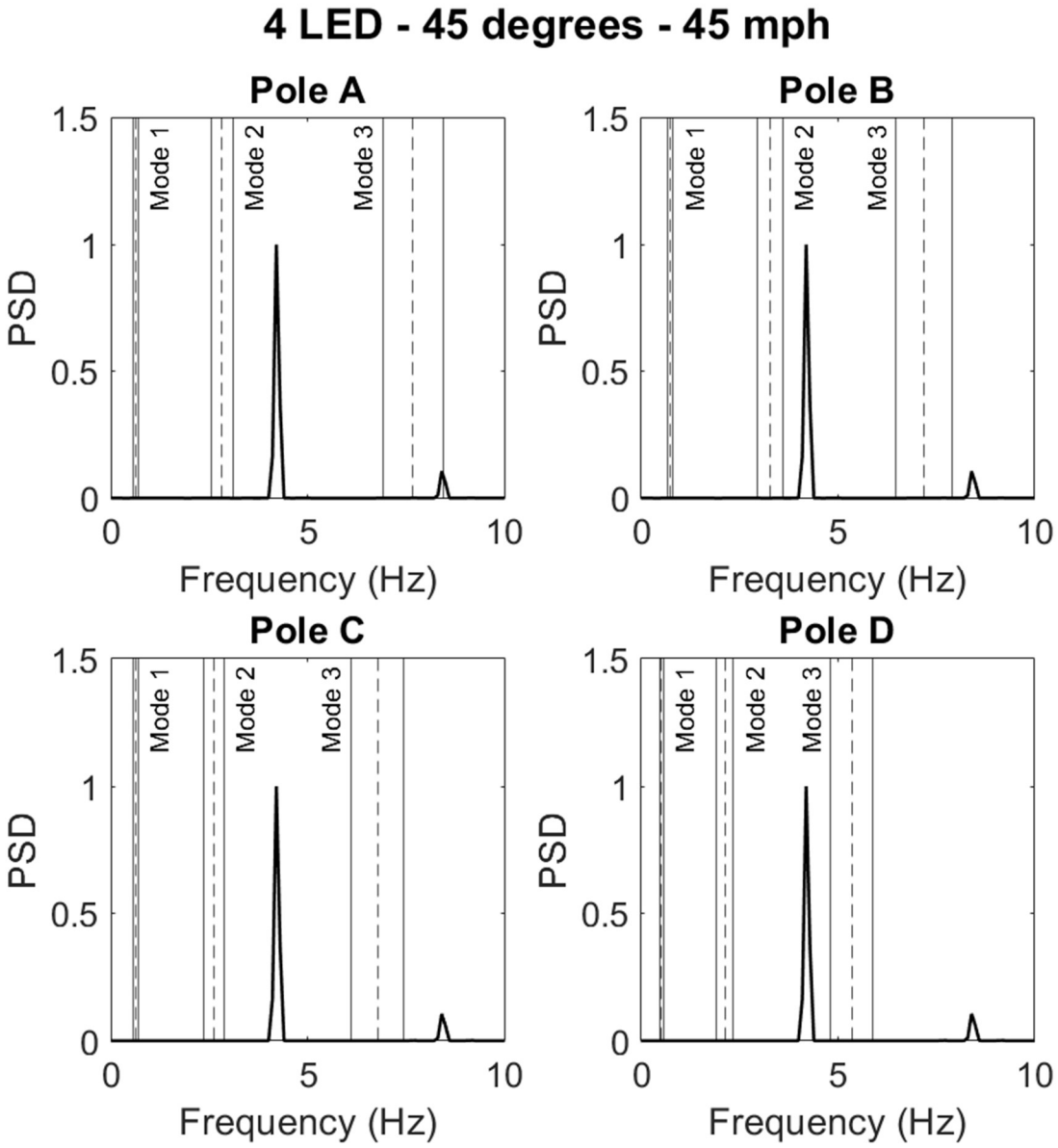
4 LED - 45 degrees - 45 mph
Pole A
Pole B
Pole C
Pole D
PSD
Frequency (Hz)
Mode 1
Mode 2
Mode 3
0
0.5
1
1.5
0
5
10

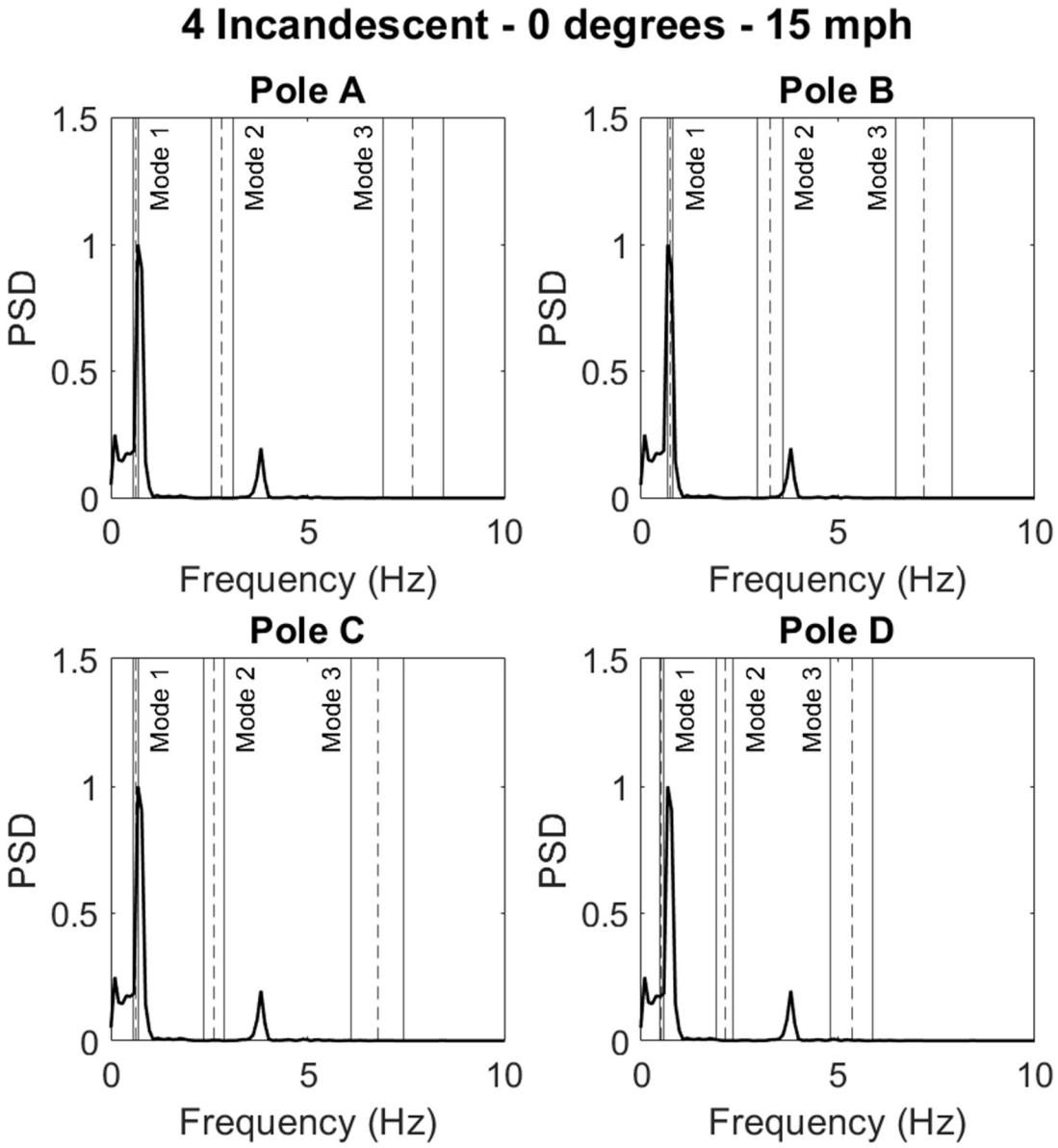
4 Incandescent - 0 degrees - 15 mph
Pole A
Pole B
Pole C
Pole D
Mode 1
Mode 2
Mode 3
PSD
Frequency (Hz)
0
0.5
1
1.5
5
10

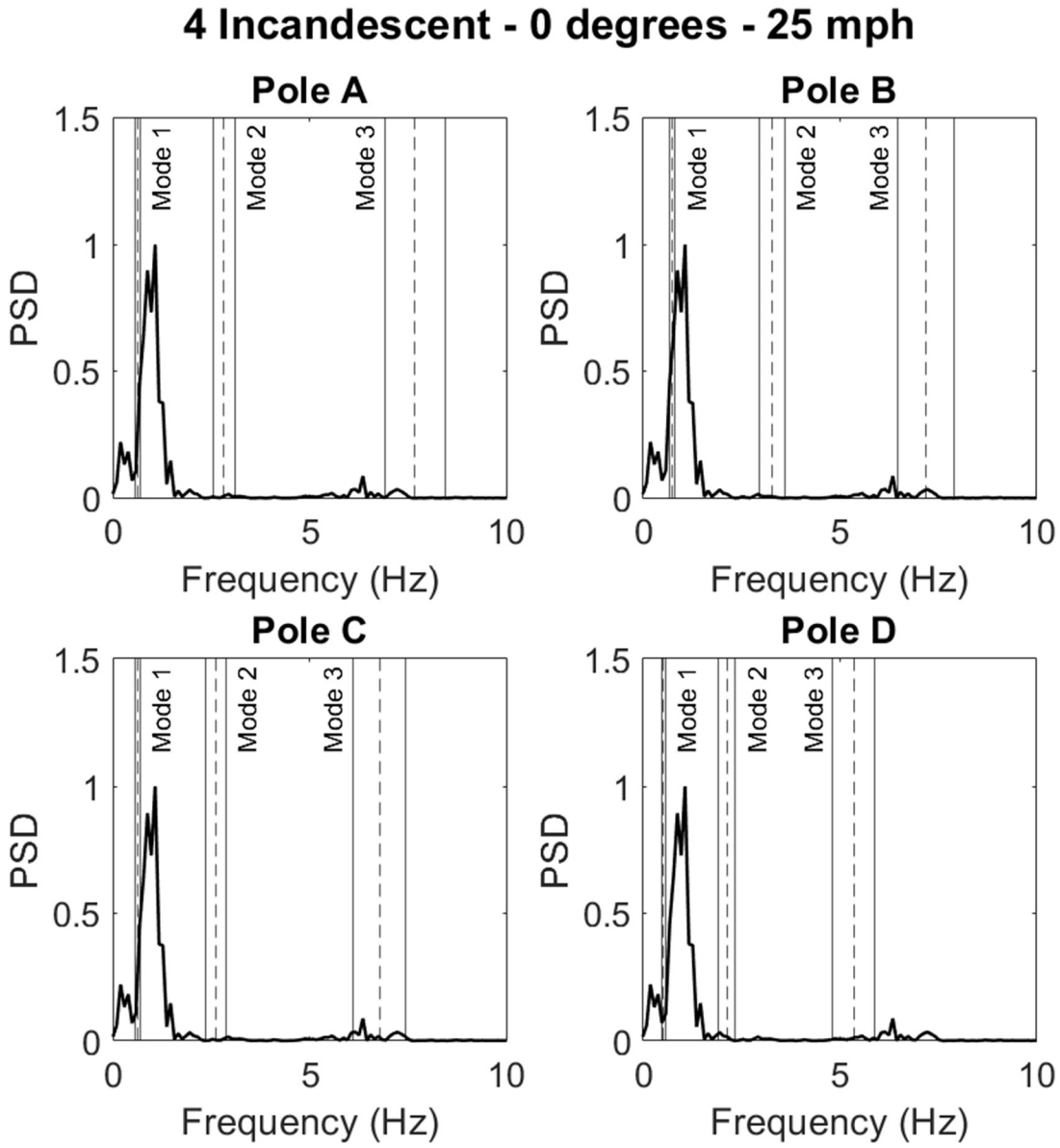
4 Incandescent - 0 degrees - 25 mph
Pole A
Pole B
Pole C
Pole D
PSD
Frequency (Hz)
Mode 1
Mode 2
Mode 3
0
0.5
1
1.5
5
10

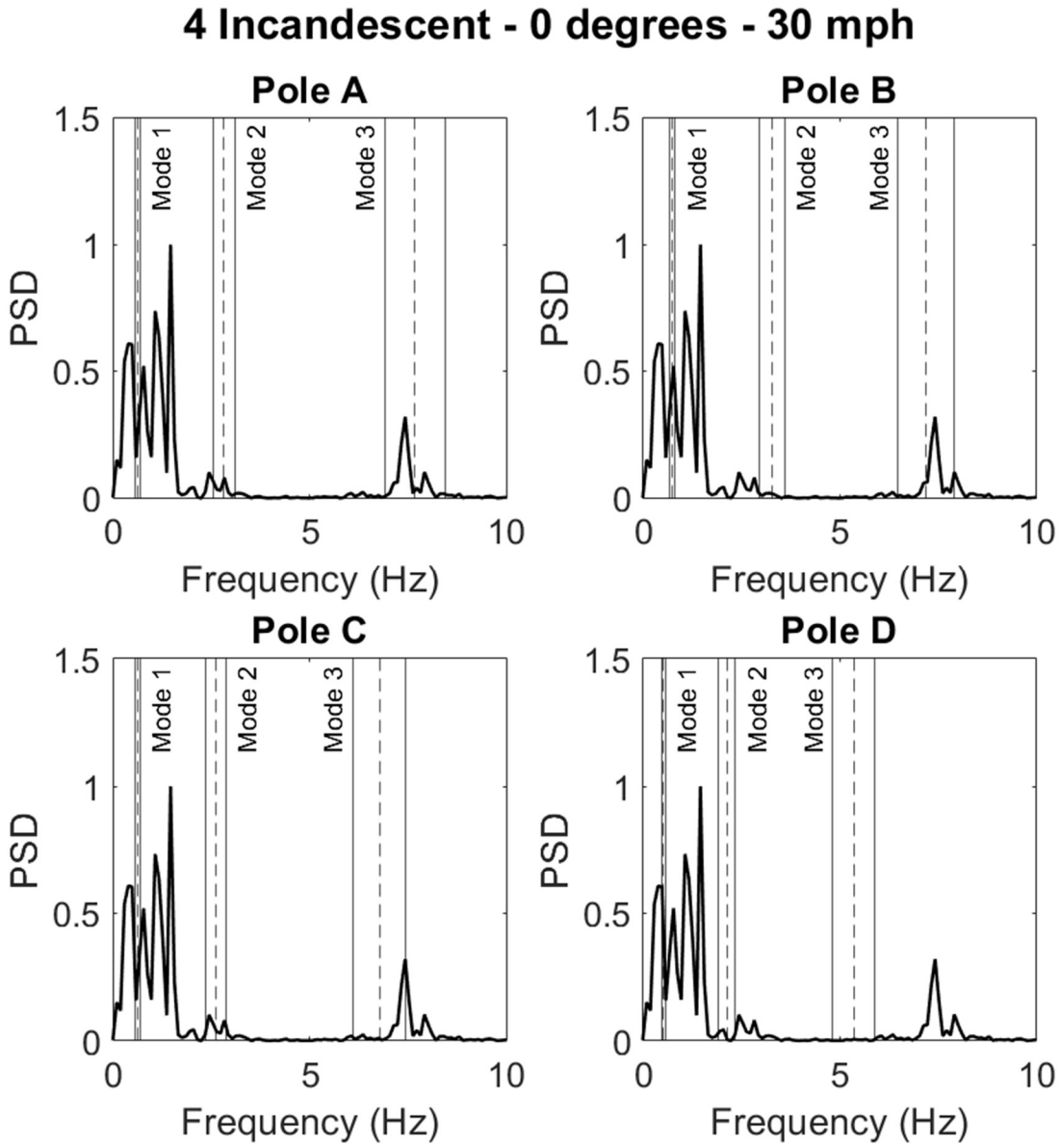
4 Incandescent - 0 degrees - 30 mph
Pole A
Pole B
Pole C
Pole D
Mode 1
Mode 2
Mode 3
PSD
Frequency (Hz)
0
0.5
1
1.5
5
10

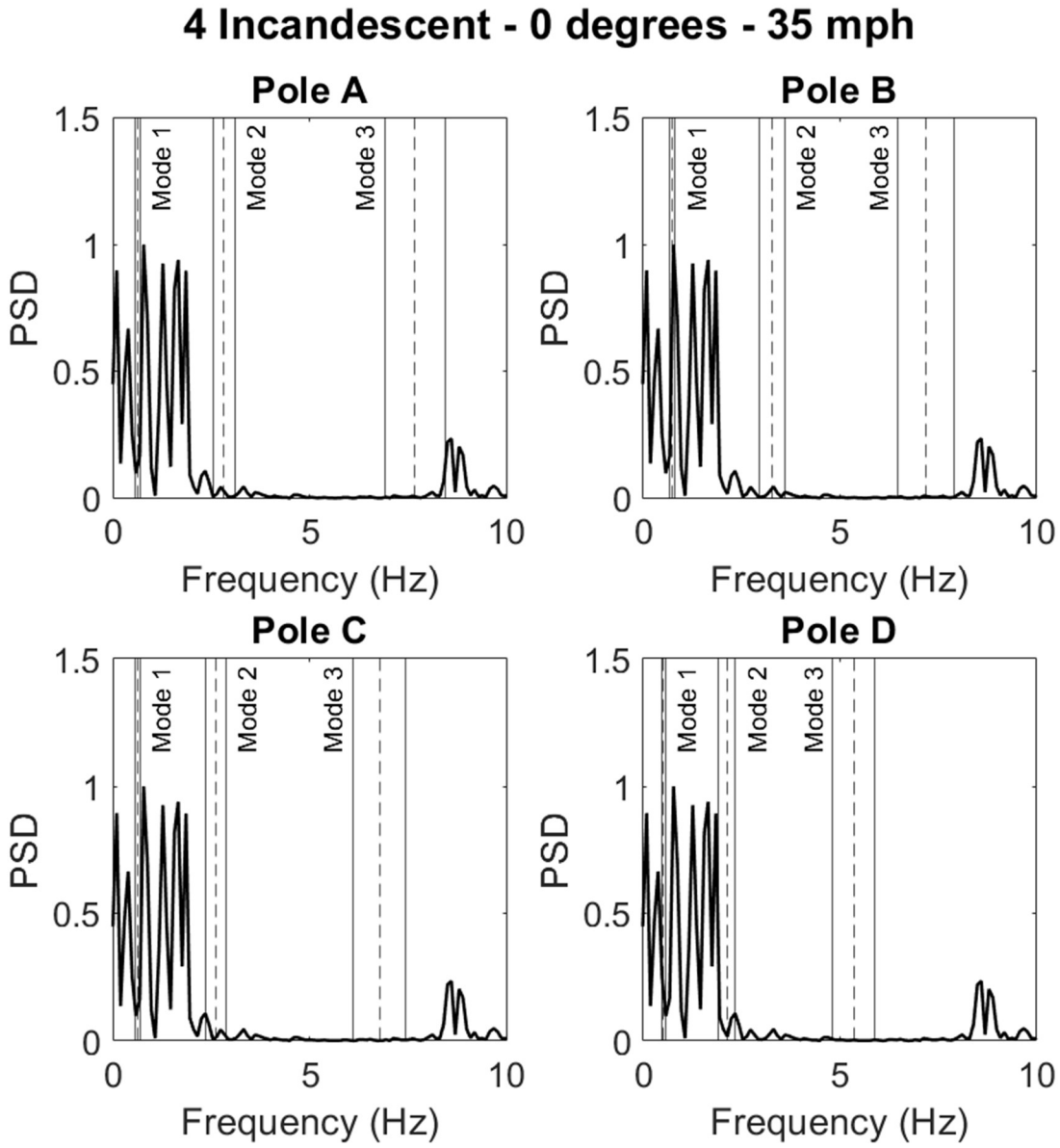
4 Incandescent - 0 degrees - 35 mph
Pole A
Pole B
Pole C
Pole D
Mode 1
Mode 2
Mode 3
PSD
Frequency (Hz)
0
0.5
1
1.5
5
10

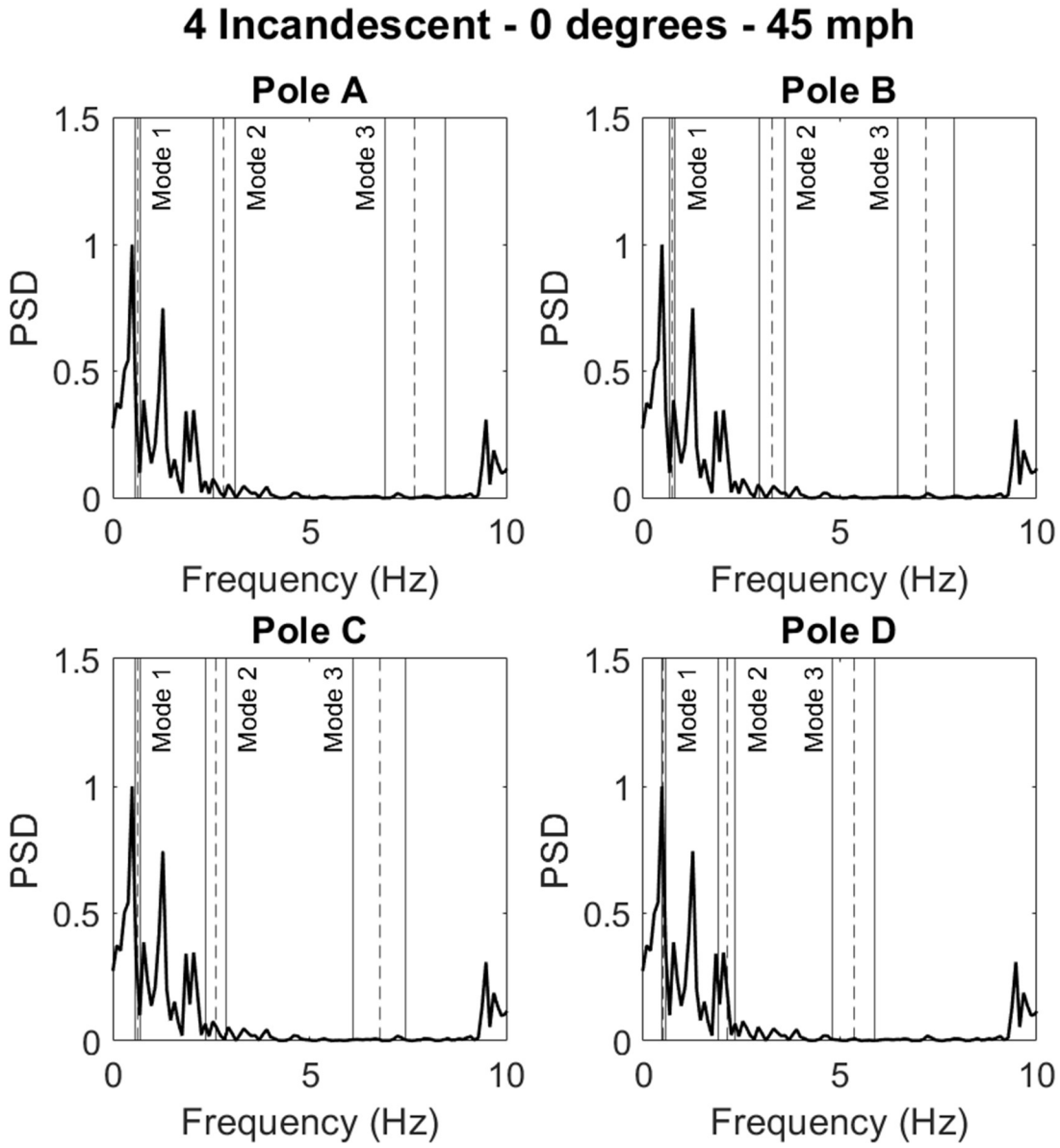
4 Incandescent - 0 degrees - 45 mph
Pole A
Pole B
Pole C
Pole D
Mode 1
Mode 2
Mode 3
PSD
Frequency (Hz)
0
0.5
1
1.5
5
10

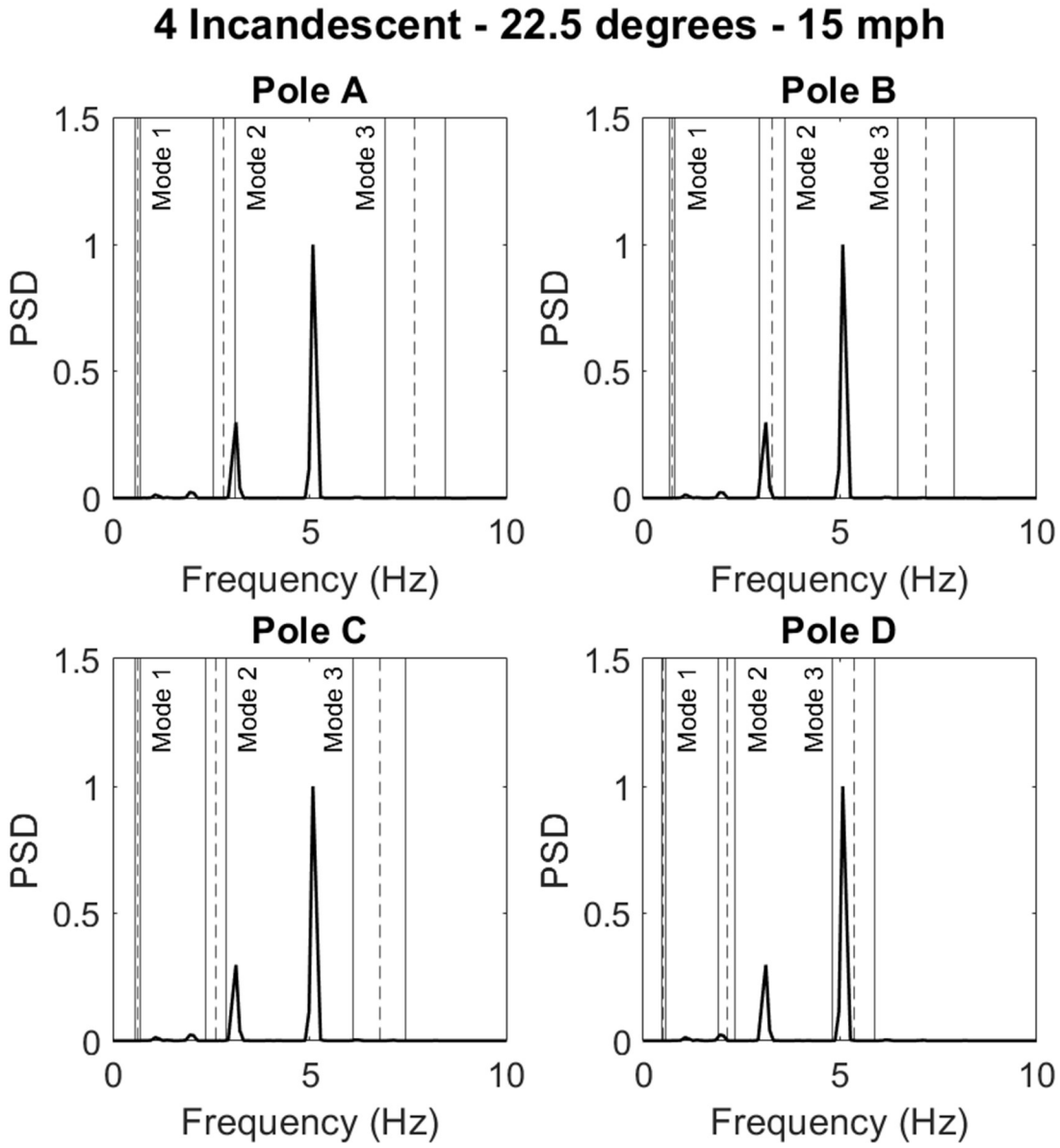
4 Incandescent - 22.5 degrees - 15 mph
Pole A
Pole B
Pole C
Pole D
Mode 1
Mode 2
Mode 3
PSD
Frequency (Hz)
0
0.5
1
1.5
5
10

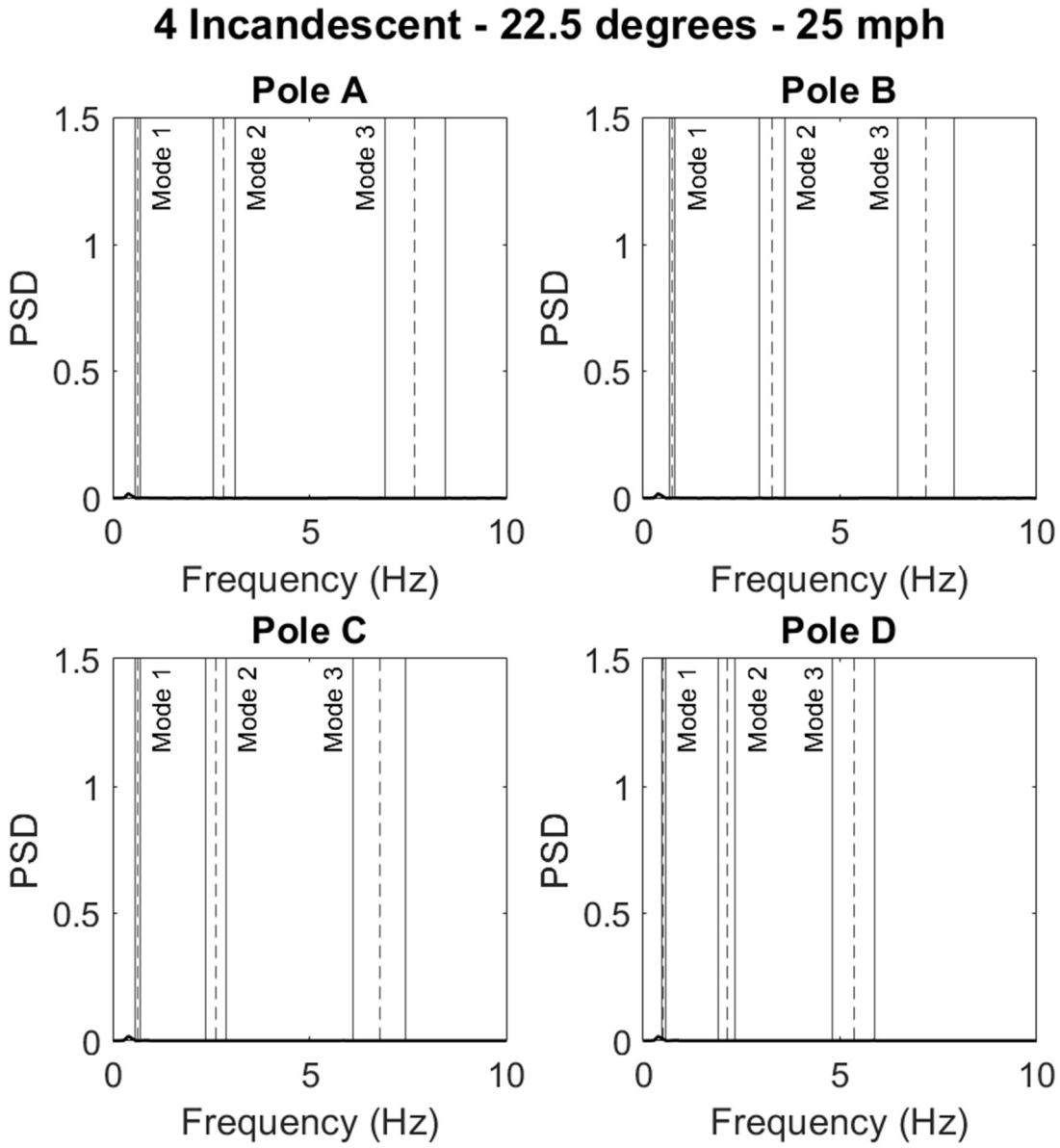
4 Incandescent - 22.5 degrees - 25 mph
Pole A
Pole B
Pole C
Pole D
PSD
Frequency (Hz)
Mode 1
Mode 2
Mode 3
0
0.5
1
1.5
5
10

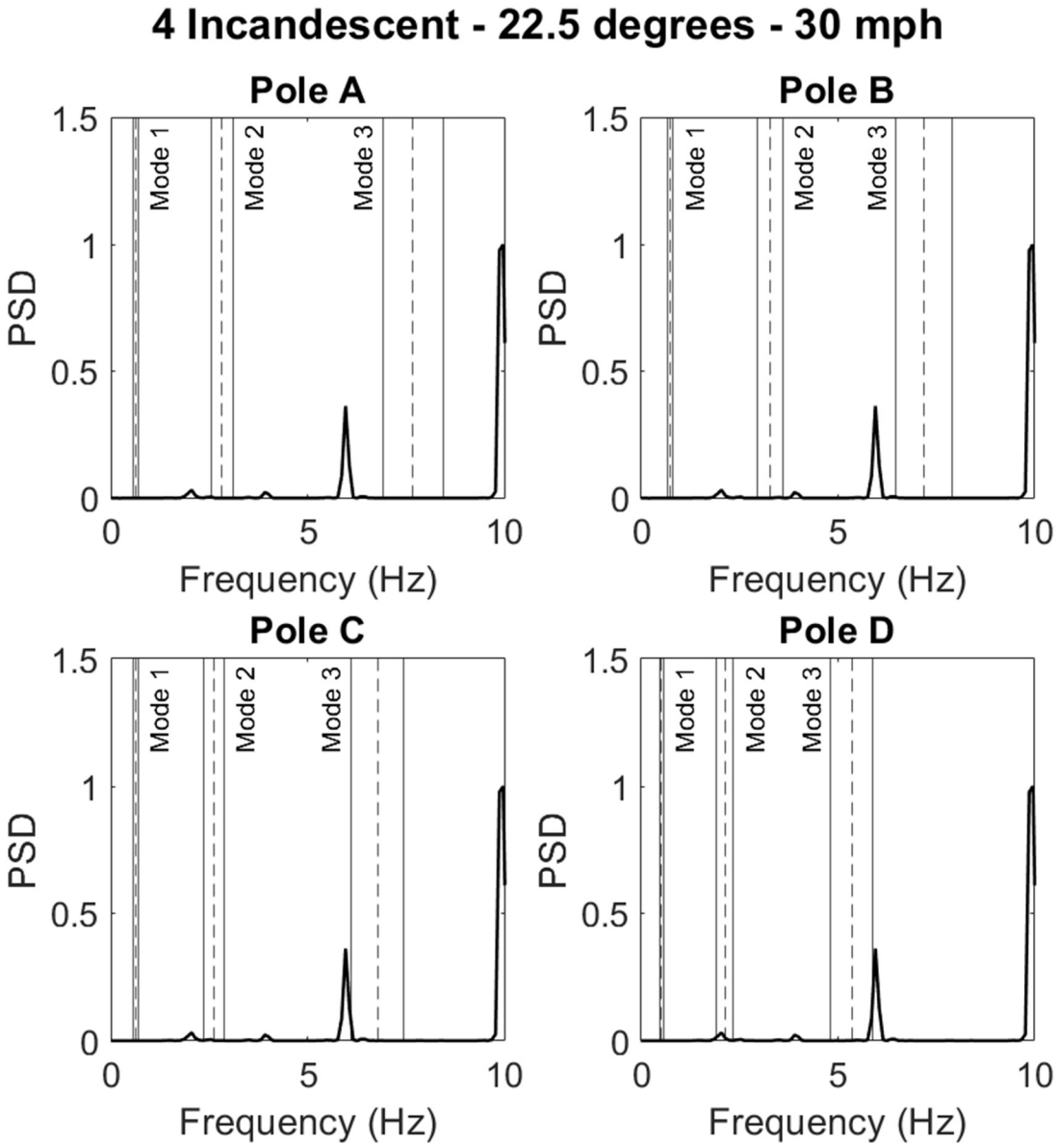
4 Incandescent - 22.5 degrees - 30 mph
Pole A
Pole B
Pole C
Pole D
Mode 1
Mode 2
Mode 3
PSD
Frequency (Hz)
0
0.5
1
1.5
5
10

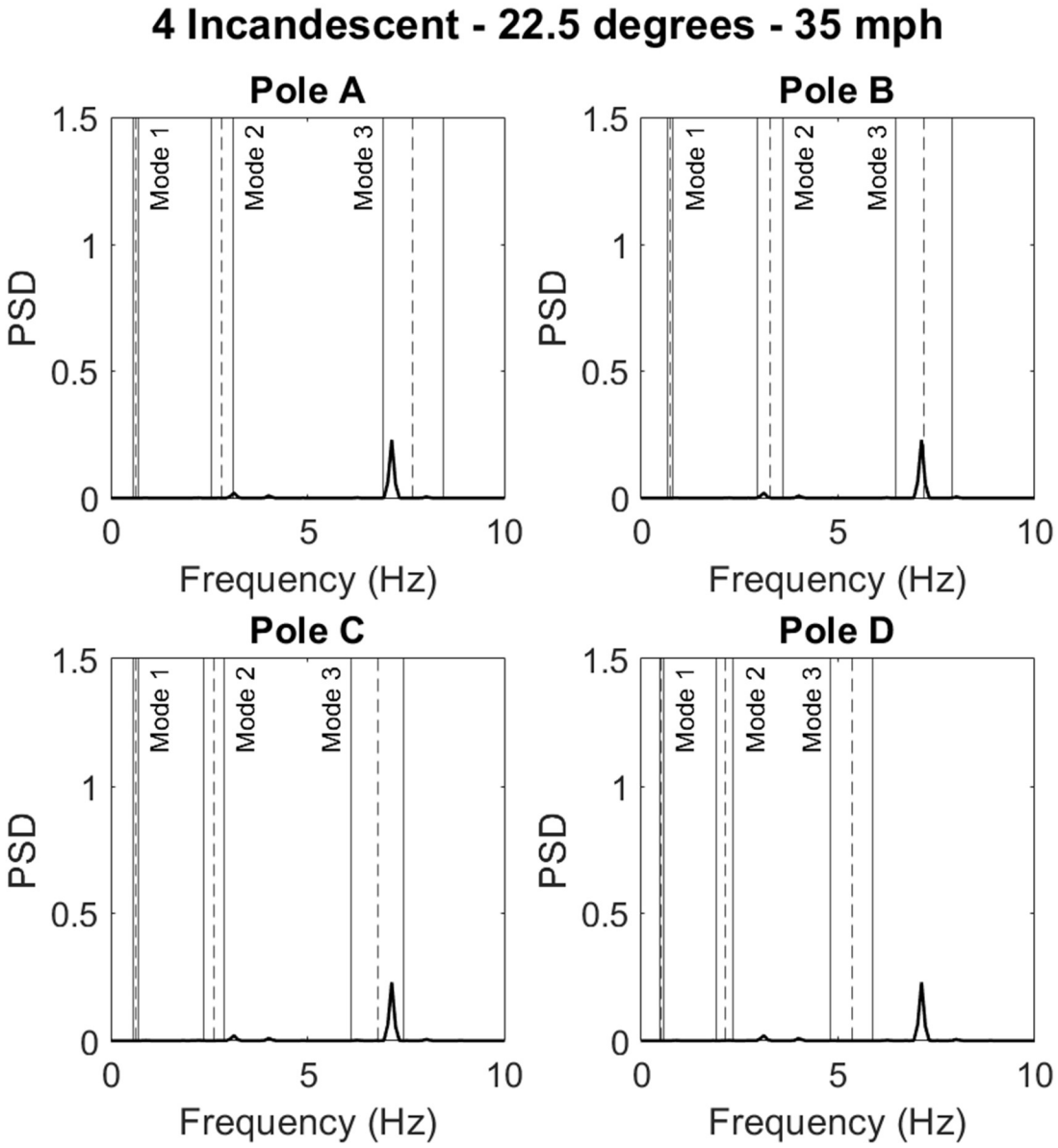
4 Incandescent - 22.5 degrees - 35 mph
Pole A
Pole B
Pole C
Pole D
Mode 1
Mode 2
Mode 3
PSD
Frequency (Hz)
0
0.5
1
1.5
5
10

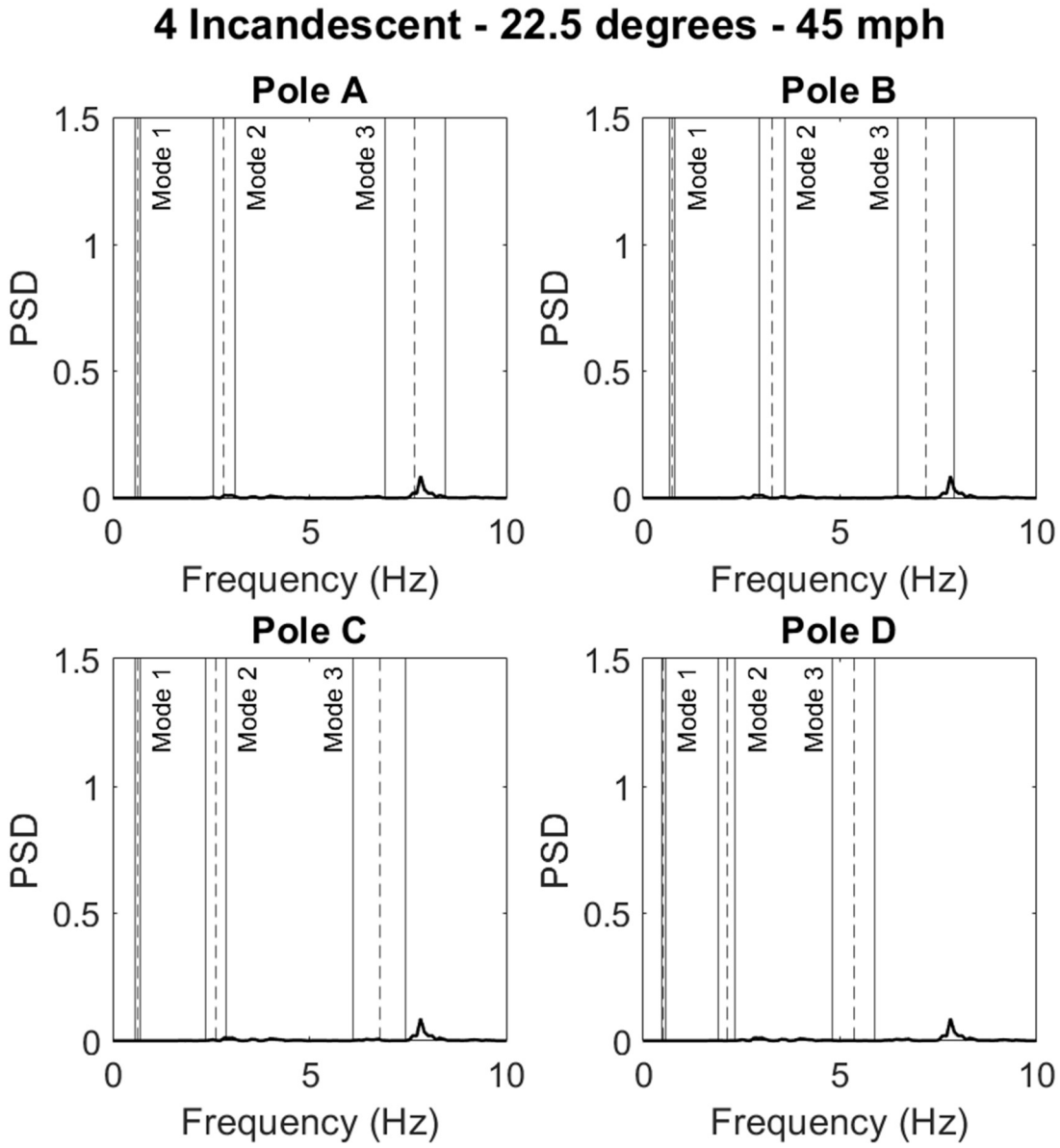
4 Incandescent - 22.5 degrees - 45 mph
Pole A
Pole B
Pole C
Pole D
Mode 1
Mode 2
Mode 3
PSD
Frequency (Hz)
0
0.5
1
1.5
5
10

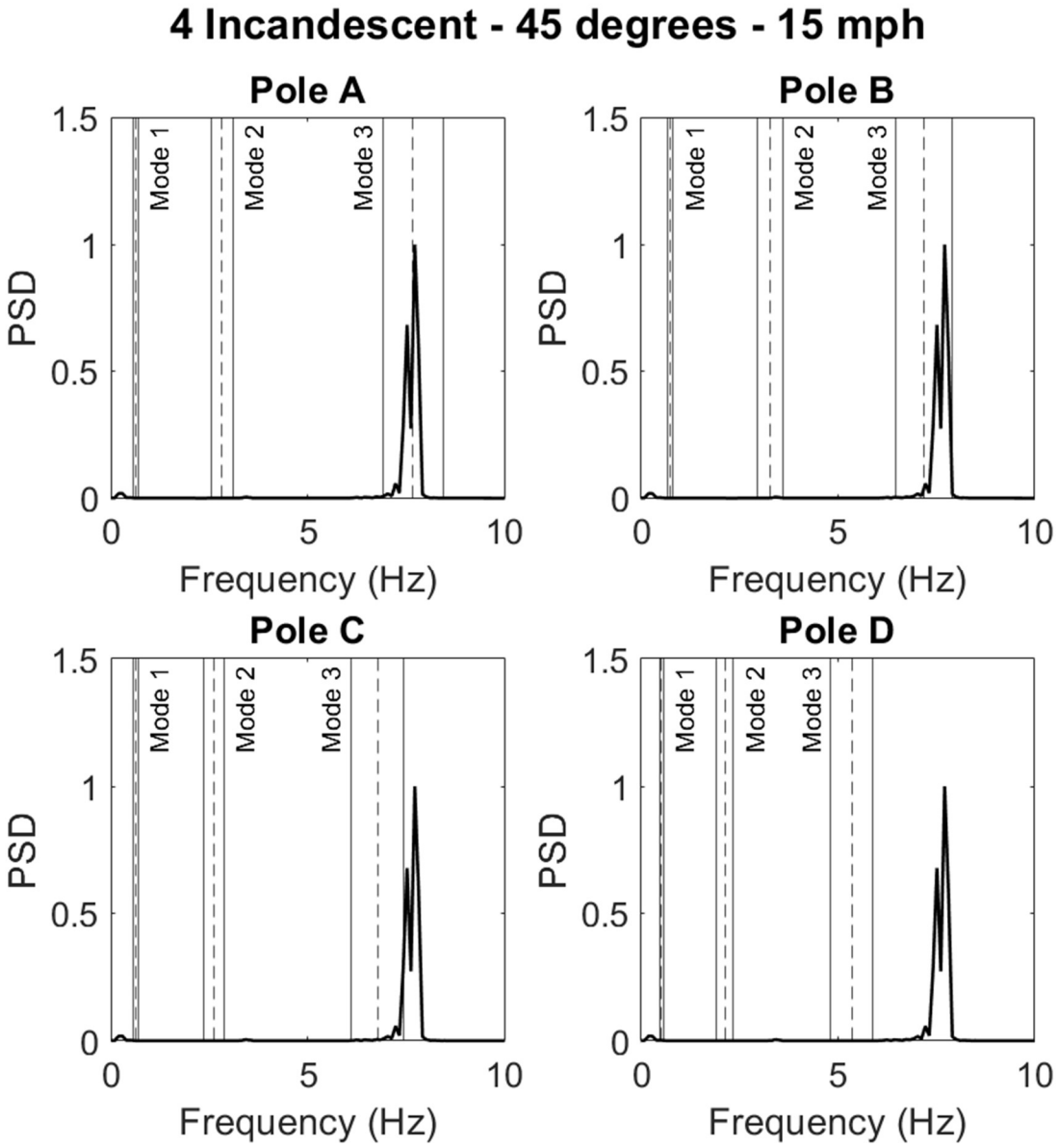
4 Incandescent - 45 degrees - 15 mph
Pole A
Pole B
Pole C
Pole D
Mode 1
Mode 2
Mode 3
PSD
Frequency (Hz)
0
0.5
1
1.5
5
10

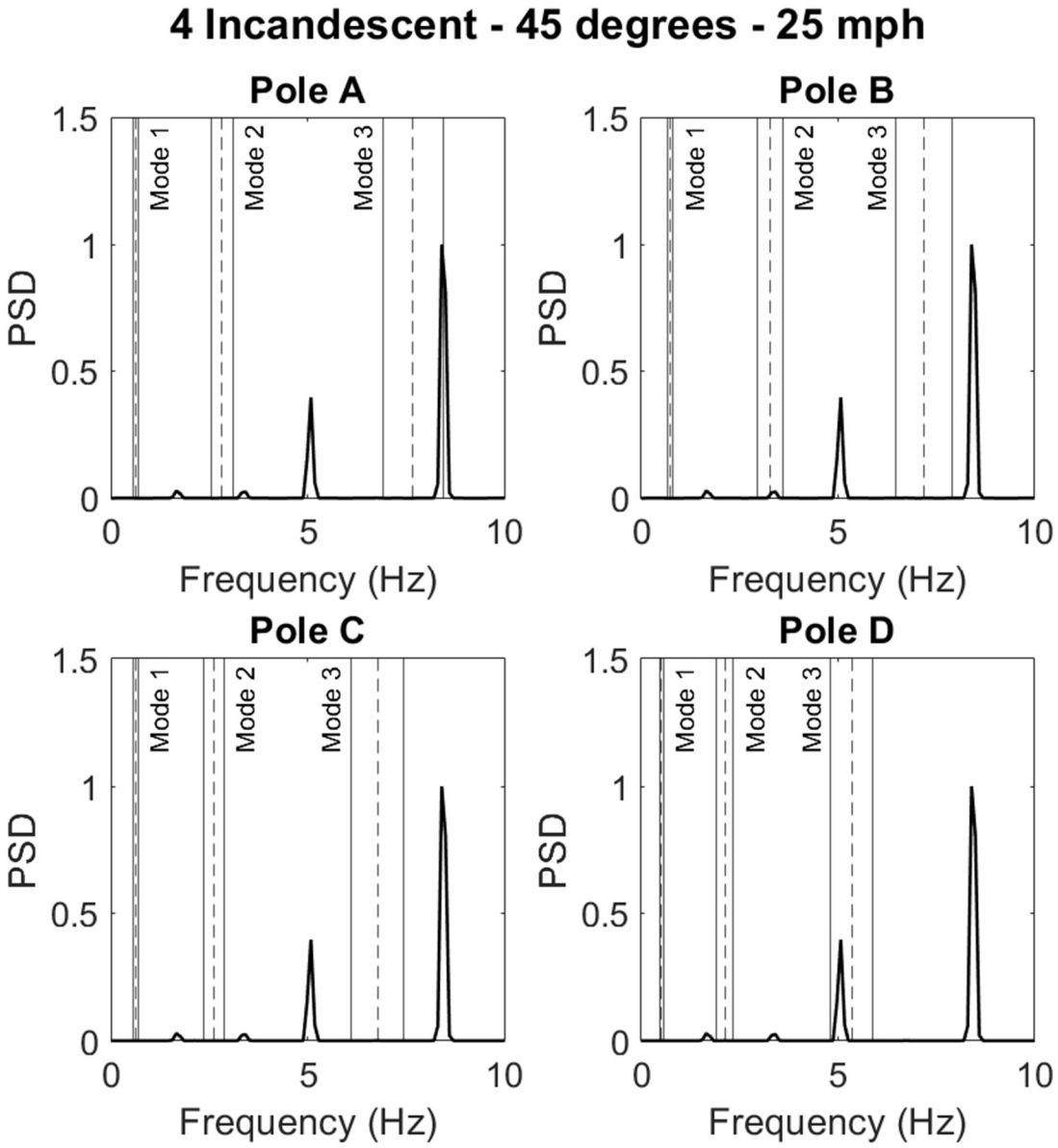
4 Incandescent - 45 degrees - 25 mph
Pole A
Pole B
Pole C
Pole D
Mode 1
Mode 2
Mode 3
PSD
Frequency (Hz)
0
0.5
1
1.5
5
10

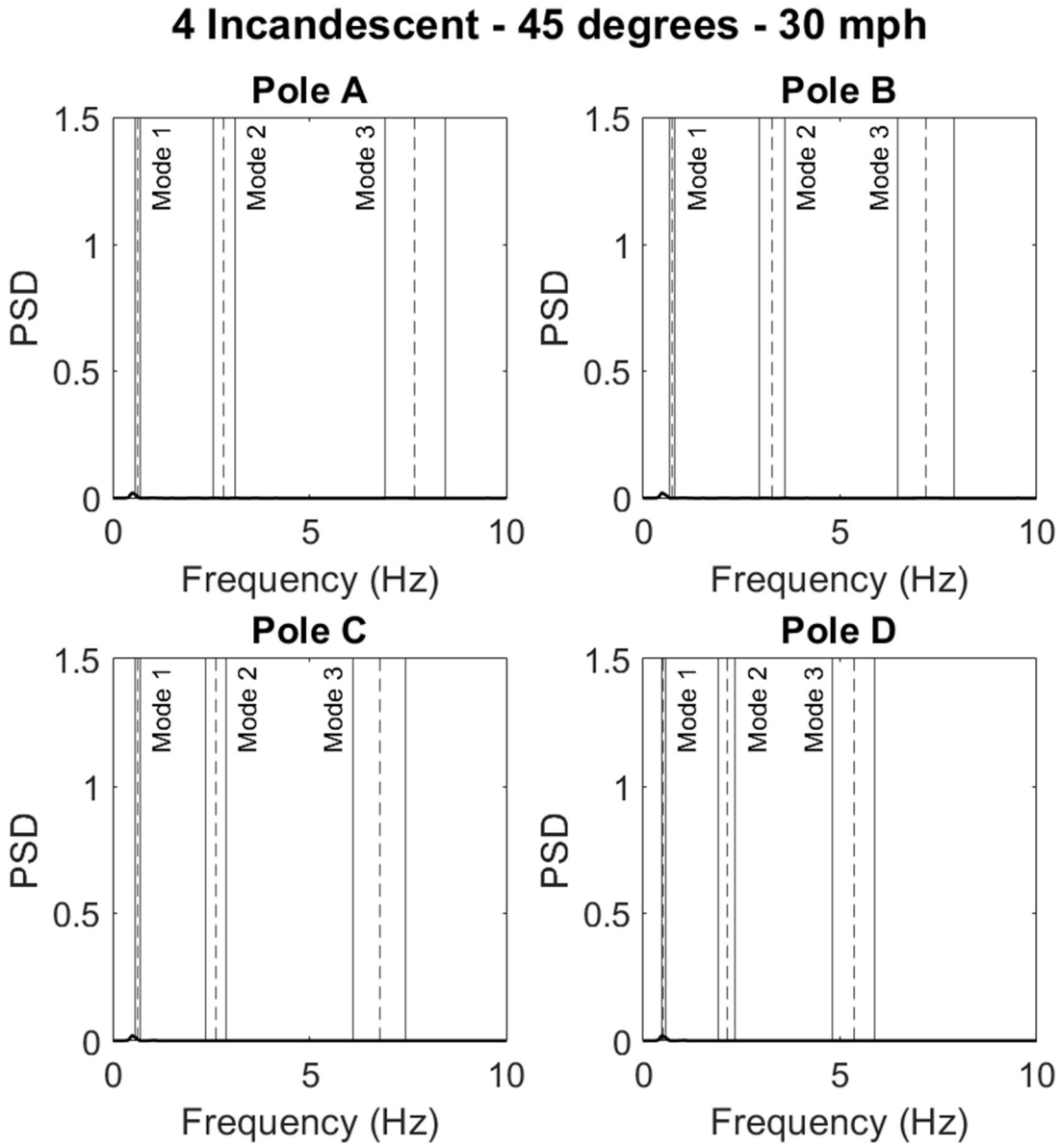
4 Incandescent - 45 degrees - 30 mph
Pole A
Pole B
Pole C
Pole D
Mode 1
Mode 2
Mode 3
PSD
Frequency (Hz)
0
0.5
1
1.5
5
10

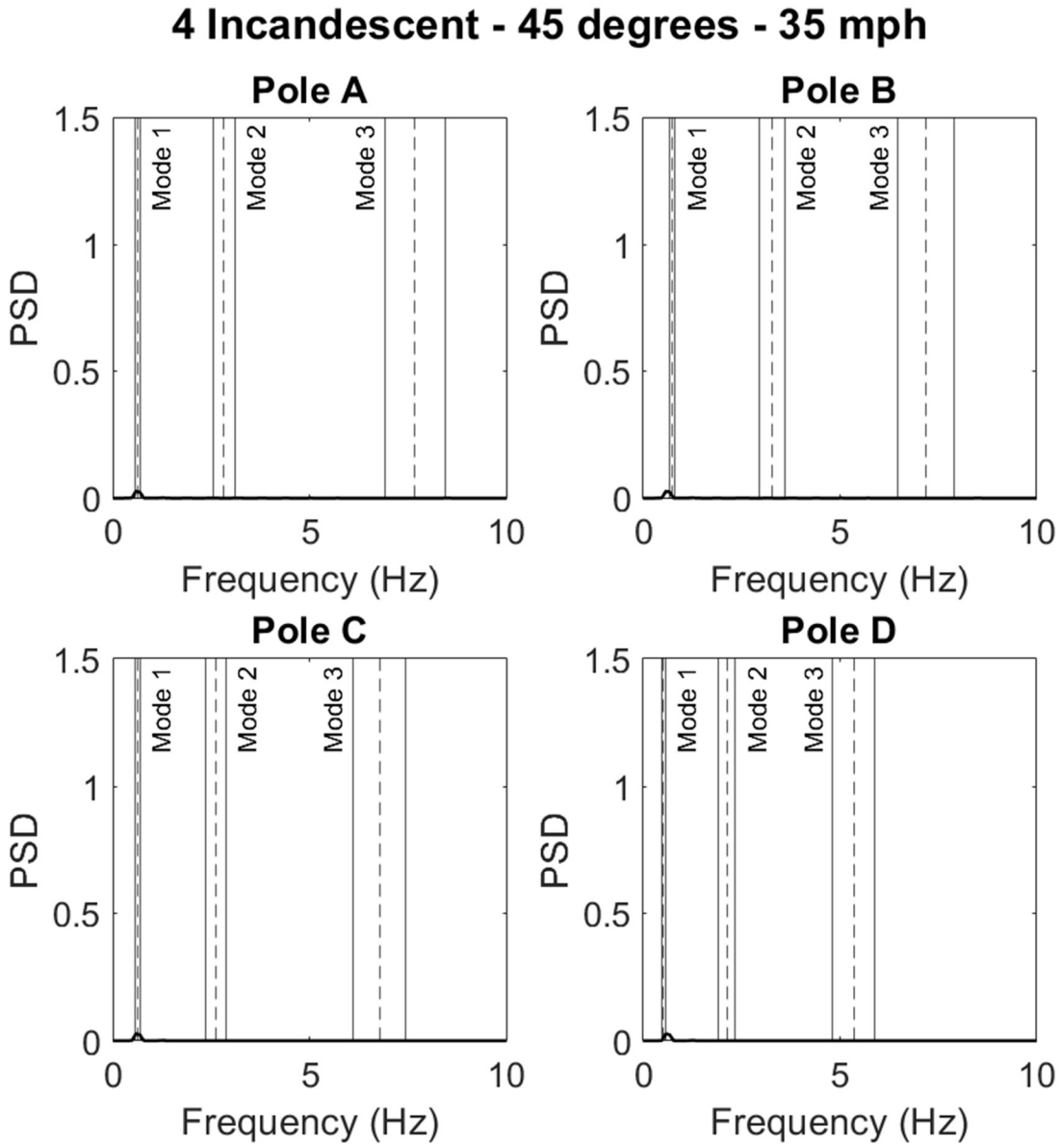
4 Incandescent - 45 degrees - 35 mph
Pole A
Pole B
Pole C
Pole D
PSD
Frequency (Hz)
Mode 1
Mode 2
Mode 3
0
0.5
1
1.5
5
10

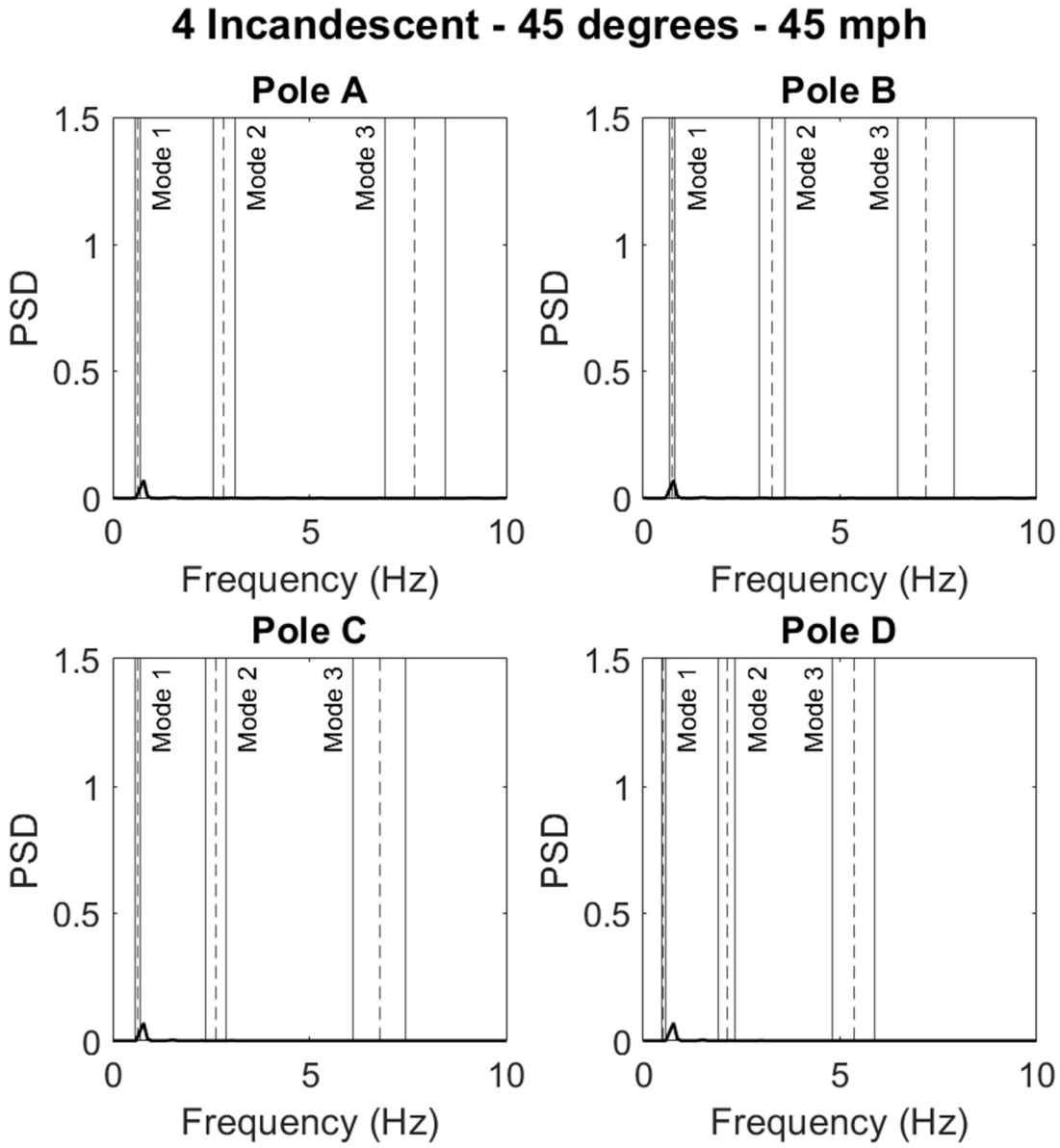
4 Incandescent - 45 degrees - 45 mph
Pole A
Pole B
Pole C
Pole D
Mode 1
Mode 2
Mode 3
PSD
Frequency (Hz)
0
0.5
1
1.5
5
10

APPENDIX A3

A3.1 Color-Band Comparison Charts for Abaqus Simulations

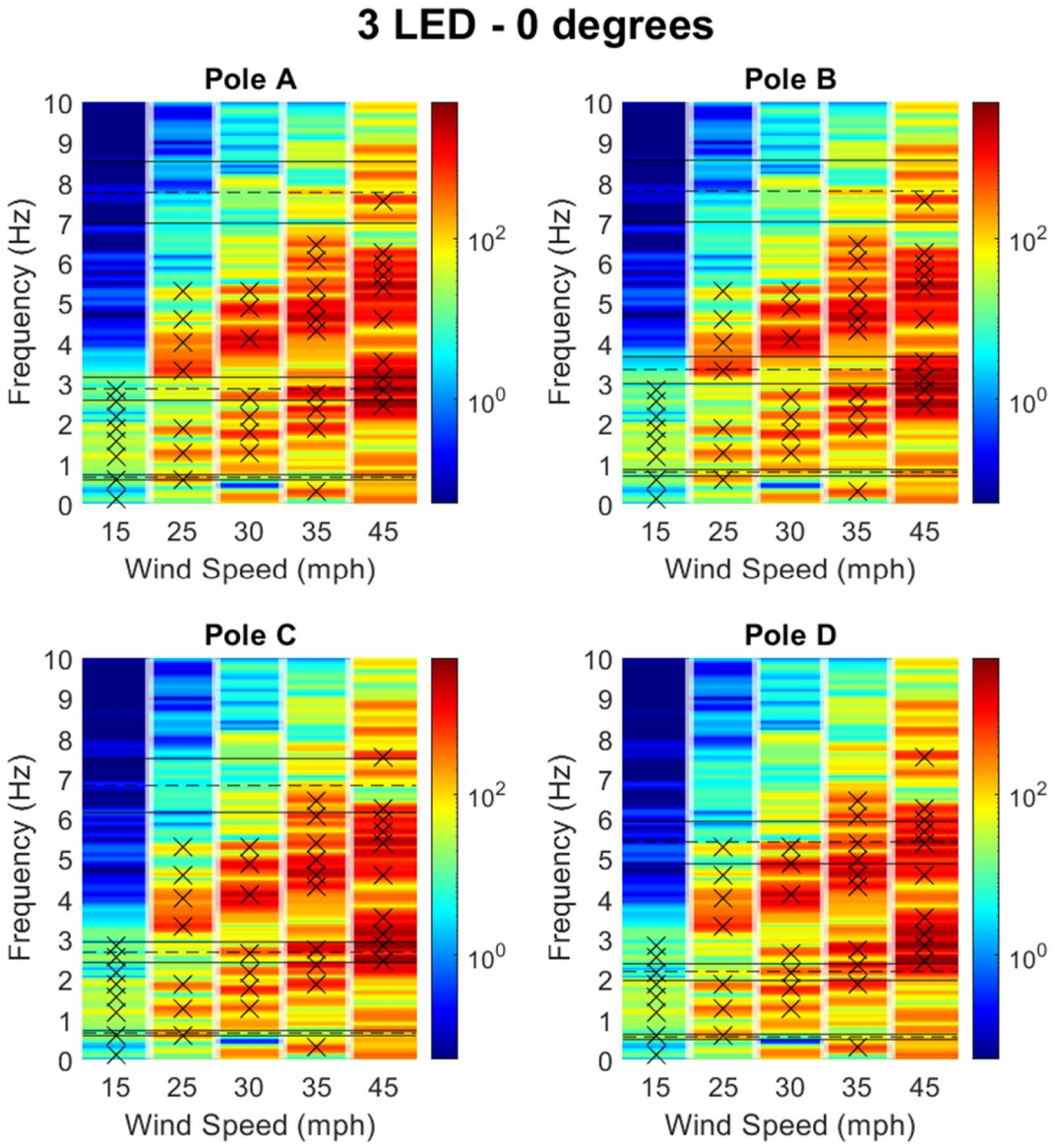

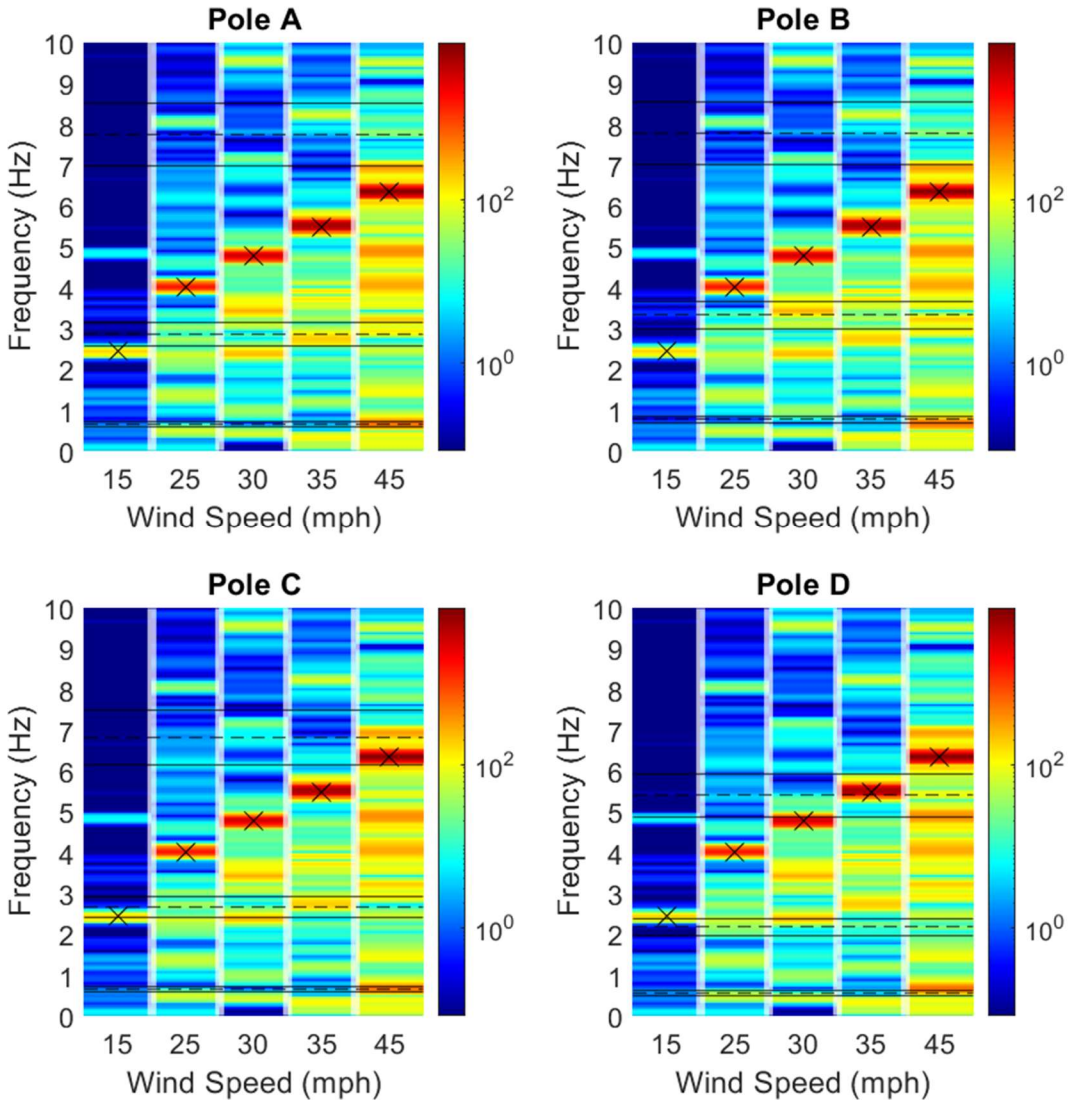
3 LED - 30 degrees
Pole A
Pole B
Pole C
Pole D
Frequency (Hz)
Wind Speed (mph)
0
1
2
3
4
5
6
7
8
9
10
15
25
30
35
45
10^2
10^0

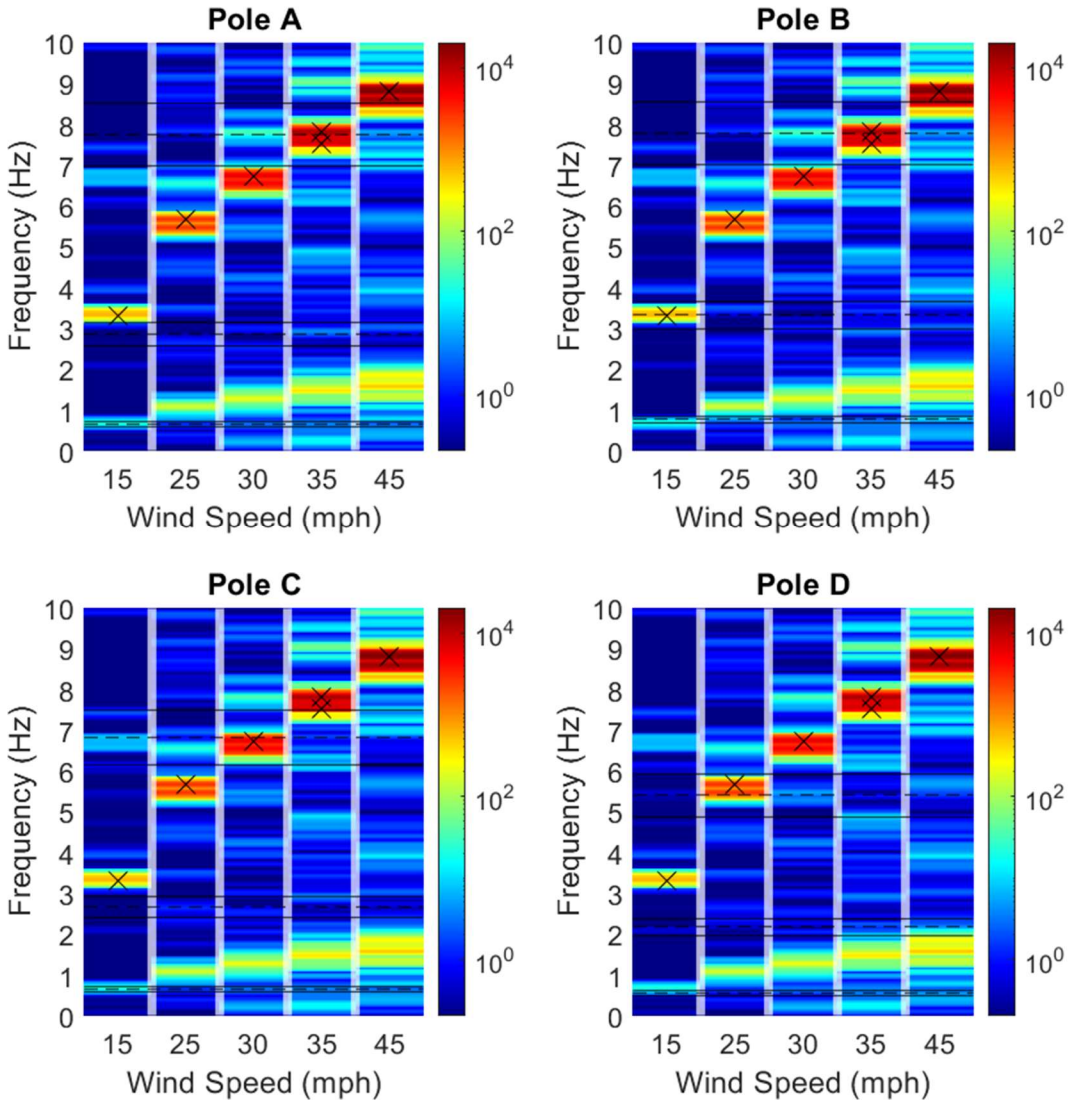
3 LED - 60 degrees
Pole A
Pole B
Pole C
Pole D
Frequency (Hz)
Wind Speed (mph)
0
1
2
3
4
5
6
7
8
9
10
15
25
30
35
45
10^0
10^2
10^4

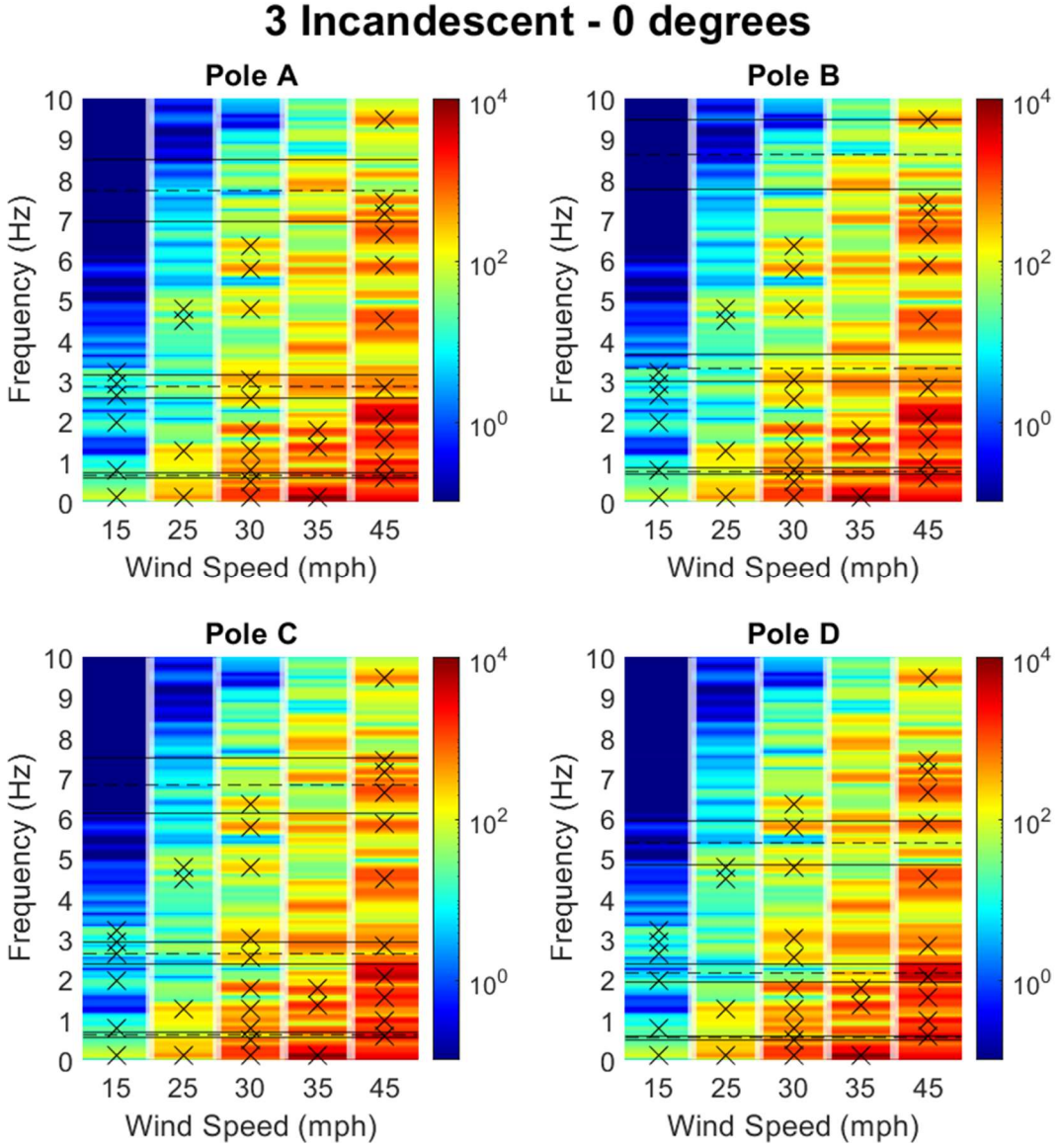
3 Incandescent - 0 degrees
Pole A
Pole B
Pole C
Pole D
Frequency (Hz)
Wind Speed (mph)
0
1
2
3
4
5
6
7
8
9
10
15
25
30
35
45
10^0
10^2
10^4

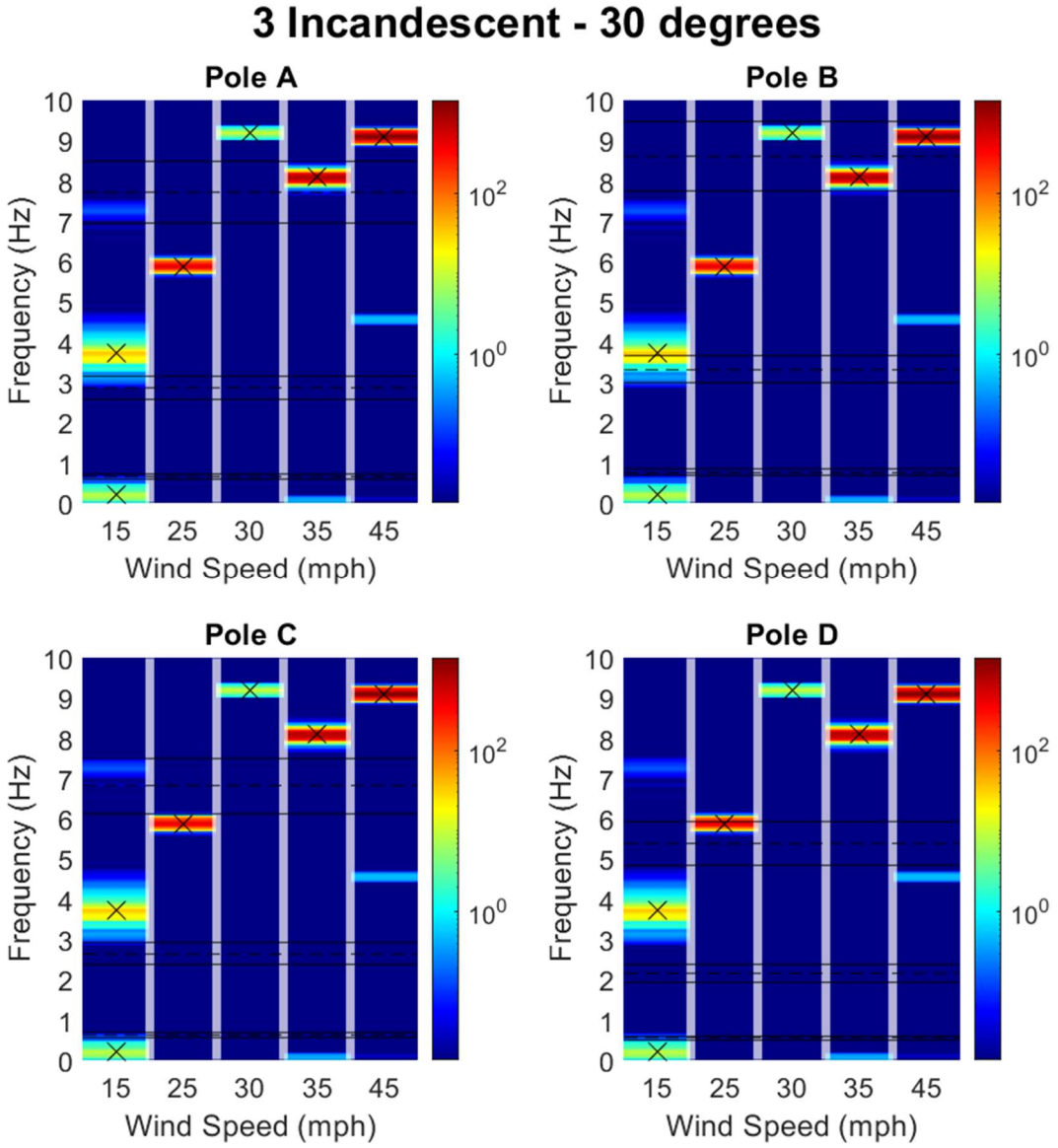
3 Incandescent - 30 degrees
Pole A
Pole B
Pole C
Pole D
Frequency (Hz)
Wind Speed (mph)
15 25 30 35 45
0 1 2 3 4 5 6 7 8 9 10
10^2
10^0

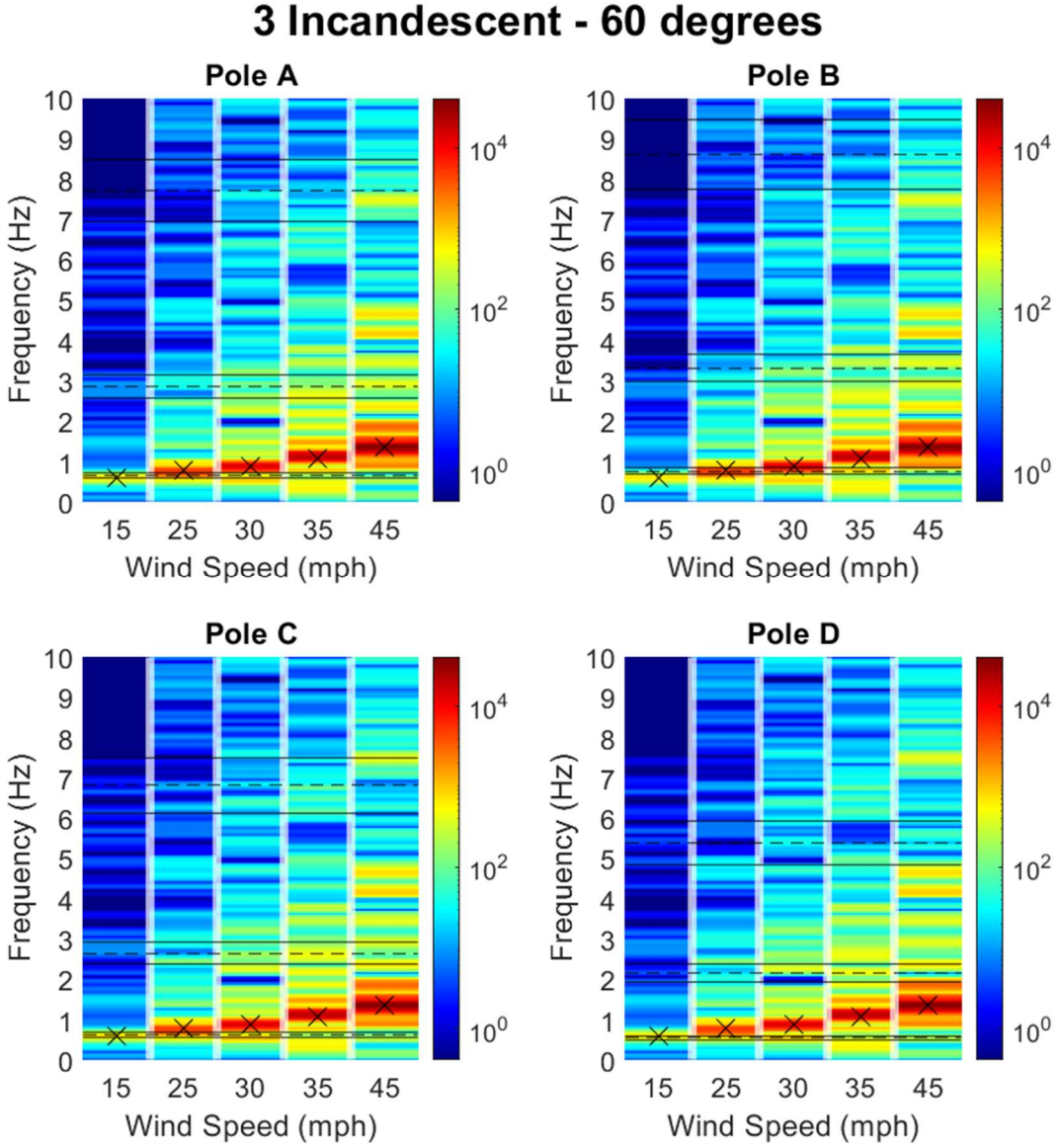
3 Incandescent - 60 degrees
Pole A
Pole B
Pole C
Pole D
Frequency (Hz)
Wind Speed (mph)
0
1
2
3
4
5
6
7
8
9
10
15
25
30
35
45
10^0
10^2
10^4

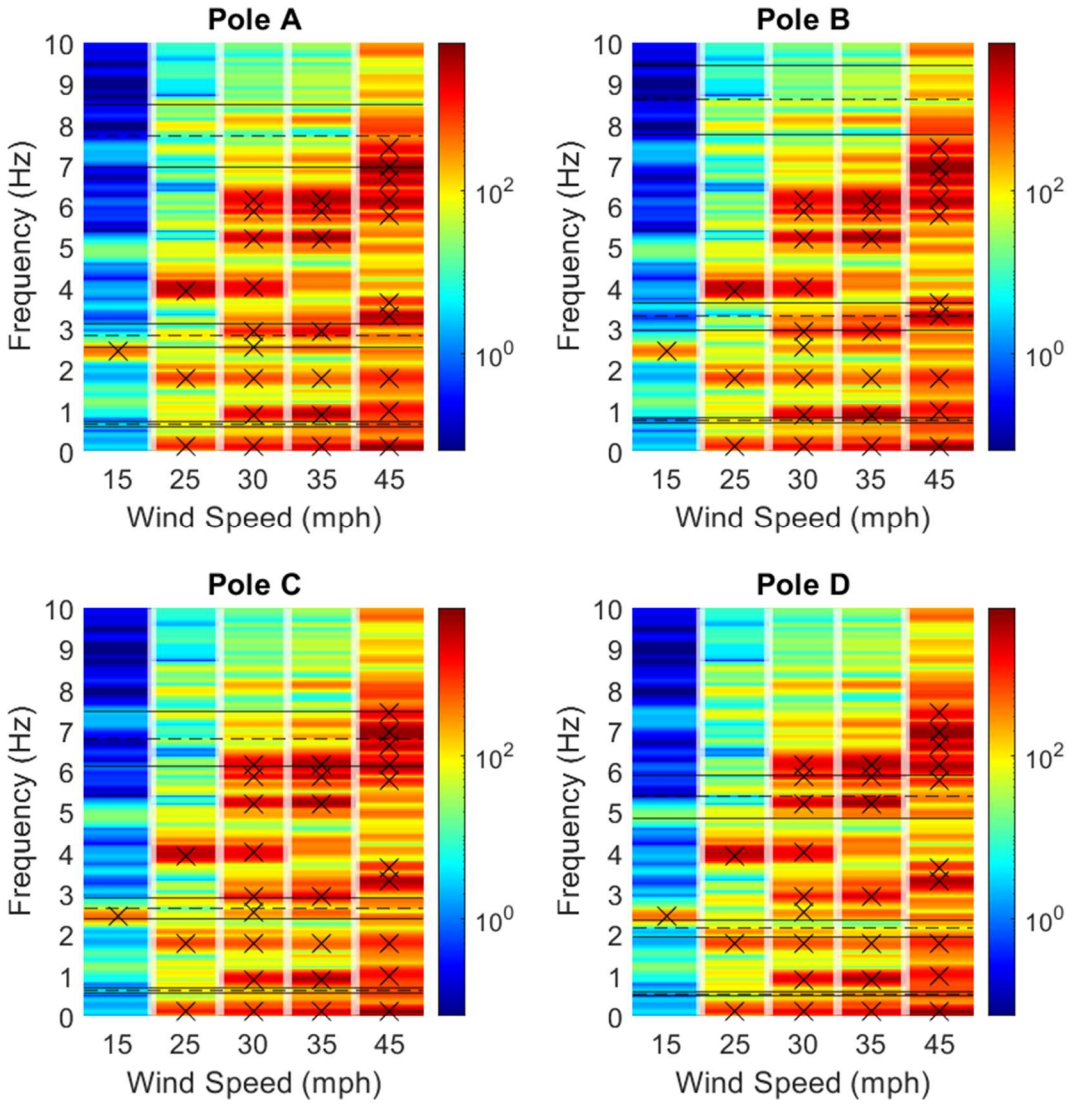
4 LED - 0 degrees
Pole A
Pole B
Pole C
Pole D
Frequency (Hz)
Wind Speed (mph)
0
1
2
3
4
5
6
7
8
9
10
15
25
30
35
45
10^2
10^0

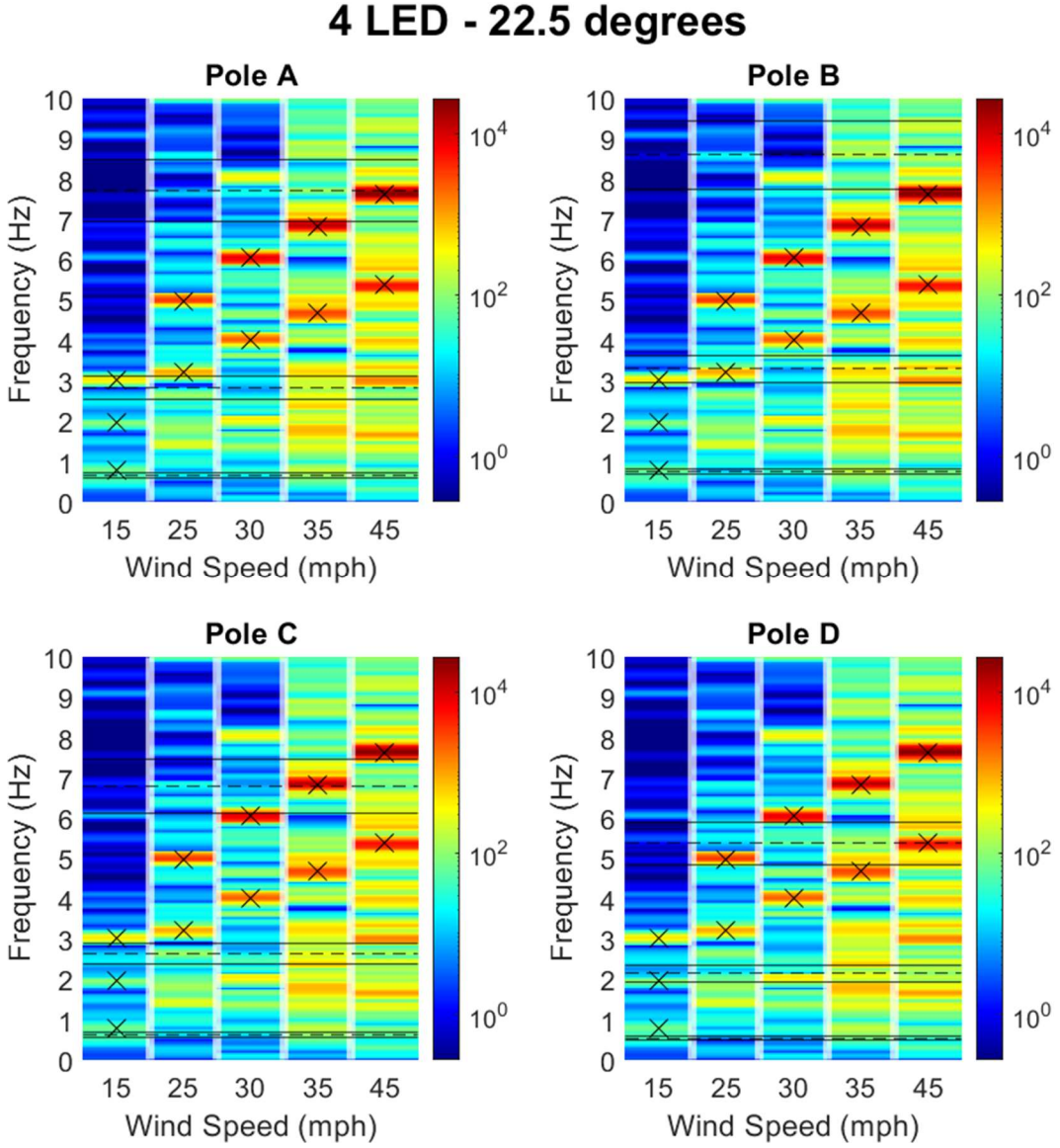
4 LED - 22.5 degrees
Pole A
Pole B
Pole C
Pole D
Frequency (Hz)
Wind Speed (mph)
0
1
2
3
4
5
6
7
8
9
10
15
25
30
35
45
10^0
10^2
10^4

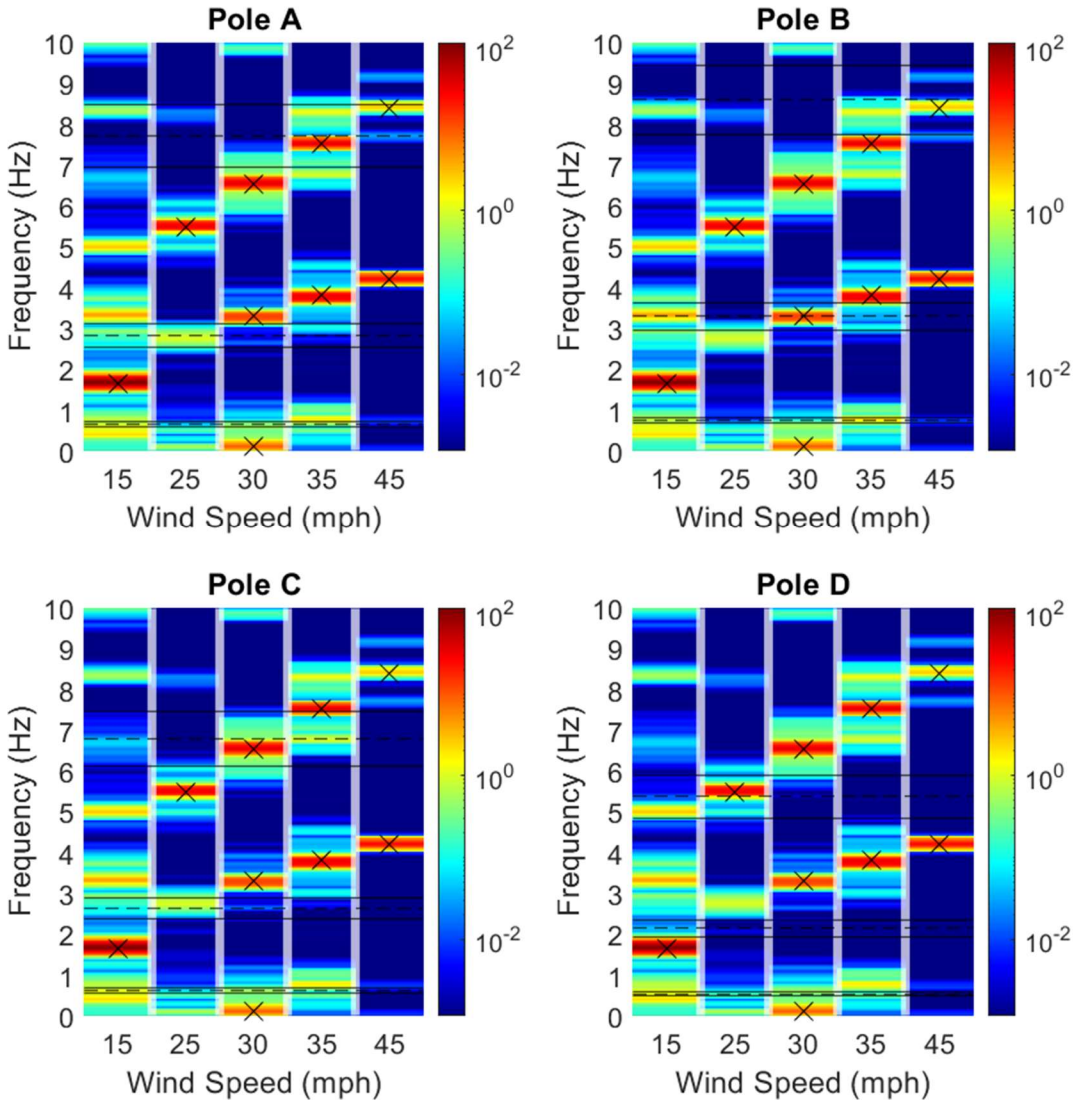
4 LED - 45 degrees
Pole A
Pole B
Pole C
Pole D
Frequency (Hz)
Wind Speed (mph)
0
1
2
3
4
5
6
7
8
9
10
15
25
30
35
45
10^2
10^0
10^{-2}

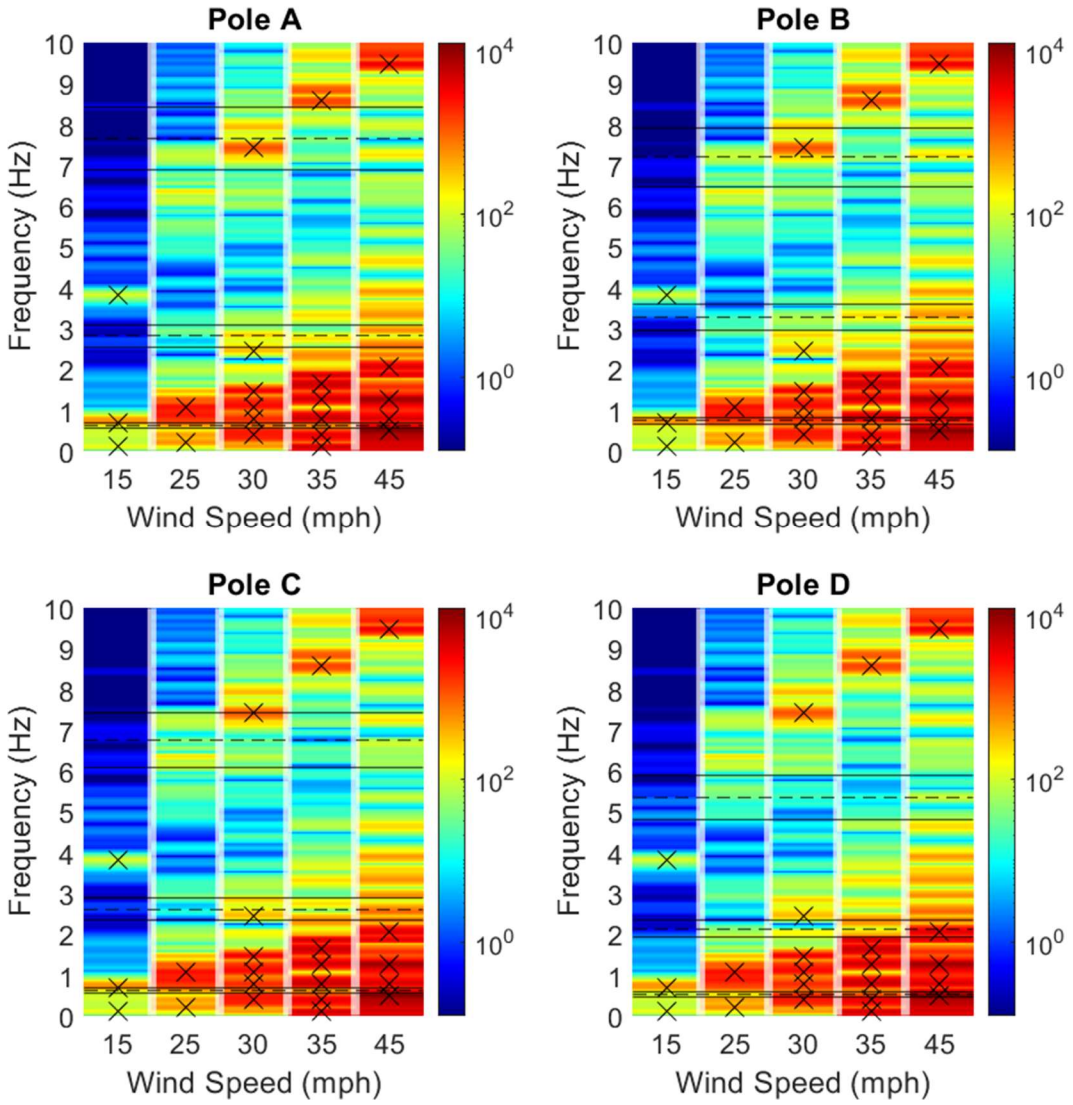
4 Incandescent - 0 degrees
Pole A
Pole B
Pole C
Pole D
Frequency (Hz)
Wind Speed (mph)
0
1
2
3
4
5
6
7
8
9
10
15
25
30
35
45
10^0
10^2
10^4

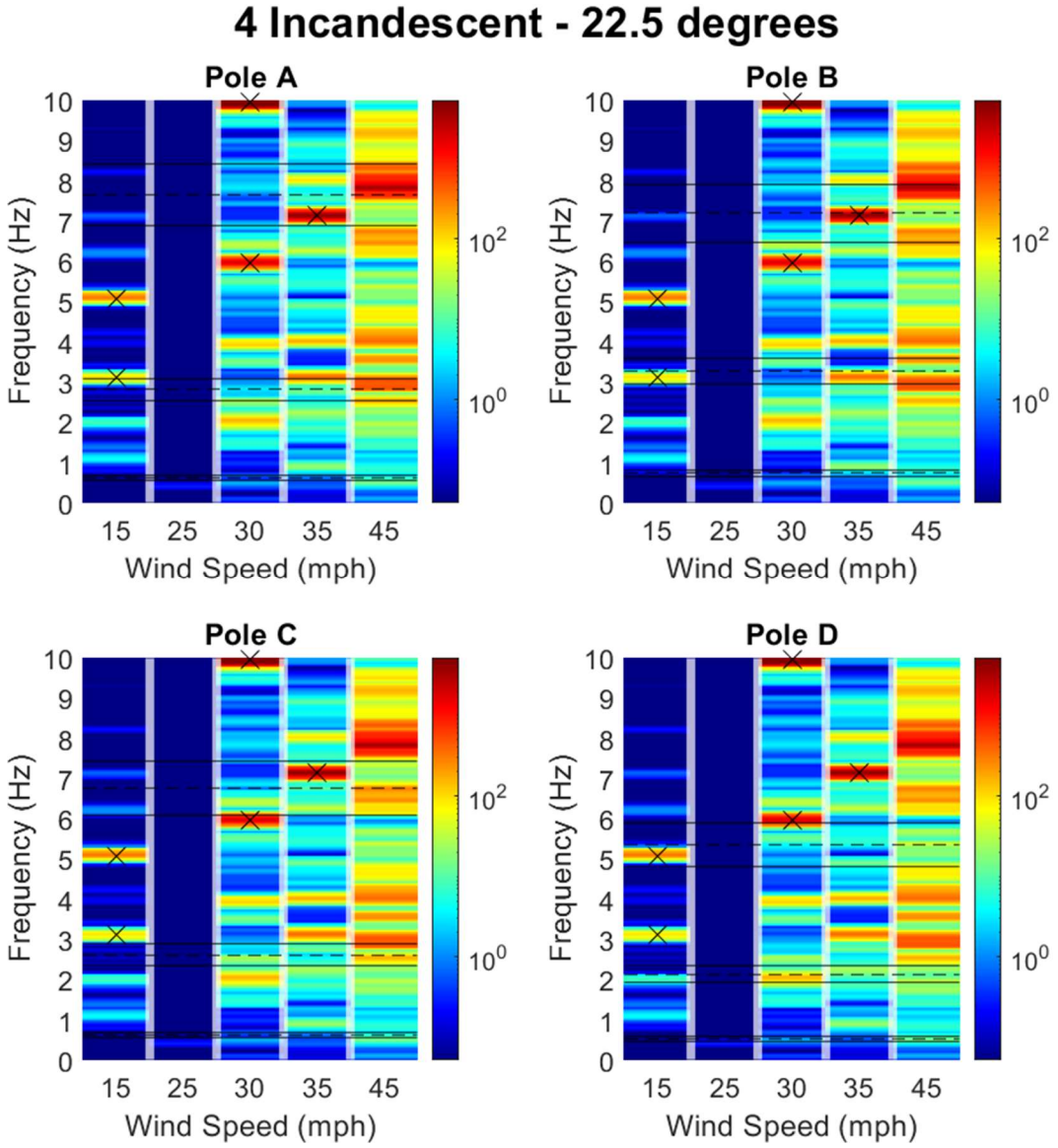
4 Incandescent - 22.5 degrees
Pole A
Pole B
Pole C
Pole D
Frequency (Hz)
Wind Speed (mph)
0
1
2
3
4
5
6
7
8
9
10
15
25
30
35
45
10^2
10^0

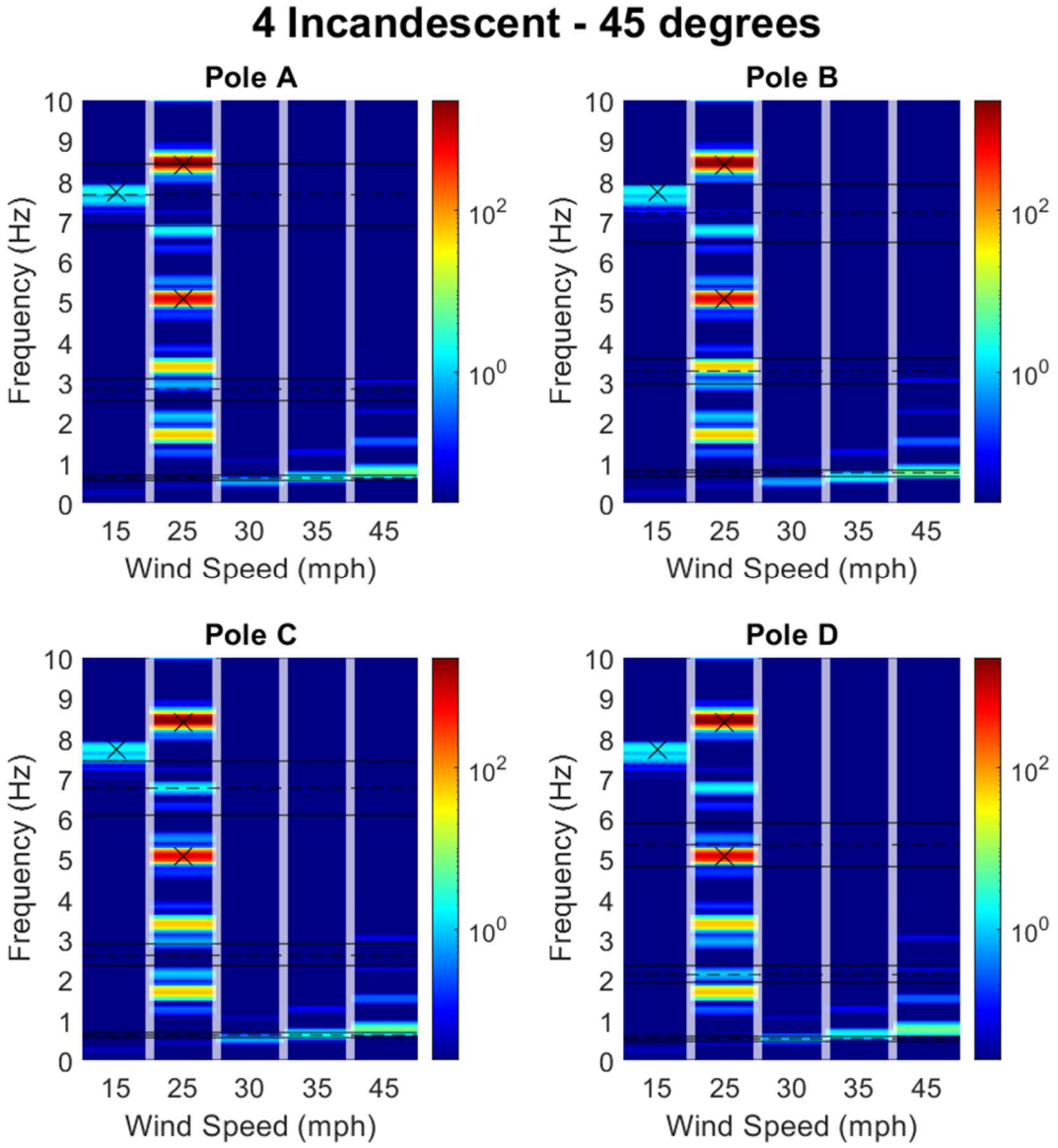
4 Incandescent - 45 degrees
Pole A
Pole B
Pole C
Pole D
Frequency (Hz)
Wind Speed (mph)
0
1
2
3
4
5
6
7
8
9
10
15
25
30
35
45
10^2
10^0

APPENDIX A4

A4.1 Bubble Comparison Charts for Abaqus Simulations

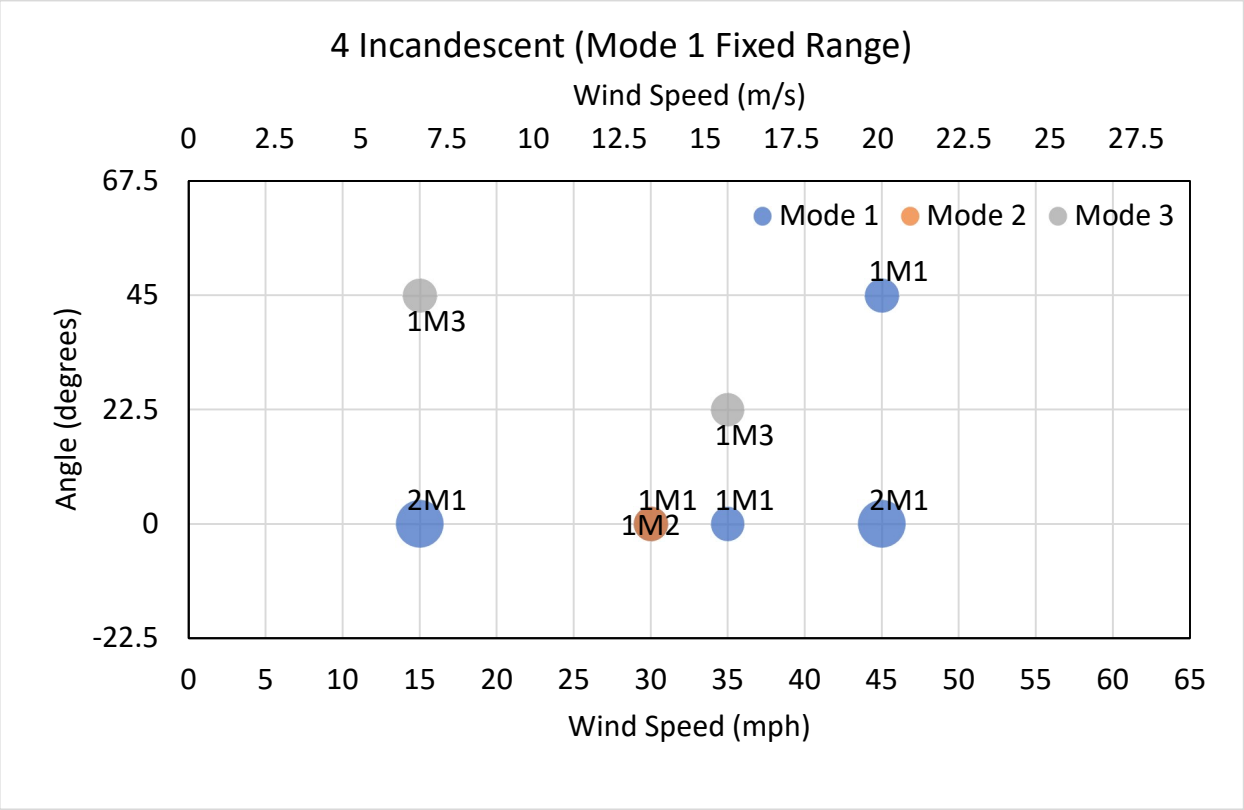

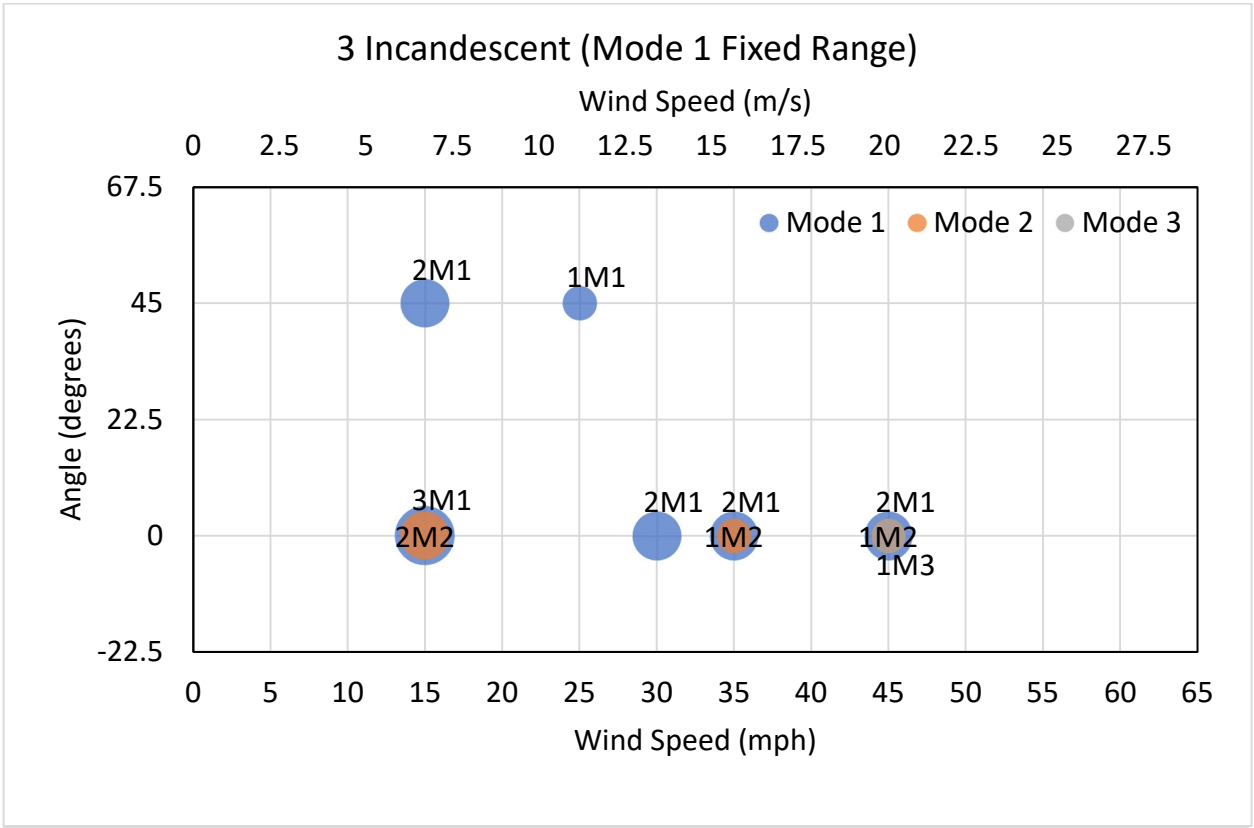
3 Incandescent (Mode 1 Fixed Range)
Wind Speed (m/s)
0 2.5 5 7.5 10 12.5 15 17.5 20 22.5 25 27.5
67.5
45
22.5
0
-22.5
Angle (degrees)
Mode 1
Mode 2
Mode 3
2M1
1M1
3M1
2M2
2M1
2M1
1M2
2M1
1M2
1M3
0 5 10 15 20 25 30 35 40 45 50 55 60 65
Wind Speed (mph)

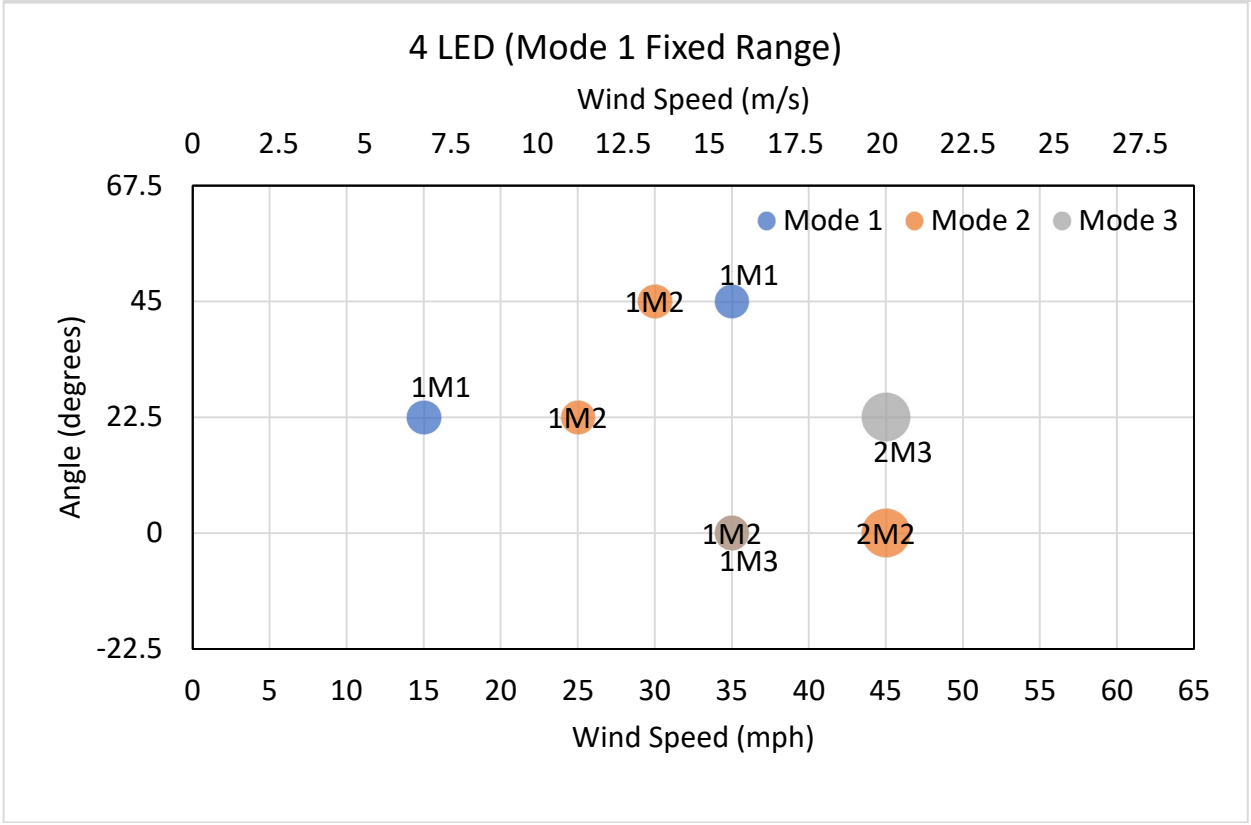
4 LED (Mode 1 Fixed Range)
Wind Speed (m/s)
0 2.5 5 7.5 10 12.5 15 17.5 20 22.5 25 27.5
67.5
45
22.5
0
-22.5
Angle (degrees)
Mode 1
Mode 2
Mode 3
1M1
1M2
1M1
1M2
2M3
1M2
1M3
2M2
0 5 10 15 20 25 30 35 40 45 50 55 60 65
Wind Speed (mph)

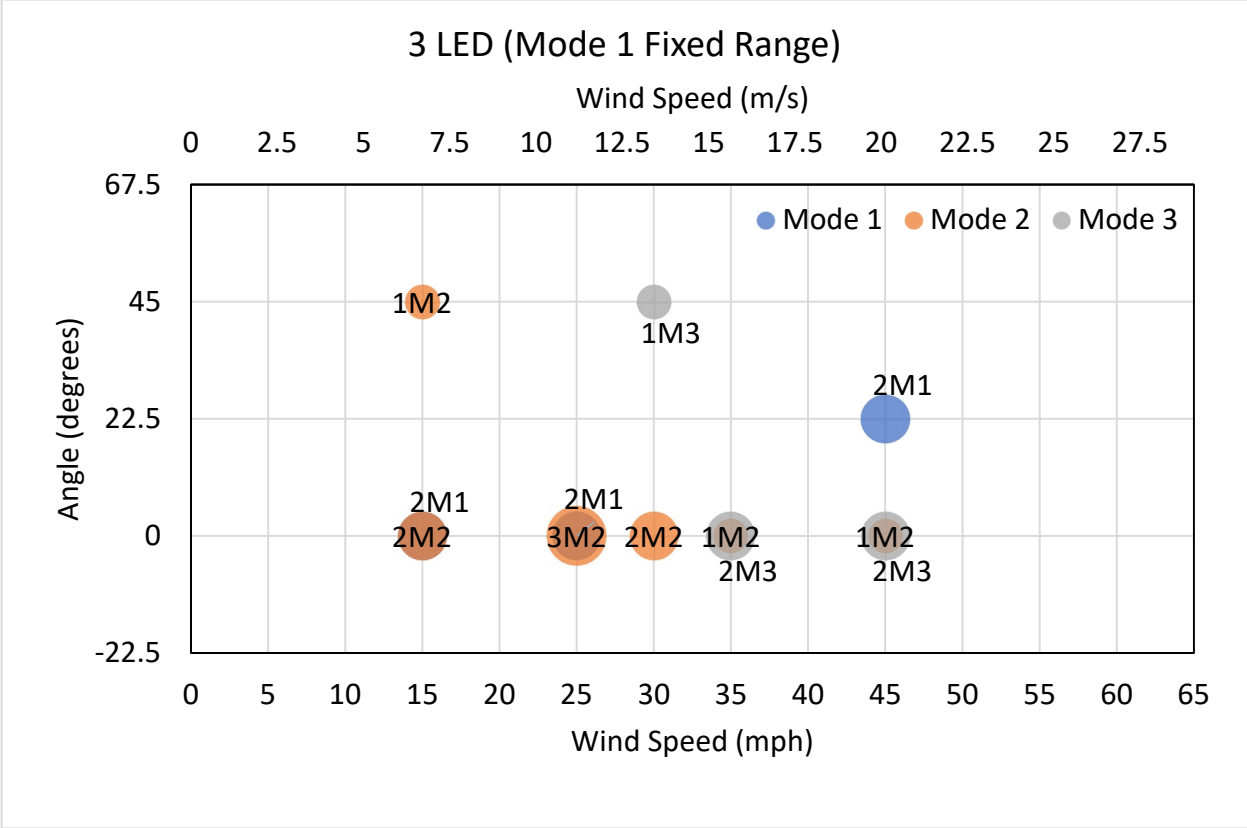
3 LED (Mode 1 Fixed Range)
Wind Speed (m/s)
0
2.5
5
7.5
10
12.5
15
17.5
20
22.5
25
27.5
67.5
45
22.5
0
-22.5
Angle (degrees)
Mode 1
Mode 2
Mode 3
1M2
1M3
2M1
2M1
2M2
2M1
3M2
2M2
1M2
2M3
1M2
2M3
0
5
10
15
20
25
30
35
40
45
50
55
60
65
Wind Speed (mph)

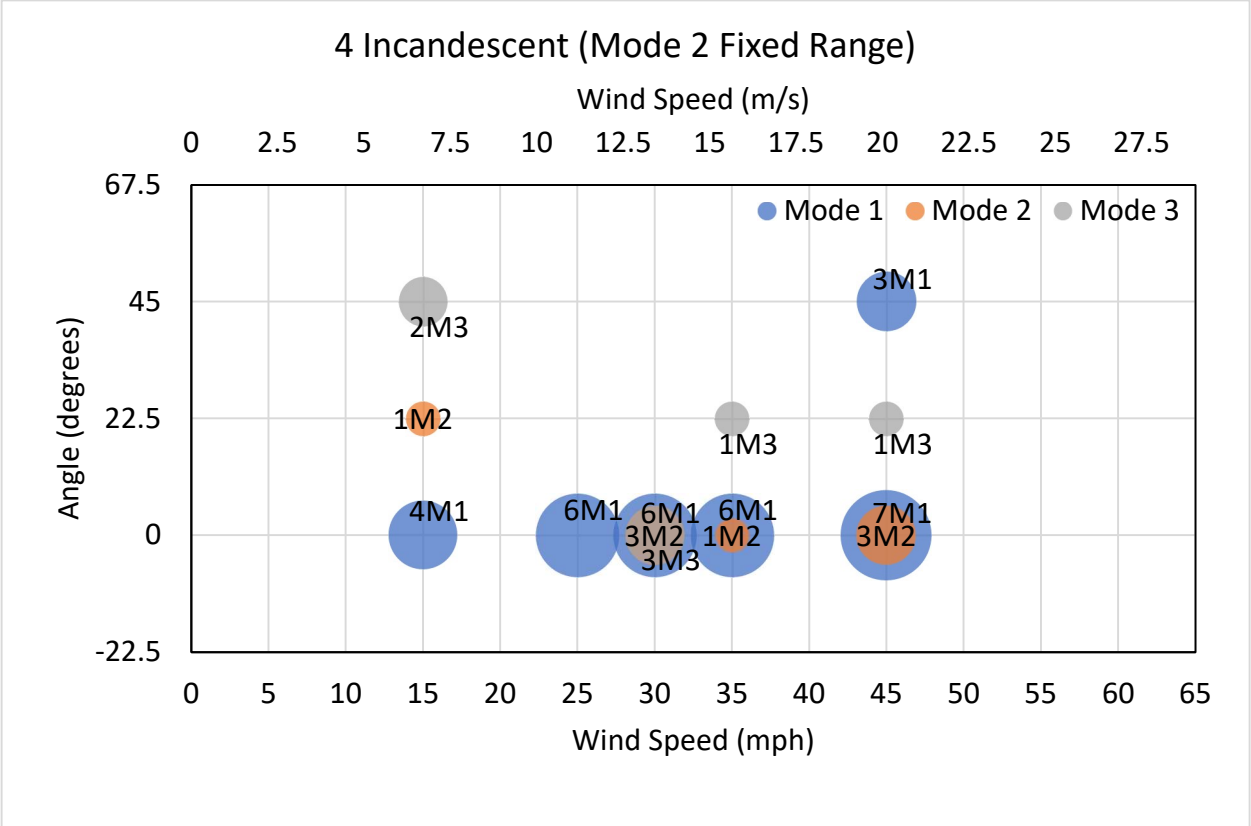
4 Incandescent (Mode 2 Fixed Range)
Wind Speed (m/s)
0
2.5
5
7.5
10
12.5
15
17.5
20
22.5
25
27.5
67.5
45
22.5
0
-22.5
Angle (degrees)
Mode 1
Mode 2
Mode 3
3M1
2M3
1M2
1M3
1M3
4M1
6M1
6M1
3M2
3M3
6M1
1M2
7M1
3M2
0
5
10
15
20
25
30
35
40
45
50
55
60
65
Wind Speed (mph)

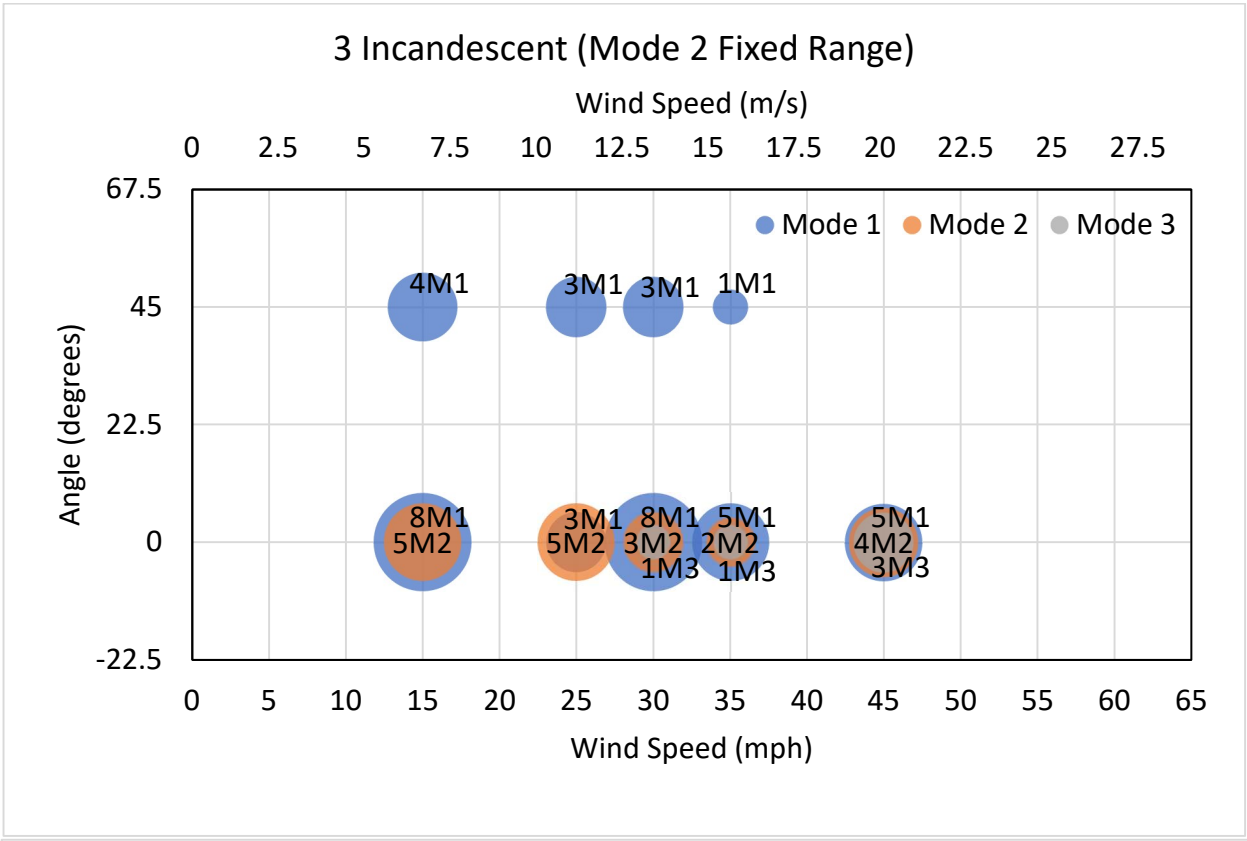
3 Incandescent (Mode 2 Fixed Range)
Wind Speed (m/s)
0 2.5 5 7.5 10 12.5 15 17.5 20 22.5 25 27.5
67.5
45
22.5
0
-22.5
Angle (degrees)
Mode 1
Mode 2
Mode 3
4M1
3M1
3M1
1M1
8M1
5M2
3M1
5M2
8M1
3M2
1M3
5M1
2M2
1M3
5M1
4M2
3M3
0 5 10 15 20 25 30 35 40 45 50 55 60 65
Wind Speed (mph)

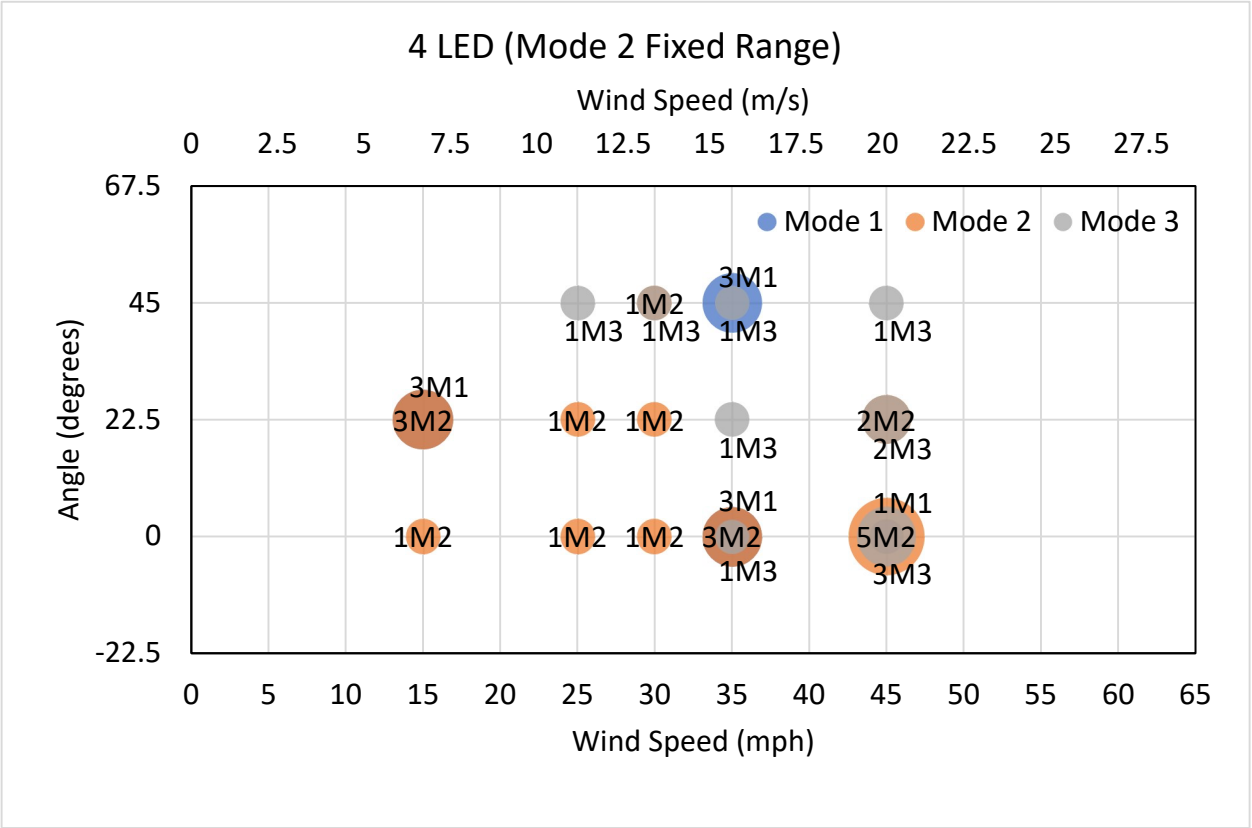
4 LED (Mode 2 Fixed Range)
Wind Speed (m/s)
0 2.5 5 7.5 10 12.5 15 17.5 20 22.5 25 27.5
67.5
45
22.5
0
-22.5
Angle (degrees)
Mode 1
Mode 2
Mode 3
3M1
1M2
1M3
1M3
1M3
1M3
3M1
3M2
1M2
1M2
1M3
2M2
2M3
3M1
1M2
1M2
1M2
3M2
1M3
1M1
5M2
3M3
0 5 10 15 20 25 30 35 40 45 50 55 60 65
Wind Speed (mph)

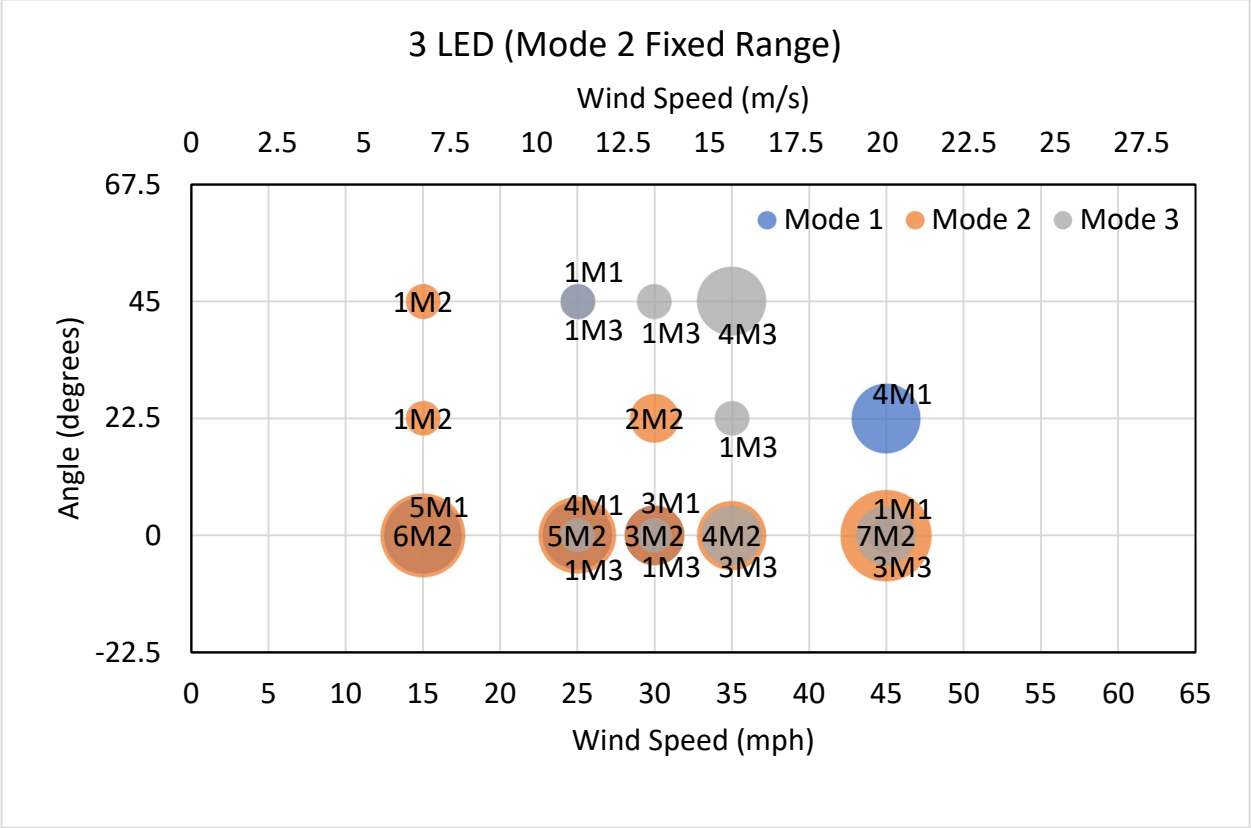
3 LED (Mode 2 Fixed Range)
Wind Speed (m/s)
0
2.5
5
7.5
10
12.5
15
17.5
20
22.5
25
27.5
67.5
45
22.5
0
-22.5
Angle (degrees)
Mode 1
Mode 2
Mode 3
1M1
1M2
1M3
1M3
4M3
4M1
1M2
2M2
1M3
5M1
6M2
4M1
5M2
3M1
3M2
4M2
1M3
1M3
3M3
1M1
7M2
3M3
0
5
10
15
20
25
30
35
40
45
50
55
60
65
Wind Speed (mph)

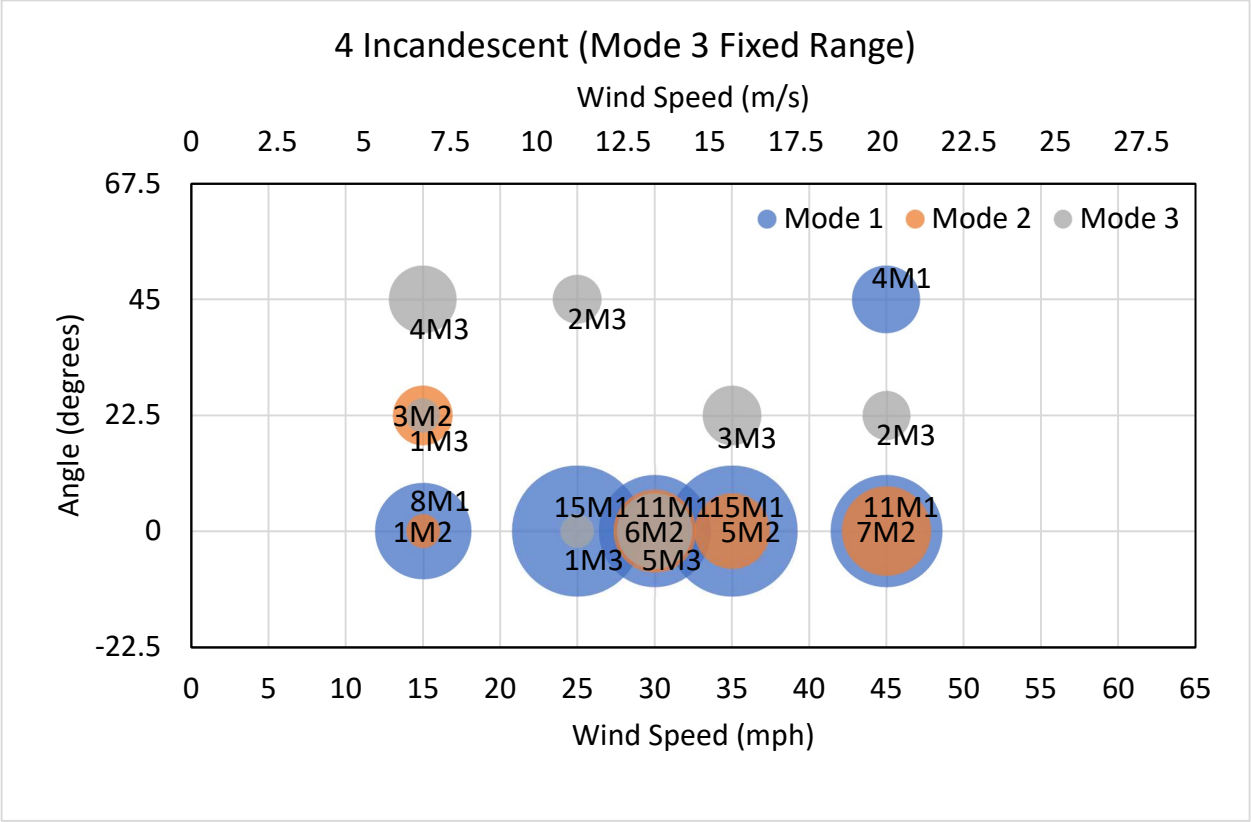
4 Incandescent (Mode 3 Fixed Range)
Wind Speed (m/s)
0
2.5
5
7.5
10
12.5
15
17.5
20
22.5
25
27.5
67.5
45
22.5
0
-22.5
Angle (degrees)
Mode 1
Mode 2
Mode 3
4M3
2M3
4M1
3M2
1M3
3M3
2M3
8M1
1M2
15M1
1M3
11M1
6M2
5M3
15M1
5M2
11M1
7M2
0
5
10
15
20
25
30
35
40
45
50
55
60
65
Wind Speed (mph)

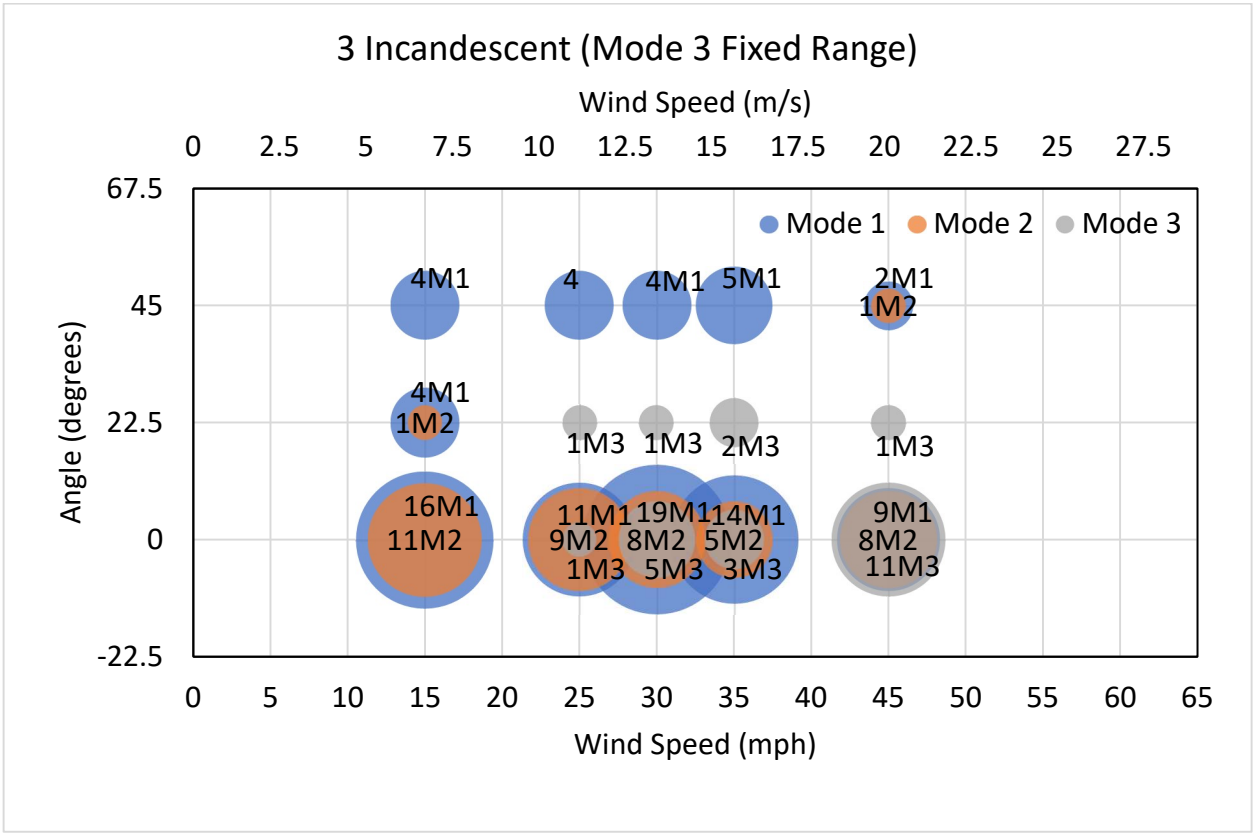
3 Incandescent (Mode 3 Fixed Range)
Wind Speed (m/s)
0 2.5 5 7.5 10 12.5 15 17.5 20 22.5 25 27.5
Mode 1
Mode 2
Mode 3
Angle (degrees)
67.5 45 22.5 0 -22.5
4M1
4
4M1
5M1
2M1
1M2
4M1
1M2
1M3
1M3
2M3
1M3
16M1
11M2
11M1
9M2
19M1
8M2
1M3
14M1
5M2
5M3
3M3
9M1
8M2
11M3
0 5 10 15 20 25 30 35 40 45 50 55 60 65
Wind Speed (mph)

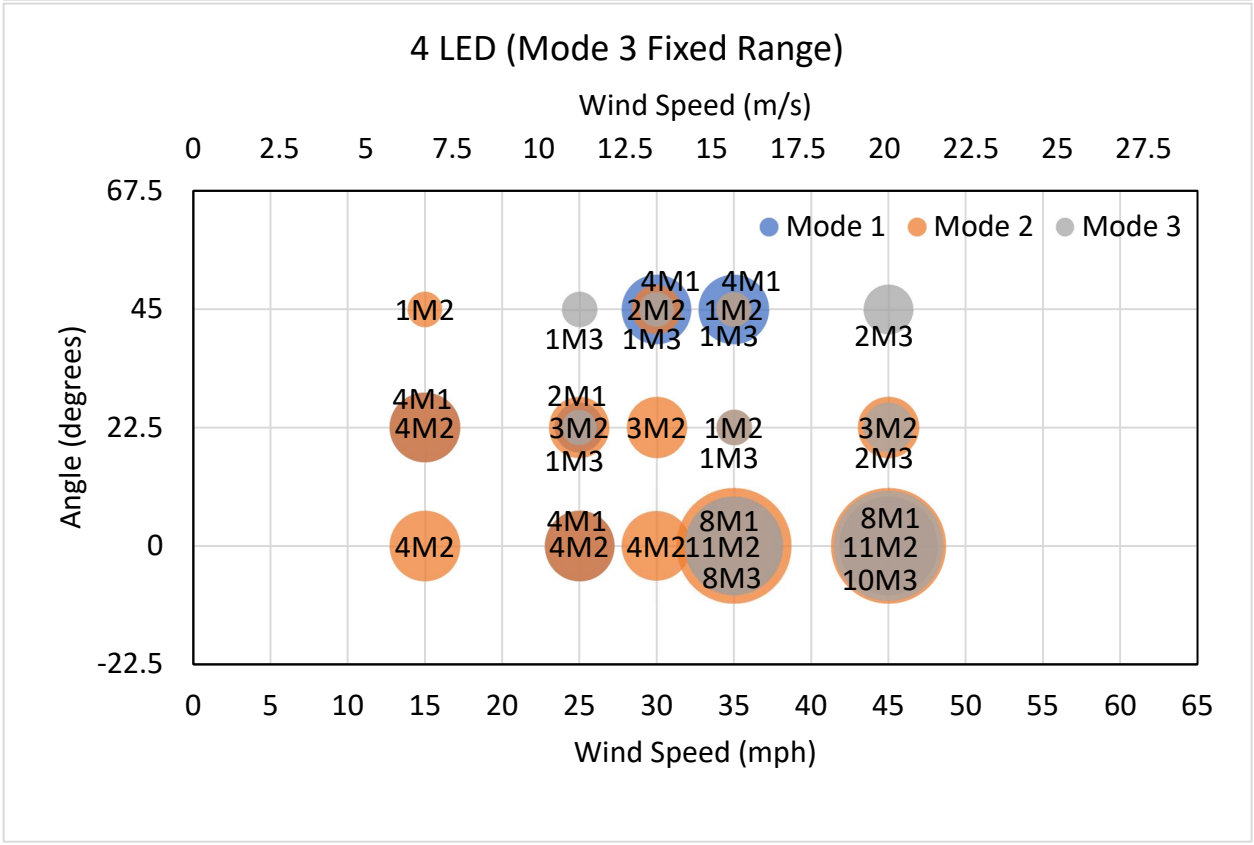
4 LED (Mode 3 Fixed Range)
Wind Speed (m/s)
0 2.5 5 7.5 10 12.5 15 17.5 20 22.5 25 27.5
Mode 1
Mode 2
Mode 3
Angle (degrees)
67.5 45 22.5 0 -22.5
1M2
4M1
2M2
1M3
4M1
1M2
1M3
1M3
2M3
4M1
4M2
2M1
3M2
1M3
3M2
1M2
1M3
3M2
2M3
4M2
4M1
4M2
4M2
8M1
11M2
8M3
8M1
11M2
10M3
0 5 10 15 20 25 30 35 40 45 50 55 60 65
Wind Speed (mph)

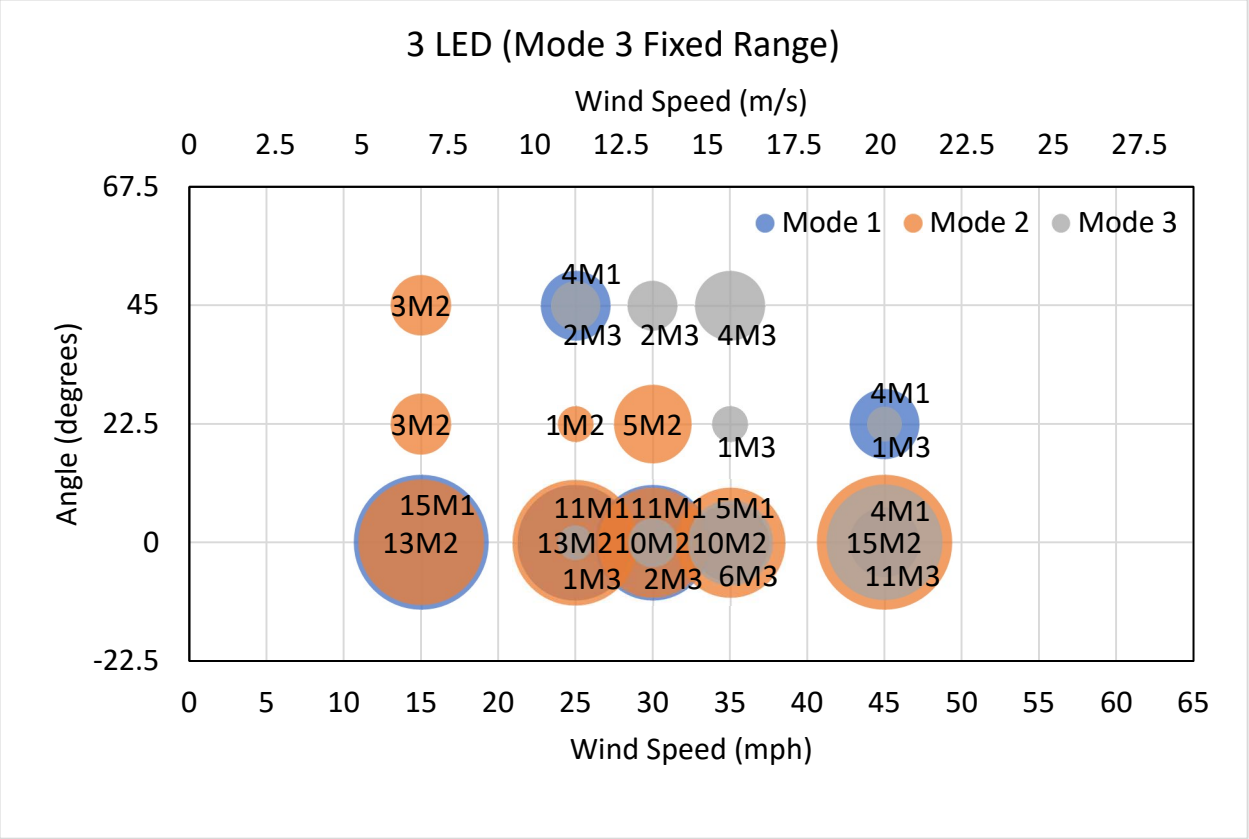
3 LED (Mode 3 Fixed Range)
Wind Speed (m/s)
0 2.5 5 7.5 10 12.5 15 17.5 20 22.5 25 27.5
67.5
45
22.5
0
-22.5
Angle (degrees)
Mode 1
Mode 2
Mode 3
4M1
3M2
2M3 2M3 4M3
4M1
3M2
1M2 5M2
1M3
1M3
15M1
13M2
11M1 11M1 5M1
13M2 10M2 10M2
1M3 2M3 6M3
4M1
15M2
11M3
0 5 10 15 20 25 30 35 40 45 50 55 60 65
Wind Speed (mph)

APPENDIX A5

A5.1 CFD STUDY OF LUMINAIRES USING ANSYS FLUENT

Ansys Fluent Study Introduction/Background

The same study was performed using Ansys Fluent. This program has more turbulence models available that would be favorable to the accuracy of the results. The Detached-Eddy Simulation (DES) turbulence solver was selected for this study. Attempt to verify previous results in Abaqus with more widely accepted software, and to explore the influence of the turbulence solver on the results.

Ansys Fluent Modeling

The fluid domain was made much larger than the geometry itself to minimize boundary effects on the results. The velocity inlet was placed 5 diameters in front of the geometry. The far field (walls) boundaries were modeled as no slip walls and located 5 diameters from the geometry as well. The fluid outlet was modeled as a pressure outlet with pressure as 0 psi. It was 10 diameters downstream from the geometry. The diameter of the geometry was measured as twice the distance between the center of the housing and the farthest point the luminaires reach. The diameters for the LED and incandescent assemblies are 126.3 in. (320.8 cm) and 109.8 in. (278.9 cm), respectively.

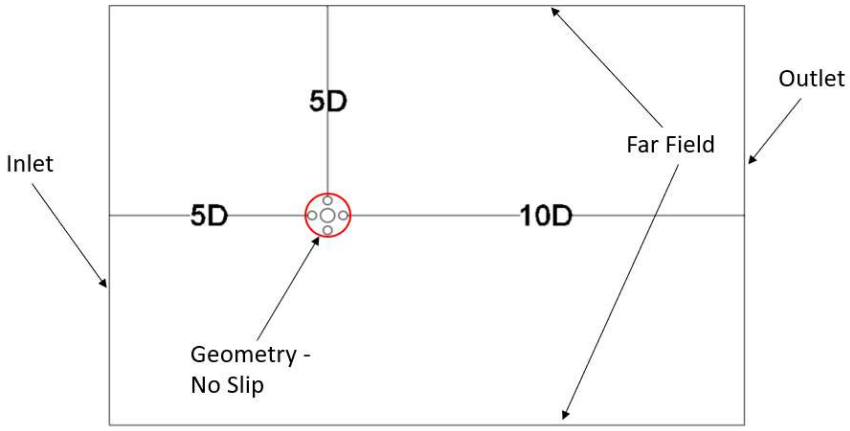

Figure 18: Ansys Fluent Fluid Domain Dimensions and Boundary Conditions

The model mesh was created using the Ansys Meshing program. The mesh sizing was defined in three sections on the model domain: the outer domain, body of influence, and near the lighting assembly wall. The meshing method was set as quadrilateral dominant for the model. The mesh sizing was set at 5 in (127 mm) on the outsides of the model (Section A). The mesh was refined to 1 in. (25.4 mm) in a smaller box (Section B), or body of influence, surrounding the geometry as shown in Figure 19. This box had the dimensions of one diameter to front the front, one diameter to the sides, and two diameters to the back. A mesh sensitivity study was performed to find the necessary level of refinement within this box. The mesh used was again refined at the wall representing the luminaire geometries. Inflation layers were used starting at 0.001 in. (0.0254 mm) for the first layer height. This value was chosen by targeting a y-plus value near 1.

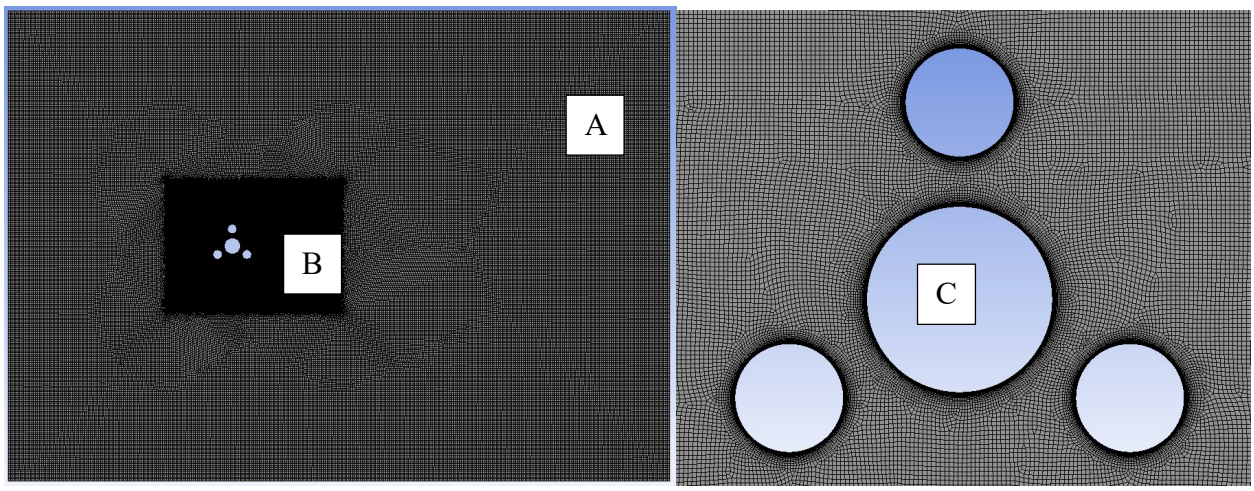

Figure 19: Ansys Fluent Model Meshing Technique

Ansys Fluent Results

The resulting PSD curves for each simulation are shown in section A5.2. The dataset developed with Fluent is far from complete and will require additional simulations to make comparisons or improve on any conclusions. This will include running each lighting assembly model at a variety of wind speeds like the Abaqus study.

A5.2 Power Spectral Density Plots for Fluent Simulations

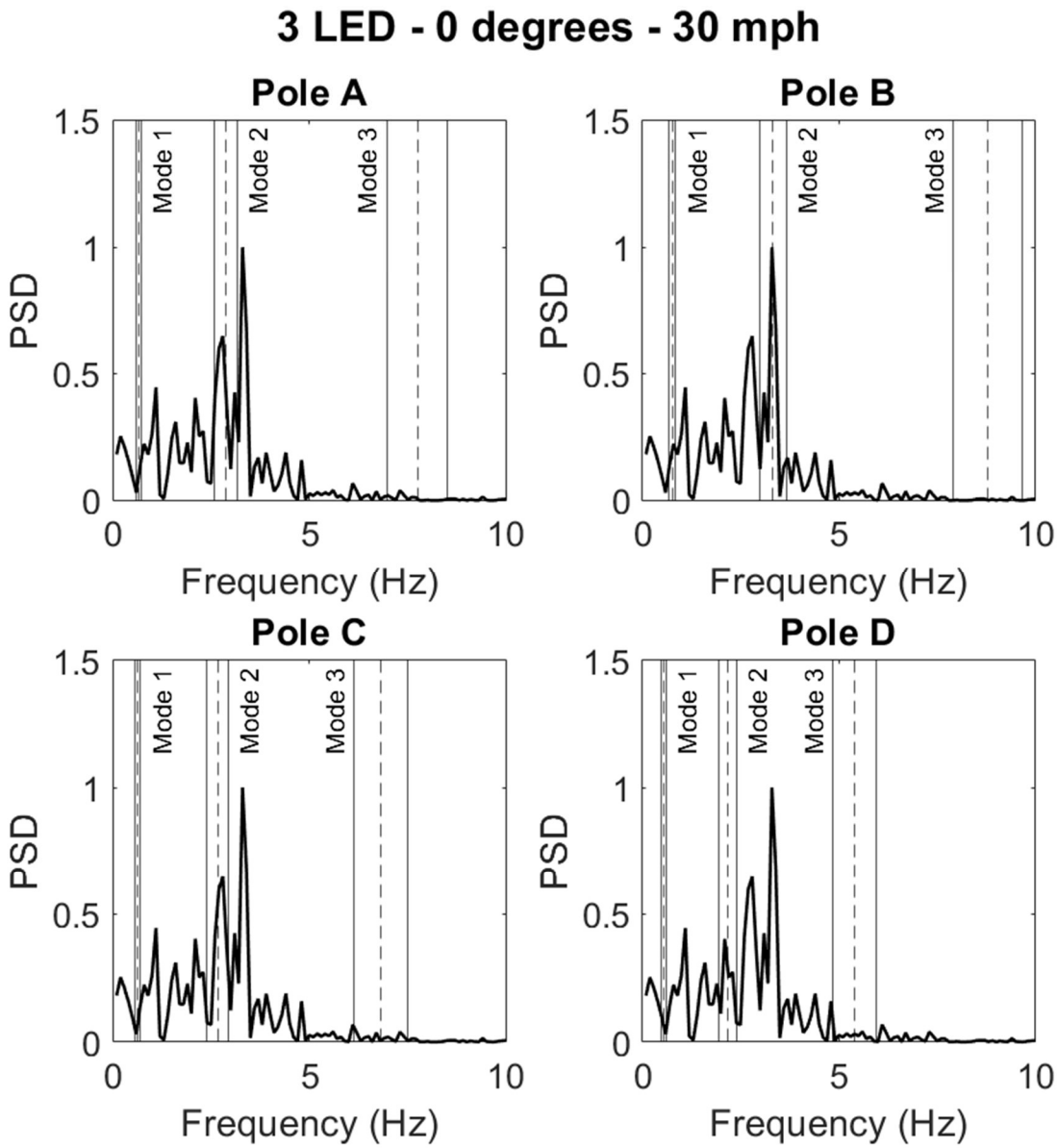

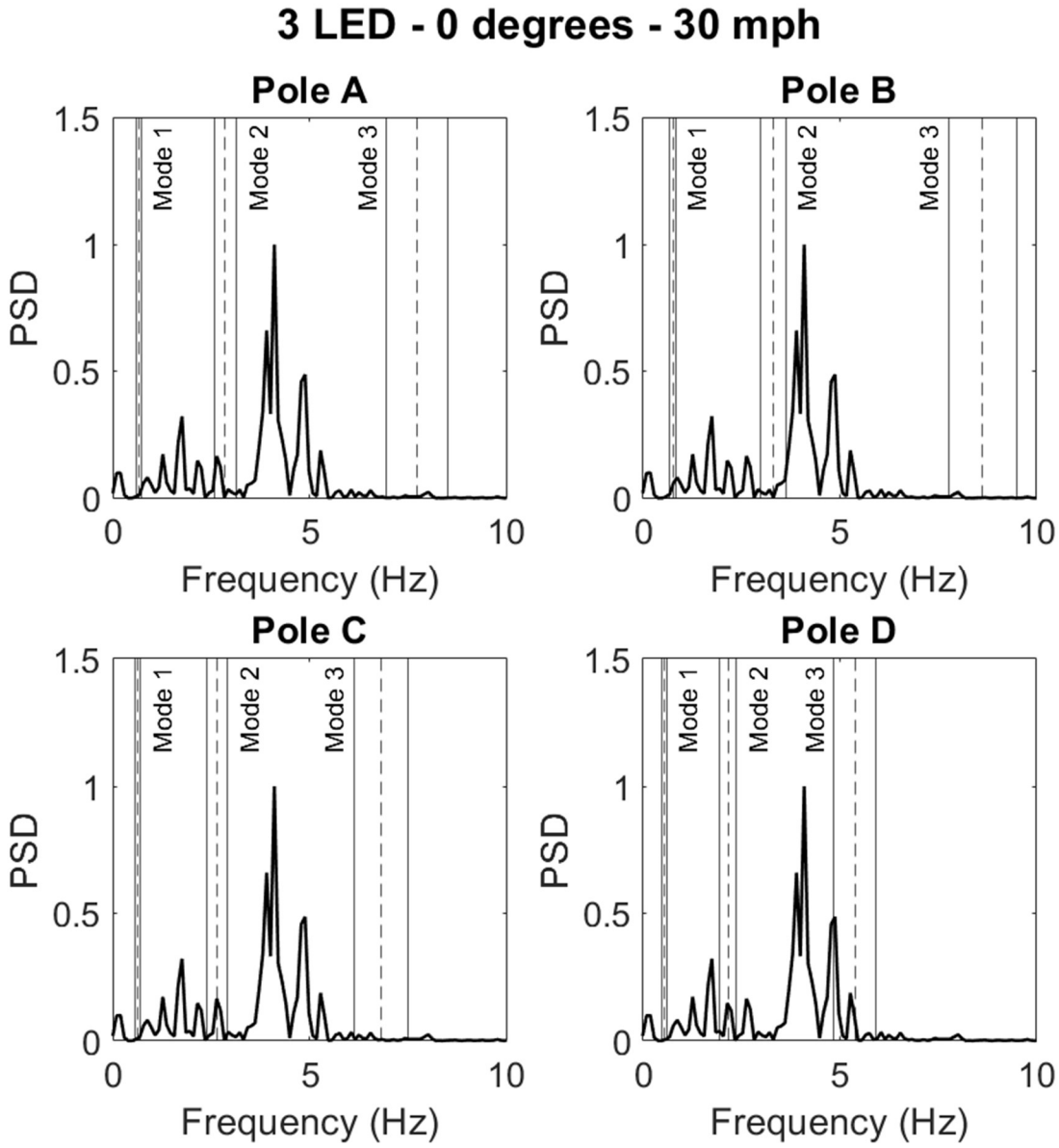
3 LED - 0 degrees - 30 mph
Pole A
Pole B
Pole C
Pole D
Mode 1
Mode 2
Mode 3
PSD
Frequency (Hz)
0
0.5
1
1.5
5
10

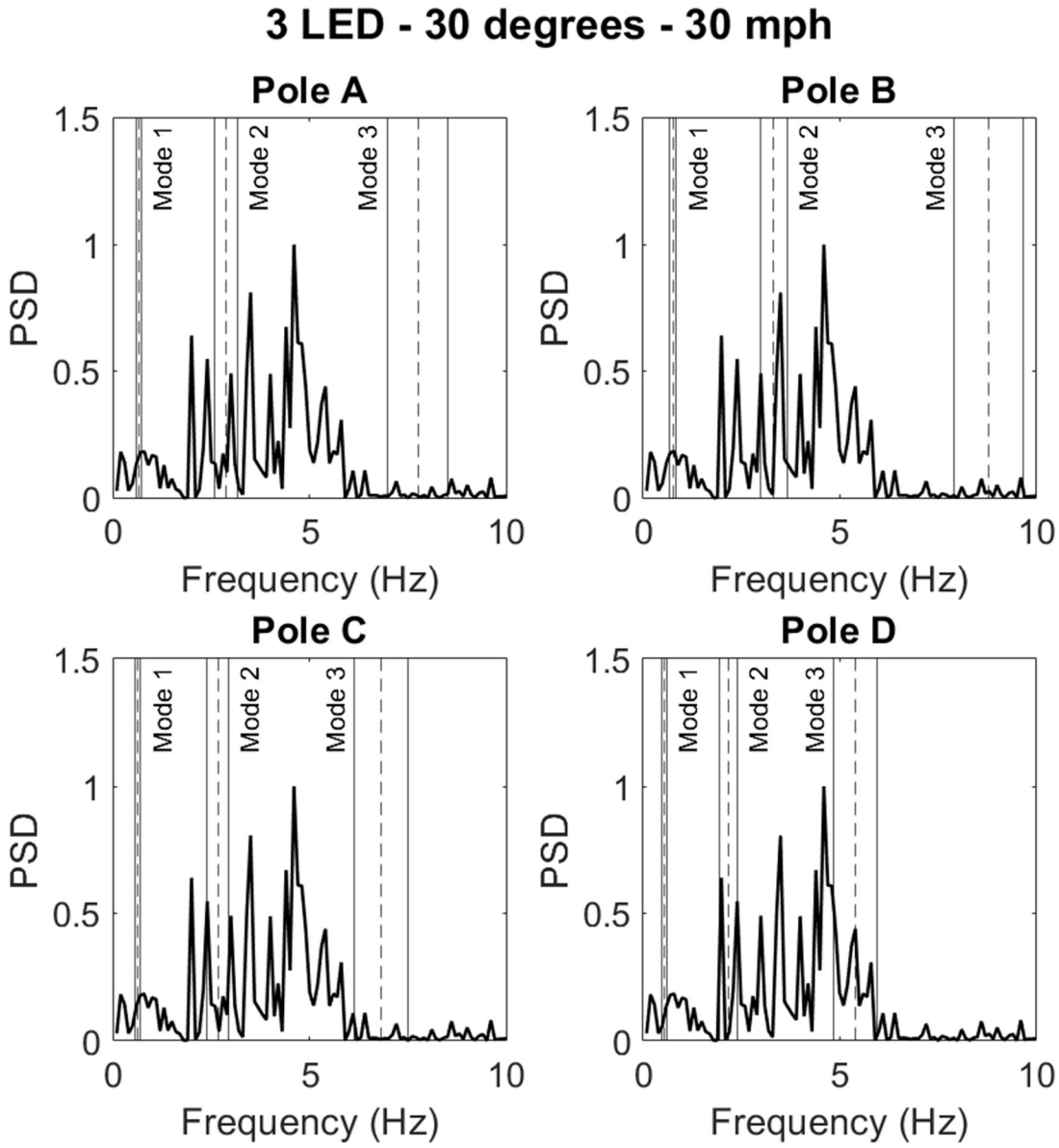
3 LED - 30 degrees - 30 mph
Pole A
Pole B
Pole C
Pole D
Mode 1
Mode 2
Mode 3
PSD
Frequency (Hz)
0
0.5
1
1.5
5
10

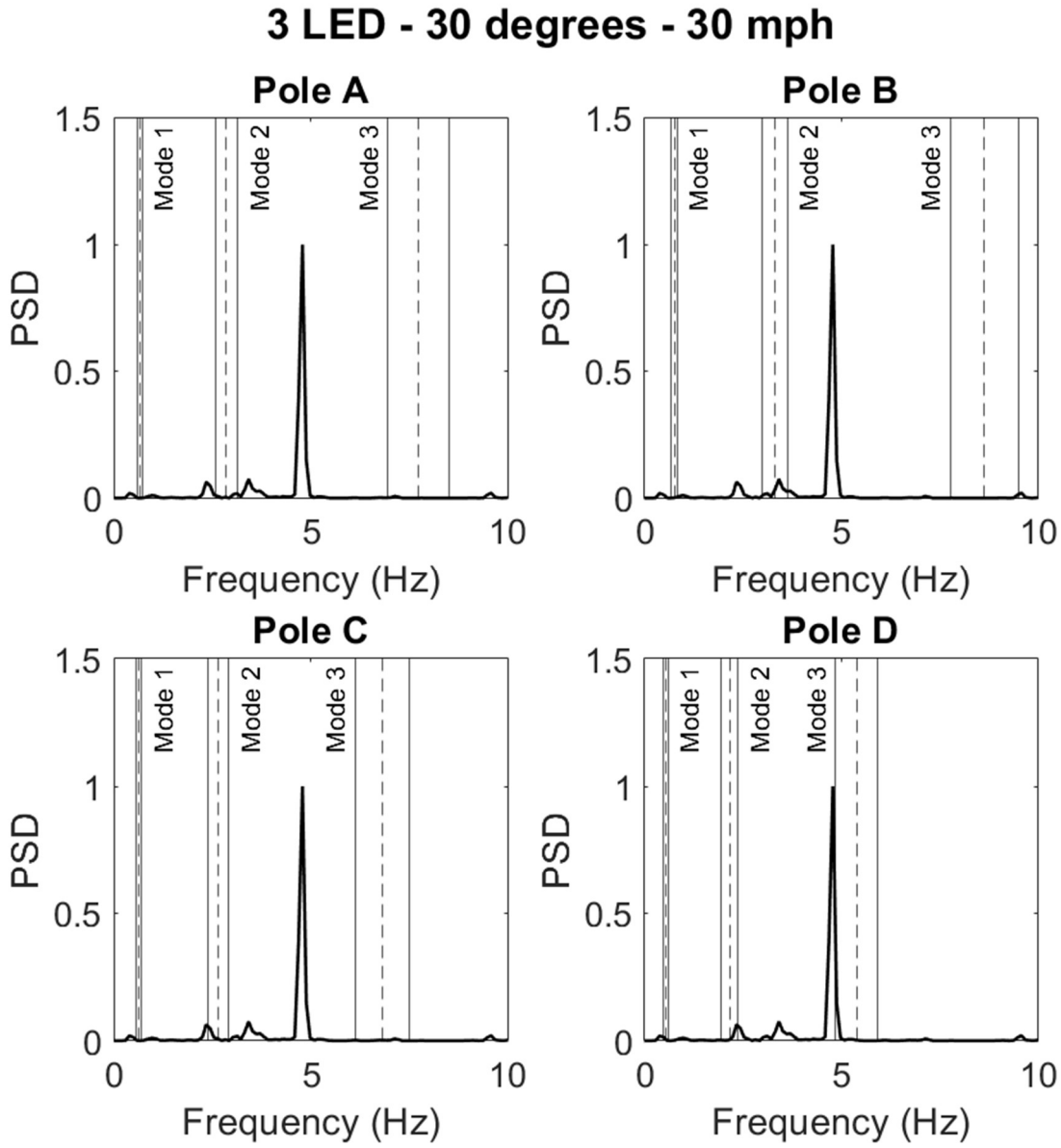
3 LED - 30 degrees - 30 mph
Pole A
Pole B
Pole C
Pole D
Mode 1
Mode 2
Mode 3
PSD
Frequency (Hz)
0
0.5
1
1.5
5
10

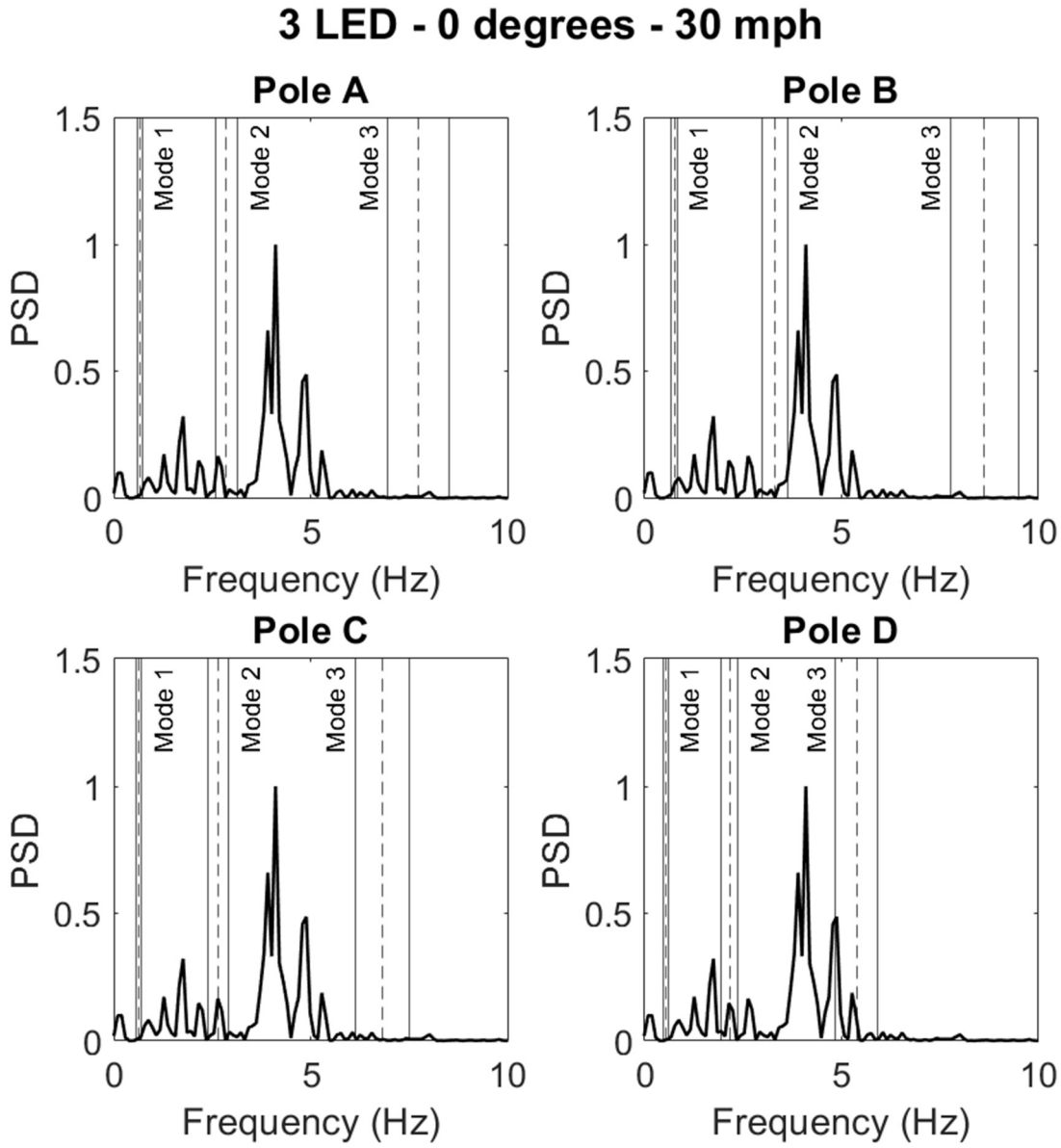
3 LED - 0 degrees - 30 mph
Pole A
Pole B
Pole C
Pole D
Mode 1
Mode 2
Mode 3
PSD
Frequency (Hz)
0
0.5
1
1.5
5
10

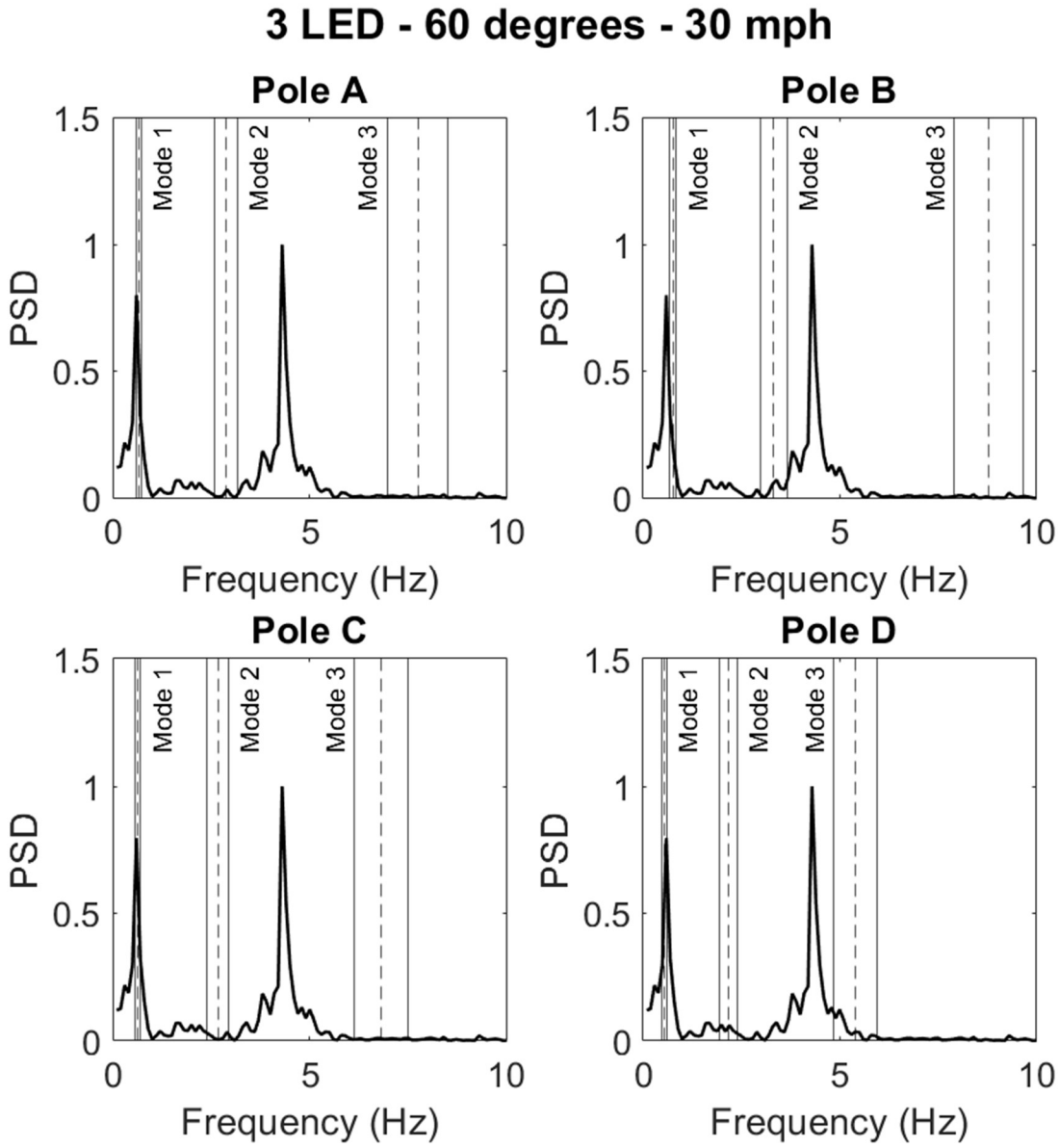
3 LED - 60 degrees - 30 mph
Pole A
Pole B
Pole C
Pole D
Mode 1
Mode 2
Mode 3
PSD
Frequency (Hz)
0
0.5
1
1.5
5
10

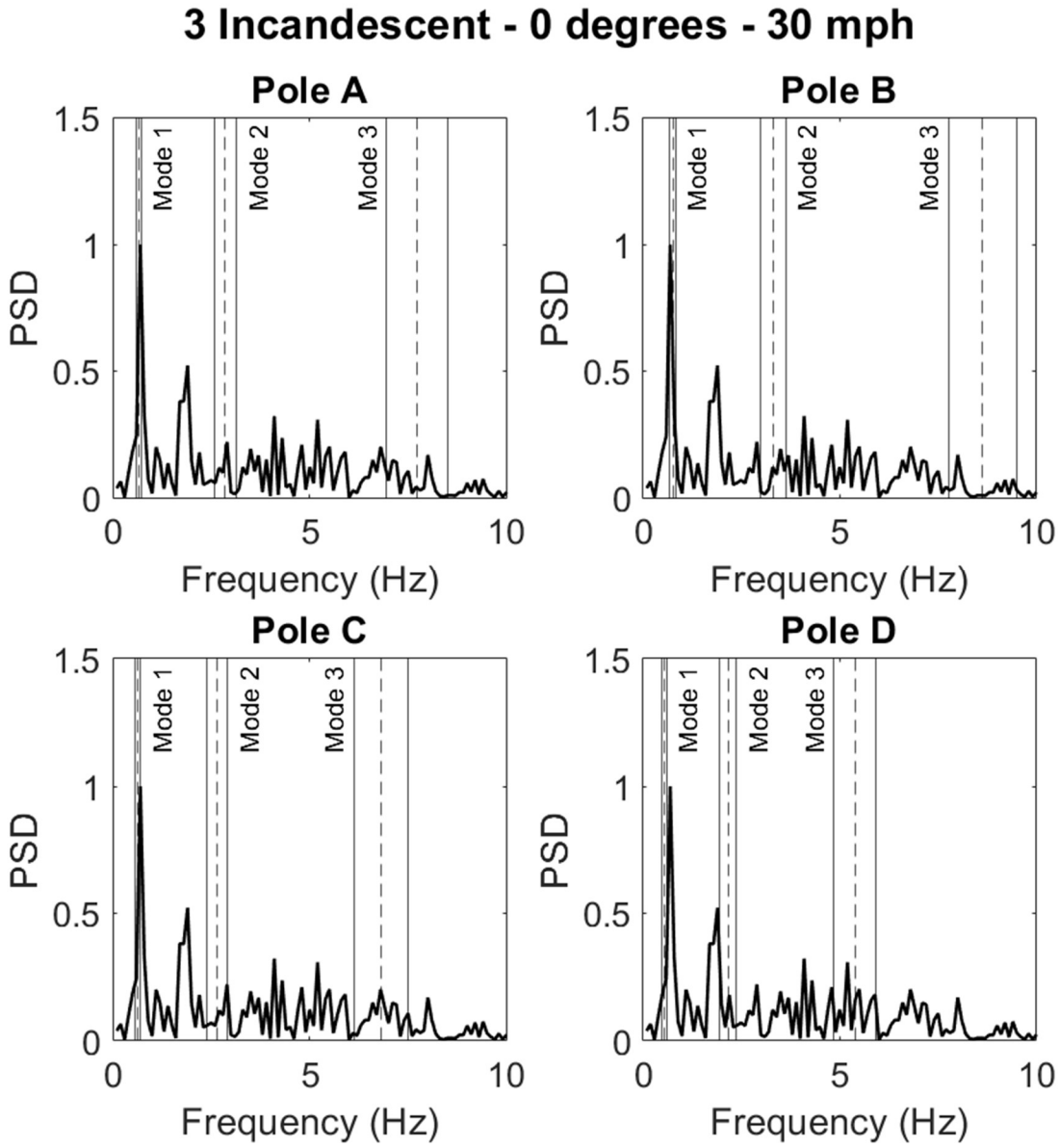
3 Incandescent - 0 degrees - 30 mph
Pole A
Pole B
Pole C
Pole D
Mode 1
Mode 2
Mode 3
PSD
Frequency (Hz)
0
0.5
1
1.5
5
10

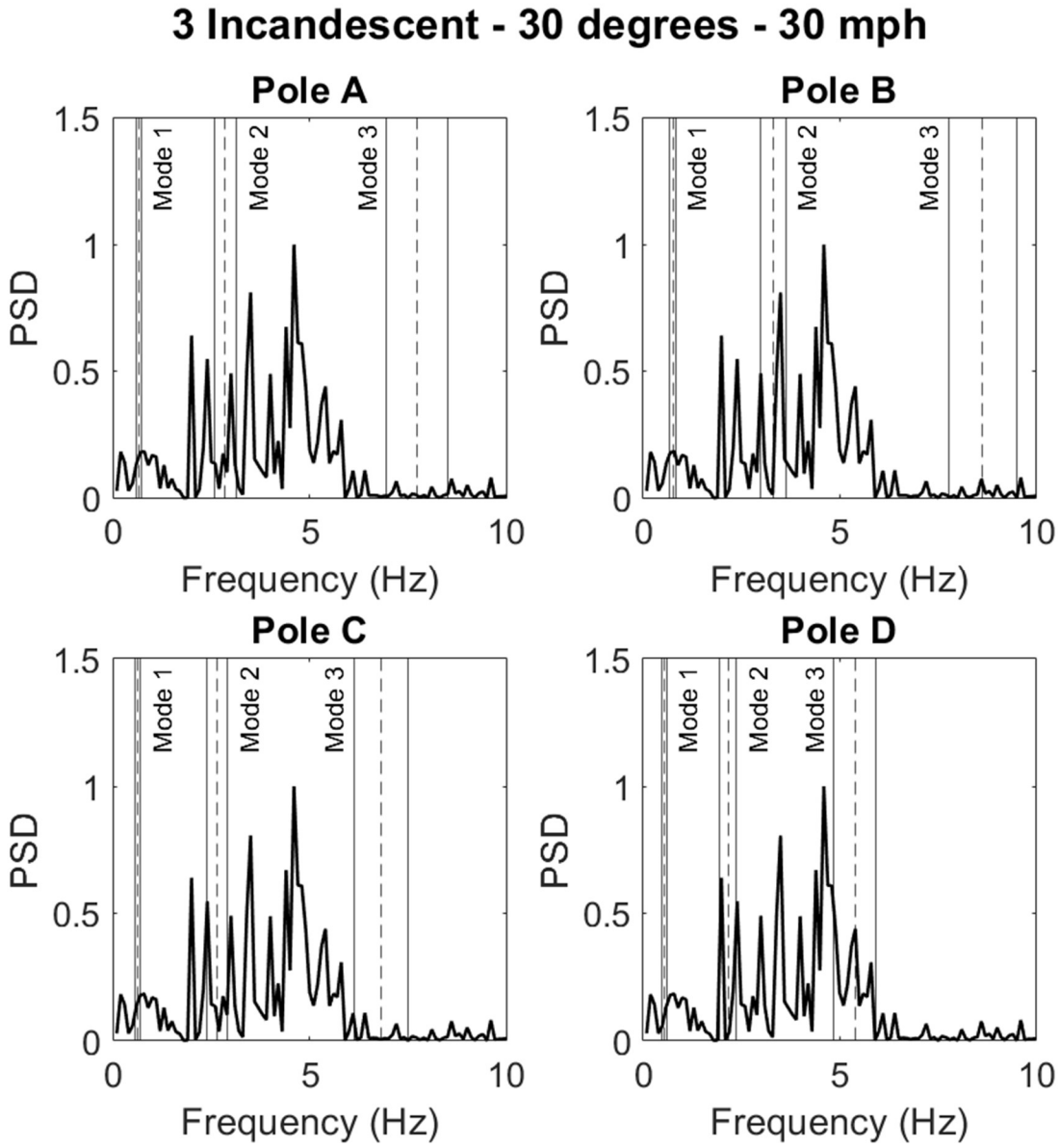
3 Incandescent - 30 degrees - 30 mph
Pole A
Pole B
Pole C
Pole D
Mode 1
Mode 2
Mode 3
PSD
Frequency (Hz)
0
0.5
1
1.5
5
10

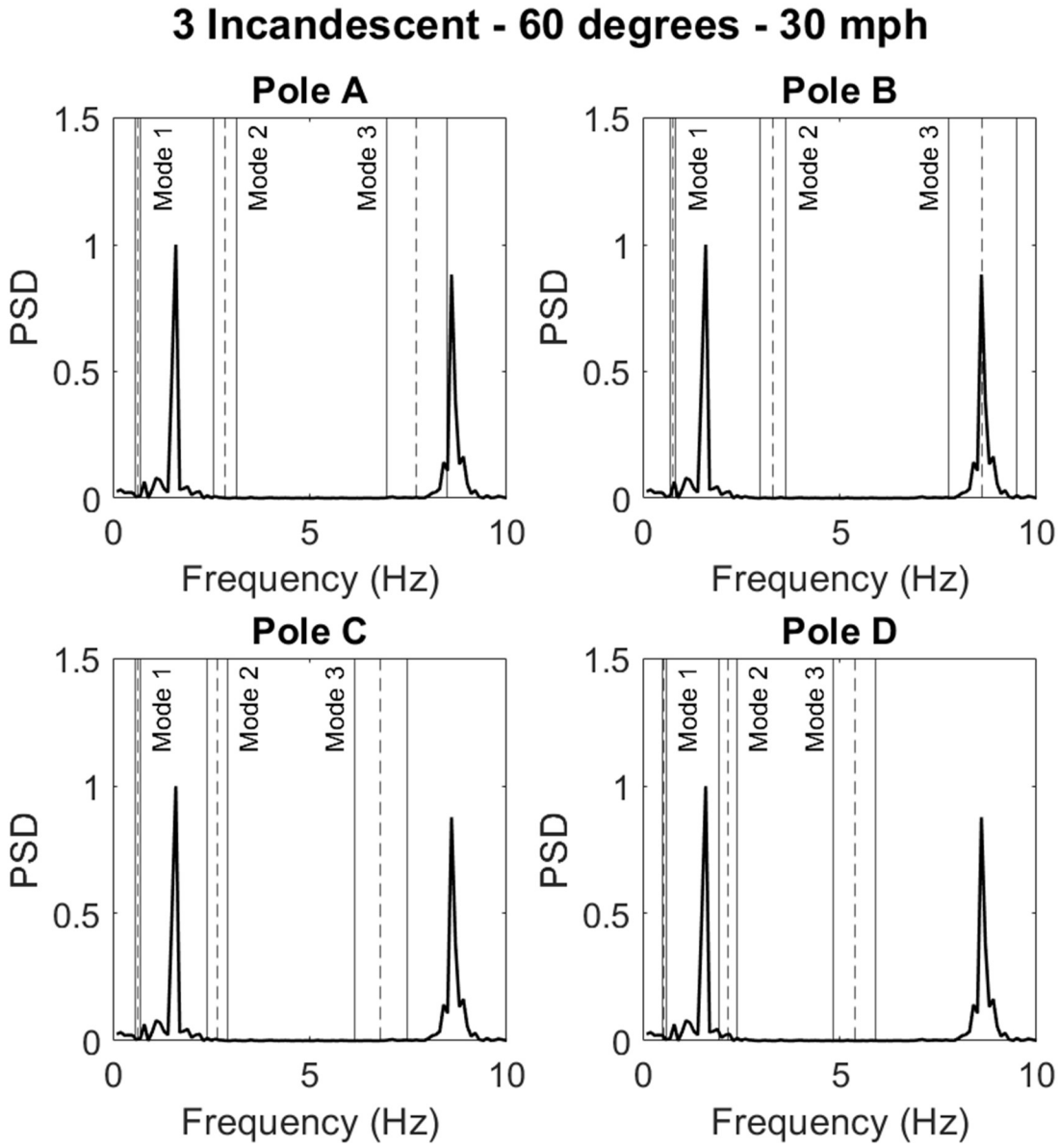
3 Incandescent - 60 degrees - 30 mph
Pole A
Pole B
Pole C
Pole D
Mode 1
Mode 2
Mode 3
PSD
Frequency (Hz)
0
0.5
1
1.5
5
10

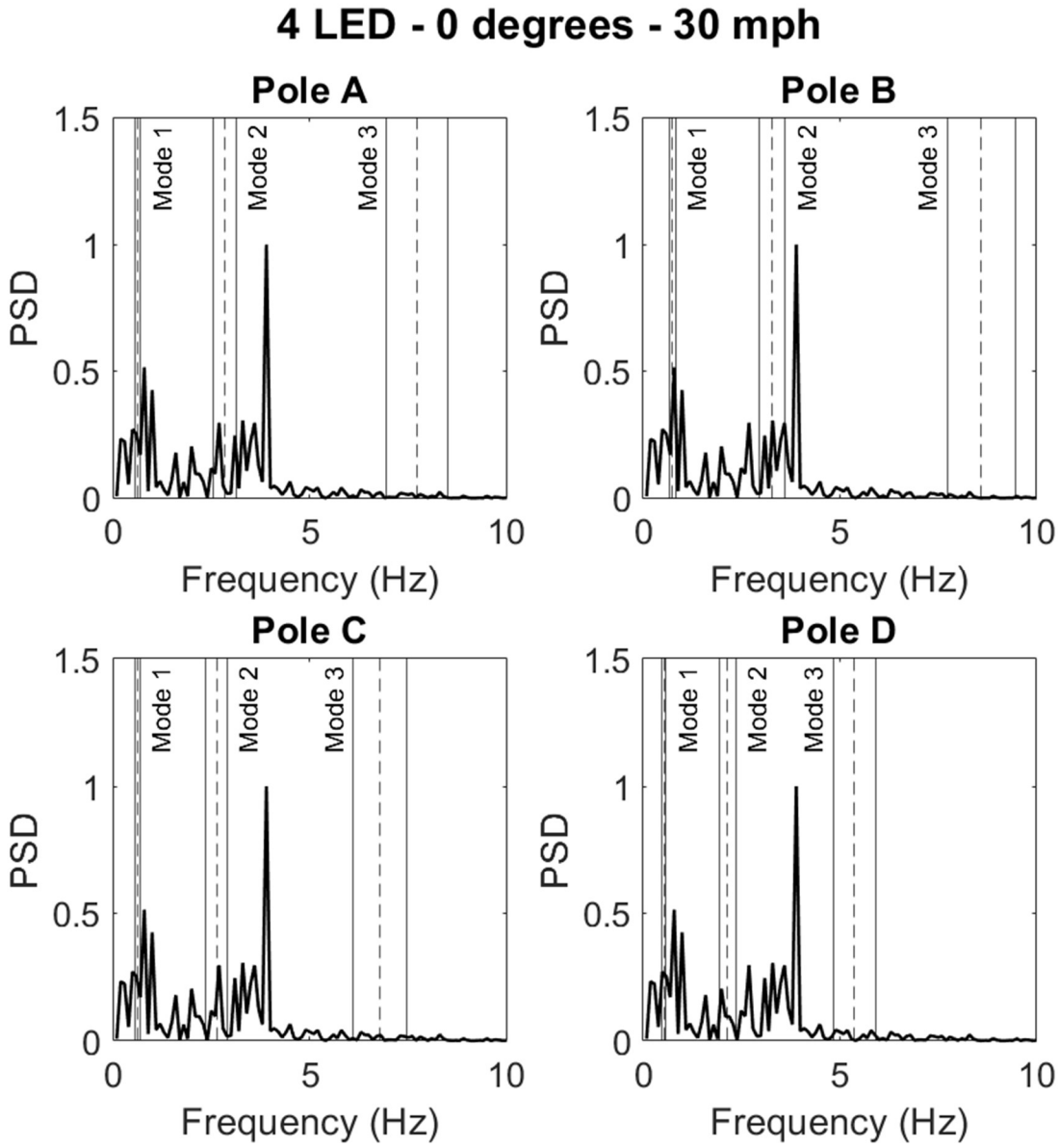
4 LED - 0 degrees - 30 mph
Pole A
Pole B
Pole C
Pole D
Mode 1
Mode 2
Mode 3
PSD
Frequency (Hz)
0
0.5
1
1.5
5
10

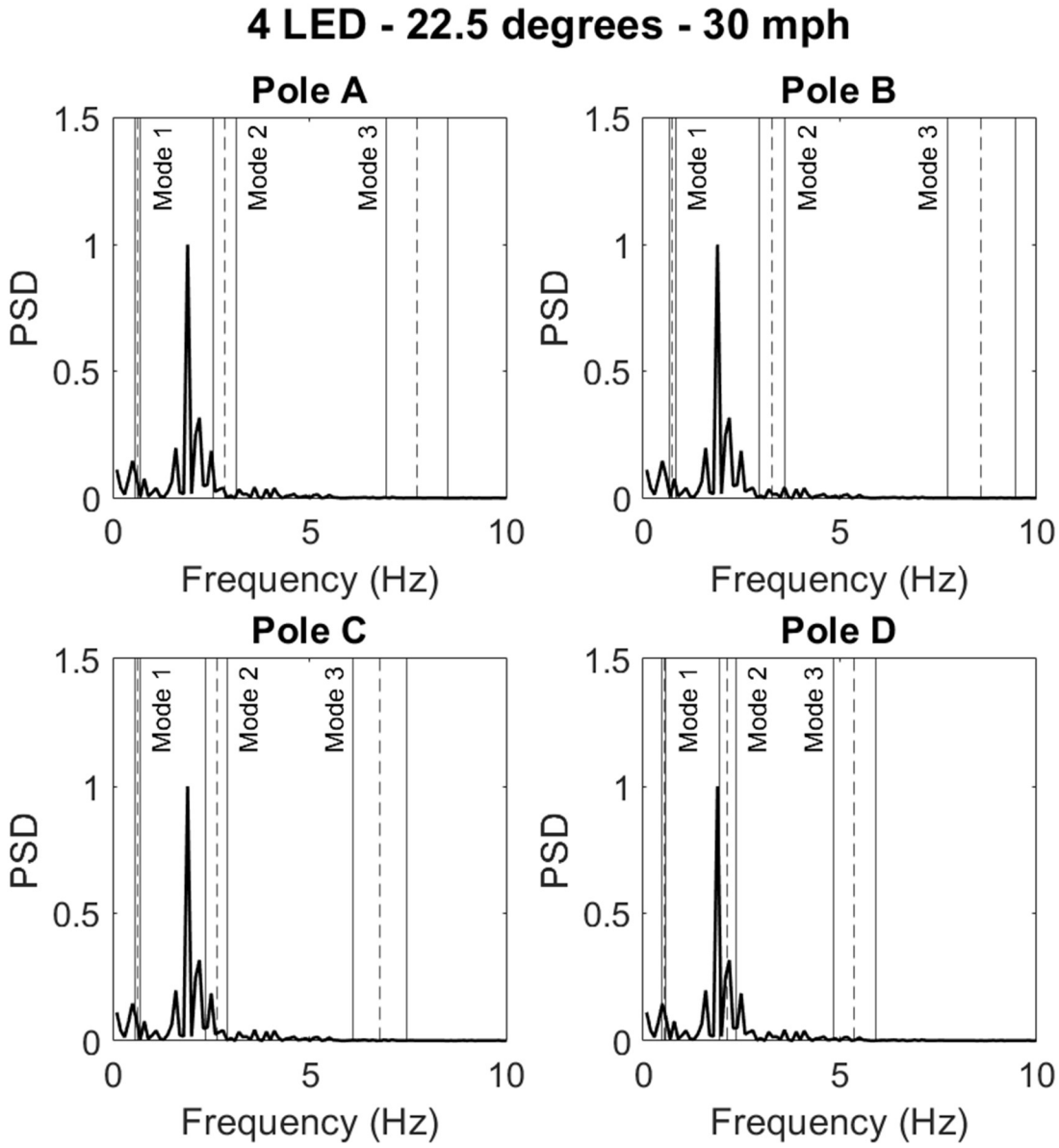
4 LED - 22.5 degrees - 30 mph
Pole A
Pole B
Pole C
Pole D
PSD
Frequency (Hz)
Mode 1
Mode 2
Mode 3
0
0.5
1
1.5
5
10

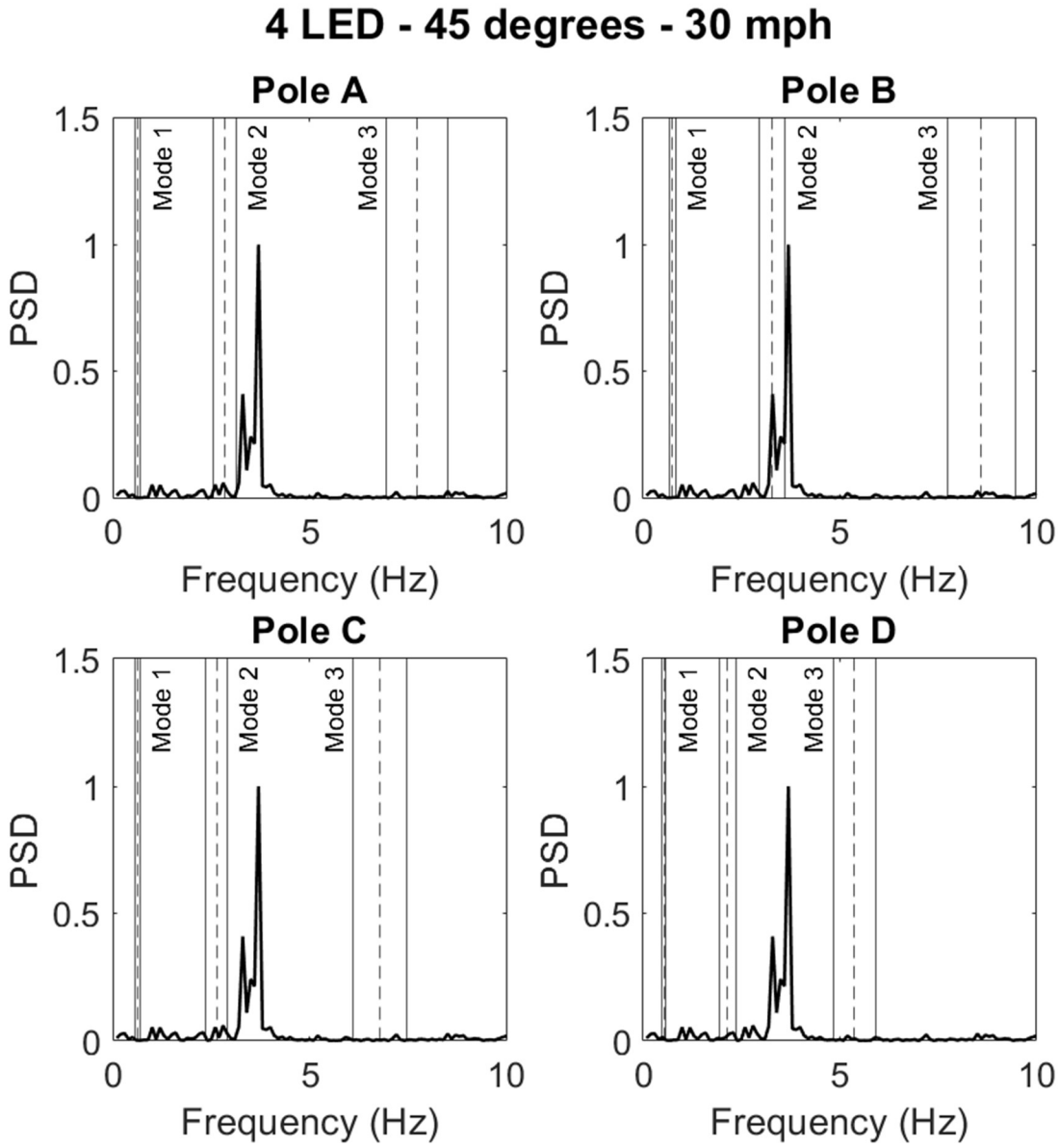
4 LED - 45 degrees - 30 mph
Pole A
Pole B
Pole C
Pole D
Mode 1
Mode 2
Mode 3
PSD
Frequency (Hz)
0
0.5
1
1.5
5
10

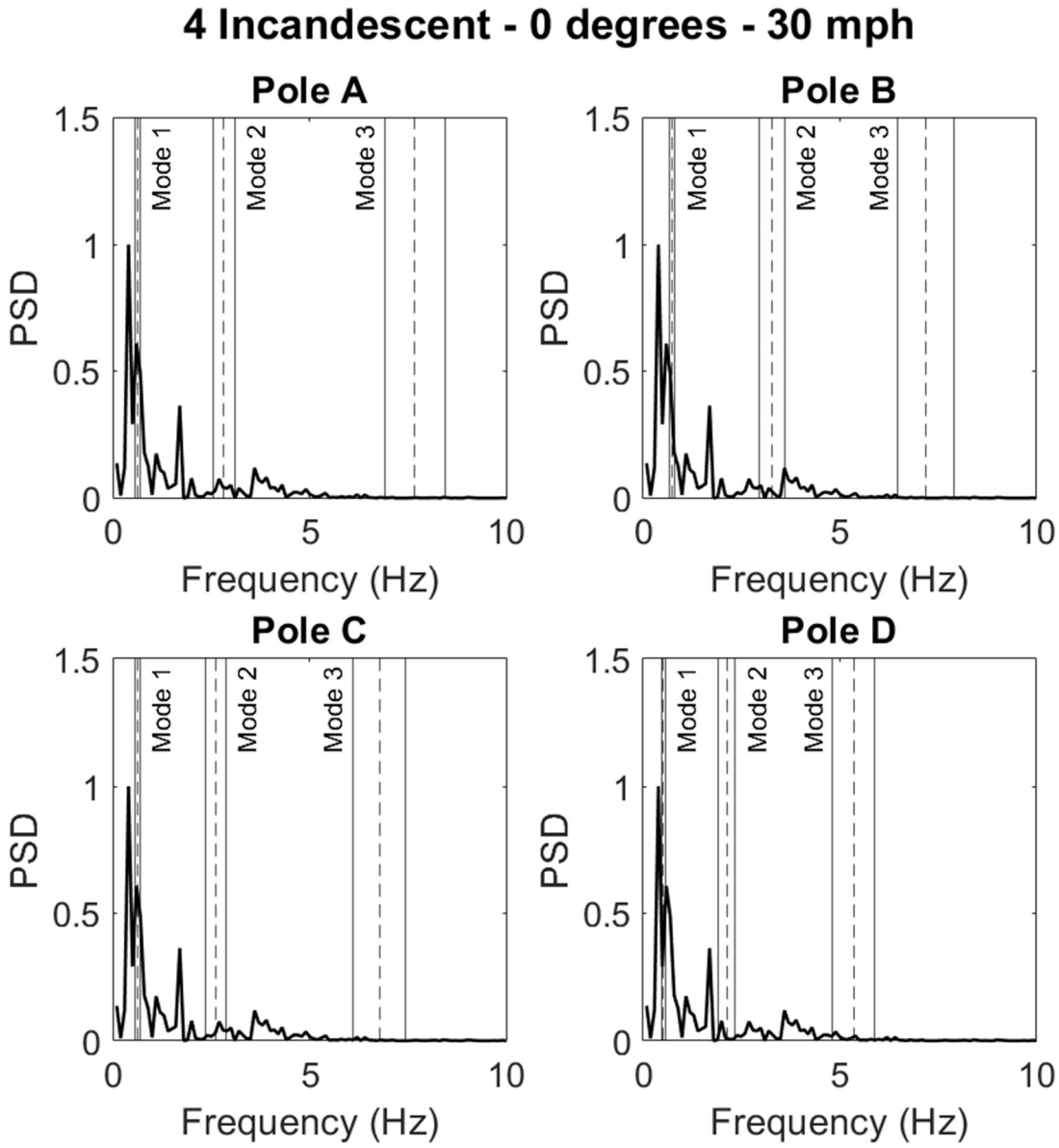
4 Incandescent - 0 degrees - 30 mph
Pole A
Pole B
Pole C
Pole D
Mode 1
Mode 2
Mode 3
PSD
Frequency (Hz)
0
0.5
1
1.5
5
10

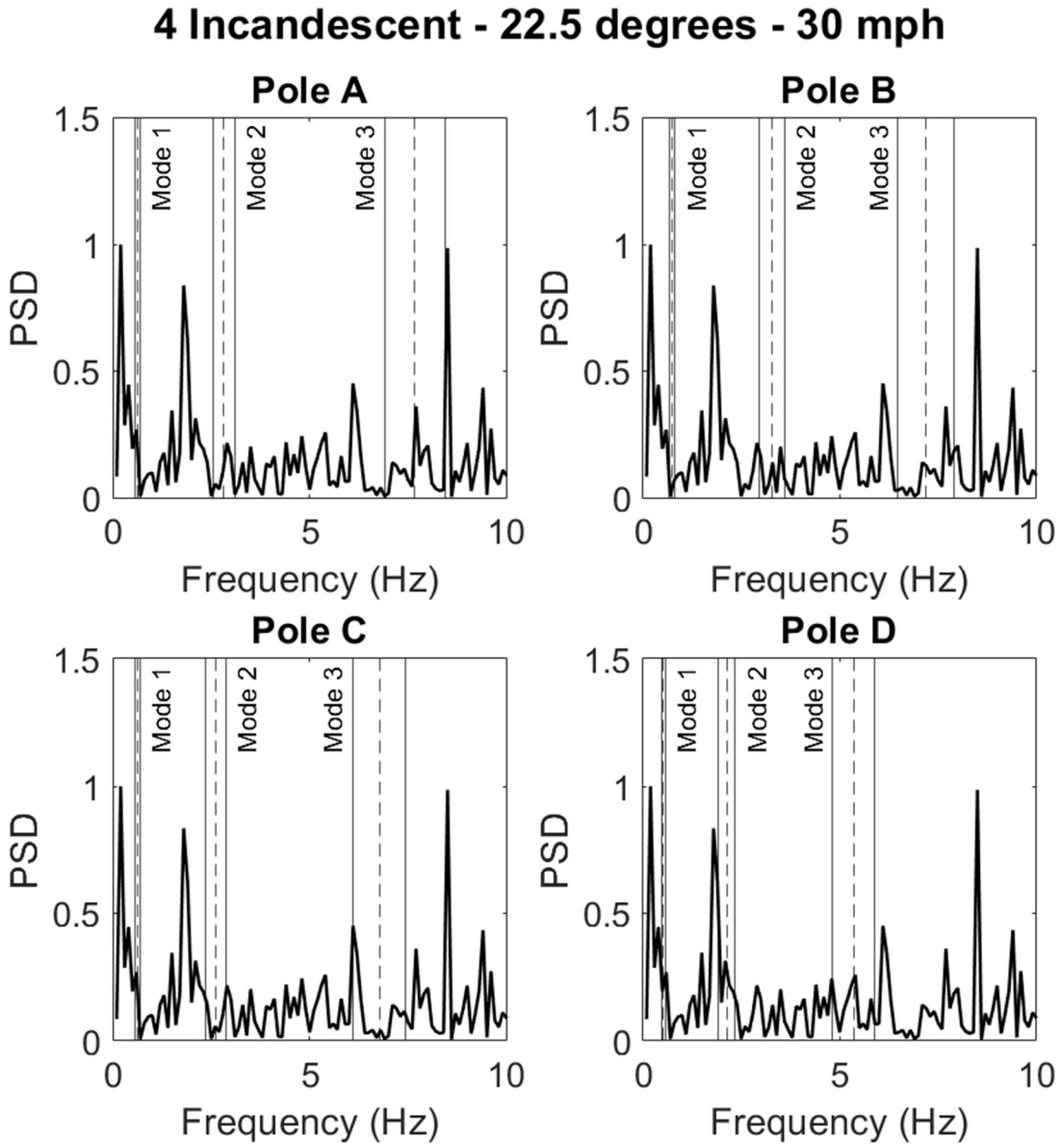
4 Incandescent - 22.5 degrees - 30 mph
Pole A
Pole B
Pole C
Pole D
Mode 1
Mode 2
Mode 3
PSD
Frequency (Hz)
0
0.5
1
1.5
5
10

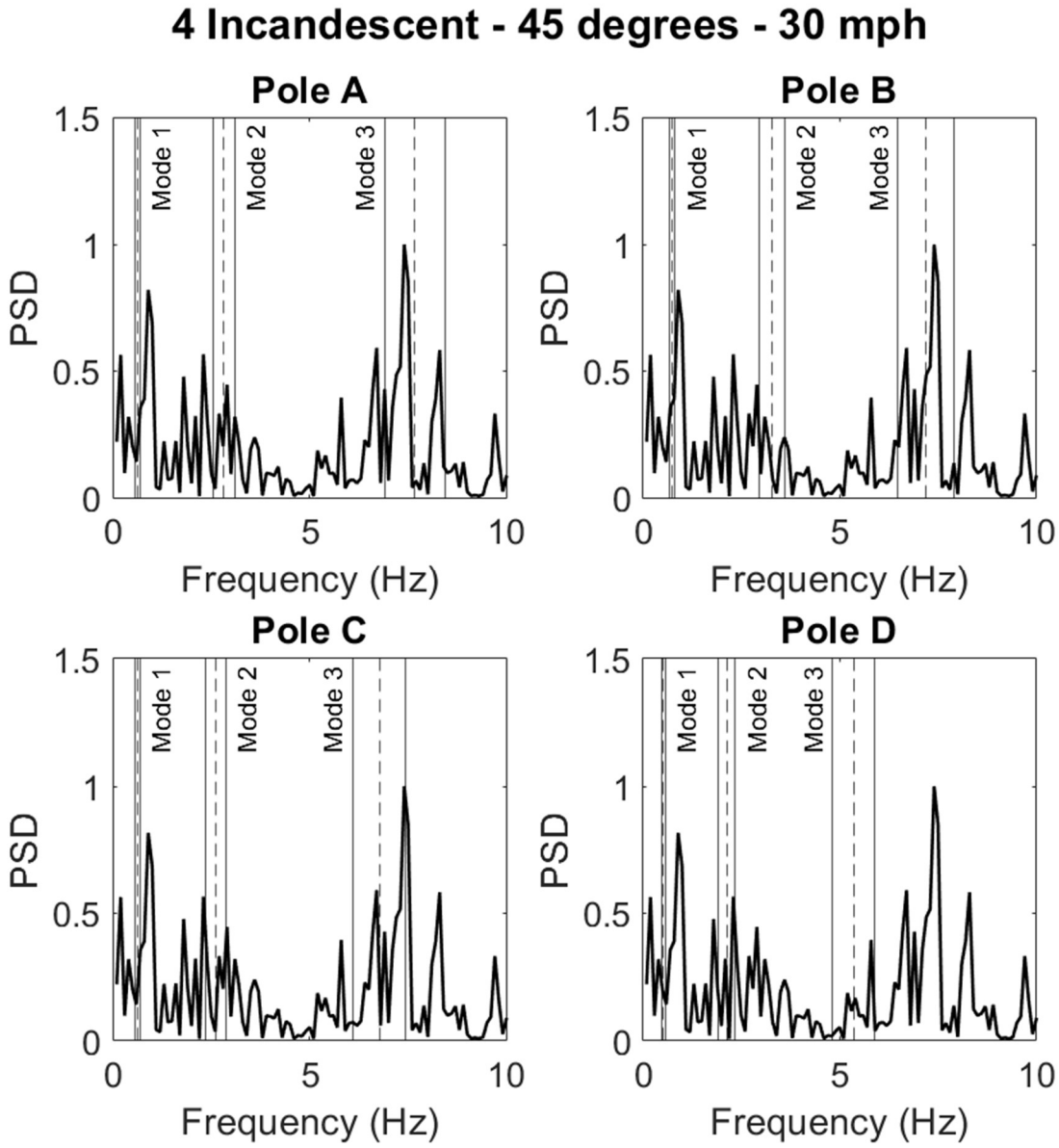
4 Incandescent - 45 degrees - 30 mph
Pole A
Pole B
Pole C
Pole D
Mode 1
Mode 2
Mode 3
PSD
Frequency (Hz)
0
0.5
1
1.5
5
10